Stem cell culture on 3D-scaffolds for cardiac regenerative medicine and *in vitro* studies



Arne A. N. Bruyneel

Merton College

University of Oxford

A thesis submitted for the degree of

Doctor of Philosophy

Michaelmas 2015

Acknowledgements

First and foremost, I would like to thank my supervisor Professor Carolyn Carr for giving me the opportunity to work on this project and for her guidance and support throughout the course of my D. Phil. I would also like to thank the British Heart Foundation for funding my project, and my second supervisor Professor Damian Tyler, and the head of our research group Professor Kieran Clarke, for their support and for welcoming me in the group.

Second, I would like to thank all the members of the CMRG group for making my time in the lab and office enjoyable. In particular, I would like to thank the Stemmies: Dr. Filippo Perbellini, Sophia Malandraki-Miller, Heba Al-Siddiqi, Khadijeh Pakzad and Colleen Lopez, for their company in the cell culture room and their friendship, technical help and advice. Next, I would to thank all other group members, Drs. Amira Abd-Jamil, Lydia Le Page, Daniel Ball, Andrew Lewis, Latt Mansor, Jack Miller, Angus Lau, Lucy Ambrose, Rhys Evans, Lisa Heather, Michael Dodd, Lowri Cochlin, Pete Cox, David Holdsworth, and Brianna Strubbs, Lucia Giles, Maria de Luz Fialho, Vicky Ball, Nicola Dixon, Yvonne Green, Matthew Kerr, and Dragana Savic, for the friendship, advice and the excellent and pleasant working environment. Special thanks to Lucia Giles, for introducing me to a new hobby, to Dr. Latt Mansor, for the breakfast/brunch trips, and to Dr. Jack Miller, for the physics/statistics/engineering chats and for the pleasant time sharing an office.

Third, I would like to thank everybody who directly contributed to experiments, Saumya Jani, Colleen Lopez, Dr. Lydia Le Page, Dr. Lucy Ambrose, Dr. Jack Miller, and our collaborators in the Material Science department: Professor Jan Czernuska, Dr. Qi Chen, and Rabia Nazir, for the excellent collaboration and producing the collagen scaffolds. I would also like to thank Dr Sally Cowley (James Martin Stem Cell Facility, University of Oxford) and Professor Chris Denning and his group (The University of Nottingham) for technical help and support in working with iPS cardiomyocytes.

Additionally, I would like to thank all the members of staff in DPAG and other departments for their assistance. In particular, Mark Howard, Daniel Heaton and Marcas O'Bardain, of the mechanical workshop in DPAG, David O'Connor in DPAG, Richard Stillion of histology facility (Pathology), Dr. Alan Wainman of the confocal microscopy facility (Pathology), and Mark Jones of the electronics workshop (Physics).

Finally, I would like to thank my parents, family and friends. In particular, many thanks to my current and former house mates, Drs. Youxin Kong, Roland Armstrong, and Imogen Large, for their friendship and for making me feel at home. Additionally, special thanks to my girlfriend Amélie Verfaillie for her love and support.

Stem cell culture on 3D-scaffolds for cardiac regenerative medicine and *in vitro* studies

Arne A. N. Bruyneel

Merton College, University of Oxford

A thesis submitted for the degree of

Doctor of Philosophy

Michaelmas 2015

Most life years lost due to death and disability in the Western world arise from non-communicable diseases, such as cancer and cardiovascular disease. Myocardial infarction (MI) and heart failure (HF) still have a particular poor prognosis, despite the development of improved pharmacological therapy and surgical interventions. No cure, other than heart transplant, is available for patients with HF. As a result, further research into new treatment strategies is paramount. Many potential avenues have been suggested, but this thesis aimed to work towards using stem cells and tissue engineering strategies as tool for *in vitro* testing and *in vivo* therapy.

In the first place, the thesis aimed to develop a humanised Langendorff perfused heart as an *in vitro* testbed. The decellularised rat heart was chosen as biomaterial, because it allows perfusion, and cardiomyocytes (CMs) derived from human induced pluripotent stem cells (hiPS) as cell source. Given the size of the constructs and to enable biomimetic mechano-electrical stimulation of the organoids, which may aid in the differentiation and maturation of the cardiomyocytes, a bioreactor was constructed for culturing the recellularised hearts. Finally, the feasibility and performance of culturing decellularised hearts seeded with iPS-CMs in the bioreactor under biomimetic conditions was assessed. The performance of this technique was currently insufficient for it to be used as an *in vitro* model of the heart. Hence, further improvements in bioreactor design and cell culture technique are required.

Secondly, the therapeutic benefit of a cell-loaded collagen scaffold was investigated in a rat ischaemia-reperfusion myocardial infarction (MI) model. A bilayer collagen scaffold was designed for this purpose and biocompatibility demonstrated both *in vivo* and *in vitro.* Cardiosphere-derived stem cells were used as cell source, given their potential to form cardiomyocytes and blood vessel structures, and their therapeutic benefit post-MI. In the present study, the cells were pre-conditioned with hypoxia, as this increased stemness and pro-angiogenic factor secretion, before implantation post-MI. However, a twelve week study using magnetic resonance imaging to study cardiac function failed to show significant improvements in function post-MI.

In summary, this thesis contributed to the development of technology for both *in vitro* and *in vivo* cardiac tissue engineering. However, further investigation and optimisation will be required before this technology can be applied in practice.

CONTENTS

Contents i

List of Figures vi

List of Tables ix

1 Introduction & literature review 1
- 1.1 Cardiovascular disease . . . 2
  - 1.1.1 The global burden of cardiovascular disease . . . 2
  - 1.1.2 Congenital heart disease . . . 2
  - 1.1.3 Coronary artery disease . . . 3
  - 1.1.4 Heart failure . . . 6
  - 1.1.5 Valve disease . . . 7
  - 1.1.6 Drug-induced cardiotoxicity and drug development . . . 8
- 1.2 Shortcomings of current therapeutic strategies for AMI and HF and avenues for further research . . . 9
- 1.3 Stem cell therapy for cardiovascular disease . . . 11
  - 1.3.1 The heart is not a post-mitotic organ . . . 11
  - 1.3.2 Embryonic and adult stem cells . . . 13
  - 1.3.3 Bone-marrow derived cells . . . 14
  - 1.3.4 Skeletal myoblasts . . . 15
  - 1.3.5 Embryonic and induced pluripotent stem cells . . . 15
  - 1.3.6 Endogenous cardiac stem cells . . . 16
- 1.4 Cardiac differentiation of stem cells . . . 18
  - 1.4.1 Differentiation . . . 18
  - 1.4.2 Gene and protein expression . . . 19
  - 1.4.3 Metabolism . . . 20
  - 1.4.4 Contraction . . . 21
  - 1.4.5 (Im)Maturity of stem cell derived cardiomyocytes . . . 21
- 1.5 Hallmarks of cardiac stem cell therapy . . . 24
  - 1.5.1 Remuscularisation . . . 24
  - 1.5.2 Paracrine signalling . . . 25
  - 1.5.3 The dying stem cell hypothesis . . . 26
- 1.6 Biomaterials and tissue engineering . . . 27
  - 1.6.1 Aims . . . 28
  - 1.6.2 Biomaterials . . . 29

1.6.3 Tissue engineering for regeneration . . . 33
1.6.4 Tissue engineering approaches for disease modelling . . . 34
1.6.5 Bioreactors and biomimetic stimulation . . . 36
1.7 Central hypothesis and aims of this thesis . . . 38

2 Materials and methods 40
2.1 Statistics and Data analysis . . . 40
2.1.1 Data and distributions . . . 40
2.1.2 Descriptive and exploratory statistics . . . 41
2.1.3 Frequentist statistics . . . 41
2.1.4 Bayesian statistics . . . 44
2.1.5 Software . . . 46
2.2 Animals . . . 46
2.2.1 Organ harvest . . . 47
2.2.2 Infarct surgery . . . 47
2.3 MR imaging and analysis . . . 47
2.4 Cell culture . . . 48
2.4.1 iPS cell culture and cardiac differentiation . . . 48
2.4.2 Cardiosphere explant culture . . . 51
2.5 Collagen scaffolds . . . 52
2.5.1 Disc-shaped collagen scaffolds . . . 53
2.5.2 Biventricular collagen cup-shaped scaffolds . . . 53
2.5.3 Bilayer collagen scaffolds for surgery . . . 54
2.5.4 Scaffold sterilisation . . . 54
2.6 Decellularisation . . . 55
2.6.1 Literature review . . . 55
2.6.2 Reactor . . . 55
2.6.3 Protocols . . . 56
2.6.4 Tissue characterisation . . . 57
2.6.5 Normalisation . . . 59
2.6.6 Tissue permeability . . . 60
2.6.7 Detergent toxicity . . . 60
2.6.8 Sterilisation and preparation of decellularised hearts for cell culture 61
2.7 Recellularisation . . . 62
2.7.1 Bioreactor design . . . 62
2.7.2 Sterilisation and preparation . . . 63
2.7.3 Cell culture . . . 63
2.7.4 Cell seeding of decellularised hearts . . . 64
2.7.5 Culture in the bioreactor . . . 64
2.8 Histology, immunohisto- and immunocytochemistry . . . 64
2.8.1 Tissue fixation, embedding and sectioning . . . 64
2.8.2 Histological staining . . . 65
2.8.3 Immunohistochemistry . . . 65
2.8.4 Immunocytochemistry . . . 66
2.8.5 RNA extraction . . . 66

2.8.6 cDNA conversion . . . 67
2.8.7 Primer design . . . 67
2.8.8 qPCR reaction . . . 67
2.8.9 Analysis of qPCR data . . . 68
2.9 ELISA . . . 71
2.10 Metabolic measurements . . . 71
2.10.1 Measurement of media glucose and lactate concentration . . . 71
2.10.2 Metabolite cell extraction using chloroform-methanol-water . . . 72
2.10.3 Metabolite extraction from cell medium . . . 72
2.10.4 NMR sample preparation . . . 72
2.10.5 NMR machine and protocols . . . 72
2.10.6 NMR Metabolomics software and data analysis . . . 73

3 hiPS culture and differentiation on matrigel and collagen scaffolds 74
3.1 Introduction . . . 74
3.1.1 Generating iPS-derived cardiomyocytes . . . 74
3.1.2 3D approach: collagen scaffolds . . . 75
3.1.3 Aims . . . 76
3.2 Results . . . 76
3.2.1 Cardiac differentiation of iPS cells on Matrigel . . . 76
3.2.2 Effect of long term culture of hiPS-CMs on gene expression . . . 77
3.2.3 iPS and iPS-CM metabolism . . . 86
3.2.4 Culture of iPS-CMs on different ECM substrates . . . 90
3.2.5 Culture of iPS-CMs on collagen scaffolds . . . 92
3.3 Discussion . . . 95
3.3.1 Cardiac differentiation of iPS cells and maturation by long-term culture . . . 95
3.3.2 Metabolism . . . 99
3.3.3 ECM and scaffolds . . . 100
3.4 Conclusion . . . 101

4 Decellularisation of isolated rat hearts 103
4.1 Introduction . . . 103
4.1.1 Decellularisation methods . . . 103
4.1.2 The mechanism of decellularisation . . . 105
4.1.3 Aims . . . 108
4.2 Results and discussion . . . 108
4.2.1 Decellularisation reactor design . . . 108
4.2.2 Decellularisation of isolated rat hearts . . . 109
4.2.3 Normalisation strategies for decellularisation . . . 111
4.2.4 Pre-treatment strategies for decellularisation . . . 122
4.2.5 Post-treatment strategies for decellularisation . . . 131
4.3 Conclusion . . . 135

5 Development of a biomimetic culture platform for recellularisation of decellularised rat hearts with synchronised mechanical and electrical stimulation 137
5.1 Introduction . . . 137
5.2 Development of a recellularisation bioreactor . . . 138
5.2.1 Fluidics . . . 139
5.2.2 Biomimetic mechano-electrical stimulation . . . 140
5.2.3 Electronics . . . 140
5.2.4 Computer client software . . . 156
5.3 Recellularisation of decellularised hearts . . . 156
5.3.1 Infused cells populate the vasculature and cavities, but fail to populate the full thickness of the construct . . . 157
5.3.2 Cells are viable and metabolically active within the recellularised heart . . . 157
5.3.3 Effect of biomimetic stimulation on gene expression of iPS-CMs . 158
5.4 Discussion . . . 160
5.5 Conclusion . . . 166

6 Therapeutic effect of transplantation of bilayer collagen scaffolds seeded with hypoxic-preconditioned cardiosphere-derived stem cells after myocardial infarction in an experimental rat model 170
6.1 Introduction . . . 170
6.1.1 Stem cell therapy and tissue engineering for the heart . . . 171
6.1.2 Mechanical considerations of scaffolds . . . 172
6.1.3 Host response to scaffolds . . . 174
6.1.4 Aims . . . 174
6.2 Results . . . 175
6.2.1 Design and manufacture of a bilayer collagen scaffold . . . 175
6.2.2 Host response to the transplantation of collagen scaffolds . . . 175
6.2.3 Cardiosphere-Derived Cells . . . 178
6.2.4 Effect of scaffold transplantation with or without cells on cardiac function . . . 182
6.3 Discussion . . . 192
6.3.1 Scaffold design and biocompatibility . . . 193
6.3.2 Characterisation of CDCs . . . 196
6.3.3 Effect of scaffold transplantation on cardiac function and adverse remodeling . . . 197
6.4 Conclusion . . . 202

7 Conclusions and future perspectives 205
7.1 Development of a humanised Langendorff perfused heart . . . 205
7.1.1 Limitations and future work aimed towards developing the humanised Langendorff perfused heart . . . 207
7.2 Development of a cardiac patch for preventing adverse remodelling post-MI . . . 209
7.3 Conclusion . . . 211

Bibliography **213**

A Additional materials and methods **246**

B Bioreactor: detailed design description **250**

List of Figures

1.1 Risk factors for disease by country and development level . . . 3
1.2 Cell metabolism . . . 22
1.3 Protein complexes involved in cardiac excitation-contraction coupling . . . 23

2.1 iPS-CM differentiation protocol time line . . . 50
2.2 Photograph of a disc-shaped collagen scaffold . . . 53
2.3 Design of a biventricular cup-shaped collagen scaffold . . . 54
2.4 VEGF ELISA . . . 71

3.1 Cell morphology changes during differentiation from iPS cell to cardiomyocyte 78
3.2 Cardiac Troponin-T expression in hiPS-CMs . . . 79
3.3 Efficiency of the differentiation of hiPS to beating cardiomyocytes . . . 79
3.4 iPS-CM long term culture-induced maturation study: PCA and Hierarchical clustering of qPCR data . . . 82
3.5 iPS-CM long term culture-induced maturation study: housekeeping gene expression . . . 83
3.6 iPS-CM long term culture-induced maturation study: contractile protein expression . . . 84
3.7 iPS-CM long term culture-induced maturation study: metabolic protein expression . . . 85
3.8 iPS-CM long term culture-induced maturation study: ECM protein expression 86
3.9 hiPS and hiPS-CM gene expression of metabolic proteins . . . 87
3.10 hiPS and hiPS-CM NMR metabolomics: cell media supplemented with 2-^{13}C glucose . . . 89
3.11 hiPS and hiPS-CM NMR metabolomics: intracellular metabolites . . . 90
3.12 hiPS and hiPS-CM NMR metabolomics: intracellular Lactate to Alanine ratio 91
3.13 Culture of hiPS-CMs on ECM substrates: success rate of forming beating cells 91
3.14 Gene expression of hiPS-CMs cultured on a variety of ECM substrates . . . 92
3.15 iPS-CMs on collagen scaffolds: histology and qPCR . . . 94

4.1 Convective flow in decellularisation: vessel model . . . 106
4.2 Decellularisation of rat hearts: methodology and reactor configuration . . . 110
4.3 Decellularised hearts retain gross anatomy morphology . . . 111
4.4 Normalisation study: normalisation in literature . . . 115
4.5 Normalisation study: heart and body weights . . . 116
4.6 Normalisation study: histology . . . 116

4.7 Normalisation study: tissue and water content of decellularised tissue 117
4.8 Normalisation study: wet and dry weight normalisation 119
4.9 Normalisation study: whole heart normalisation 120
4.10 Effect of perfusion pressure and permeabilisation strategy on detergent use and permeability 125
4.11 Effect of pressure and permeabilisation technique on the DNA content of decellularised tissue 127
4.12 Effect of pressure and permeabilisation technique on the GAG content of decellularised tissue 128
4.13 Effect of pressure and permeabilisation technique on the collagen content of decellularised tissue 129
4.14 The effect of DNase treatment of the DNA content of decellularised hearts . . 131
4.15 SDS content of decellularised heart after treatment with TX-100 133
4.16 Toxic effect of SDS and TX-100 133

5.1 Schematic of the biomimetic stimulation features of the bioreactor 138
5.2 Schematic and photo of the bioreactor fluidics path 141
5.3 Ventricular pressure and volume during the cardiac cycle 142
5.4 Linear actuator fitted with syringe for inducing mechanical stimulation . . . 143
5.5 Bioreactor power supply board: PCB 144
5.6 Bioreactor MCU board: PCB 146
5.7 SRAM-ADC algorithm 147
5.8 Bioreactor amplifier board: PCB 148
5.9 Bioreactor Stimulation board: PCB 149
5.10 Biphasic electrical stimulation pulse by charge dumping 153
5.11 Synchronised mechanical and electrical stimulation: triangular or trapezoidal pulse 154
5.12 Histology on decellularised hearts reseeded with CDCs 158
5.13 Metabolic activity of recellularised hearts: CDCs and hiPS-CMs 159
5.14 iPS-CMs on collagen scaffolds and decellularised hearts 160

6.1 Design of bilayer collagen scaffold for implantation on the LV wall post-MI . 176
6.2 Retention and integration of collagen scaffolds two and six weeks post implantation on the heart 177
6.3 Scaffold colonisation by macrophages and blood vessels *in vivo* 178
6.4 CDC cell morphology during the cell isolation protocol 180
6.5 CDC colony types under normoxic and hypoxic culture conditions 181
6.6 CFU potential in normoxia and hypoxia 182
6.7 VEGF and lactate secretion by CDC-seeded scaffolds in normoxia and hypoxia 183
6.8 Experimental overview scaffold surgery study 184
6.9 Descriptive statistics: PCA on MRI data 186
6.10 Effect of MI and scaffold treatment on LV mass 188
6.11 Effect of MI and scaffold treatment on heart rate, ejection fraction and cardiac output 189
6.12 Effect of MI and scaffold treatment on end systolic and diastolic lumen . . . 190

6.13 Effect of MI and scaffold treatment on infarct size 192
6.14 Scaffold degradation *in vivo* 193
6.15 Histological quantification of scarred area 194

7.1 A vascularised hydrogel as a humanised Langendorff perfused heart 209

B.1 Power board: Schematics 252
B.2 MCU board PCB: Schematics 253
B.3 Amplifier board PCB: Schematics 254
B.4 Stimulation board PCB: Schematics 255

List of Tables

2.1 Compounds used in the cardiac differentiation protocol . . . 49
2.2 ECM components and concentration for culture of iPS-CMs . . . 51
2.3 CEM media composition . . . 52
2.4 CGM media composition . . . 52
2.5 Krebs-Henseleit buffer composition . . . 56
2.6 qPCR cycle protocol . . . 68
2.7 qPCR modelling notations . . . 69
2.8 Batman NMR metabolomics: metabolite list . . . 73

3.1 ES/iPS cardiac differentiation protocols . . . 76
3.2 List of gene transcripts assessed in the long term culture-induced maturation of hiPS-CMs . . . 80
3.3 hiPS and hiPS-CM glucose and lactate concentration in the culture medium 88

4.1 Heart and body weights of SD rats used to assess the effect of pressure and permeabilisation technique on decellularisation performance . . . 124
4.2 Wet weight of the hearts after decellularisation . . . 126
4.3 LD50 of SDS and TX-100 . . . 134
4.4 Literature toxicity levels for SDS and TX-100 . . . 135

5.1 Bioreactor design: Power supplies . . . 143
5.2 Linear actuator characteristics . . . 151
5.3 Overview of mechanical stimulation parameters used in literature . . . 167
5.4 Overview of electrical stimulation parameters used in literature . . . 168
5.5 Overview of whole organ recellularisation bioreactor studies . . . 169

6.1 Overview of the cine-MRI data . . . 191
6.2 Overview of *in vivo* studies using collagen scaffolds with or without cells post-MI . . . 204

A.1 qPCR primers for human samples . . . 246
A.2 Primary antibodies used for immunohistochemistry and immunocytochemistry . . . 249
A.3 Secondary antibodies used for immunohistochemistry and immunocytochemistry . . . 249

B.1 Instructions list . . . 250

B.2 Instructions list 251
B.3 Instructions list 251
B.4 Stimulation instructions list 256
B.5 Parallel communication instructions to configure oxygenation 256
B.6 Parallel communication instructions to configure electrical and mechanical stimulation 257

ABBREVIATIONS

AC	alternating current
ACE	angiotensin-converting enzyme
ACS	acute coronary syndrome
ADC	analog-to-digital convertor
ADHF	acute decompensation heart failure
ADR	adverse drug reaction
ADSC	adipose-derived stem cell
AIC	Akaike information criterion
AMI	acute myocardial infarction
ANOVA	analysis of variance
ARB	angiotensin II receptor blocker
ATP	adenosine-5'-triphosphate
bFGF	basic fibroblast growth factor
BM	bone marrow
BM-MSC	bone marrow-derived mesenchymal stem cell
BME	β-mercaptoethanol
BMMNC	bone marrow-derived mononuclear cell
BMP	bone morphogenetic protein
bp	base pairs
BSA	bovine serum albumin
CABG	coronary artery bypass graft
CAD	coronary artery disease
CASQ2	calsequestrin-2
CDC	cardiosphere-derived stem cell
cDNA	complementary deoxyribonucleic acid
CE	Conformité Européenne
CEM	complete explant medium
CFU	colony forming unit
CGM	cardiosphere growth medium
CHD	coronary heart disease
CICR	Ca^{2+}-induced Ca^{2+} release
CM	cardiomyocyte
CO	cardiac output
CPC	cardiac progenitor cell

CS	citrate synthase
CSC	cardiac stem cell
CSV	comma-separated value
CVD	cardiovascular disease
Cx40	connexin 40
Cx43	connexin 43
Cx45	connexin 45
DAPI	4',6-diamidino-2-phenylindole
DC	direct current
DDR2	discoidin domain-containing receptor-2
DMEM	Dulbecco's modified eagle medium
DNA	deoxyribonucleic acid
DNP	dynamic nuclear polarisation
dNTP	deoxynucleotide triphosphate
DPBS	Dulbecco's phosphate buffered saline
ds	double stranded
EB	embryoid body
EC	endothelial cell
ECG	electrocardiogram
ECM	extracellular matrix
EDC	explant-derived cell
EDL	end diastolic lumen
EF	ejection fraction
EGF	epidermal growth factor
EHT	engineered heart tissue
ELISA	enzyme-linked immuno sorbent assay
ES	embryonic stem cell
ES-CM	embryonic stem cell-derived cardiomyocyte
ESL	end systolic lumen
FA	fatty acid
FBS	fetal bovine serum
FDA	U. S. Food and Drug Administration
FGF	fibroblast growth factor
FISH	fluorescence in situ hybridisation
FLC	fetal lung cell
FS	fractional shortening
G-CSF	granulocyte-colony stimulating factor
GAG	glycoamino glycan
GLM	general linear model
GLS	generalised linear least squares
GLUT	glucose transporter

GLUT1	glucose transporter-1
GLUT4	glucose transporter-4
GOI	gene of interest
GUI	graphical user interface
H&E	Hematoxylin and Eosin
HF	heart failure
HFPEF	heart failure with preserved ejection fraction
HFREF	heart failure with reduced ejection fraction
HGF	hepatocyte growth factor
HMBC	heteronuclear multiple-bond correlation spectroscopy
HUVEC	human umbilical vein endothelial cell
I^2C	inter-integrated circuit
I/R	ischaemia/reperfusion
IGF-1	insulin-like growth factor-1
IL-10	interleukin-10
IL-6	interleukin-6
IMDM	Iscove's modified Dulbecco's medium
IP	intraperitoneal
iPS	induced pluripotent stem cell
iPS-CM	induced pluripotent stem cell-derived cardiomyocyte
IRS1	insulin receptor substrate-1
IRS2	insulin receptor substrate-2
LAD	left anterior descending
LCD	liquid crystal display
LD50	lethal dose 50
LDH	lactate dehydrogenase
LDL	low-density lipoprotein
LM	linear model
LV	left ventricle
LVEF	left ventricular ejection fraction
LVIDd	left ventricle internal diameter at end diastole
LVIDs	left ventricle internal diameter at end systole
LVPWDd	left ventricle posterior wall dimension at end diastole
LVPWDs	left ventricle posterior wall dimension at end systole
MCU	microcontroller unit
MEF	mouse embryonic fibroblast
MI	myocardial infarction

MR	magnetic resonance
MRI	magnetic resonance imaging
MSC	mesenchymal stem cell
MT	Masson's trichrome
NAD+	nicotinamide adenine dinucleotide
NADH	reduced nicotinamide adenine dinucleotide
NKC	neonatal kidney cell
NMR	nuclear magnetic resonance
NSTEMI	non-ST-segment elevation myocardial infarction
OCT	optimal cutting temperature
OXPHOS	oxidative phosphorylation
PAA	peracetic acid
PBMC	peripheral blood mononuclear cell
PBS	phosphate buffered saline
PC	personal computer
PCA	principal component analysis
PCB	printed circuit board
PCR	polymerase chain reaction
PDC	pyruvate dehydrogenase complex
PDF	portable document format
PDH	pyruvate dehydrogenase
PDK4	pyruvate dehydrogenase kinase isozyme-4
PE	polyethylene
PES	polyethersulfone
PET	polyethylene terephthalate
PFA	paraformaldehyde
PGA	polyglycolic acid
PGC1A	peroxisome proliferator-activated receptor gamma coactivator 1 alpha
PI3K	phosphoinositide 3-kinase
PLA	polylactic acid
PLGA	poly(lactic-co-glycolic acid)
POETE	polyoxyethelene (10) tridecyl ether
PPARA	peroxisome proliferator-activated receptor alpha
PTFE	polytetrafluoroethylene
qPCR	quantitative polymerase chain reaction
RAEC	rat aortic endothelial cell
RF-M	reduced factor Matrigel

RNA	ribonucleic acid
ROM	read-only memory
RPMI	Roswell Park Memorial Institute
RT	room temperature
RV	right ventricle
SCID	severe combined immune deficiency
SCIPIO	Stem Cell Infusion in Patients with Ischemic cardiOmyopathy
SD	Sprague Dawley
SDF-1	stromal cell-derived factor-1
SDS	sodium dodecyl sulfate
SEM	scanning electron microscopy
SPGA	software programmable gain amplifier
SPI	serial peripheral interface
SR	Sirius Red
SR	sarcoplasmic reticulum
SRAM	static random-access memory
ss	single stranded
STEMI	ST-segment elevation myocardial infarction
SV	stroke volume
TCA	tricarboxylic acid
TEP	trans-epithelial potential
TGF	transforming growth factor
TSA	trial sequential analysis
TX-100	triton X-100
UA	unstable angina
UK	United Kingdom
USA	United States of America
USB	universal serial bus
VAD	ventricular assist device
VEGF	vascular endothelial growth factor
VSMC	vascular smooth muscle cell
vWF	von Willebrand factor
WB	Western blot

CHAPTER 1

INTRODUCTION & LITERATURE REVIEW

Most life years lost due to death and disability in the Western world arise from non-communicable diseases, such as cancer and cardiovascular disease (CVD) (1). Myocardial infarction (MI) and heart failure (HF) have a particular poor prognosis, with up to 30 % of patients with acute myocardial infarction (AMI) dying within the first 24 hours, depending on the severity class. Surviving patients recover initially but will progress toward HF for which no cure, other than heart transplant, is available.

Despite the development of improved pharmacological therapy and surgical interventions over the last few decades resulting in an improved prognosis, further research into new treatment strategies is paramount since CVD remains the leading cause of death world wide.

Many potential avenues have been suggested as strategies to give rise to improved clinical outcomes. This thesis aimed to work towards using stem cells and tissue engineering strategies as drug testing platforms or as regenerative tool.

1.1 Cardiovascular disease

1.1.1 The global burden of cardiovascular disease

All of us die eventually, but the mechanism by which we die varied throughout history, geographical location and social status. Whereas infectious diseases, maternal and child illness, and malnutrition caused most of the deaths historically, and currently in high mortality developing countries, in the Western world most life years lost due to death and disability arise from non-communicable diseases, such as cancer and CVD (Figure 1.1). However, whereas the risk of death by CVD is decreasing in developed countries, it is becoming more prevalent in developing and transitional countries, with 80% of CVD-related deaths occurring in low or middle-income countries, partly as a result of increasing longevity, society and lifestyle changes (2–4).

In the United Kingdom (UK), CVD was the second biggest cause of death in 2014, causing 27 % of all deaths. Cancer preceded CVD and caused 29 % of all deaths. Coronary heart disease (CHD) and stroke are the predominant forms within CVD, with CHD the biggest single cause of death in the UK, causing 45 % of CVD deaths (5).

The different forms of cardiovascular disease, their prognosis and treatment strategies will be discussed in the next Sections.

1.1.2 Congenital heart disease

Gross structural abnormality of the heart or intrathoracic great vessels with actual or potential for functional significance, or congenital heart disease, has an incidence of about 75/1000 live births and is the most common birth defect (6–8).

Although many congenital defects are associated with considerable morbidity or mortality, the benefit of surgical intervention has increased dramatically and currently about 85% of these babies survive into adult life in the United States of America (USA)

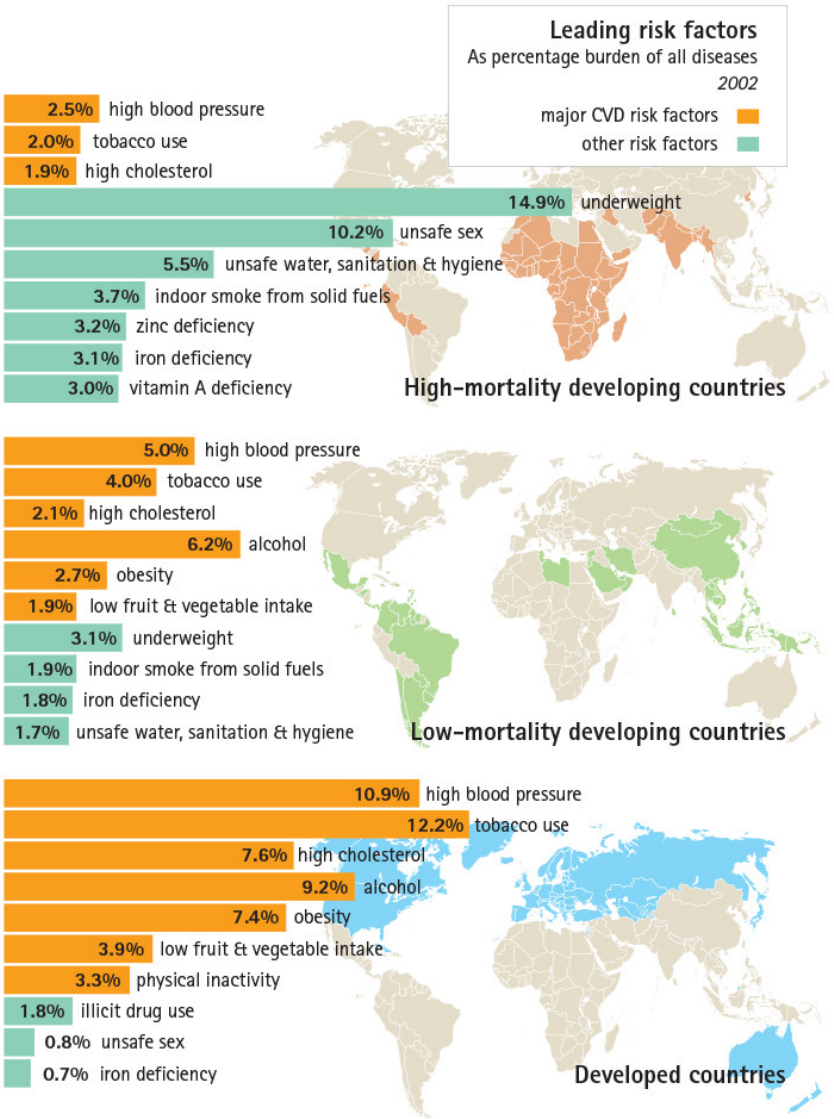


Figure 1.1: Risk factors for disease by country and development level Adapted from WHO (3).

(6). Patients do however need repeated surgery in order to accomodate survival.

1.1.3 Coronary artery disease

CHD or coronary artery disease (CAD) is caused by atherosclerotic plaque formation and narrowing and/or occlusion of the blood vessels in the heart. Atherosclerosis is a silent process that may start during the second or third decade in life and 20 to 30

years before patients present with clinical symptoms. Risk factors such as hypercholesterolemia and hypertension damage the endothelium layer of the blood vessel, and aid in allowing macrophages to infiltrate and low-density lipoprotein (LDL) to accumulate, resulting in a lipid-filled atherosclerotic plaque, which can rupture and cause clot formation. Coronary occlusion, by the clot, results in persistent ischaemia in the myocardial regions perfused by the occluded artery (9–13). Depending on the severity and magnitude of the thrombus formation, different subtypes can be distinguished, with chest pain as a common symptom: stable angina, unstable angina (UA), non-ST-segment elevation myocardial infarction (NSTEMI), and ST-segment elevation myocardial infarction (STEMI). Stable angina is a CAD, but not necessarily an acute coronary syndrome (ACS). Chest pain as a result of stable angina is usually physical activity dependent. A patient is diagnosed with UA when ischemic chest pain occurs in the absence of activity and when the symptoms worsen over time. Moreover, UA does not coincide with increased circulatory levels of cardiac proteins. NSTEMI and STEMI patients have elevated biomarker levels of cardiac necrosis. STEMI patients additionally have ST-segment elevation on their electrocardiogram (ECG), which is an indicator of total occlusion.

1.1.3.1 Therapeutic strategies

It is vital that the tissue at risk is reperfused imminently, as prolonged occlusion results in myocardial necrosis and impaired left ventricular function (13). As a result, clinical strategies are aimed at restoring perfusion, destroying the thrombi, preventing further blood clot formation and reducing the workload of the heart, by using drug therapy and surgical procedures (11, 12).

Pharmacological A variety of drugs are used in order to limit damage and prevent further ischaemia in patients with ACS. First of all, anticoagulants, antiplatelet and anti-

thrombotic agents are used. For UA and NSTEMI patients, antiplatelets and anticoagulants, such as aspirin, heparin, thienopyridines and glycoprotein IIb/IIIa, are prescribed. Whereas STEMI patients are also given thrombolytic treatment to dissolve the clots. A second class of drugs commonly used are the anti-ischaemic agents, which include nitrates, nitroglycerin, β-blockers, calcium antagonists, and potassium channel activators. These drugs result in vasodilation and reduce the workload, and hence the oxygen requirements of the heart. Angiotensin-converting enzyme (ACE) inhibitors, which reduce blood pressure and left ventricle (LV) workload, can additionally be prescribed. Finally, statins, typically administered to lower cholesterol levels, have been shown to have the additional benefits of improving coronary plaque stability by improving endothelial function, decreasing vascular inflammation and reducing platelet aggregation and instability (14).

Angioplasty Angioplasty is an endovascular procedure to widen narrowed blood vessels by use of an inflatable balloon. A stent may be placed to keep the vessel open.

CABG In order to improve blood flow downstream of a narrowed blood vessel, a surgical procedure termed coronary artery bypass graft (CABG) can be applied, in which a blood vessel from another part of the body is grafted to bypass the narrowed blood vessels of the heart.

1.1.3.2 Prognosis

Despite significant improvements in treatment strategies and survival rates, ACS account for half of all cardiovascular deaths, with 18 % of men and 23 % of women older than forty dying within a year of a first heart attack (3, 15). Mortality in STEMI patients is highest, with approximately one third of STEMI patients dying within twenty-four hours of ischemia. Whereas, 15 % of patients with UA or NSTEMI die or experience another infarction within thirty days.

Moreover, over time the necrotic regions become replaced by non-contractile scar tissue and the LV hypertrophies in order to maintain cardiac output. Unfortunately, the compensatory mechanisms may not be sufficient, leading to heart dilation and HF in the majority of patients.

1.1.4 Heart failure

Heart failure is a condition in which the heart function is limited in such a way that it cannot pump enough blood to meet the needs of the body for blood and oxygen. Inappropriate neurohormonal activation is associated with this condition which contributes to progressive ventricular remodelling and worsening of clinical phenotype (16). Hypertension, CAD, diabetes, and valvular heart disease most frequently preceded the diagnosis of HF. This condition has a dire prognosis of approximately 50 % mortality at 5-years post diagnosis (17), and although CVD mortality has decreased in the industrialised world because of prevention and better care, HF has become more prevalent (18). Three types of HF can be distinguished with different clinical-hemodynamic profiles: heart failure with preserved ejection fraction (HFPEF) (ejection fraction (EF) > 50 %, diastolic HF), heart failure with reduced ejection fraction (HFREF) (systolic HF) and acute decompensation heart failure (ADHF) (19).

1.1.4.1 Therapeutic strategies

There has been considerable improvement in survival of patients with HFREF over the last couple of decades, whereas the development of new drugs for patients with HFPEF or ADHF has been limited (20). Nonetheless, there is no curative treatment available for heart failure, other than transplantation. Given the complex pathophysiology of heart failure and adverse remodelling of the heart tissue, therapeutic strategies should aim to both alleviate symptoms and attenuate further adverse ventricular remodelling.

Pharmacological A variety of drugs are prescribed, such as anticoagulants, antiplatelets, ACE inhibitors, angiotensin II receptor blockers (ARBs), inotropic drugs, diuretics, vasodilators, β-blockers, and aldosterone antagonists. These drugs aim to prevent clotting, reduced blood pressure, drain retained fluids, lower the heart rate and increase the strength of contraction.

Transplantation Transplantation is the ultimate curative strategy for heart failure. However, donor organs are sparse, and transplanted patients are required to take lifelong immunosuppressive drugs leading to the development of other illnesses (21). Moreover, it is very difficult to predict the prognosis of this treatment strategy, given the heterogenous nature of both the patients requiring the procedure and the status of the donors (22). In general, the mortality is highest in the first year post-surgery with $15-20$ % of patients dying in this timeframe. In the subsequent years, mortality is constant at 4 % per annum.

Mechanical devices Heart pumping can be supported by implantation of a ventricular assist device (VAD). Replacement with a mechanical VAD is limited by an increased risk of infection and thromboembolism and finite durability. More than fifty years ago, when the development of these devices started, they were mainly used to treat post-operative HF, to aid the heart in self-recovery, whereas nowadays, these devices are either used as a bridge to transplantation or as destination therapy (defined as long-term home treatment). The major focus is using these devices as temporary measures, with destination therapy limited to elderly patients and patients otherwise unfit for transplantation (23, 24).

1.1.5 Valve disease

The heart is equipped with valves in order to obtain unidirectional flow. Three types of heart valve problems can be distinguished: regurgitation, stenosis, and atresia (25, 26).

Heart valve diseases can be congenital or can develop later in life. The risk factors for congestive valve disease are first of all old age, and secondly some infectious diseases, AMI, HF and the same risk factors as those of coronary heart disease. Regurgitation or backflow is frequently caused by prolapse, when the flaps of the valve bend back into an upper heart chamber during contraction. Stenosis is the stiffening or thickening of the heart valve leaflets and may prevent the valve from opening fully. Atresia is the condition in which the heart valve lacks an opening for blood to flow through.

1.1.5.1 Therapeutic strategies

Heart valve disease can not be cured by drugs, albeit these can alleviate some of the complications arising from this disorder. The only curative strategy is heart valve replacement. Three classes of heart valves for transplantation are available: prosthetic, bioprosthetic, and homograft valves. Prosthetic valves are made of plastic and/or metal, and are the most long lasting. However, patients are required to take anticoagulants to prevent blood clotting. Homograft valves are uncommon, given the limited availability of donor tissue, and also last for about two decades. Bioprosthetic valves combine heterograft tissue with prosthetic material, and last for about 10-20 years, with calcification as major lifetime limiting factor (27).

1.1.6 Drug-induced cardiotoxicity and drug development

New drugs are characterised in detail and screened for effectivity and safety using *in vitro* and *in vivo* models. Subsequently, the drug is tested in human subjects. In phase-I trials, the drug is administered to a small group (20 to 100) of healthy volunteers or patients affected with the illness. The primary aim is to study safety and dosage. About 70 % of drugs progress to phase-II testing, which involves several hundred patients and assesses efficacy and side effects. These studies last up to two years and are a more significant hurdle with only about 33 % of drugs progressing to the next phase. Phase-

III/IV trials last multiple years and involve multiple thousand patients. Taken together, the route from discovery to marketing is long and expensive and the pharmaceutical industry would benefit from tools that would enable them to identify failed drugs sooner in the process.

At the time a new drug reaches the market, not all potential adverse drug reactions (ADRs) are known and hence post-marketing review of drugs is essential (28). ADRs are considered a major source of death and disability, since the overall incidence of serious ADRs (requiring hospitalisation, permanently disabling, or resulting in death) was 6.7 % and of fatal ADRs was 0.32 % of hospitalised patients (29). Cardiotoxicity is a primary cause of compound failure during drug development, and post-launch withdrawal (30).

Potential attributes of drug-induced cardiac toxicity are *inter alia* altered contractility, ion channel block, arrhythmia (long QT), and ischemia (28, 31). BMS-986094, a drug by Bristol-Myers Squibb is such an unfortunate story. The development of this novel nucleotide-polymerase inhibitor for the treatment of chronic hepatitis C infection was terminated in August 2012 during the phase-II trial, after a 25-year old patient treated with this compound developed rapidly progressing heart failure (EF $<$ 10 %) and died (32). Cardiotoxicity was not observed during phase-I testing and was only thoroughly investigated after the death of the index case, since patients failed to present with any symptoms whilst having a reduced EF. The investigation concluded that 14 out of 34 treated patients experienced cardiac dysfunction (six patients had EF $<$ 30 % and eight had EF $30-50$ %).

1.2 Shortcomings of current therapeutic strategies for AMI and HF and avenues for further research

As discussed above, the current treatment strategy for AMI is to initiate myocardial reperfusion, whereas for HF, therapy aims to enhance cardiac efficiency and ameliorate side

effects or impaired cardiac function (such as fluid retention). However, these strategies, although they reduce symptoms and prolong life, are not curative.

Cardioprotection There is considerable interest in cardioprotective interventions to enhance the hearts resistance to cell death (33). Myocardial ischaemia rapidly leads to depression of contractile force, as a result of immediate biochemical perturbations inhibiting contractile proteins (34). These effects are initially reversible, but if the perfusion deficit is left uncorrected, may cause permanent damage to the myocyte sarcolemmal membrane. Indeed, loss of the mitochondrial membrane integrity compromises their ability to effectively execute oxidative metabolism, and the release of mitochondrial proteins can directly trigger programmed cell death pathways (35). In addition, when unable to generate energy through oxidative metabolism, the cells shift to anaerobic respiration, leading to acidification, which is counteracted by exchanging protons for sodium. This is in turn counteracted by the Na^+/Ca^{2+} exchanger, leading to the accumulation of intracellular calcium and eventually to calcium overload, and cell death, by activating apoptosis (33, 36).

Although reperfusion is essential for survival, reperfusion *per se* can cause further damage by rapid correction of intracellular pH, calcium overload and oxidative stress (37). Based on this understanding, ischaemic preconditioning and drugs limiting reperfusion damage were proposed for clinical application post-MI. Currently, no treatment strategy based on this technology has been successful and has reached clinical practice (33, 38–42).

Therapeutic angiogenesis Therapeutic angiogenesis, defined as strategies to induce therapeutic vascular growth in the ischaemic myocardium, have been proposed as a novel therapeutic strategy. Multiple angiogenic agents, such as vascular endothelial growth factor (VEGF) and fibroblast growth factor (FGF) have been clinically evaluated in recent years, but none have shown sufficient efficacy to be translated into routine

clinical practice (43–45). Multiple reasons have been proposed, including the difficulty of maintaining the local VEGF concentration at an effective level and the fact that additional signalling is likely to be required to have adequate and sustained vascular development (46).

Stem cell therapy and tissue engineering Alternatively, stem cell therapy and tissue engineering have been proposed as potential curative treatments, since these cells can give rise to new muscle. This technology is the main focus of this thesis, and will be discussed in greater detail in the next Sections.

1.3 Stem cell therapy for cardiovascular disease

The human heart, in contrast to various other organs like the liver, skin and gut, is unable to cope with severe tissue damage, although it contains a resident stem cell pool. Stem cells have been suggested as a tool to regenerate damaged contractile tissue and/or prevent adverse remodelling post-MI. Unfortunately, the stem cell hype has resulted in very few new treatment options so far, as clinical trials have failed to show any clinically relevant benefit.

1.3.1 The heart is not a post-mitotic organ

Whether or not the heart is a terminally differentiated organ or has a stem cell population has been a contentious issue, in strong contrast to various other tissues in which there is a substantial turnover of cells and the associated stem cell population and its regenerative potential were rapidly accepted. This in part stems from the observation that the heart is known to predominantly grow by hypertrophy (47), that primary tumours in the heart are very rare (48), and that the heart forms scar tissue in response to damage (49).

However, the notion that the heart is a terminally differentiated organ was challenged (50–52), and many groups tried to determine the cardiomyocyte (CM) turnover rate in the heart, and rates around 1 % per year were most commonly reported (53–56).

Bergmann *et al.* (55) determined CM turnover using the incorporation of carbon-14 (^{14}C) from nuclear bomb tests in genomic deoxyribonucleic acid (DNA). Atmospheric $^{14}CO_2$ is incorporated by plants through photosynthesis and digested by humans and animals. Hence, because the ^{14}C concentration in the human body mirrors the atmospheric concentration and because DNA is stable after cell division, it is possible to use the concentration of ^{14}C in DNA as a date mark for when a cell was born. Bergmann *et al.* (55) demonstrated that CM DNA synthesis continues throughout life at annual rates ranging from 0.5 to 2 %, but decreases with age. A follow-up study by Senyo *et al.* (53), using ^{15}N imaging mass spectrometry, reported a similar annual rate of about 0.76 % per year in the young adult mouse. Interestingly, they also observed an increases after myocardial injury in the border region, as was reported previously (52). Similarly to Bergmann *et al.* (55), the rate also declined with age. Moreover, Mollova *et al.* (56) also observed CM cytokinesis in human infants, which decreased with age and is absent in adults.

An annual rate of 1 % implies that less than 50 % of the CMs in the heart will be exchanged during the life span (55). This also means that CMs mainly rely on intracellular repair mechanisms to maintain structure and function, in contrast to organs such as the skin and gut, where cells are rapidly shedded and replaced.

There is considerable confusion with respect to where those few new CMs arise from. There are at least three different potential sources: (a) pre-existing CMs, (b) resident stem or progenitor cells, or (c) circulating stem or progenitor cells. Bergmann's study did not determine the origin of these newly derived CMs (55). In zebra fish, existing CMs were shown to contribute to regeneration post-myocardial injury (57). Similarly, the study by Senyo *et al.* (53) demonstrated that new CMs formed from pre-existing CMs

and that cardiac progenitors played an insignificant role in myocardial homeostasis in health and disease. In contrast, other studies identified resident stem cell populations with the capability to give rise to all lineages of the heart (58, 59).

Hence, since very few new CMs are generated post injury, the concept of supplying the heart with exogenous stem cells or with factors capable of inducing the resident cells to promote regeneration is currently investigated as a potential therapeutic strategy for AMI and HF.

1.3.2 Embryonic and adult stem cells

All stem cells share a set of characteristics: self-renewal and differentiation potential (potency) (60). Self-renewal implies that a given cell can give rise to progeny with identical properties. Stem cells can have different levels of potency, in order of reducing potency: totipotent, pluripotent, multipotent, oligopotent and unipotent. Totipotent or omnipotent stem cells can differentiate into embryonic and extra-embryonic cell types, and hence can give rise to all the cells in an organism. Pluripotent stem cells are derived from the latter, and can differentiated into all embryonic lineages. Multipotent stem cells have the capability to differentiate into a number of a closely related cell types, whereas oligopotent and unipotent stem cells can differentiate into a few types, or only one type, respectively (61).

Stem cells are identified and characterised based upon source or origin, morphology, function, cell surface markers, transcription factors and expressed proteins (62, 63). Two broad types of stem cells can be distinguished: embryonic and adult stem cells. Adult stem cells reside within organs and tissues in order to aid in maintenance and regeneration in case of wear and tear or disease, whereas embryonic stem cells are present during development to form an organism and all the tissues it comprises (61).

Both adult and embryonic stem cell (ES) based approaches have been suggested to be suitable to aid the heart in regeneration post-MI or HF and have been tested in animal

models and in the clinic, as discussed in the following Sections.

1.3.3 Bone-marrow derived cells

Historically, the first studies which tried to use stem cells for repairing damaged heart tissue involved using skeletal myoblasts or bone marrow (BM)-derived stem cells, because of availability and existing experience with BM transplantations.

The BM contains a huge variety of different cell types, including mesenchymal stem cells (MSCs), hematopoietic stem cells, and endothelial progenitor cells. Infusion or injection of BM cells was shown to regenerate myocardium *in vivo* and had beneficial effects to overall cardiac function (64, 65). In addition, bone marrow-derived mesenchymal stem cells (BM-MSCs) were shown to be able to differentiate *in vitro* to CMs (64–66). However, later studies called into question the cardiomyogenic potential of BM-derived cells (67, 68).

Clinical scientists across the world rapidly attempted to translate these promising findings, with little and variable success. A 2012 meta-analysis reported that transplantation with BM cells improved LV function, infarct size, and remodeling in patients with ischemic heart disease compared with standard therapy, and that these benefits persist long-term (69). However, a 2013 meta-analysis reported improved EF, but no change in infarct size (70). Moreover, discrepancies and misrepresentations are commonplace in these trials, which makes their results uninterpretable and as a result it is currently impossible to numerate the magnitude of the beneficial effect of BM treatment, if there is any (71, 72). The latest Cochrane review also concluded that there is currently insufficient evidence for a beneficial effect of cell therapy for AMI patients (73). Whereas for HF, a recent trial sequential analysis (TSA) report suggested that current randomised controlled trials administering autologous BM-derived cells to HF patients offer a reduction of the risk of mortality and hospitalisation for HF (74).

1.3.4 Skeletal myoblasts

CMs do not proliferate *in vitro* and can as a result not be harvested and expanded for subsequent transplantation. However, skeletal muscle is easily accessible and contains myoblasts that are able to proliferate and repair or replace damaged or old tissue, and are resistant to ischemia (75, 76). This observation led various groups to explore the feasibility of applying skeletal myoblasts for cardiac regeneration.

Myoblast transplantation showed improved cardiac function in animal studies (76). Milieu-dependent differentiation of myoblast satellite cells into cardiac-like muscle cells was observed in some studies (77), however this observation is heavily disputed by others (75). Nonetheless, this technology was soon translated into a first human patient (78). In this study, no arrhythmias were observed and a 9 % increase in EF (from 21 to 30 %) was recorded.

Encouraged by the beneficial effects of myoblast transplantation in both animal models and in pilot studies in humans, clinical trials were started in Europe and the US (79, 80). Although some patients developed ventricular arrhythmias, phase-I studies demonstrated safety and promised hope for heart failure patients. However, they failed to fulfil the promised results in phase-II clinical studies (81). Indeed, beneficial effects on left ventricular ejection fraction (LVEF) were only moderate and rarely clinically relevant (82). Since myoblasts do not differentiate to form CMs in significant numbers, and the transplanted cells failed to gain electromechanical coupling with the host tissue, interest in these cells diminished (83).

1.3.5 Embryonic and induced pluripotent stem cells

ES cells are typically derived from the inner cell mass of pre- or peri-implantation mammalian embryos. These cells can give rise to all three germ layers and thus can differentiate into all tissues. ES cells have considerable ethical issues as they are derived from

fertilised eggs. Additionally, care should be taken in clinical translation as ES cells are not autologous and may thus be rejected after transplantation, and these stem cells have the potential to form tumours. The induced pluripotent stem cell (iPS) is ES cell-like and can be derived from somatic cells by manipulating the gene expression profile to induce stemness (84), and can be an autologous sources of cells since they can be derived from the patient (85). Reprogramming to form iPS from somatic cells was originally accomplished by overexpression of pluripotency-related transcription factors: OCT4, SOX2, KLF4 and MYC, using a retroviral approach. Nowadays, significant improvements have made the process more efficient and made the use of integrating vectors obsolete (86).

Given their strong potential to differentiate, these cells have been suggested as an *in vitro* model for development & pathology, and as cell source for tissue engineering and cell therapy. Indeed, these cells have been successfully differentiated into beating CMs *in vitro* and have been shown to improve cardiac function *in vivo* in animal models (87).

There are very few clinical trials on using ES-derived therapies for regeneration. In 2015, Schwartz *et al.* (88) reported the first results from their study in using retinal pigment epithelial cells derived from ES cells in patients with macular degeneration or dystrophy, and concluded that the procedure is safe. However, the study was not powered to assess the clinical benefit. With respect to the heart, feasibility of using embryonic stem cell-derived cardiomyocytes (ES-CMs) on a clinical scale was recently demonstrated in a non-human primate model (89), to make way towards clinical translation.

1.3.6 Endogenous cardiac stem cells

More recently, multiple ways to isolate or identify endogenous cardiac stem cells (CSCs) have been reported, *inter alia* c-kit (58), Sca-1 (90), ALDH (91), side population (92), epicardial (93, 94) and cardiospheres-derived cells (95), and the longstanding theory that the heart is a terminally differentiated organ was abandoned (55). Multiple endogenous stem cell isolation protocols have been published, but it remains unclear how these pop-

ulations differ and how they relate to the endogenous cells in the cardiac stem cell niche.

C-kit stem cells, which have probably been studied the most, have been shown to give rise to CM *in vitro* and regenerate hearts *in vivo* (59). In 2011, the Anversa group published the promising results of the phase-I Stem Cell Infusion in Patients with Ischemic cardiOmyopathy (SCIPIO) trial (96)[1]. However, apart from fraud allegations raised against Anversa, new evidence also suggests that c-kit cells may not be cardiac progenitor cells (98, 99).

In our lab, we have established protocols to isolate and expand cardiosphere-derived stem cells (CDCs) from cardiac biopsies, which allows the production of patient-specific stem cells without the risk of rejection (95). CDCs are typically isolated by waiting for cells to appear from cardiac tissue fragments (usually atria and apex) attached to fibronectin coated dishes. The population of cells at this stage is a mixture of fibroblasts and progenitors cells, with phase-bright cells growing on top of the fibroblasts. These cells are subsequently collected and grown on poly-D-lysine coated plates to form spheres (95, 100). CDCs are a mixed population of cells and contain cells expressing markers such as c-kit, CD90, CD105, and discoidin domain-containing receptor-2 (DDR2) (101, 102).

CDCs can be differentiated into CMs and endothelial cells *in vitro* (103, 104), and CDCs have been shown to have beneficial effects after transplantation in experimental infarction models (101, 105, 106). Moreover, these cells underwent phase-I testing (CADUCEUS trial) on 17 patients. The initial results demonstrated safety, and a reduction in scarring after myocardial infarction, without any improvement of the patients' ejection fraction (102, 107). Phase-II testing is required to further assess clinical benefit.

[1] Prof Piero Anversa is currently under investigation for scientific misconduct and The Lancet published an expression of concern with respect to the integrity of the clinical trial (97).

1.4 Cardiac differentiation of stem cells

A CM has an unique phenotype, it distinguishes itself morphologically from its progenitors by its internal filamentous structure and its contractility. CMs also have a typical metabolic profile and calcium handling system. The suitability of stem cell derived-CMs for regenerative medicine and *in vitro* drug testing depends on appropriate heart development and maturation gene expression, leading to the generation of *true* CMs. Essential characteristics comprise *inter alia* the formation of sarcomeric filaments, expression of relevant ion transport channels and transporters, excitation-contraction coupling, and oxidative metabolism.

1.4.1 Differentiation

After fertilisation, the single layer blastula reorganises *in vivo* into a trilaminar structure, by a process named gastrulation (108). The three layers formed are called: the endoderm, the ectoderm, and the mesoderm. Each of these layers will further pattern and organise itself to form the different organs and tissues of the body. The ectoderm will form multiple tissues, including the epidermis and the nervous system. The mesoderm gives rise to muscle, blood and blood vessels, bone, and connective tissue. The endoderm forms the epithelium of the digestive system and respiratory system, and organs associated with the digestive system, such as the liver and pancreas. The heart is derived from the mesoderm and is the first organ to form and function during vertebrate development (109).

The embryonic development can be mimicked *in vitro* in order to differentiate pluripotent stem cells to beating CMs. Four main steps are essential to gain CMs from pluripotent stem cells: (a) mesoderm generation, (b) the mesoderm patterning towards anterior/cardiogenic mesoderm, (c) formation of cardiac mesoderm, and (d) maturation of early CMs (110). It is well established that mesoderm can be induced during the car-

diac differentiation from pluripotent stem cells using Wnt (111), bone morphogenetic protein (BMP) (112), and transforming growth factor (TGF) β-family member Nodal or Activin A (113). The next steps are less well understood, but Nodal and Wnt inhibition have been found to be effective for the formation of cardiac mesoderm (114). The last step is the acquisition of beating CMs, a process of which the exact mechanism has not been established yet and typically occurs spontaneously *in vitro*. The adult stem cells have already obtained an intermediate differentiated profile, and hence do not have to undergo the same four steps. However, they rarely differentiate to beating CM *in vitro* (115).

1.4.2 Gene and protein expression

Upon differentiation the gene and protein expression profile of the cells undergoes dramatic changes in order to accommodate for the newly obtained phenotype. Xu *et al.* (116) compared ES, embryoid body (EB) cultures, enriched differentiated CMs derived from ES, fetal and adult heart using gene chip analysis (116) and concluded that although purified CMs displayed similar overall gene expression similarities with heart tissue, they expressed in some aspects a different expression pattern. Four classes of genes are differentially expressed in CMs and heart, compared to EB and ES cells: sarcomere, ion transport, metabolism and heart development genes. In particular, the myosin genes have been used to demonstrate the cardiac phenotype. Interestingly, these authors also identified a set of genes transiently upregulated in fetal heart, and genes lowly expressed in ES-CMs and higher in fetal and adult heart: MYL2, MYH7, MYL3, and MYH11. The latter are particularly interesting since they might be related to CMs maturation.

1.4.3 Metabolism

Cells are equipped with various pathways to metabolise a range of compounds for energy (Figure 1.2). These pathways are crucial to life and intensely regulated.

Glycolysis is the metabolic pathway that breaks down glucose into pyruvate by a sequence of ten cytosolic enzyme-catalyzed reactions which do not require the presence of oxygen. Energy is release by this reaction in the form of adenosine-5'-triphosphate (ATP) and reduced nicotinamide adenine dinucleotide (NADH). Pyruvate can be oxidised in the tricarboxylic acid (TCA) cycle in aerobic conditions, after conversion into acetyl-CoA by the pyruvate dehydrogenase complex (PDC), or can be reduced to lactate in anaerobic conditions by lactate dehydrogenase (LDH), which also regenerates nicotinamide adenine dinucleotide (NAD+).

Fatty acids are metabolised by β-oxidation which splits the carbon chains of the fatty acid into acetyl-CoA, which can be oxidised further in the TCA cycle.

The citric acid cycle, TCA cycle, or Krebs cycle is a cyclic series of oxygen-dependent enzyme-catalyzed chemical reactions to generate energy through the oxidation of acetyl-CoA. Acetyl-CoA can be derived from degradation of either carbohydrates, fats or proteins. The TCA cycle produces metabolic intermediates (which can be utilised in anabolic reactions) and reduced proton carriers, which are subsequently used in the respiratory chain to form ATP.

The heart is a metabolic omnivore which can use a variety of substrates to generate energy for contraction and switches substrates depending on availability and physiological conditions (117, 118). The healthy heart uses exogenous free fatty acids for about 70 % of its ATP production, whereas glucose oxidation results only in about 20 % of the total ATP production. About 70 % of the ATP produced is used for contractile function (118, 119).

In contrast, stem cells and proliferating cells *in vitro* predominantly metabolise glu-

cose and glutamine via aerobic glycolysis and the glutaminolytic pathway respectively, regardless of the availability of oxygen (120, 121). The metabolism of differentiated stem cells has not been studied in detail. However, there is some evidence that mitochondrial oxidative metabolism is required for cardiac differentiation of murine ES cells (122). Interestingly, the ability of CMs to utilise lactate as sole energy source has been utilised to purify differentiated populations (123, 124).

1.4.4 Contraction

CMs are uniquely characterised by their contractile apparatus and excitation-contraction coupling, which is distinct from that of a skeletal muscle or smooth muscle cell (125). Upon electrical stimulation from a neighbouring cell, through gap junctions, the cardiac cycle is initiated by depolarising the membrane (Figure 1.3). Voltage-gated fast Na^+ channels are opened and Na^+ enters the cell, leading to the reversal of the membrane potential. The fast Na^+ channels are only open for a few thousands of a second, and then the action potential is kept at a plateau phase by influx of Ca^{2+} through L-type calcium channels and efflux of K^+. Ca^{2+} entry then triggers the release of more Ca^{2+} from the sarcoplasmic reticulum (SR) through the ryanodine channels, by a mechanism called Ca^{2+}-induced Ca^{2+} release (CICR). The calcium-binding protein calsequestrin-2 (CASQ2) enables the SR to maintain very high calcium concentrations. The large cytosolic concentration of calcium initiates and maintains contraction. Next, the L-type Ca^{2+} channels close, whilst the K^+ channels remain open leading to rapid repolarisation. Calcium reuptake to the SR and extracellular space by the Na^+/Ca^{2+} exchanger and the Na^+/K^+ pump bring back intracellular ion homeostasis.

1.4.5 (Im)Maturity of stem cell derived cardiomyocytes

It is well established that induced pluripotent stem cell-derived cardiomyocytes (iPS-CMs) have an immature phenotype resembling embryonic or fetal CMs (126, 127). In-

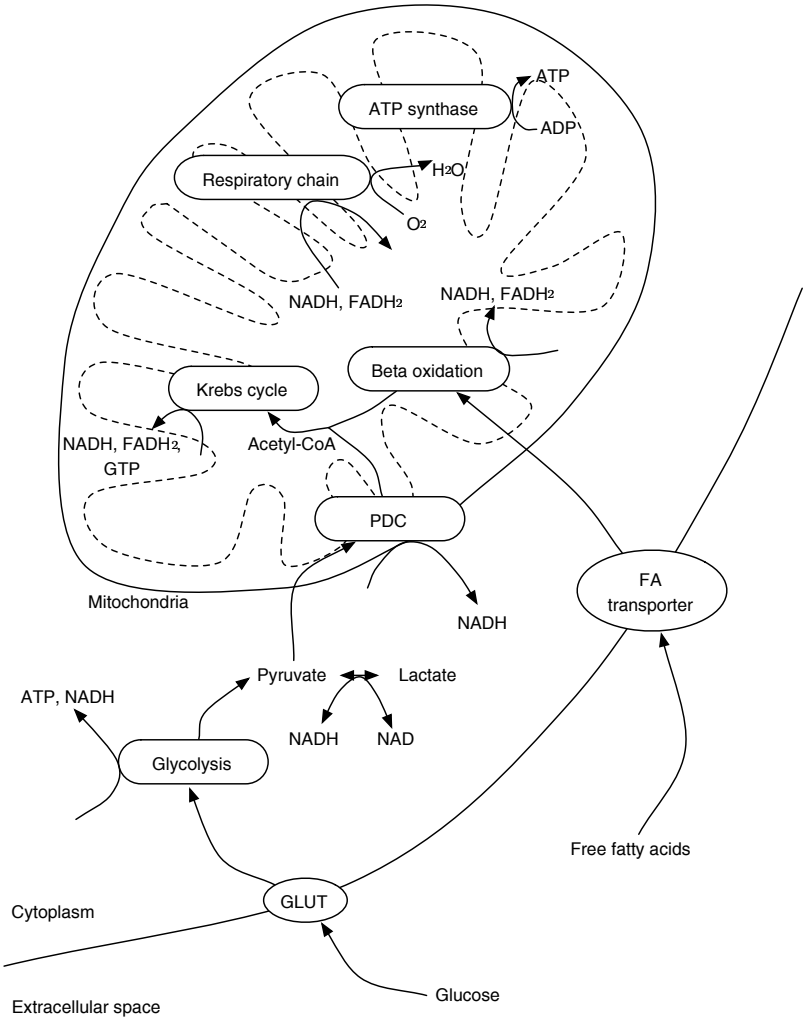


Figure 1.2: Cell metabolism In order to provide for their energy requirements, cells can digest a multitude of fuel sources, including sugars and fats. Metabolites (glucose and fatty acids) enter the cell via specialised transporters (glucose transporter (GLUT) and fatty acid transporters). Glucose is converted into pyruvate by glycolysis, and then into acetyl-coA by the pyruvate dehydrogenase complex (PDC) which enters the Krebs cycle in the mitochondria. Fatty acids are converted into acetyl-coA by β-oxidation, before feeding into the Krebs cycle. The transfer of electrons from NADH to oxygen allows the generation of a proton gradient that drives ATP synthase for the generation of ATP. In the absence of oxidative metabolism, NADH is regenerated by the generation of lactate. Adapted from Neubauer (118).

deed, the CMs are generally small, round and mono-nucleated cells, whereas adult CMs are large cylindrical cells with two or more nuclei. Moreover, the stem cell derived CMs do not have t-tubules (128), hence calcium primarily enters the cell through the sar-

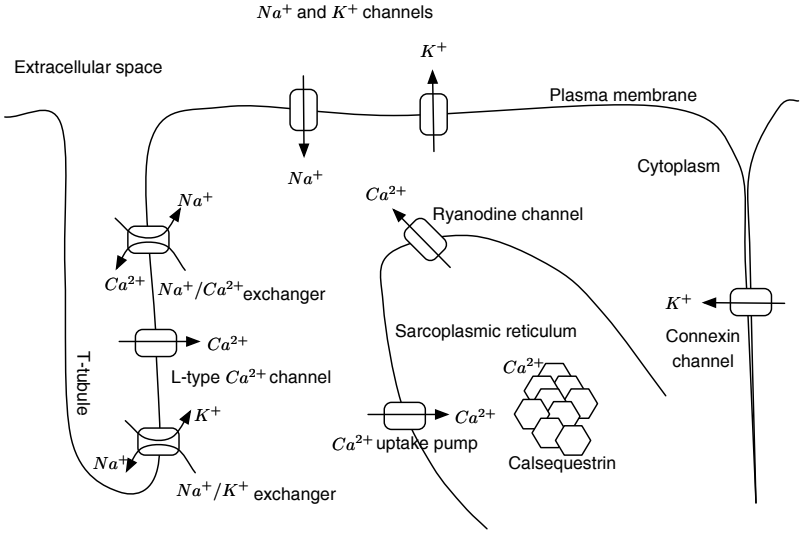


Figure 1.3: Protein complexes involved in cardiac excitation-contraction coupling Upon membrane depolarisation by an electrical signal originating from a neighboring cell, voltage gated Na^+ are opened leading to reversal of the membrane potential. The fast Na^+ channels rapidly close again and the action potential is kept at a plateau phase by influx of Ca^{2+} through L-type calcium channels and efflux of K^+. Ca^{2+} entry then triggers the release of more Ca^{2+} from the SR through the ryanodine channels (CICR). The cytosolic concentration of calcium initiates and maintains contraction. Then the membrane repolarises as the L-type Ca^{2+} channels close, whilst the K^+ channels remain open. The calcium reuptake/extrusion and the Na^+/K^+ pump restore intracellular ion homeostasis and prepare the cell for the next cycle. Adapted from Knollmann & Roden (125).

colemma instead of being released from the SR causing slower excitation-contraction coupling. There is some indication that the CMs undergo some level of maturation by prolonged culture (> 1 month) (129).

Metabolism is regulated by both transcription regulators and post-translational modifications or interactions with activators or inhibitors (130). An enzyme may be activated by the binding of an activator, which often is the enzyme substrate itself, according to the classic allosteric control mechanism. Also, post-translational modifications such as proteolytic cleavage, phosphorylation, glycosylation, may shift the activity or protein stability. These first two mechanisms give high frequency regulatory ability to the cells. Alternatively, the level of expression of certain enzymes or metabolic factors may un-

dergo transcriptional regulation, which leads to longer time scale effects.

Stem cells generate most of their energy from glycolysis, whereas the heart uses fat oxidation for most of its energy requirements (120, 121). Although, post-translational enzymatic regulation may upregulate the oxidative behaviour of cells, it is well understood that the cells would need to undergo significant mitochondrial biogenesis to gain a comparable level of oxidation as that of the heart.

1.5 Hallmarks of cardiac stem cell therapy

Although stem cell therapy has been shown to have a beneficial effect in animal models, the underlying mechanism is highly controversial and poorly understood and may underpin the difficulty in translating this technology to the clinic. In general, three non-mutually exclusive mechanism may be involved: direct differentiation to new contractile muscle tissue, paracrine signalling, or immune modulation. It is currently unknown to what extend each of these potential mechanisms contributes to the beneficial effects seen *in vivo*. However, it is reasonable to expect that the extent to which these different mechanisms contribute may depend on the setting (acute vs. chronic injury) and the cell type (131).

1.5.1 Remuscularisation

Given the significant loss of contractile tissue and the generation of scar tissue, *de novo* remuscularisation is considered the silver bullet for HF treatment. Multiple studies have presented evidence in favour of exogenous or endogenous stem cell contribution to the generation of new CMs (59, 101, 132). However, in most cases only very few *de novo* CMs can be identified. In addition, cell retention post injection or infusion is typically very low (133, 134), suggesting that direct remuscularisation likely only has a small contribution to any beneficial effect seen.

1.5.2 Paracrine signalling

Although the transplanted stem cells may form new CMs by transdifferentiation, cell fusion or cardiac differentiation, these events appear too infrequent to account for the improvements seen. Chimenti *et al.* (135) quantified the relative contribution of paracrine signalling and direct regeneration to improved myocardial function in the severe combined immune deficiency (SCID) mouse model after injection of human CDCs, by quantifying the proportion of cells that were of human origin versus the overall improvement in cardiac parameters. The study revealed that paracrine interactions significantly outweighed direct regeneration.

The mixture of paracrine signalling molecules expressed by stem cells, depends hugely on the type of stem cell, and its effects may include preventing death, promoting neovascularisation, preventing adverse remodelling, maintaining cardiac contractility and promoting cardiac regeneration (136).

MSCs have been shown to secrete anti-apoptotic factors and to modulate the immunoinflammatory response post-MI (137). The phosphoinositide 3-kinase (PI3K)-Akt pathway plays a central role in pro-survival signalling (138). Insulin-like growth factor-1 (IGF-1) is a potent activator of the Akt pathway leading to survival of CMs and is secreted by MSCs and endogenous CSCs (139). Du *et al.* (140) reported that transplantation of MSCs inhibited the activity of NF-κB, attenuated the production of pro-inflammatory proteins including tumor necrosis factor-α and interleukin-6 (IL-6), and increased the expression of the anti-inflammatory protein interleukin-10 (IL-10) in peri-infarct myocardium. Furthermore, Ohnishi *et al.* (141) demonstrated that MSC-conditioned medium upregulated the expression of anti-proliferation genes and downregulated the expression of collagen I and III in cardiac fibroblasts.

Paracrine induction of neovascularisation involves mediators such as VEGF and basic fibroblast growth factor (bFGF), which induce endothelial cell (EC) and vascular smooth

muscle cell (VSMC) migration and proliferation, are secreted by a variety of cells, including CDCs and MSCs (136, 142, 143).

Exogenous stem cell transplantation may activate resident CSCs and stimulate CM replication via paracrine signalling, to induce regeneration. For example, Linke *et al.* (144) injected hepatocyte growth factor (HGF) and IGF-1 intramyocardially to stimulate resident CSCs, resulting in the formation of new myocytes and bloodvessels. Similarly, Yoon *et al.* (145) reported that a population of BM-derived stem cells can induce endogenous and exogenous cardiomyogenesis. The cytokine stromal cell-derived factor-1 (SDF-1) can promote cell survival, endogenous stem cell recruitment, and vasculogenesis (146–148). However, a recent phase-II trial using a single dose of SDF-1 gene therapy failed to meet its primary end point, although it did show beneficial effects in one of the patient subgroups (149).

1.5.3 The dying stem cell hypothesis

Thum *et al.* (150) hypothesized that the beneficial effect of stem cell transplantation can be explained by the modulation of local immune reactions in response to apoptosis of the infused cells. Dying cells release danger signals, which may trigger innate or adaptive immune responses. Even though there is a considerable amount of cell death occurring in the infarcted heart, the mode of cell death differs between the native heart cells and the injected stem cells. Indeed, necrotic cell death is the major contributor to cell death in the infarcted heart (151, 152), and endogenous ligands released by stressed or necrotic cells can activate toll-like receptor signaling, resulting in inflammation (153). While necrotic cells stimulate inflammation, apoptotic cells inhibit inflammation (154, 155).

Stressed peripheral blood mononuclear cells (PBMCs) have been shown to enhance angiogenesis and wound healing resulting in tissue repair through paracrine signalling pathways (156, 157). In fact, large numbers of PBMCs can easily be obtained, in strong

contrast with most stem cells which usually require long culture periods to acquire a therapeutic dose of cells. Burt *et al.* (158) demonstrated that irradiated, and mitotically inactivated, ES cells were capable of improving myocardial function, similarly to non irradiated ES cells, after injection into the infarcted heart. Histological examination revealed insignificant levels of cell engraftment and no improvement of cardiac function was seen after injection of conditioned medium, suggesting that the beneficial effect observed is at least dependent on the transitory presence of the cells. Interestingly, injection of mouse embryonic fibroblast (MEF) cells did not ameliorate cardiac function post-MI, suggesting that the type of dying cell might be relevant to the beneficial effect observed.

1.6 Biomaterials and tissue engineering

Tissue engineering was defined by McIntire (159) as:

> *The application of principles and methods of engineering and life sciences to obtain a fundamental understanding of structure-function relationships in novel and pathological mammalian tissues and the development of biological substitutes to restore, maintain or improve tissue function.*

Hence, in many cases, tissue engineering involves the combination of both cells and scaffolding materials to form new, engineered tissue (160). The hope is that tissue engineering would alleviate what is believed to be the main failure of standard stem cell injection protocols: low cell retention and engraftment. Alternatively, cell-free tissue engineered constructs can be utilised to provide localised drug delivery. Moreover, scaffold material may also give mechanical strength to the developing or recovering tissue.

1.6.1 Aims

Developments in tissue engineering have two main aims, either for direct medical applications, or as *in vitro* model systems.

1.6.1.1 Organs and tissues for transplant

Organs and tissues in the body have different levels of complexity, which affects their ease of manufacture. Flat organ structure, such as the skin, are considered the least complex, and most progress has been made in this area of research (161). Tubular organs, such as the vagina, have also been engineered and have been tested in patients (162, 163). Hollow organs, such as the bladder, have also been thoroughly investigated and tested in the clinic (164). However, even though these organs are structurally quite simple, and for some the initial trials were reported a decade ago, the tissue engineering of bladders and vaginas has not entered routine clinical practice. Solid organs, including kidney, lung, heart, are considered the most complex, and no large animal or clinical trials have been performed with these.

In many cases, whole organ replacement may not be required and a patch alone might offer symptomatic relief. Multiple types of such constructs can be distinguished, depending on their potential for scalability and initial *ex vivo* culture period. Initially there has been considerable interest into tissue engineered constructs with long *in vitro* cell preparation period, before transplantation (165). However, with the idea of making regulatory approval and translation to the clinic easier, the focus has somewhat shifted towards *in situ* tissue engineering of cell-free materials with the required signalling clues to direct regeneration *in vivo* (166, 167).

1.6.1.2 3D *in vitro* model systems

Cells behave differently when cultured in a monolayer rather than in 3D, which suggests that disease modelling and drug testing protocols will also benefit from tissue engineering strategies.

1.6.2 Biomaterials

Materials play an important role in surgery, and a huge variety of materials has been developed with different physical features and requirements depending on the application, ranging from dissolving sutures, to metal pins for orthopaedic surgery and artificial skin for burns victims. Materials can be segregated into artificial or biological, depending on their origin or as integrating or inert depending on their behaviour in the body. Whereas historically the main developmental interest was to create inert materials that degrade or integrate with the body, nowadays researchers are actively researching materials with the potential to integrate and interact with the body to drive regenerative processes.

Many types of materials are currently being investigated. Successful medical materials need to (a) support functional replacement, (b) be inert to negative host responses, (c) have compatible mechanical properties and (d) degrade within a reasonable time span into non-toxic waste products (168). These material properties are not static and change during the lifespan of the implanted material (169, 170). Scaffolds can be formed by layering or mixing multiple different material compositions, which may be utilised to induce different cell responses (171, 172).

1.6.2.1 The ECM

Cells in organs and tissue are surrounded by extracellular matrix (ECM), the naturally occurring scaffold material (173). ECM is present in all tissues and is deposited and

maintained by the resident cells. The ECM is more than a structural component and also contributes to cell signalling. ECM is essential for life, as demonstrated by the wide range of tissue defects or embryonic lethality caused by mutations in ECM related genes (174). The structure and composition of the ECM varies hugely depending on the tissue type, developmental stage, disease state and age. Around 300 proteins have been identified to encode for ECM components, such as collagen, laminin, fibronectin, and glycoamino glycans (GAGs) like chondroitin-sulphate and hyaluronic acid. Two main types of ECM can be distinguished: interstitial connective tissue matrix and the basement membrane. The former surrounds cells and provides structural support in all tissues, whereas the latter is the ECM that separates the epithelium, mesothelium and endothelium from the underlying connective tissue.

1.6.2.2 Biological materials

Cadaver tissue can be used as the starting material for the production of biological materials. However, it is paramount that cellular material is absent from the produced material as this may cause an inflammatory response and rejection *in vivo* (175).

Macromolecular proteins such as collagen, elastin, fibrin, fibronectin and GAGs can be extracted from tissue and are sold commercially. These purified ECM proteins can subsequently be used for the production of scaffolds or hydrogels (176–178).

Secondly, scaffolds can be obtained by decellularisation. Decellularisation is a process to generate biomaterials in which the ECM is isolated from the cellular material by sequential application of physical, chemical or biochemical procedures. Initial attempts for decellularisation go back to the 1950's (179–181). The process aims to maintain gross anatomy and structure of the organ or tissue post decellularisation. There is considerable interest in decellularisation since it has the potential to give rise to appropriately structured scaffolds for organ replacement.

Decellularised tissues have entered mainstream clinical practice as surgical meshes

for soft tissue repair, or for heart valve replacement (182). In terms of soft tissue repair, the rational is to provide the tissue with a scaffold material that supports tissue regeneration by allowing rapid revascularisation and cell population. The scaffold material is ultimately integrated in and replaced by host tissue. Human dermis derived products, such as AlloDerm®, have been used successfully in multiple surgical procedures, such as *inter alia* abdominal wall, breast, and head and neck reconstruction (183).

Heart valves can lose proper function as a result of old age, infection or AMI/HF and may require replacement by either synthetic or (semi-)biological prosthetic analog. Mechanical valves require anti-coagulation therapy. Xenogeneic biological values require fixation (glutaraldehyde) to decrease the immune response, are non-viable and eventually calcify. There is currently a considerable interest in developing tissue engineered heart valves, derived from decellularised vales, that are less likely to calcify, have the possibility to harbour cells and to remodel and grow (184–186). This would be very promising, especially in the area of paediatric heart valve replacement, where otherwise repeated surgery is required to accommodate for the growth of the patient (187).

The tissue engineering of solid organs has attracted much interest in preclinical research, however it has not be translated to the clinics because of lack of efficacy and complexity. Transplantation of cell seeded decellularised tracheas has been attempted in patients, with initial beneficial results reported (188). However, the outcome and efficacy is currently unknown and questioned, since one of the chief researchers in this field is under investigation for scientific fraud.

1.6.2.3 (Semi-)synthetic materials

Material properties are more controllable and modifiable in synthetic polymers. The most commonly used synthetic biomaterials for tissue engineering are: polylactic acid (PLA), polyglycolic acid (PGA), and poly(lactic-co-glycolic acid) (PLGA) copolymers (189, 190).

1.6.2.4 Constructing 3D scaffolds from materials

Cell sheeting Cell sheeting is a method which forms scaffolds with cells in their own secreted ECM, by detaching the whole monolayers from the tissue culture dishes without enzymatic treatment, using covalently attached poly(N-iso-propylacrylamide) (PIPAAm) to regular polystyrene tissue culture dishes (191). Temperature reduction from 37 to 32°C, causes the polymer, which was initially hydrophobic, to become hydrophilic and hydrated. As a result, the whole monolayer detaches from the tissue culture dish (192). These monolayers can subsequently be stacked to generate thicker constructs (193, 194).

Hydrogels In the hydrogel approach, cells are encapsulated in the scaffold during synthesis of the scaffold. The main advantages are that this method allows homogenous seeding. Gels can be transplanted with or without *in vitro* pre-culture (195–197). When cells are mixed with gelating scaffold material and injected directly *in vivo*, gels will set in the provided cavity and limit cell wash-out (198).

Porous scaffolds Porous scaffolds can be generated by feeze-drying suspensions poured in moulds (199). This type of manufacturing gives flexibility in shape and composition, but limits cell seeding efficacy. Indeed, most of the seeded cell suspension will initially cover the surface of the scaffold (in contrast to hydrogel scaffolds where gel and cells can be mixed before gelation, leading to homogenous seeding throughout the scaffold). The degree to which cells will be able to colonise deeper layers of solid porous scaffolds depends *inter alia* on the pore size and interconnectivity of the pores within the scaffold, which can be manipulated by varying manufacturing conditions such as solvent, freezing rates, and freeze-dry conditions (200, 201).

Fibrous scaffolds Fibrous scaffolds can be manufactured from a large variety of materials, for example by electrospinning. This technique gives control over the nano-scale

structure and mechanical properties of the scaffold, but again limits the seeding efficiency (189, 202).

1.6.3 Tissue engineering approaches for stimulating regeneration or organ replacement

Most progress has been made in devising cell-free tissue engineering methods, giving their easier design and less restrictive U. S. Food and Drug Administration (FDA) approval guidelines. Material based strategies to give the failing ventricle additional support have been around for decades. For example, Dor *et al.* (203) proposed to excise the akinetic portion of the myocardial wall, restore normal LV geometry and to close the ventricle with a polyethylene terephthalate (PET) patch (204, 205). Additionally, LV restraining devices (or Cardiac Support Devices) have been applied to prevent further dilation. These devices are polymer meshes which can be wrapped around the heart to offer end-diastolic support and limit further dilatation by reducing wall stress (206–208).

Cell-free constructs often only have one mode of action: mechanical support. Cells can be utilised to deliver sustainable therapy, by integrating in the host tissue and secreting soluble factors. This is particularly interesting since low cell retention is believed to be one of the reasons for the limited clinical benefit of stem cell therapy for CVD. Depending on the cells or growth factors within the scaffold, the idea is either to support the injured tissue or the replace lost muscle tissue.

Growth factors can be included into scaffolds to induced a localised response. Lin *et al.* (209) produced self-assembling peptide nanofibers loaded with VEGF, a potent pro-angiogenic factor. Injection of the loaded nanofibers post-MI was superior to nanofibers and VEGF alone. Wang *et al.* (190) produced PLGA scaffolds loaded with bFGF, and demonstrated enhanced myocardial neovascularisation and perfusion in a mini-swine myocardial infarction model. bFGF was chosen because of its mitogenic properties towards fibroblasts, smooth muscle cells, and vascular endothelial cells, and be-

cause bFGF is capable of inhibiting apoptosis and protecting acute ischaemic myocardium (210). An epicardial scaffold loaded with Fstl1, an epicardial cardiomyogenic factor, was shown to stimulate cell cycle re-entry and devision of CM, leading to improved cardiac function post-MI (211).

The first clinical trial which aims to transplant a stem cell loaded fibrin patch containing human ES-derived cardiac-committed $CD15^+$ $ISL\text{-}1^+$ progenitors onto the epicardium of the infarcted area, has recently started [2].

1.6.4 Tissue engineering approaches for disease modelling

Traditionally, much of the cardiac physiology was described using the *Langendorff* perfused heart model established in 1898 (212). In this method, cadaveric organs are isolated and blood or synthetic buffers are perfused into the heart through the ascending aorta (retrograde flow), which closes the leaflets of the aortic valve and hence the perfusate enters the coronary arteries at the aortic root, providing the heart with the necessary nutrients and oxygen, and eventually drains into the right atrium via the coronary sinus. After more than hundred years, this method is still actively applied to study whole heart physiology, as it allows the quantification of a wide range of parameters, such as *inter alia* heart rate, contractile function, coronary vascular function, cardiac metabolism (oxygen consumption and substrate metabolism) and electrical activity.

However, with the establishment of cell lines, and the expense of animal experiments, cellular models of cardiac biochemistry are pursued. As human or animal derived CMs cannot be maintained in culture for long, there are no satisfactory *in vitro* models available to test for drug toxicity or to study cardiac disease. In fact, for large cardiac drug discovery and toxicity screenings, immortalised cell lines overexpressing single ion channels are typically used (213). The major disadvantage of the cell lines is that these usually focus on a single channel rather than offering an holistic approach,

[2] `http://www.clinicaltrials.gov`, ID: NCT02057900

whereas for the isolated organ model the limitations are the animal origin and physiology (mouse versus man).

There is considerable interest in stem cell technology and tissue engineering strategies for disease modeling. iPS-CMs have been suggested as a novel diagnostic tool for cardiac toxicity investigations in drug discovery, since they offer the potential to generate large quantities of human CMs. Hitherto in most iPS-based cardiac disease models, cell-autonomous defects, such as changes in electric properties or calcium cycling, were investigated. However, many clinically relevant cardiac diseases, including developmental defects, MI and HF, cannot be sufficiently explained at the single-cell level (214). In addition, iPS-CMs have a very immature phenotype, which makes them currently a poor model for single-cell CM physiology.

3D constructs are believed to be phenotypically superior to single cell or monolayer culture for disease modeling. Most progress has been made in microfabrication techniques for disease modeling. Microfluidics and organ-on-chip technology allow the development and maintenance of 3D-organoids in defined structures, are scalable to high throughput configurations and are compatible with real time data gathering using microsensors and life cell imaging (215). This technology has been successfully applied for a variety of model systems, including heart and lung (216–219). Alternatively, the engineered heart tissue (EHT) model pioneered by Thomas Eschenhagen and Wolfram-Hubertus Zimmermann is currently arguably one of the furthest developed 3D *in vitro* model of the heart (220, 221). These EHTs are generated by casting cell loaded collagen type I/Matrigel®) gel solution in moulds of different shape and size, and these constructs display spontaneous contractile activity within days and have the potential of studying the effect of drugs on contraction frequency and force.

1.6.5 Bioreactors and biomimetic stimulation

Cells are typically cultivated in flasks or dishes in CO_2-incubators, which provide the cells with optimal temperature, humidity and pH for growth. However, since oxygen and nutrient diffusion is restricted these incubators are not suitable for culturing thicker scaffolds (222). Bioreactors are specially designed incubators which promote delivery of metabolites and oxygen and may also provide the growing tissue with biomimetic stimuli, such as electrical and mechanical stimulation, shear stress, to steer the differentiation process.

1.6.5.1 Mass transfer

Compound concentrations (substrates, growth factors, waste products, oxygen and carbon dioxide) are non-uniform and non-stationary during tissue culture in a bioreactor (222). Two mass transfer phenomena can be distinguished: transfer by molecular diffusion or convection. In a quiescent fluid, only diffusion occurs, whereas in a moving fluid both mass transfer by convection and diffusion occur. Diffusion is also crucial for mass transfer across phase boundaries as fluid velocity near the phase interphase is decreased.

In the absence of perfusion, tissue growth is limited to about to 200 µm due to limited oxygen diffusion and washout of waste products (222). Hence, for the culture of large tissue engineered constructs with high cell densities, bioreactor systems are equipped with a stirring mechanism or perfusion to enable convective mass transfer.

1.6.5.2 Biomimetic stimulation

Two types of biomimetic stimulation are typically considered in the field of cardiac tissue engineering: mechanical and electrical stimulation.

Mechanical stimulation Cells respond to mechanical stimuli (pressure, flow, stretching and shear) by amongst others their cytoskeleton and mechanosensitive channels (223). Multiple ways to induce mechanical stimulation have been devised (224).

Stretching has been shown to play a beneficial role in tissue engineering of muscle tissues by upregulating the expression of myogenic factors (225–227). Zimmermann *et al.* (195) seeded neonatal rat CMs in collagen/matrigel and subjected the construct to cyclic mechanical strain. These scaffolds beat *in vitro*, and upon engraftment onto infarcted rat hearts, LV function was improved. Egusa *et al.* (225) demonstrated that cell alignment parallel to the strain vector resulted in the upregulation of various skeletal myogenic markers in mouse BM-MSCs. In cardiac progenitor cells (CPCs), Kurazumi *et al.* (227) showed that mechanical stretching lowered c-kit levels, but elevated troponin-I and smooth muscle actin (226, 227). Taken together, mechanical stimulation limits proliferation and stemness, but enhances differentiation.

Shear stress has been shown to contribute to induced expression of endothelial cell specific surface markers and tube formation in shear stress treated cells (228).

Electrical Stimulation Electricity plays indisputable roles in the human body, during development, repair, pathological and normal physiology. Ion gradients across cell membranes give rise to the membrane potential. Many cells together parallel their potentials, which gives rise to the trans-epithelial potential (TEP), which is around $15-65$ mV (229). This TEP plays a major role in skin and wound healing, where skin disruption results in the formation of an electrical field (230). This in turn affects cell orientation, migration and division (231). In the heart, electricity initiates and synchronises the contractile activity. Indeed, the heart is equipped with a conductive system comprising cardiac muscle cells and conducting fibers with the purpose of initiating and conducting impulses rapidly through the heart. The primary aim is to initiate the cardiac cycle and coordinate the contractions of cardiac chambers (first both atria contract together, then

the ventricles).

Different types of electrical fields are used for different applications. Direct current (DC) systems generate a uniform continuous electrical field. This configuration is amongst others used to align cells, induce migration or differentiation (232). Alternatively, alternating current (AC) systems provide bidirectional electrical fields, and are frequently generated using direct contact between metal electrode and the medium or tissue, or by capacitive or inductive coupling. AC setups are typically used for stimulating cardiac and skeletal muscle.

Electrical stimulation has been shown to maintain contractile activity of CMs *in vitro* using carbon rod electrodes (233–235). Radisic *et al.* (236) demonstrated that electrical stimulation during construct culture resulted in enhanced differentiation, this effect was attributed to gap junction formation and cytoskeleton rearrangements (197, 236).

Integrated approach Although individual stimuli have been shown to have beneficial effects, tissue engineering could potentially benefit more from combining multiple stimuli together. Feng *et al.* (237) developed an electro-tensile bioreactor which synchronises electrical stimulation with extra-mechanical contraction. Unfortunately, these authors did not report any biochemical data. Ott *et al.* (238) decellularised whole isolated rat hearts and recellularised the scaffold with endothelial cells and neonatal CMs in a bioreactor system under biomimetic conditions. These recellularised hearts generated about 2% of the pump function of an adult rat heart.

In summary, for cardiac tissue engineering, multiple forms of biomimetic stimulations may be used to induce further maturation of the seeded cells.

1.7 Central hypothesis and aims of this thesis

The overarching hypothesis of this thesis is that the 3D environment might be beneficial for cell behaviour and maturation. The experiments and technology developed in this

thesis aimed to investigate this hypothesis both *in vitro* and *in vivo*.

The underlying hypothesis for the *in vitro* experiments was that 3D culture of CMs would enable them to be used as *in vitro* testing models. To develop this technology and test this hypothesis, we proposed to develop a human iPS-derived Langendorff perfused heart, which can subsequently be used with all the traditional techniques available for studying whole organ cardiac physiology, such as metabolic profiling using radiolabelled substrates or dynamic nuclear polarisation (DNP) & nuclear magnetic resonance (NMR) spectroscopy. The decellularised heart matrix was chosen as a scaffold material to develop humanised hearts, and given the diffusion limitation of oxygen and nutrients in thick scaffolds, a bioreactor system for culturing the recellularised hearts was developed.

The aims and chapter outline of the *in vitro* experiments:

1. Differentiate human iPS cells to CM and establish protocols to culture these cells on collagen scaffolds (Chapter 3)

2. Develop protocols for isolated rat heart decellularisation and augment the understanding of the process (Chapter 4)

3. Develop a bioreactor and protocols for rat heart recellularisation under biomimetic (perfusion, electrical and mechanical stimulation) conditions (Chapter 5)

The central hypothesis of the *in vivo* experiments in this thesis was that a collagen scaffold may be applied to as a therapeutic vehicle for delivering stem cells to the infarcted heart to provide support and overcome the problem of limited cell retention. This hypothesis was tested by developing collagen scaffolds capable of delivering CDCs to the heart and performing an *in vivo* magnetic resonance imaging (MRI) study to assess cardiac function post ischaemia/reperfusion (I/R). Additionally, we proposed that hypoxic pre-treatment of the cells may provide additional therapeutic advantage (Chapter 6).

CHAPTER 2

MATERIALS AND METHODS

2.1 Statistics and Data analysis

Next to the standard t-test and analysis of variance (ANOVA), some more advanced statistical methods were applied in this thesis, which will be discussed briefly in the following sections.

Descriptive and inferential statistics are the two main statistical methodologies. As suggested by its name, descriptive statistics mainly aims to describe the properties of a sample, whereas inferential statistics, aims to draws conclusions about the population by studying a random sample.

2.1.1 Data and distributions

A framework within which the probability of random phenomena can be enumerated is required in order to make inferences. Probability distributions assign probabilities to all possible outcomes. Discrete and continuous probability distributions can be distinguished depending on whether the outcomes are restricted to a predefined set (flipping

a coin), or are continuous.

Typically, the normal distribution is assumed for most statistical tests. In case the data does not follow this distribution, non-parametric methods are advised. However, some types of experiments generate data that follow a parametric distribution, distinct from the normal, and for those cases alternative statistical methods are available.

2.1.2 Descriptive and exploratory statistics

Descriptive and exploratory techniques are commonly used to inspect data and to try to identify patterns. For high dimensional multivariate data, principal component analysis (PCA) is a very simple but powerful method to visualise data in two or three dimensions.

Multi-dimensional data is difficult to plot and graphically represent. However, in many cases, many of the variables are not very informative (for example highly correlated). PCA is able to transform the data into a new set of dimensions without loss of information, by deconstructing the data by its eigenvectors and eigenvalues. Every eigenvector is paired with an eigenvalue, in which the eigenvector is the direction and the eigenvalue is a measure of the variance explained by this new dimension. Since not all dimensions necessarily explain equal amounts of variance in the data, PCA may be applied to reduce the dimensions of the data set.

2.1.3 Frequentist statistics

The key concept in frequentist statistics is deciding whether or not a particular predefined value of a parameter can be rejected. This is formally done by estimating the probabilities of all outcomes, and calculating the probability of getting an outcome more or as extreme as the observed outcome when the null hypothesis is considered to be *true*, this probability is called the p-value. If the p-value is sufficiently *small*, the null hypothesis (H_0) can be rejected (typically p-value < 0.05), in favour of the alternative hypothesis (H_1). However, it is important to note that the estimation of the probability of all

outcomes and hence the p-value is conditional on the sampling and testing procedure (a. o. stopping rules and multiple testing), and that as a result multiple different p-values can be computed from one single set of data.

In practice, when using frequentist statistics, a test statistic is calculated based on the data observed. Under the null hypothesis, the test statistic follows a certain distribution (i. e. t-test, F-test), which allows the calculation of the probability that the measure is larger or smaller than a certain value (critical value), assuming the null hypothesis is true.

2.1.3.1 Analysis of Variance (ANOVA) and General Linear Models

The ANOVA method is a statistical technique in which multiple treatments can be compared by attributing the total observed variance in the data to different sources. The assumptions are comparable to those of the standard t-test, i. e. the observations are independent and the samples are randomly selected from the population that approximates the Gaussian distribution with identical standard deviation for all groups (homoscedasticity).

Fixed effects Fixed effects models are used to estimate the fixed effect of a treatment group, where the effects are considered population characteristics in which the researcher is interested it.

The standard fixed effect one factor ANOVA has following hypothesis:

$$\begin{cases} H_0: & \mu_1 = ... = \mu_p \\ H_1: & \text{at least one of the groups have different means} \end{cases} \tag{2.1}$$

In order to formally test the null hypothesis, a linear model (Equation 2.2) is fitted to the data $Y_{i,j}$, where Y is the recorded response for treatment i and repeat j (assume an experiment with p treatments and r repeats and total sample size $n = r\,p$):

$$Y_{i,j} = \mu + \tau_i + \epsilon_{i,j}, \tag{2.2}$$

with μ the intercept, τ_i is the real effect of treatment i and $\epsilon_{i,j}$ experimental error on observation $Y_{i,j}$. The τ values are not random variables, do not have distributions, quantify the effect of a particular treatment group as a deviation from μ ($\tau_i = \mu_i - \mu$), and are restricted by $\sum_{i=1}^{p} \tau_i = 0$. One of the underlying assumptions of ANOVA is that $\epsilon_{i,j}$ follows the Gaussian distribution $\mathcal{N}(0, \sigma^2)$ and is independently distributed from τ_i. These assumptions can conveniently be assessed graphically.

Random and Mixed effects Random effects describe variation associated with samples that are repeatedly sampled (longitudinal studies, batch studies, or paired studies), and/or not particularly of interest, but can be isolated from residual and fixed effect variance. Hence, in such cases that the assumptions hold for random effects, such models are superior. The keys assumption is that the sample specific random effects are uncorrelated with the independent variables. Mixed effects models contain both random and fixed effects terms.

General linear models ANOVA (fixed, random, or mixed effects) are part of large class of statistical methods, named general linear model (GLM). GLM allows more complex models (Equation 2.3a), including multivariate models, with atypical distributions and variance structures (not necessarily homoscedastic). A linear model (LM) is a model in which unknown parameters are multiplied by observed variables, which are then summed to give a prediction for the response variable. ANOVA is commonly used for hypothesis testing, whereas the purpose of GLM is to quantify effect sizes and eventually make predictions. Typically, the underlying assumptions are independence of measurements, correct distribution of the residuals and variance structure, and linear

relationship between the response and the linear predictor.

$$E[\boldsymbol{y}] = \boldsymbol{X}\boldsymbol{\beta}, \tag{2.3a}$$

$$\boldsymbol{y} \sim \mathcal{N}(\boldsymbol{X}\boldsymbol{\beta}, \sigma_e^2 \boldsymbol{I}) \tag{2.3b}$$

with $\boldsymbol{y}$ are the responses, $\boldsymbol{X}$ is the design matrix, and $\boldsymbol{\beta}$ is the parameter matrix. $\boldsymbol{I}$ is an identity matrix. This expression of the variance structure implies that the residuals are uncorrelated and that all have the same variance σ_e^2.

GLM extends further than LM in that they also allow other distribution than the normal distribution, and this has implications on the specification of the model. First, in some instances link functions, such as $log(E[\boldsymbol{y}])$ are fitted rather than the mean response $E[\boldsymbol{y}]$. Second, alternative distributions may have different parameterisations for which the estimation of the variance structure is not required (single parameter distributions, example: Poisson distribution).

2.1.4 Bayesian statistics

The two foundational ideas behind Bayesian analysis are that Bayesian inference is the reallocation of credibility across possibilities and that the possibilities across which credibility is allocated are parameter values in mathematical models (239). Whereas traditional frequentist statistics uses sampling distributions to calculate the probability of imaginary outcomes given a parameter value (p-value, inference from maximal likelihood), Bayesian statistics calculates the probability of parameter values given the data observed (inference from posterior distribution).

The likelihood is defined as $Pr(\boldsymbol{D}|\boldsymbol{\theta})$, with $\boldsymbol{D}$ data under investigation from a distribution with parameters $\boldsymbol{\theta}$. Thus, the likelihood is a conditional distribution[1], in which model parameters are taken as fixed and known. Although this is what is typically done

[1]Conditional probability: $p(c|r) = \frac{p(r,c)}{p(r)}$

in frequentist statistics, is seems far more useful to investigate the posterior distribution: $Pr(\boldsymbol{\theta}|\boldsymbol{D})$:

$$\underbrace{Pr(\boldsymbol{\theta}|\boldsymbol{D})}_{\text{Posterior}} = \frac{\overbrace{Pr(\boldsymbol{D}|\boldsymbol{\theta})}^{\text{Likelihood}}\overbrace{Pr(\boldsymbol{\theta})}^{\text{Prior}}}{\underbrace{Pr(\boldsymbol{D})}_{\text{Marginal}}} \tag{2.4}$$

Bayesian analysis allows one to take prior knowledge into consideration: $Pr(\boldsymbol{\theta})$. Although this seems to suggests that one can *fiddle* with the analysis and bias the results into a certain direction, this does not necessarily have to be the case. In fact, even though prior knowledge is not utilised in frequentist statistics, is commonly used in every day reasoning. For example, patients are typically not sampled for certain illnesses, unless there is some clinical indication that warrants executing such a test. This is not only because it could be a waste of money, but because every test can result in a false positive or false negative result. Hence, prior knowledge is used to indicate which tests are appropriate to further determine the clinical phenotype. Alternatively, a positive test result in a patient who is very unlikely to be positive, means it is more likely that the outcome was a false positive. Hence, it may be informative to take prior knowledge into consideration when analysing the outcome of experimental results.

2.1.4.1 Bayesian null hypothesis testing

Bayesian statistics can be used to test whether or not a treatment has a non-null effect in two ways (239). First, one can assess whether or not the null value belongs to the group of most credible values in the posterior. Secondly, two different models can be fitted using the data: (a) a model with prior that allows only the parameter value of interest, (b) a model that allows a broad range of parameter values. Then, both models are compared.

Bayesian p-values Some packages for Bayesian inference compute bayesian 'p-values'. In the R-package *MCMCglmm* (240), pMCMC is defined as two times the smaller of the

two quantities: the probability that $\beta < 0$ or the probability that $\beta > 0$, where β is the parameter value.

2.1.4.2 Bayesian modelling

The true power of Bayesian analysis is arguably in fitting complex models. In this thesis, Bayesian modelling was used for quantitative polymerase chain reaction (qPCR) and NMR metabolomics analysis, and prior knowledge was considered in determining the posterior (241–244). In case of qPCR analysis (Section 2.8.9), housekeeping genes were provided as prior, whereas in the fitting of NMR spectra (Section 2.10.6), experimenter assigned shifts were provided to aid the model in fitting the spectra in order to deal with pH-dependent peak shifts.

2.1.5 Software

R, a free software environment, was the preferred statistical software in this thesis (245). For some graphs, Prism GraphPad or Matlab was utilised. Thousands of libraries are available for R to do specialised types of analysis and the packages utilised in this thesis were cited where appropriate. Custom code or packages were developed where required to aid in the analysis of the acquired data.

2.2 Animals

The experimental procedures for the studies described in thesis were approved by The University of Oxford Animal Ethics Review Committees and the Home Office (London, UK) under Project License 30/2755. Animals were kept under controlled conditions for temperature, humidity and light, with water and rodent chow available *ad libitum*.

2.2.1 Organ harvest

The animals were anaesthetised by overdose of isofluorane or with sodium pentobarbital (200 $mg\,kg^{-1}$ body weight, intraperitoneal (IP) injection; Euthatal®, Merial, UK) to allow tissue removal.

2.2.2 Infarct surgery

The left anterior descending (LAD) coronary artery of female Sprague Dawley (SD) rats (200−250 g) was occluded using established methods (101, 246). Briefly, following anaesthesia, using 2 % isoflurane in O_2, and thoracotamy, the pericardium was removed and a 5-0 prolene suture placed under the LAD, about 2 mm from the origin. The suture was tied around a small piece of polyethylene (PE) tubing, occluding the LAD, and the chest closed temporarily to prevent dehydration. After 40 minutes, the chest was re-opened and the tube removed to allow reperfusion. Then, the scaffolds were attached to the infarct region at one or two points using sutures. In sham animals, the thoracotomy was performed, but no stitch was place in the heart. The surgery was performed by Professor Carolyn Carr.

2.3 MR imaging and analysis

The animals were positioned with their hearts at isocentre in a horizontal bore 7 T magnetic resonance (MR) scanner (Varian Inc., Yarnton, UK) and a stack of $7-8$ sequential 1.6 mm true short axis ECG-gated cine images were acquired to span the entire left ventricle. MR images were processed using ImageJ/Fiji (247, 248) by determining blood and tissue area and perimeter at end systole and diastole. For quantifying cardiac performance parameters based on the areas and perimeters measured in ImageJ, a custom-build R-package was developed.

2.4 Cell culture

2.4.1 iPS cell culture and cardiac differentiation

2.4.1.1 Routine culture, media and matrigel coating

The iPS cells used in this thesis were obtained from Dr. Sally Cowley from the James Martin Stem Cell Facility (University of Oxford, UK). iPS cells were cultured on matrigel-coated plates or flasks (Matrigel® hESC-Qualified Matrix, Corning®, USA). For coating matrigel plates, matrigel was diluted (according to the batch-dependent dilution factor) in Dulbecco's modified eagle medium (DMEM)/F12 (gibco®, Life Technologies™, UK), and pipetted into plates (1.5 mL well^{-1} in six-well plate). The plates were incubated for 45 – 60 minutes at room temperature (RT) in the hood, before immediate use, or stored for up to two weeks in the fridge for later use. The iPS cultures were subcultured every 3 – 5 days when confluent. The media of the iPS cells was changed daily, and the cells were cultured in mTeSR™1 media (Stemcell Technologies™, France).

2.4.1.2 Subculturing iPS

The media was removed and the wells were washed with Dulbecco's phosphate buffered saline (DPBS) (Sigma-Aldrich®, UK). Next, 1 mL of TrypLE™ Express (Life Technologies™, Denmark) was used per well (six-well plate), and the plate was incubated (7 minutes). The cells were collected in DPBS and centrifuged (3 min, 1300 rpm). The supernatant was discarded and the pellet resuspended in mTeSR™1 containing rock inhibitor (10 µM Y-27632, Calbiochem®, Merck Chemicals Ltd, China) and then plated into freshly coated matrigel plates.

2.4.1.3 Cardiac differentiation

iPS cells were cultured on Matrigel plates until confluent. Then, the cells were transferred to reduced factor Matrigel (RF-M) plates (Matrigel® Growth Factor Reduced Basement Membrane Matrix, Corning®, USA) for the differentiation (DMEM/F12 at 1/100, 384 kcells cm^{-2}). The next day (Day −1, Figure 2.1), RF-M (1/200) was added to the mTeSR™1 media and the plates were transferred to an hypoxic incubator (5 % oxygen, 5 % CO_2). The following day (Day 0, Figure 2.1), the medium was changed to Roswell Park Memorial Institute (RPMI) 1640 (gibco®, Life Technologies™, UK), containing 1 % B27 minus Insulin (gibco®, Life Technologies™, USA), 12 µM CHIR99201 (Stratech Scientific Ltd), 10 ng mL^{-1} Activin A (R&D Systems Europe Ltd) and 1/200 RF-M (Table 2.1). The next day, the media was changed to RPMI 1640, containing 1 % B27 minus insulin. On day 3, half of the media was changed to RPMI 1640, containing 1 % B27 minus insulin and 10 µM IWP4 (tebu-bio, final concentration of IWP4 in medium is 5 µM). On day 5, the medium was changed again to RPMI 1640, containing 1 % B27 minus Insulin. On day 7, the media was changed to RPMI 1640, containing 1 % B27 Complete (gibco®, Life Technologies™, USA), and the plates were cultured under normoxia (room air with 5 % CO_2). From this point on the medium was replenished every two days.

Table 2.1: Cardiac differentiation compounds

Agent	Class	Function	Concentration
CHIR99021	Compound	GSK-3β inhibitor, Wnt activation	12 µM
Activin-A	Recombinant protein	TGF-β signaling	10 ng mL^{-1}
IWP4	Compound	Wnt inhibitor	5 µM

2.4.1.4 Replating of iPS-CMs

Human iPS cells were differentiated to cardiomyocytes as described above in T25 flasks (Corning®) coated with RF-M. Around day 15-45, the cells were harvested using a collagenase and trypsin based method. Briefly, the cells were incubated for 10 minutes with

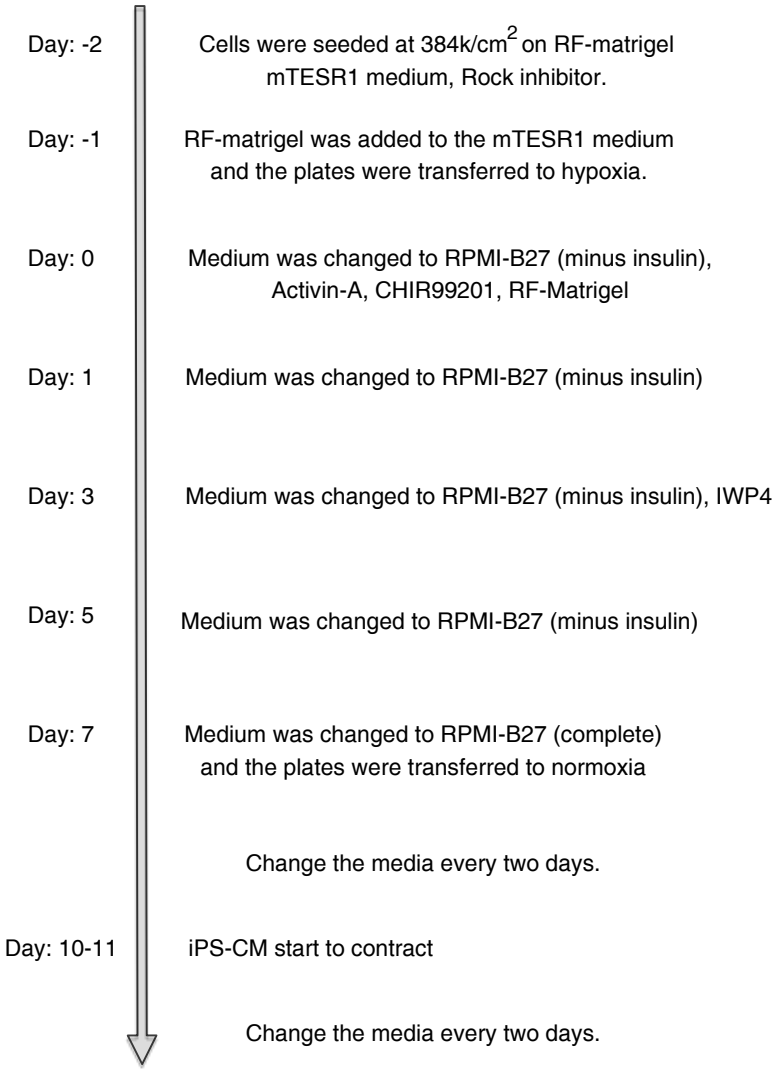


Figure 2.1: iPS-CM differentiation protocol time line

1 mg mL^{-1} collagenase (Type I-A, Sigma-Aldrich®, UK) and then 6 minutes of cell dissociation solution (40 % RPMI, 40 % enzyme-free cell dissociation buffer, and 20 % 0.05 % Trypsin-EDTA, all gibco®, Life Technologies™, UK). The dissociation reaction was then stopped using fetal bovine serum (FBS) (gibco®, Life Technologies™, South America) and the cells were collected and centrifuged. To remove any remaining enzyme, the pellets were washed with DPBS and subsequently resuspended in RPMI medium supplemented with B27, 20 % FBS, and Rock inhibitor (Y-27632). The cells were then replated on coated well plates (Corning®, Table 2.2). After one day, the medium was changed

to RPMI medium supplemented with B27, but without serum. The cells were fed again every few days.

Table 2.2: ECM components and concentration for culture of iPS-CMs For a 12-well plate a volume of at least 600 µL per well was used, and for a 24-well plate a volume of at least 300 µL per well was used.

ECM component	Manufacturer	Concentration	Coating
Fibronectin	F1141, Sigma-Aldrich®	20 µg mL^{-1}, DPBS	> 1 hr, 37 °C
Gelatin	G6144, Sigma-Aldrich®, USA	1 mg mL^{-1}, ddH_2O	> 1 hr, 37 °C
Collagen I	C8919, Sigma-Aldrich®, USA	100 µg mL^{-1}, ddH_2O	> 2 hrs, 37 °C
RF-M	Corning®, USA	1/100, DMEM/F12	> 1 hr, RT

2.4.2 Cardiosphere explant culture

2.4.2.1 Harvesting fresh CDCs

CDC were isolated from adult SD rats and expanded, in accordance with previously published protocols (95, 100, 101). Briefly, SD rats were killed, the hearts explanted and washed with DPBS and minced into small explant pieces in 0.05 % Trypsin-EDTA (Invitrogen, UK). Explants were plated on fibronectin-coated (Sigma-Aldrich®, UK) 60 mm petri dishes with 2 mL Iscove's modified Dulbecco's medium (IMDM) containing complete explant medium (CEM) (Table 2.3), and incubated in a standard tissue culture incubator at 37 °C with 5 % CO_2. After a few days, small, round, phase bright cells grew out from the explants. Upon reaching 80 – 90 % confluency, these explant-derived cell (EDC) were isolated using trypsin and re-plated in poly-d-lysine (Sigma-Aldrich®, USA) coated 24 well plates in cardiosphere growth medium (CGM) (Table 2.4). Cardiospheres formed after 2 – 3 days, when they were harvested by mechanical trituration and plated in CEM in fibronectin-coated flasks and formed CDC. EDC could be harvested from the explants multiple times.

Table 2.3: CEM media composition.

Reagent	Concentration
IMDM (gibco®, Life Technologies™, UK)	80 %
FBS (gibco®, Life Technologies™, South America)	20 %
Penicillin (gibco®, Life Technologies™, USA)	1 U mL^{-1}
Streptomycin (gibco®, Life Technologies™, USA)	1 µg mL^{-1}
L-glutamine (gibco®, Life Technologies™, USA)	0.2 mM

Table 2.4: CGM media composition.

Reagent	Concentration
DMEM/F12 (gibco®, Life Technologies™, UK)	63.4 %
IMDM (gibco®, Life Technologies™, UK)	27.3 %
FBS (gibco®, Life Technologies™, South America)	6.8 %
B27 (gibco®, Life Technologies™, USA)	2 %
Cardiotrophin (Peprotech EC, USA)	25 ng mL^{-1}
Epidermal growth factor (EGF) (Peprotech EC, USA)	16 ng mL^{-1}
bFGF (Promega, France)	20 ng mL^{-1}
Thrombin (Sigma-Aldrich®, USA)	25 µg mL^{-1}
Penicillin (gibco®, Life Technologies™, USA)	1 U mL^{-1}
Streptomycin (gibco®, Life Technologies™, USA)	1 µg mL^{-1}
L-glutamine (gibco®, Life Technologies™, USA)	0.2 mM

2.4.2.2 Colony forming unit assay

The colony forming unit (CFU) assay was performed by plating 180 cells $well^{-1}$ into a six-well plate (20 cells cm^{-2}). After 14 days of culture, the plates were washed twice with DPBS, fixed with 70% ethanol (two hours, 4 °C), air dried, stained with Crystal Violet (Sigma-Aldrich®, UK) for 5 minutes and washed with water. A cluster of cells was considered a colony if it consisted of more than 30 cells.

2.5 Collagen scaffolds

The collagen scaffolds were designed and manufactured in collaboration with Prof. Jan Czernuszka's group (Material Science, Oxford). The scaffolds used in this thesis were

made by Dr. Qi Chen and Rabia Nazir.

The collagen scaffolds were produced by freeze drying a moulded 1% collagen-I suspension, as described previously (178, 249). Briefly, a suspension of collagen-I (from bovine Achilles tendon, Sigma-Aldrich®, UK) in 0.05 M acetic acid (pH 3.2) was cast into polytetrafluoroethylene (PTFE) moulds according to the required dimensions of the samples, frozen at −20 °C, and freeze-dried (Christ I-5, Martin Christ) for 24 hours in a vacuum of 0.05 mbar, removing the ice crystals by sublimation and leaving behind the porous solid scaffolds.

2.5.1 Disc-shaped collagen scaffolds

1 % collagen-I suspensions were poured into PTFE moulds to form disc-shaped scaffolds (diameter: 13 mm, height: 4 mm, Figure 2.2). Next, the moulds were frozen and subsequently freeze dried, as described previously (178, 249).

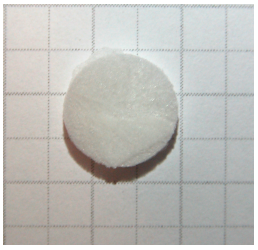
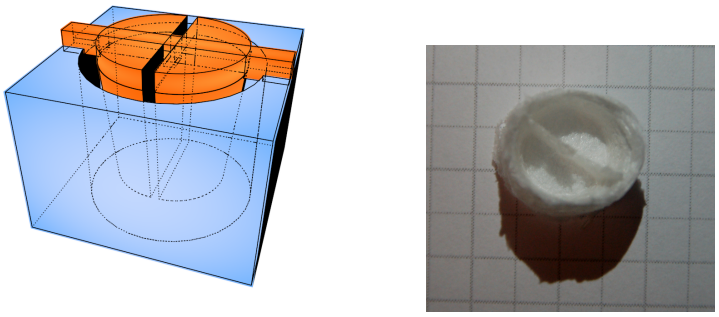


Figure 2.2: Photograph of a disc-shaped collagen scaffold. Top view photograph of disc-shaped collagen scaffold on 5 mm graph paper.

2.5.2 Biventricular collagen cup-shaped scaffolds

A 3D mould to cast biventricular collagen cup-shaped scaffolds was designed using computer aided design software (Figure 2.3(a)) and 3D printed in glass-filled nylon (3T, UK). The plug was 12.0 mm × 20.0 mm × 13.5 mm and the base was 20.0 mm × 20.0 mm × 14.0 mm. 1 % collagen-I suspensions were poured into the moulds to form cup-shaped scaffolds (Figure 2.3(b)).



(a) (b)

Figure 2.3: Design of a biventricular cup-shaped collagen scaffold (a) Diagram of the design of the mould for making cup-shaped collagen scaffolds. Image and improved design, courtesy of Dr. Jack Miller. Scale: the length and width of the blue base mould were 20.0 mm × 20.0 mm. (b) Top view photograph of a cup-shaped collagen scaffold on 5 mm graph paper.

2.5.3 Bilayer collagen scaffolds for surgery

The collagen film was made by air-drying a 20 mL 1 % collagen suspension per petri-dish. The collagen disc layer (Section 2.5.1) was subsequently casted and processed on top of the collagen film, as described above.

2.5.4 Scaffold sterilisation

The collagen scaffolds were sterilised by submersion and infusion of 100 % ethanol (3× 30 min). Next, in order to remove all traces of ethanol, the scaffolds were washed 3× 30 min with DPBS containing antibiotics (100 U mL^{-1} penicillin, 0.1 mg mL^{-1} streptomycin and 0.25 µg mL^{-1} amphotericin B, Sigma-Aldrich®, UK) and were washed once with medium.

2.6 Decellularisation

2.6.1 Literature review

A Pubmed search was run on *decellularization*, *decellularized*, *decellularisation* or *decellularised* and went through all papers published since January 2014 in order to assess which normalization strategy had been applied. All papers quantifying at least one of the components of interest (DNA, collagen, GAG) were included. For those papers that assessed multiple components, we determined whether they were consistent in their approaches.

2.6.2 Reactor

The decellularisation reactor comprises plastic tubing, plastic and glass bottles, and pumps enabling flow through the heart and buffer recirculation (Figure 4.2). Decellularisation buffers were stored in bottles (Duran® bottles or Nalgene® carboys) equipped with inlet and outlet tubing fittings. Tygon® S-50-HL and 2001 tubing (Cole-Parmer, USA) and Masterflex® PharMed® tubing (Saint-Gobain) were used for fluid handling. The coordinated action of two pumps (Masterflex®, Cole-Parmer) maintained a constant fluid level in an elevated vessel to enable constant pressure perfusion of the hearts. The perfusion pressure can be modified by altering the height of the elevated reservoir. The inlet to the elevated reservoir was equipped with particulate filters (fibre glass prefilter and 0.45 – 0.8 µm membrane filter, Merck Millipore). The aorta of the hearts was cannulated for retrograde perfusion of decellularisation buffers into the coronary arteries. Eventually, the spend buffers will drain out of the heart through the coronary sinus into the bottle and are subsequently collected and discarded.

2.6.3 Protocols

2.6.3.1 Decellularisation for normalisation study

Hearts were cannulated via the ascending aorta, heparinised and perfused with Krebs-Henseleit buffer (10 – 20 min, Table 2.5) to wash out the blood. The hearts were decellularised by constant pressure perfusion (72 mmHg) for about 18 hours with detergent: 1% sodium dodecyl sulfate (SDS) in ddH_2O or 1% polyoxyethelene (10) tridecyl ether (POETE) in 50 mM Tris-HCl pH 7.4, washed for 5.5 hours with ddH_2O, and subsequently fixed for histology or freeze clamped in liquid nitrogen for further analysis.

2.6.3.2 Decellularisation for pretreatment study

Hearts were canulated via the ascending aorta, heparinised and treated with one of the three pre-treatment strategies: (a) perfusion with warm Krebs-Henseleit buffer (10 – 20 min, Table 2.5), (b) perfusion with phosphate buffered saline (PBS) containing 10 µM adenosine (10 – 20 min), or (c) a $-80^{\circ}C$ freeze-thaw cycle (> overnight). Subsequently, the hearts were decellularised with 1% SDS in ddH_2O at 58 or 72 mmHg (or 7.7 kPa and 9.6 kPa) for about 18 hours. Then, the hearts were washed for 5.5 hours with ddH_2O, and subsequently freeze clamped in liquid nitrogen for further analysis.

Table 2.5: Krebs-Henseleit buffer composition.

Reagent	Concentration
NaCl	118 mM
KCl	4.7 mM
$MgSO_4 \cdot 7\,H_2O$	1.2 mM
$CaCl_2 \cdot 2\,H_2O$	1.75 mM
Na_2EDTA	0.5 mM
Glucose	11.0 mM
$NaHCO_3$	25 mM

2.6.3.3 DNase treatment

Decellularised hearts were perfused with and submerged in a 156 Kunitz mL^{-1} DNase-solution for 16 hours at RT, to degrade the residual DNA present within the decellularised heart.

2.6.4 Tissue characterisation

2.6.4.1 Histology

Decellularised hearts were fixed in 4 % paraformaldehyde (PFA), embedded in wax and processed as discussed in Section 2.8.

2.6.4.2 DNA quantification

DNA content was determined in both control and decellularised tissue using the Qiagen® DNeasy® blood and tissue kit according to the supplied protocol (Qiagen®, UK). Briefly, tissue was digested using 20 µL proteinase K stock solution and 180 µL ATL buffer per sample on a dry block heater (56 °C, overnight). Then, 200 µL AL buffer and 200 µL ethanol was added per sample, and the mixture was subsequently loaded on a DNeasy® Mini spin column and centrifuged (1 min, >6000 g). Next, the column was washed with AW1 and 2× with AW2 buffer and centrifuged (1 min, >6000 g, final wash: 3 min, 20 000 g). Finally, the DNA was eluted using 180 µL AE buffer (1 min, >6000 g). The eluted DNA was subsequently quantified using a NanoDrop™ spectrometer.

2.6.4.3 Collagen quantification

Collagen content was determined in both control and decellularised tissue by quantifying hydroxyproline with the Ehrlichs reagent (250–256). Crushed tissue was weighed out (100 mg) and dried on a heating block (70 °C until constant weight). The tissue was hydrolysed in 1 mL 6 N HCl at 105 °C overnight and subsequently cooled and dried at

60 °C. The dry residue was resuspended in 1 mL buffer solution (0.7 M Sodium Acetate, 0.2 M Trisodium citrate, 45 mM Citric Acid, pH 6.0) and filtered (0.22 µm). 60 µL of the filtered solution was added to 340 µL buffer solution (6 : 4 diluted with isopropanol). 100 µL chloramine T oxidant solution (300 mM Chloramine T in buffer solution 6 : 4 diluted with isopropanol) was added to all samples and incubated (25 °C, 5 min), after which 1.3 mL of the Erhlichs reagent (3.5 M dimethylaminobenzaldehyde in 72 % perchloric acid, diluted 1 : 4 with isopropanol) was added, and the samples were incubated on a heat block (60 °C, 30 min). Absorbance was measured at 550 nm with a plate reader (Multiskan™ FC, Thermo Fisher Scientific) and converted into absolute concentration based on linear regression on the standard curve samples (0 - 5 µg OH-proline).

2.6.4.4 GAG quantification

The Blyscan Glycosaminoglycan Assay (Biocolor, UK) was used to quantify retained GAG in decellularised and control tissue according to the standard protocol. Briefly, crushed tissue was digested with papain (Sigma-Aldrich®, UK) overnight at 65 °C. 1 mL of dye reagent was incubated with the lysate (30 min, RT, gently rocking), then the GAG-complex was pelleted (12 000 rpm, 10 min, RT), the unbound dye was removed and the pellets subsequently resuspended in dye dissociation reagent. The foam was removed from the resuspended samples by centrifugation (12 000 rpm, 5 min). Absorbance of the samples was then measured with a plate reader at 656 nm (BMG Labtech), and quantified using a standard curve (0 - 5 µg chondroitin-sulphate).

2.6.4.5 SDS quantification

Dyes such as methylene green or blue (257–259) and Stains-all (260) have affinity for SDS and can be used to determine SDS content in solutions by spectrophotometry.

When an SDS solution is added to methylene green and chloroform, the SDS and methylene green will ionically bind, and partition in the organic phase. Hence, the

colour intensity of the chloroform layer relates to the amount of SDS present in the original solution. Briefly, 0.5 mL of 0.005 % methylene green in 0.7 mM Tris-HCl (pH 7.0) was added to 1 mL sample (259). Then, 3 mL chloroform was added and the solution vortexed, and subsequently centrifuged (2000 rpm, 3 min, RT). Next, the chloroform layer was collected and placed in a cuvette and the optical density recorded at 659 nm using ultraviolet-visible light spectroscopy (UV-1700 PharmaSpec, Shimadzu). The concentration of SDS was determined using a standard curve.

2.6.5 Normalisation

Heart weights (wet) were recorded before and after decellularisation. Frozen tissue was crushed under liquid nitrogen and a representative sample taken for dry weight determination by drying in an oven to a constant weight (48 hrs, 70 °C).

Since experiments were performed on wet tissue, analysis immediately gives rise to results normalised to final wet weight. For normalisation to initial wet weight the following equation was used (for compound Q):

$$\mu\text{g Q/mg initial wet weight} = \frac{\mu\text{g Q/mg final wet weight} \times \text{total final heart wet weight (mg)}}{\text{total initial heart weight (mg)}} \tag{2.5}$$

For normalisation to final dry weight:

$$\mu\text{g Q/mg final dry weight} = \frac{\mu\text{g Q/mg final wet weight}}{\text{mg dry weight/mg final wet weight}} \tag{2.6}$$

Normalisation to whole organ weight:

$$\mu\text{g Q/whole organ} = \mu\text{g Q/mg final wet weight} \times \text{total final heart weight (mg)} \tag{2.7}$$

2.6.6 Tissue permeability

At the end of the decellularisation cycle, for a couple of minutes the spend perfusate was collected and weighed, to determine the flow through the decellularised heart. For retrograde perfused hearts, the perfusate enters the heart through the aorta and subsequently enters the coronary arteries, and eventually escapes the hearts through the coronary sinus in the right atria. The same mechanism applies for decellularised hearts, however it is reasonable to assume that the valves and coronaries are a lot leakier and hence perfusate will exit at different other points of the circulation too. For the purpose of calculating the permeability or alternatively the vascular resistance of the whole decellularised heart, the heart was considered a *black box* with one inlet and one outlet, and one *net* permeability variable, and as a result computed using Darcy's law (Equation 4.6a):

$$\frac{Q}{\Delta P} = \frac{kA}{\mu L} \tag{2.8a}$$

$$\text{Permeability} = \frac{Q}{\Delta P} \tag{2.8b}$$

The permeability measure as defined in Equation 2.8 has units $\frac{\text{m}^3}{\text{Pa s}}$.

2.6.7 Detergent toxicity

Cells were seeded in a 96-well plate and were allowed to attach and reach confluency. Non-sterile detergent was added to an aliquot of tissue culture medium and subsequently filter sterilised (Millex® GP Filter Unit 0.22 µm, Millipore Express® polyethersulfone (PES) membrane, Merck Millipore, Ireland). The cells were treated with medium containing detergent for 24 hours. Next, the plates were washed with DPBS and incubated with medium containing 10% AlamarBlue® (AbD Serotec®, UK). After 6 hours, the fluorescence of the medium was measured according to the manufacturers protocol

(BMG Labtech FLUOstar® Omega).

A four-parameter log-logistic function (Equation 2.9) was fitted to the viability data obtained by the AlamarBlue® assay using Matlab (261).

$$f(x) = \beta_{\text{Upper}} + \frac{\beta_{\text{Lower}} - \beta_{\text{Upper}}}{1 + (x/\beta_{\text{LD50}})^{\beta_{\text{Slope}}}} \tag{2.9a}$$

$$f(x) = \beta_{\text{Lower}} + \frac{\beta_{\text{Upper}} - \beta_{\text{Lower}}}{1 + \exp(\beta_{\text{Slope}}(\log(x) - \log(\beta_{\text{LD50}})))}, \tag{2.9b}$$

with x the concentration, $f(x)$ the % cell viability and the βs the four parameters in the model: β_{Lower} is the minimum asymptote, β_{Upper} is the maximum asymptote, β_{Slope} is the slope or steepness of the curve, and β_{LD50} the inflection point.

2.6.8 Sterilisation and preparation of decellularised hearts for cell culture

Decellularised hearts were sterilised by submersion and infusion of 100 % ethanol (3× 30 min). Next, in order to get rid of all traces of ethanol, the samples were washed 3× 30 min with DPBS containing antibiotics (100 U mL^{-1} penicillin, 0.1 mg mL^{-1} streptomycin and 0.25 µg mL^{-1} amphotericin B, Sigma-Aldrich®, UK). The decellularised hearts used for iPS-CMs recellularisation were incubated with FBS (4 °C, > overnight) to reduced the potential toxic effects of residual SDS. Before seeding, the decellularised hearts were washed with culture medium.

2.7 Recellularisation

2.7.1 Bioreactor design

2.7.1.1 Fluidics

To provide temperature control, the bioreactor was enclosed in a heated chamber (Stuart incubator S160D, UK). The fluidics circuit for the perfusion loop of the bioreactor was composed of medical or pharmaceutical grade Tygon® S-50-HL and 2275 tubing (Saint-Gobain), and to accommodate gas exchange, wound Silastic™ (Dow Corning™) tubing was used. Peristaltic pumps were used for the fluid handling (Gilson, Inc, Minipuls® 3, USA). The fluid path was composed of shorter leads which can be assembled using the Luer-Lok™ system (Becton Dickinson) and Duran® bottles fitted with tubing connections were used for holding the medium and the heart. The entire fluid path can be disassembled, washed, and autoclaved to allow sterile operation.

2.7.1.2 Electronics

Circuit/PCB design and manufacturing Diptrace (Novarm) was used for drawing circuit diagrams and printed circuit board (PCB) design. Circuits were tested on prototype boards or *in silico* using Tina (DesignSoft). Two or four layer panels with through-hole technology were used given their ease to produce, solder and manipulate. The PCBs were manufactured by Eurocircuits (Eurocircuits, Belgium).

PIC microcontroller software development MPLAB® X (Microchip) was used to program the microcontroller units (MCUs) in C and a PICkit™ 2 was used to write the software to the chipset.

C++ & Qt GUI software development The graphical user interface (GUI), to operate the bioreactor and communicate with the PCBs, was implemented in C++ using Qt Cre-

ator/Designer on a personal computer (PC) running Debian as operating system.

2.7.2 Sterilisation and preparation

Before usage the bioreactor setup was rinsed with ddH_2O, bagged and autoclaved. The bags and their content were then dried and the bioreactor was reassembled in a laminar flow hood.

2.7.3 Cell culture

CDC CDC were cultured as discussed in Section 2.4.2. Cells were dissociated, pelleted and resuspended using the standard Trypsin-EDTA method, $5-10$ million cells were typically seeded per heart (T175 flask).

iPS-CM Human iPS cells were cultured and differentiated to CM as discussed in Section 2.4.1.3. Around day 15-45 the cells were harvested using a collagenase and trypsin based method. Briefly, the cells were incubated for 10 minutes with $1\,mg\,mL^{-1}$ collagenase and then 6 minutes of cell dissociation solution (40 % RPMI, 40 % enzyme-free cell dissociation buffer, and 20 % 0.05 % Trypsin-EDTA). The dissociation reaction was then stopped using FBS and the cells were collected and centrifuged. To remove any remaining enzyme, the pellets were washed with PBS and subsequently resuspended in RPMI medium supplemented with B27, 20 % FBS, and 10 µM Rock inhibitor. These cells were then replated in coated well plates, collagen scaffolds or infused into decellularised hearts. Typically, about a T25 flask was seeded per decellularised heart ($4-6$ million cells). After one day, or after cell attachment (5 hrs), the medium was changed to RPMI medium supplemented with B27 and antibiotics ($100\,U\,mL^{-1}$ penicillin, $0.1\,mg\,mL^{-1}$ streptomycin and $0.25\,\mu g\,mL^{-1}$ amphotericin B, Sigma-Aldrich®, UK), but without serum.

2.7.4 Cell seeding of decellularised hearts

Coronary infusion Cells were dissociated, pelleted and resuspended in medium, as discussed above. The suspension was loaded onto a syringe and perfused into the aorta and coronary vessels through the cannula. Then, the heart was either cultured immediately in the bioreactor or cultured in a dish in a regular incubator before being transferred into the bioreactor.

LV infusion Cells were dissociated, pelleted and resuspended in medium, as discussed above. Then, the suspension was infused into the LV through the atrial opening and the heart was cultured in a dish in a regular incubator before being transferred into the bioreactor.

2.7.5 Culture in the bioreactor

After sterile reassembly of the bioreactor, the seeded heart was aseptically connected to the connection points in the bioreactor. The medium reservoir was filled with approximately 100 mL medium. All bioreactor components were then transferred into the heated chamber and the pump tubing connected to the peristaltic pumps. iPS-CM-seeded hearts were perfused at $35\,\mu L\,min^{-1}$, whereas CDC-seeded heart were perfused at much higher rates: $\geqslant 320\,\mu L\,min^{-1}$. The flow rate was reduced for recellularisation of iPS-CM-seeded hearts to limit wash-out.

2.8 Histology, immunohisto- and immunocytochemistry

2.8.1 Tissue fixation, embedding and sectioning

Tissues were fixed in 4 % PFA (4 °C or RT, overnight). Then, the samples were either embedded in optimal cutting temperature (OCT) or paraffin. Before OCT embedding,

the samples were equilibrated in 30 % sucrose in PBS overnight. In order to prevent the OCT or tissue from cracking, the samples were immersed slowly in cold (dry ice) isopentane. The paraffin embedding and sectioning was performed by Richard Stillion (Dept. of Pathology, Oxford).

2.8.2 Histological staining

Tissue slides were stained with Hematoxylin and Eosin (H&E), Masson's trichrome (MT), or Sirius Red (SR) to visualise nuclei, cytoplasm and extracellular matrix. The staining was performed by Richard Stillion (Dept. of Pathology, Oxford).

2.8.3 Immunohistochemistry

Frozen sections were defrosted and allowed to dry, washed with DPBS, permeabilised (0.5 % triton X-100 (TX-100) in DPBS) and incubated with blocking solution (DPBS, 10 % donkey serum, 1 % bovine serum albumin (BSA), and 0.1 % TX-100) at RT for 90 minutes. Then, the samples were incubated with primary antibody (Table A.2) diluted in blocking solution (4 °C, overnight). The next day, the samples were rinsed four times, washed three times (5 minutes, DPBS 0.1 % TX-100) and incubated with the appropriate secondary antibodies (one hour, RT, Table A.3). Then, the slides were washed three times (10 minutes, DPBS 0.1 % TX-100). For Rhodamine Phalloidin staining (Life Technologies™, UK), 5 µL methanolic stock solution was used per 200 µL blocking solution, and the samples were incubated for 20 min at RT. For the staining of nuclei, 4',6-diamidino-2-phenylindole (DAPI) (Sigma-Aldrich®) was added to the final wash, and then the slides were rinsed twice in PBS. The slides were mounted with 50 : 50 DPBS/glycerol and stored in the dark at 4 °C.

2.8.4 Immunocytochemistry

The cells were washed with DPBS and fixed in 4 % PFA (30 minutes, 4°), and washed again in DPBS. Next, the cells were incubated with blocking media (DPBS, 2 % FBS, 2 % BSA) to limit aspecific staining (30 – 60 min, RT).Then, the samples were incubated with primary antibody (Table A.2), diluted in blocking media (1 hour at RT, or overnight at 4 °C). Next, the samples were washed twice with DPBS, and incubated with secondary antibody (one hour, RT, Table A.3), and washed twice again. DAPI was added to the final wash, and then the slides were rinsed twice in DPBS. The slides were mounted with 50 : 50 DPBS/glycerol and stored in the dark in the fridge.

2.8.5 RNA extraction

Cells were collected using trypsination and stored as pellets, or were lysed directly in the plates using RLT buffer containing 1 % β-mercaptoethanol (BME) (Sigma-Aldrich®, Germany) and were stored (−80 °C). Collagen scaffolds or decellularised hearts were partly digested using collagenase (1 mg mL^{-1}), and shredded through QIAshredder™columns, before being processed further using the Qiagen® RNeasy® kit for total ribonucleic acid (RNA) extraction (Qiagen®, UK), according to the supplied protocol. Briefly, one volume of 70 % ethanol was added to the lysed samples, which were subsequently loaded onto RNeasy® Mini spin columns and centrifuged (15 s, >8000 g). Next, the column was washed with 700 µL RW1 (15 s, >8000 g) and 2× 500 µL RPE buffer (15 s and 2 min, >8000 g), and dried (1 min, >8000 g). Finally, the RNA was eluted twice from the column using 20 µL of ddH_2O (1 min, >8000 g). RNA samples were processed on the same day of extraction and stored at −80 °C for further use.

2.8.6 cDNA conversion

RNA concentration was determined using NanoDrop™ UV spectrometry (NanoDrop™ Lite, Thermo Fisher Scientific), and 1 µg of RNA was converted into complementary deoxyribonucleic acid (cDNA) using the high capacity cDNA reverse transcriptase kit (Applied Biosystems™) according to the supplied protocol. Briefly, 1 µg of RNA, 1 µL enzyme, 2 µL random primers, 0.8 µL deoxynucleotide triphosphate (dNTP) solution and 2 µL buffer was used per reaction, water was added to a total volume of 20 µL per reaction. The samples were then incubated on a thermal cycler: 10 min at 25 °C, 120 min at 37 °C, and 5 min at 85 °C. cDNA samples were stored at −20 °C for further use.

2.8.7 Primer design

Primers were designed using Primer Blast[2], so that the amplicon would contain exon-exon interface and would be of length 170 to 230 bp. Primers were produced by Sigma-Aldrich® UK, and tested by assessing the melt curve and by calculating the primer efficiency (Equation 2.10). Primers without primer-dimers visible in the melt curve and with an efficiency between 90 and 110% were used.

$$E = -1 + 10^{-1/m} \ (\%) \tag{2.10}$$

with m being the slope of Ct plotted versus log(concentration).

The primers for human iPS and iPS-CM cells, can be found in Table A.1.

2.8.8 qPCR reaction

qPCR was performed using the SYBR® detection method (Applied Biosystems™, REF 4309155, UK). Briefly, a 20 µL reaction volume was used per reaction, containing typically 12.5 ng cDNA, 10 µL SYBR® reagent master mix, and 2 µL primers (10 µM stock). The

[2]URL: www.ncbi.nlm.nih.gov/tools/primer-blast/

samples were loaded on 96-well format qPCR plates (MicroAmp® Fast, Applied Biosystems™, China), and a standard SYBR® cycle (Table 2.6) was started using a StepOnePlus™ Real-Time PCR System (Applied Biosystems™).

Table 2.6: qPCR reaction: two step SYBR® green protocol.

	Step	Time (s)	Temperature (°C)
40 times	Enzyme activation	600	95
	Denaturation	15	95
	Amplification and measurement	30	60
	Meltcurve determination		

2.8.9 Analysis of qPCR data

The traditional method for relative quantification of qPCR data is the $\Delta\Delta C_t$ method. However, more versatile modelling approaches have been proposed, and were utilised in this thesis.

One of the key aspects of qPCR analysis is the usage of an appropriate normalisation strategy. Typically housekeeping genes are utilised for this purpose (262). However, data driven approaches (such as quantile normalisation) or model driven (Bayesian inference), may be applied as alternative.

2.8.9.1 $\Delta\Delta C_t$ method

The $\Delta\Delta C_t$ method is a simple analysis method that enables the pair wise comparison of two treatment groups, for one gene of interest (GOI), taking into consideration one housekeeping gene (Equation 2.11). Adaptations are available for considering multiple housekeeping genes, however the issue of pairwise comparison is troublesome. Secondly, the propagation of error is challenging and inflexible.

$$\Delta\Delta C_t = (C_t^{GOI,reference} - C_t^{HK,reference}) - (C_t^{GOI,sample} - C_t^{HK,sample}) \tag{2.11a}$$

$$\text{Fold change} = E^{\Delta\Delta C_t}, \tag{2.11b}$$

with E, the primer efficiency coefficient. E equals to 2 for a primer that is 100% efficient.

2.8.9.2 Modelling approach

Rather than calculating $\Delta\Delta C_t$ values for each individual combination of genes and treatments, all data can be modelled using a single GLM using the C_t values or therefrom derived measures. Both frequentist and Bayesian methods can be applied, but a Bayesian model was used in this thesis (notations in Table 2.7).

Table 2.7: qPCR modelling notations.

Variable	Description
g	gene
i	level of a treatment condition
j	level of a grouping variable (block)
k	biological replicate
r	technical replicate

Frequentist modelling approach Steibel *et al.* (263) developed a mixed linear effects model for C_t values, that takes into consideration random effects of specific animals within different litters on the expression of individual genes:

$$y_{gijkr} = TG^*_{gi} + I_{gj} + B_{gijk} + D_{ijk} + \epsilon_{gijkr}, \tag{2.12}$$

where y_{gijkr} is the Ct value for gene g, technical replica r, corresponding to the kth animal in the jth litter subjected to treatment i. T_{gi} is the gene g specific effect of

treatment i, $I_{gj} \sim \mathcal{N}(0, \sigma^2_{I_g})$ is a gene-specific random effect of the jth litter and $B_{gijk} \sim \mathcal{N}(0, \sigma^2_{B_g})$ is a gene-specific random effect of the kth animal in the jth litter, $D_{ijk} \sim \mathcal{N}(0, \sigma^2_D)$ is a random sample-specific effect (common to all genes), such as total mRNA concentration, differential extraction or amplification efficiencies among samples. $\epsilon_{gijkr} \sim \mathcal{N}(0, \sigma^2_e)$ is the residual term.

Bayesian modelling approach Matz *et al.* (241) described a model in which gene expression is modelled as mRNA copy number y, assuming it is derived from a Poisson-lognormal distribution:

$$y_{gijkr} = \text{PLN}(\lambda_{gijk}, \sigma^2_g) \tag{2.13}$$

The log-rate $\psi = log(\lambda_{gijk})$, is expressed as follows:

$$\psi_{gijkr} = I_g + B_{ig} + t_k + a_{jg} + s_{kg} + \epsilon_g, \tag{2.14}$$

where I_g is the gene-specific intercept, B_{ig} is the fixed effect of treatment i on gene g, t_k is a random effect in biological replicate k (quality and quantity of cDNA), a_{jg} is the gene-specific random effect associated with the jth level of the grouping variable, s_{kg} the random effect to capture residual variation between biological replicates, and ϵ_g the gene-specific residual variance.

Genes which were not specified as housekeeping genes, were initialised with a diffuse prior ($\mu = 0$, $\sigma^2 = 10^8$). For control genes, a smaller variance was implemented (default is to allow 1.2-fold on average across experimental conditions).

In terms of statistical significance testing, Bayesian p-values were computed and corrected for multiple testing (across all genes and groups) by controlling the false-discovery rate (Benjamini-Hochberg method).

2.9 ELISA

An enzyme-linked immuno sorbent assay (ELISA) for rat VEGF (R&D Systems) was performed on the scaffold tissue culture supernant samples. The medium was changed on the 6^{th} day of culture and was collected the next day. The standard protocol was followed and the sample concentrations were estimated using a standard curve fitted with a four parameter logistic curve (Figure 2.4), using R (264).

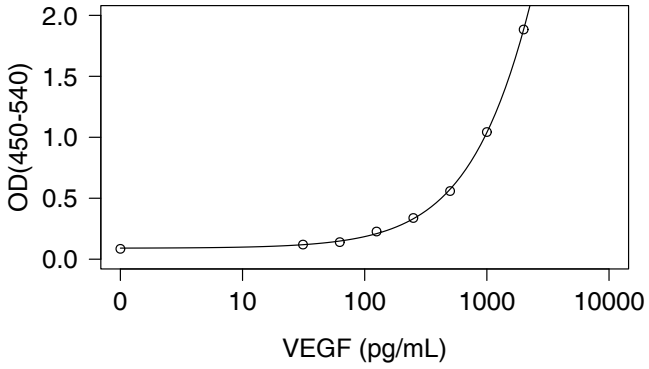


Figure 2.4: VEGF ELISA. The standard curve for the VEGF ELISA was determined using non-linear regression (four-parameter logistic curve-fit) in R (264).

2.10 Metabolic measurements

2.10.1 Measurement of media glucose and lactate concentration

Cell culture medium glucose and lactate concentrations were determined using a Horiba ABX Pentra 400 blood plasma analyser according to the standard protocols.

2.10.2 Metabolite cell extraction using chloroform-methanol-water

After the culture medium was aspirated, the flasks or well plates were washed twice with DPBS, to remove any residual medium. Then, one unit of methanol (typically 2 mL) was added, and the cells were lysed and collected by scraping and placed in a conical tube. Next, one unit of chloroform and one unit of distilled water, was added, and the solution was vortexed each time. The metabolite extract was subsequently centrifuged (3000 rpm, 20 min, 4 °C) to enable phase separation. The water layer was collected and 20 – 30 mg of Chelex® 100 was added, to absorb polyvalent cations. The solution was vortexed and subsequently centrifuged to pellet the Chelex® (3000 rpm, 5 min, 4 °C). Finally, the supernatant was collected, frozen down and freeze dried overnight (Edwards Vacuum).

2.10.3 Metabolite extraction from cell medium

Cell medium was frozen at −80 °C and subsequently freeze dried overnight (Edwards Vacuum).

2.10.4 NMR sample preparation

The dry residue from either the chloroform-methanol-water extraction or the culture medium was subsequently resuspended in D_2O. Calcium formate was added to the samples as concentration reference (265), and the sample was placed in a 5 mm NMR tube for analysis.

2.10.5 NMR machine and protocols

The NMR samples were analysed using a Bruker DPX-300 300 MHz NMR spectrometry apparatus equipped with a 5 mm dual $^{13}C/^{1}H$ probe (Dept. of Chemistry, Oxford). The following spectra were recorded: standard 1D ^{1}H, water saturated 1D ^{1}H, 1D ^{13}C, and

2D heteronuclear multiple-bond correlation spectroscopy (HMBC). The 1D ^{1}H spectra were used for quantitative analysis, and the 1D ^{13}C spectra where use to determine the fate of ^{13}C labelled substrates. 2D HMBC was used for compound identification.

2.10.6 NMR Metabolomics software and data analysis

The NMR spectra were fitted to determine metabolite content using the *batman* R-package (242–244). *batman* is a Bayesian based statistical modelling package that is able to identify and quantify compounds within complex spectra without overlapping peaks. For this purpose, *batman* utilises a metabolite list (Table 2.8) which contains the chemical shifts, coupling constants, multiplet type and relative intensity for all peaks for all molecules of interest. The software accepts prior knowledge to aid in the fitting in the form of operator assigned peaks, which is of considerable importance since changes in sample pH may result in deviations of the predicted chemical shifts.

Table 2.8: Batman NMR metabolomics: metabolite list

Metabolite	Peak position (ppm)	J-coupling	Multiplet	Relative intensity
L-alanine	1.46	7.14	1	3
L-alanine	3.67	7.20	3	1
Lactic acid	1.32	6.93	1	3
Lactic acid	4.10	6.92	3	1
Formate	8.45	-	0	2

CHAPTER 3

HIPS CULTURE AND DIFFERENTIATION ON MATRIGEL AND COLLAGEN SCAFFOLDS

3.1 Introduction

iPS cells have been proposed as a tool to study human disease in a dish using patient-derived material since Yamanaka's group published protocols to generate these embryonic-like cells from small biopsies in 2006 (84, 85). The technology has the presumed theoretical advantage that all tissue types can be derived from iPS cells from patients with mutations and/or combinations of polymorphisms in their genome. Secondly, unwanted drug side effects can be assessed in human cells during preclinical drug testing. Additionally, different treatment strategies can be compared *in vitro* for personalised medicine purposes (214).

3.1.1 Generating iPS-derived cardiomyocytes

Differentiation protocols to generate cardiomyocytes from these cells are required to facilitate such experiments (Table 3.1). There has been considerable improvement in the

efficacy to generate cardiomyocytes, since the first protocols were published more than a decade ago for ES cells (266). When human ES cells are allowed to spontaneously differentiate, they form EBs which are comprised of derivatives of all three germ layers, and include contractile patches (266). The EB method has also been applied to iPS cells (267), but this method is considered to be very inefficient since spontaneously contractile regions appear in only about 8% of the EBs.

Coculture strategies can also be applied to induce cardiomyocyte differentiation, for example by utilising a visceral endoderm-like cell line (END-2) (268). The effect is mediated by cell-cell contact and cell secreted factors (a. o. insulin depletion, p38 MAPK inhibition and PGI_2).

Finally, modern protocols are aimed at driving the cells through a differentiation process similar to that occurring during development using TGFβ and Wnt signalling. During development, canonical Wnt signaling exerts stage-dependent effects: it is activated during mesoderm induction and inhibited for the induction of precardiac-mesoderm (114). Traditional protocols modulated cell signalling using proteins, however there is currently considerable interest in cutting the cost using small molecules.

In this thesis a Activin-A, CHIR99021 and IWP4 based protocol was used, based on previous work of Lian *et al.* (269, 270), modified by Heba Al-Siddiqi, a colleague in the lab. Activin-A and Wnt activation using CHIR99021 were used to induce mesoderm formation, whereas IWP4 mediated inhibition of Wnt drives the cells further to cardiac mesoderm.

3.1.2 3D approach: collagen scaffolds

Traditionally, cells are grown in monolayer culture *in vitro* and most focus in literatures lies in the functional assessment of individual cells (patch clamp, action potentials) (275). However, *in vivo* all cells are located within a 3D organ or tissue structure, with cell-cell contact. Hence, for many disease models, single cell characterisation is in-

Table 3.1: ES/iPS cardiac differentiation protocols Adapted from Rajala *et al.* (110).

Method	Efficiency	Stem cell type	Reference
Spontaneous EB method	< 10%	hES	(266)
		hiPS	(267)
END-2 method	20 – 25%	hESC	(268, 271)
(Insulin depletion, PGI_2, p38 inhibition)		hiPSC	(272)
Guided differentiation method	> 30%	hESC	(273)
(Activin A, BMP4)		hiPS	(85)
Guided differentiation method	40 – 50%	hESC	(274)
(Activin A, BMP4, bFGF, VEGF, Dkk-1)			
Guided differentiation method	80 – 98%	hiPS	(269, 270)
(Activin A, CHIR, IWP4)			

sufficient, for example for the study of structural malformation and metabolic toxicity, it makes sense to look at integrated tissues (214).

3.1.3 Aims

In this Chapter, the aim was to determine the gene expression of our iPS-CMs by qPCR and to assess the metabolic phenotype by $^{1}H/^{13}C$ NMR metabolomics. Moreover, the feasibility of culturing iPS-CMs on collagen scaffolds or decellularised hearts (Chapter 4) was investigated to grow 3D constructs for further maturation of iPS-CMs.

3.2 Results

3.2.1 Cardiac differentiation of iPS cells on Matrigel

iPS cells seeded on RF-M, a gelatinous protein mixture derived from Engelbreth-Holm-Swarm mouse sarcoma cells rich in laminin and collagen IV, were differentiated into cardiomyocytes by utilising a differentiation protocol that exploits Wnt modulation (Figure 2.1, Table 2.1). In the first step, hypoxia, matrigel sandwich, activin-A and Wnt stimulation in the absence of insulin are used to generate mesoderm (111, 113, 276). This

step is particularly harsh, since 30 – 70% of the cells die at this stage (Figure 3.1(b)). Two days later, cardiac mesoderm is induced by Wnt inhibition in the absence of insulin (114, 269, 270). Cardiac mesoderm forms beating cardiomyocytes spontaneously around day 10-11, when cultured in normoxia and upon insulin stimulation. The beating pattern at this stage is irregular and varies depending on location within the plate. Indeed, most beating clumps of cells are located at the edge of the plates. With time, the contractile area becomes larger and different areas will start to beat in synchrony (Figure 3.1(d)). Antibody staining for cardiac Troponin-T confirmed that the cells were indeed cardiomyocytes (Figure 3.2). At least some of the cells had the typical elongated morphology, however most did not (Figure 3.2(b)). The efficiency of the protocol is not perfect and for reasons that are not entirely understood, the protocol does not always result in beating cardiomyocytes (Figure 3.3). Unfortunately, it was not possible to enumerate the percentage of Troponin positive cells by flow cytometry, as we failed to generate viable single cell suspensions.

3.2.2 Effect of long term culture of hiPS-CMs on gene expression

iPS cells were differentiated to CMs and the gene expression was assessed using qPCR after harvests at days 7, 12 – 15 or 31 (Table 3.2). Day 7 differentiated cells were used as the reference of the least mature cell type: these cells have formed cardiac mesoderm, but do not have a contractile phenotype. Day 12 – 15 cells represent the cells at the stage of the first contractions. Cells were harvested from two independent batches of differentiation of the same cell line, and three biological replicates of each time point were analysed within each batch using Bayesian model for qPCR analysis (241).

3.2.2.1 Descriptive statistics

Descriptive statistical techniques were used to identify key factors of interest within the gene expression data (Figure 3.4). 90% of the variance in the raw C_t values was explained

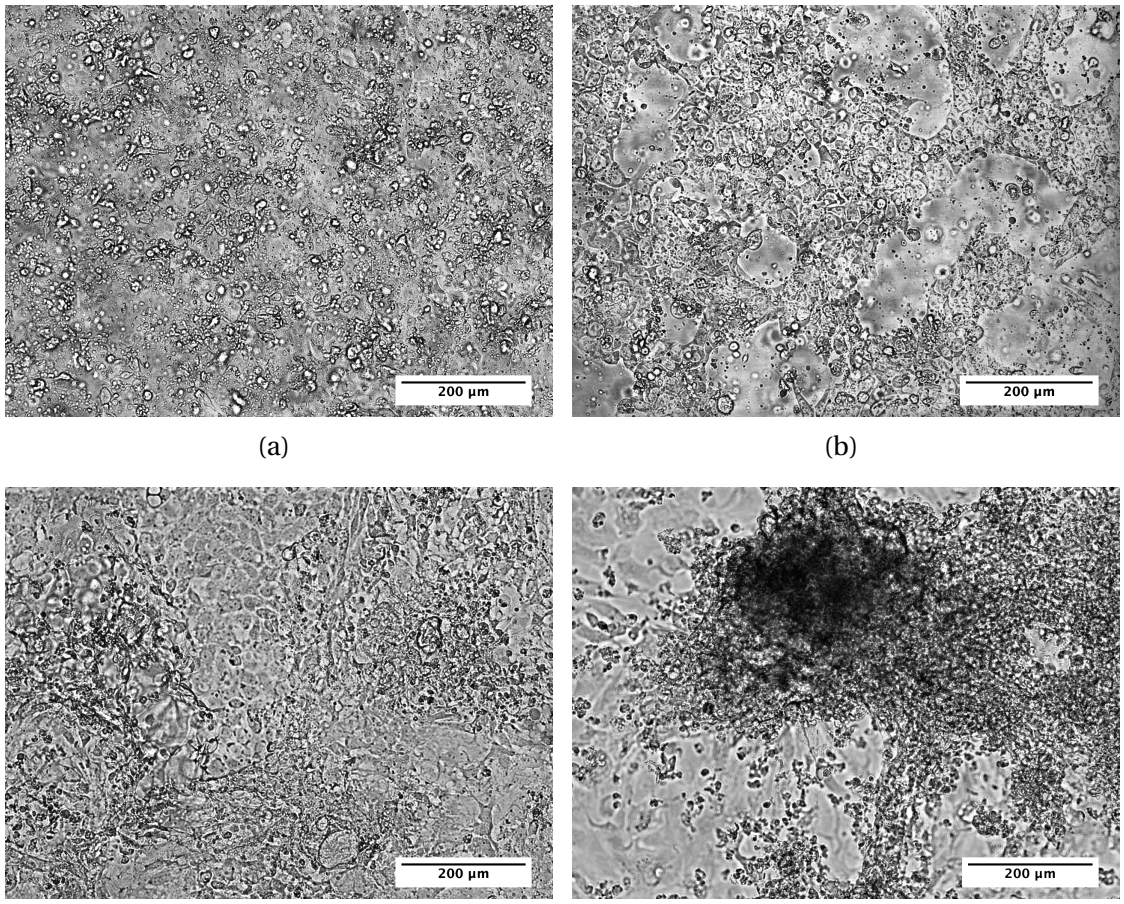
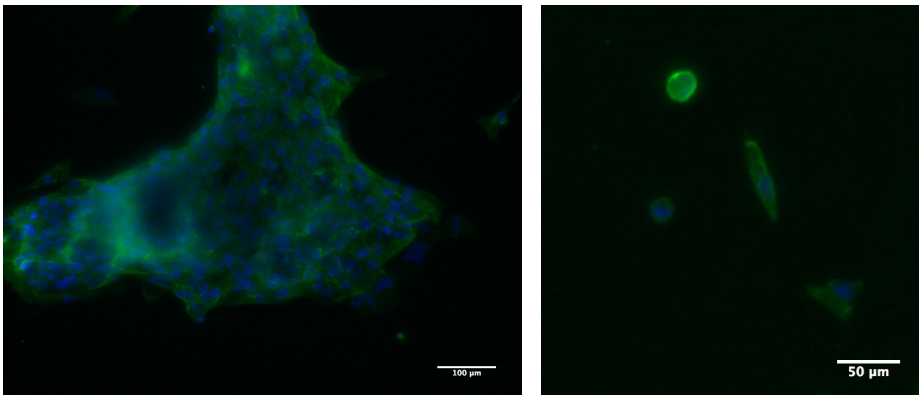


Figure 3.1: Cell morphology changes during differentiation from iPS cell to cardiomyocyte iPS cells were differentiated to CMs and microscopic recordings made at different time points during the differentiation protocol to assess cell morphology. (a) Day 0: fully confluent monolayer, (b) Day 1: considerable loss of cells leading to gaps in the monolayer, (c) Day 11: confluent monolayer and initiation of the formation of small clumps of cells, (d) 4 months post induction of cardiomyocye differentiation: large contractile clumps of cells. Scale bar: 200 µm.

by the first two eigenvalues, according to PCA (245, 277). The first component (explaining 75 – 92%) was dominated by the transcripts of contractile proteins (*MYH6*, *MYH7*) and transcripts for proteins involved in calcium cycling (*SERCA2A*, *PLN*, *CASQ2*). The interpretation of the second component is not as clear cut, since it was also affected by the same factors as component one, and the effect sizes were reasonably small. Nonetheless, the most domiant factors in component 2 were the transcription factor *PGC1A*, the



(a) (b)

Figure 3.2: Cardiac Troponin-T expression in hiPS-CMs iPS cells were differentiated to iPS-CM and subsequently transferred to gelatin-fibronectin coated microscope compatible tissue culture dishes (ibidi µ-slides, Germany). The cells were fixed with PFA and stained with an antibody raised against cardiac troponin-T. (a) Image of a beating cell clump, (b) Image of single iPS-CMs.

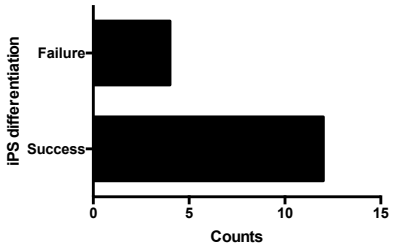


Figure 3.3: Efficiency of the differentiation of hiPS to beating cardiomyocytes. Counts represent independent batches of differentiated cells that either failed or succeeded in forming beating cells. Not every batch that generated contractile cells, contained similar numbers of contracting cells, suggesting that there is considerable variation between different batches of differentiation.

Ca^{2+}-channel *CACNA1D*, the metabolic regulator *PDK4* and the collagen isoforms one and three (Figure 3.4(a)).

PCA and hierarchical clustering also indicate which samples are more similar compared to the others, at least within the context of the applied metric. In PCA analysis, treatment groups can be correlated with principle components. In general, it is clear from Figure 3.4(c) and 3.4(d), that the first PCA dimension governs the difference between day seven on the one hand, and day 12 – 15 and 31 on the other hand.

Table 3.2: List of gene transcripts assessed in the long term culture-induced maturation of hiPS-CMs

Gene transcript	Description
TBP	housekeeping gene
POLR2A	housekeeping gene
HPRT1	housekeeping gene
B2M	housekeeping gene
TNNT2	contractile protein
SERCA2A	calcium handling
RYR2	calcium handling
PLN	calcium handling
NKX2.5	cardiac transcription factor
MYL7	contractile protein
MYH7	contractile protein
MYH6	contractile protein
KCNJ2	channel, KIR2.1
CX43	gap junction
CASQ2	calcium handling
CACNA1D	L-type Ca^{2+} channel
PPARA	metabolic transcription factor
PGC1A	mitochondrial biogenesis
PDK4	regulation of glucose metabolism
IRS2	insulin signalling
IRS1	insulin signalling
GLUT4	glucose transporter
GLUT1	glucose transporter
CS	mitochondrial metabolism
COL3A1	ECM, collagen
COL1A1	ECM, collagen

Additionally, hierarchical clustering analysis was used to compare the similarity between time points. In batch B, the three differentiation time points could be distinguished on the hierarchical clustering plot, whereas there is overlap between one of the samples of the seven day time point (*7b*) and the day 12 group in batch A (Figure 3.4(e) and 3.4(f)). This conclusion was also supported by PCA. Taking into consideration the weight of the second principal component and the distance in the clustering analysis, the raw gene expression data suggests that cells at $12-15$ and 31 days are the most similar and distinct from day seven.

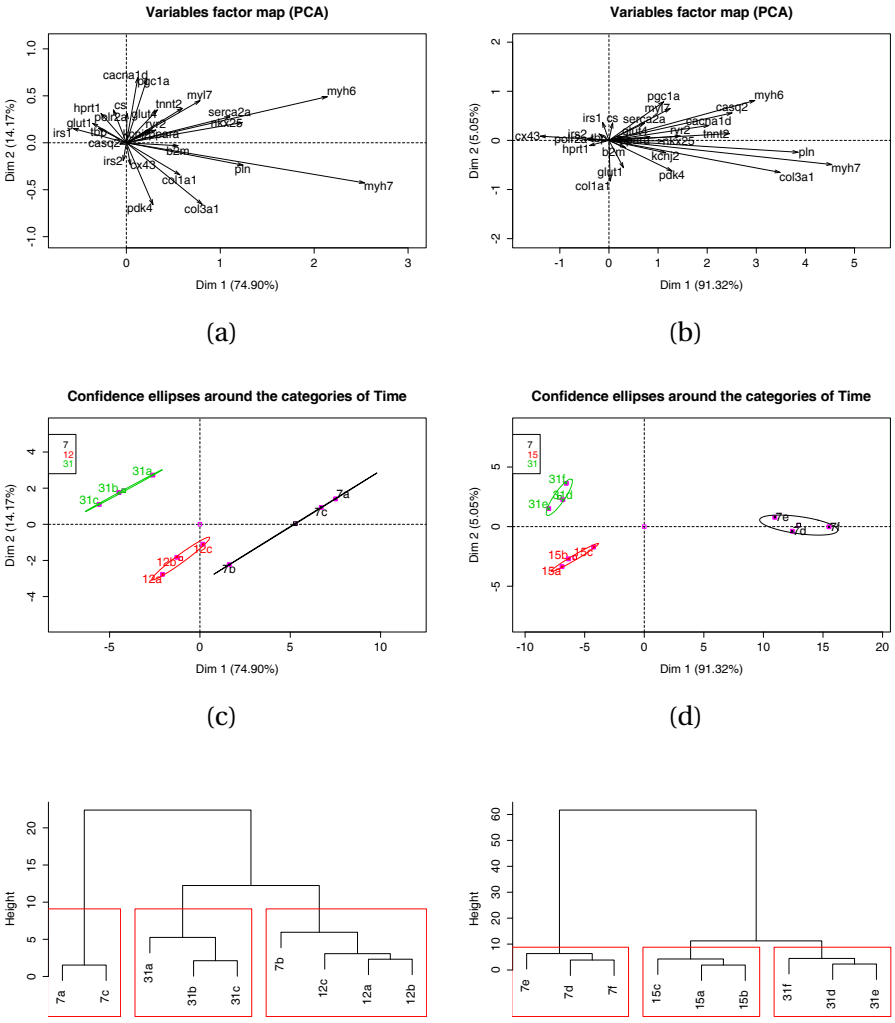
It is not unexpected that the largest variability within the data is between day seven and both days 12 – 15 and 31, since only the cells at day seven did not exhibit a contractile phenotype. Secondly, the observation of the overlap between one of the samples of the day seven group and the day twelve group can be explained by the fact that the cell populations under study are positioned within a spectrum. Indeed, within a biological replicate the population will be comprised of cells ranging from progenitors/stem cells to cardiomyocytes and some replicates within a group may have progressed slightly more than others within the same group, since transition between day seven and 12 – 15 occurs spontaneously and is poorly understood (110). The PCA data also suggests that major differences between and within the groups are dominated by the expression of the myosins, and to a lesser extend by factors that would suggest phenotypical maturations, such as *inter alia* metabolic regulators.

3.2.2.2 Stability of the housekeeping genes and the model

MCMC.qpcr was used to analyse the gene expression data obtained by SYBR green qPCR. This *R*-package allows mixed-effect Bayesian inference on raw C_t values, without the absolute need for housekeeping genes (241). In order to assess the validity of the obtained models, the diagnostic plots were assessed for linearity, normality, homoscedasticity and convergence. Housekeeping genes were used as priors in the model, and their stability was also assessed (Figure 3.5). None of the housekeeping genes were significantly up or down regulated. Nonetheless, *B2M* was excluded as housekeeping gene, given its large variability.

3.2.2.3 Contraction related proteins

Batch A and B had a markedly different gene expression profile in terms of contractile and contraction-associated genes (Figure 3.6).

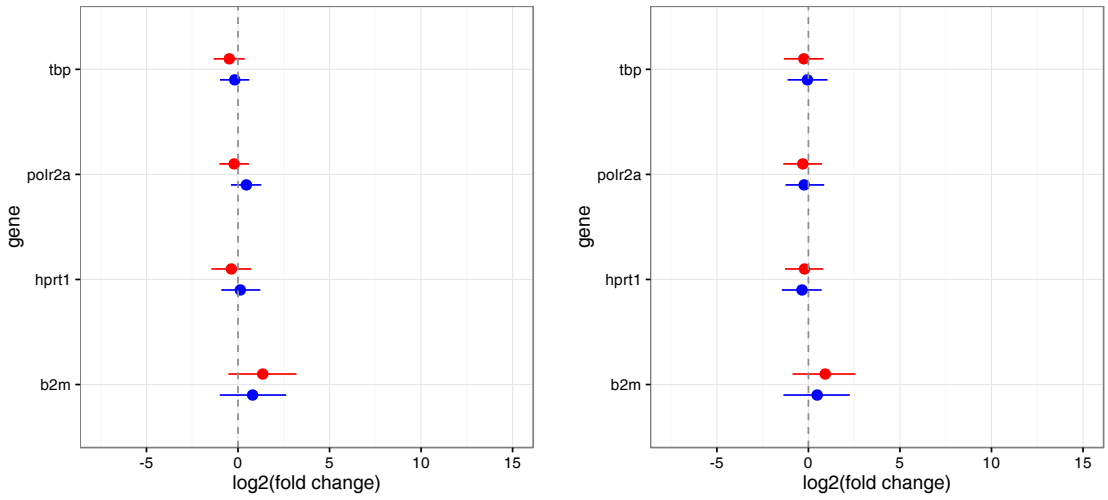


(a) (b) (c) (d) (e) (f)

Figure 3.4: iPS-CM long term culture-induced maturation study: PCA and Hierarchical clustering of qPCR data Raw C_t values were analysed using *hclust* or *PCA* in R (245, 277). (a) PCA, variables map of batch A, (b) PCA, variables map, batch B, (c) PCA, samples map, batch A, (d) PCA, samples map, batch B. The seven day group was represented in black, the 12 – 15 day group in red, and the day 31 group in green. (e) Hierarchical clustering, batch A, (f) Hierarchical clustering, batch B. The samples were clustered into three groups, as indicated in red. The clustering analysis was performed using *hclust* (euclidian distance, ward.D method).

In batch A, only *MYH6*, *MYH7* were upregulated at day 12 and 31 compared to day 7. Additionally, *MYH7* was significantly higher at day 31 compared to day 12.

In batch B, on the other hand, the expression of *TNNT2*, *RYR2*, *PLN*, *MYH6*, *MYH7*,



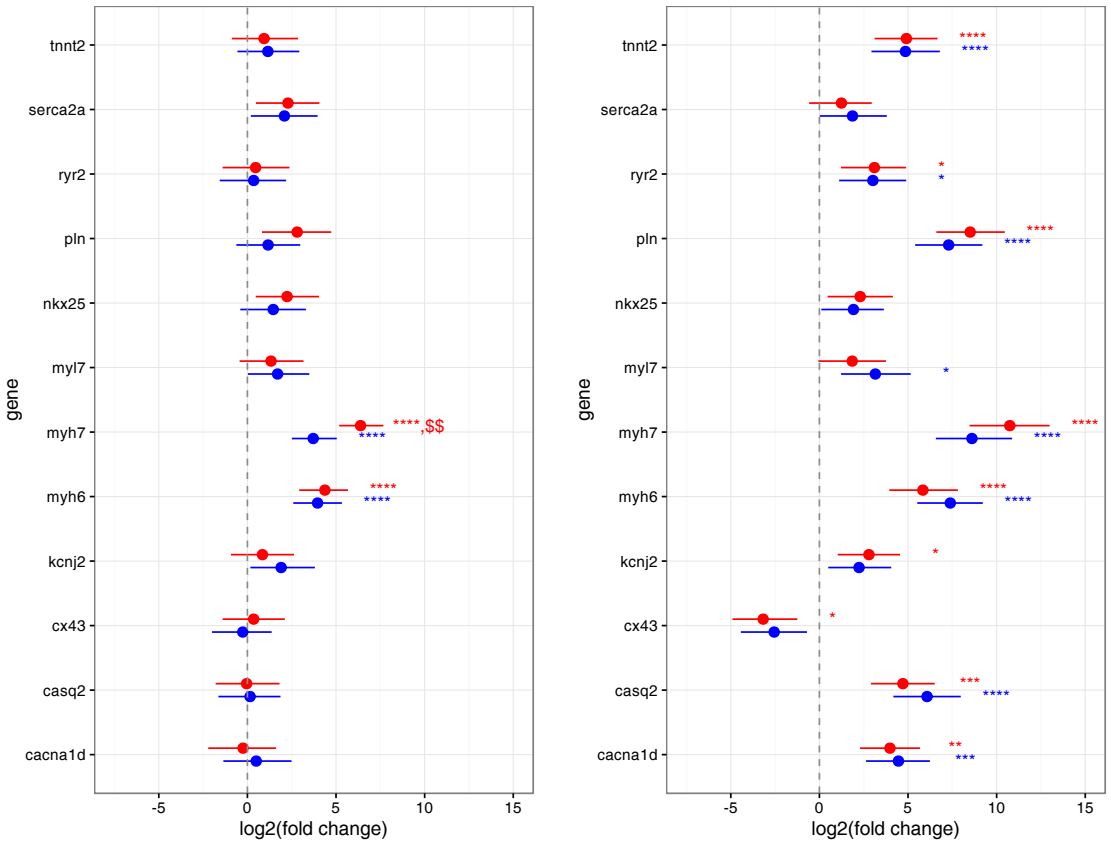
(a) (b)

Figure 3.5: iPS-CM long term culture-induced maturation study: housekeeping gene expression Housekeeping genes were coded as priors in the model, this means that no hard normalisation was applied, but that housekeeping genes were taken into consideration for estimating inter- and intra- sample variability within treatment groups. (a) housekeeping genes expression batch A, (b) housekeeping genes expression batch B. The point represents the mean, and the line the 95% credibility interval. Red represents the 31 days group, whereas blue represents the 12 – 15 days group, compared to do day 7. No significant differences in housekeeping gene expression were observed between groups.

CASQ2 and *CACNA1D* were significantly higher at both day 15 and 31 compared to day 7. The expression of *KCNJ2* was only higher at 31 days compared to day 7, whereas the expression of *MYL7* was only higher at day 15 but not day 31, compared to day 7. The expression of *CX43*, on the other hand, was significantly lower at day 31 compared to day 7.

3.2.2.4 Metabolic proteins

qPCR was performed for peroxisome proliferator-activated receptor gamma coactivator 1 alpha (PGC1A), a transcription cofactor of mitochondrial biogenesis, peroxisome proliferator-activated receptor alpha (PPARA), a transcription factor and metabolic regulator, pyruvate dehydrogenase kinase isozyme-4 (PDK4), the cardiac mitochondrial

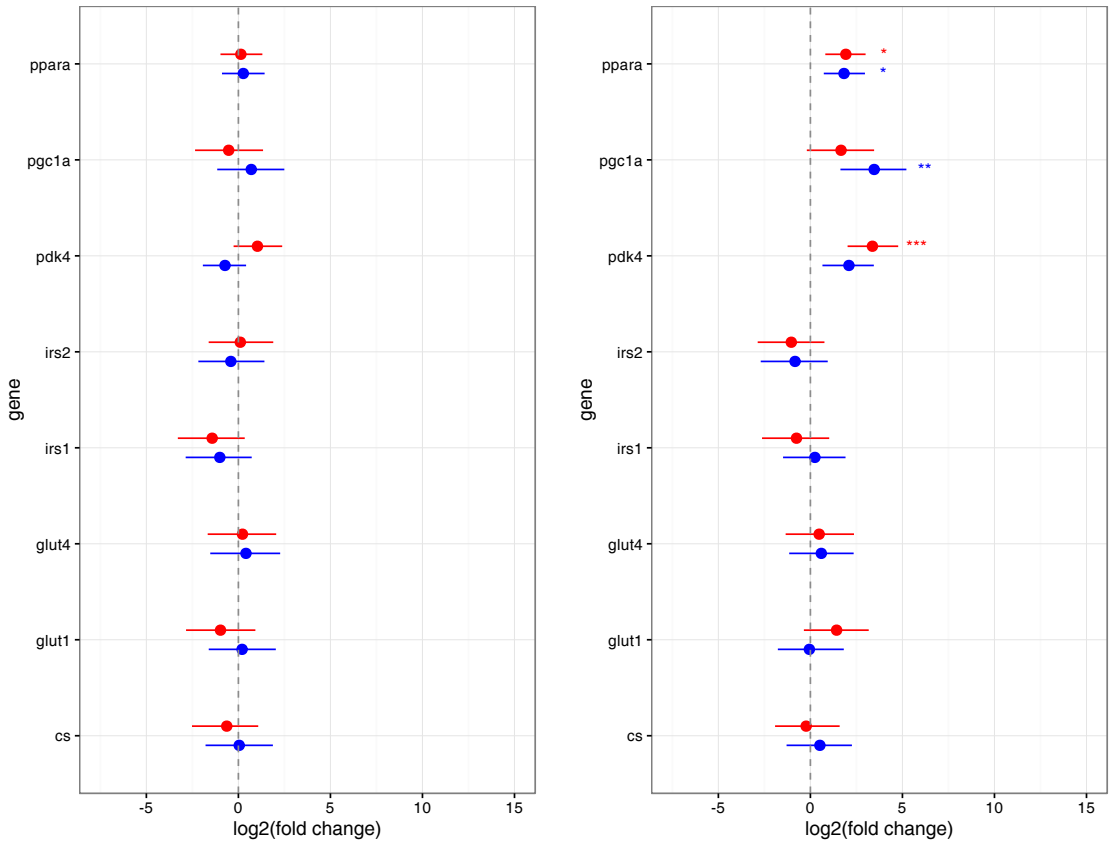


(a) (b)

Figure 3.6: iPS-CM long term culture-induced maturation study: contractile protein expression (a) batch A, (b) batch B. The point represents the mean, and the line the 95% credibility interval. Red represents the 31 days group, whereas blue represents the 12−15 days group, compared to do day 7. The '*' symbol refers to the level of significance for the comparison to seven days differentiation, whereas the '$' refers to the comparison 12 − 15 versus 31 days. '*' denotes $p \leq 0.05$, '**' $p \leq 0.01$, '***' $p \leq 0.001$ and '****' $p \leq 0.0001$ (idem for '$').

regulator of glucose metabolism, insulin receptor substrate-1 (IRS1) and insulin receptor substrate-2 (IRS2), proteins involved in insulin signalling, glucose transporter-1 (GLUT1) and glucose transporter-4 (GLUT4), and citrate synthase (CS).

There is no evidence to suggest that there were any changes in the gene expression of this set of metabolic proteins in batch A. In batch B, on the other hand, the expression of *PPARA* was upregulated at both time points, whereas the expression of *PGC1A* was only higher at 15 days, and *PDK4* was only higher at 31 days compared to day 7 (Figure 3.7).

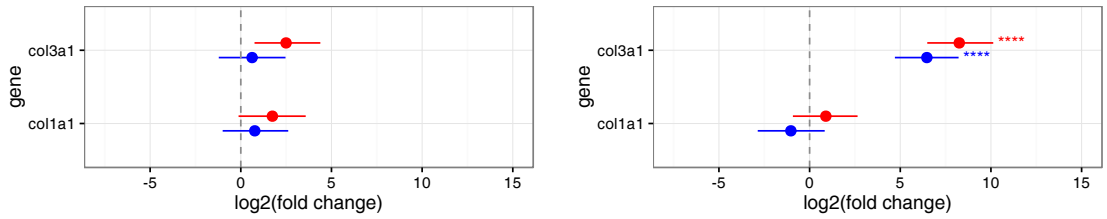


(a) (b)

Figure 3.7: iPS-CM long term culture-induced maturation study: metabolic protein expression (a) batch A, (b) batch B. The point represents the mean, and the line the 95% credibility interval. Red represents the 31 days group, whereas blue represents the 12−15 days group, compared to do day 7. The '*' symbol refers to the level of significance for the comparison to seven days differentiation, whereas the '$' refers to the comparison 12 − 15 versus 31 days. '*' denotes $p \leq 0.05$, '**' $p \leq 0.01$, '***' $p \leq 0.001$ and '****' $p \leq 0.0001$ (idem for '$').

3.2.2.5 Extracellular matrix

Since collagen is the major ECM protein and in the heart collagen I and III are the most abundant, the gene expression of these two proteins was investigated using qPCR. In batch A, there was no significant difference in either the expression of *COL1A1* or *COL3A1*. Whereas in batch B, *COL3A1* was significantly higher at both 15 and 31 days compared to control.



(a) (b)

Figure 3.8: iPS-CM long term culture-induced maturation study: ECM protein expression (a) batch A, (b) batch B. The point represents the mean, and the line the 95% credibility interval. Red represents the 31 days group, whereas blue represents the 12 – 15 days group, compared to do day 7. The '*' symbol refers to the level of significance for the comparison to seven days differentiation, whereas the '$' refers to the comparison 12 – 15 versus 31 days. '*' denotes $p \leq 0.05$, '**' $p \leq 0.01$, '***' $p \leq 0.001$ and '****' $p \leq 0.0001$ (idem for '$').

3.2.3 iPS and iPS-CM metabolism

CMs *in vivo* have a totally different metabolic profile compared to most cells cultured *in vitro*. Cells in culture, including stem cells, gain energy predominantly from glycolysis, whereas adult CMs in the body generate most energy though the oxidative phosphorylation (OXPHOS) of fats.

Since little maturation was observed during prolonged culture *in vitro*, iPS and iPS-CM about one month after initiation of differentiation were compared using qPCR and NMR metabolomics, rather than differentiated cells with or without culture-induced maturation.

3.2.3.1 Metabolic gene expression changes between hiPS and beating iPS-CMs

Gene expression of the metabolic transcription regulators PPARA and PGC1A, the insulin signalling complexes IRS1 and IRS2, the glucose transporters GLUT1 and GLUT4, and the mitochondrial enzyme CS, were compared using the aforementioned Bayesian model for qPCR analysis (241) (Figure 3.9).

Both the gene expression of PPARA and PGC1A were significantly upregulated af-

ter differentiation. Moreover, the gene expression of the ubiquitous glucose transporter GLUT1 and PDK4 were also upregulated, but none of the other transcripts under study were affected.

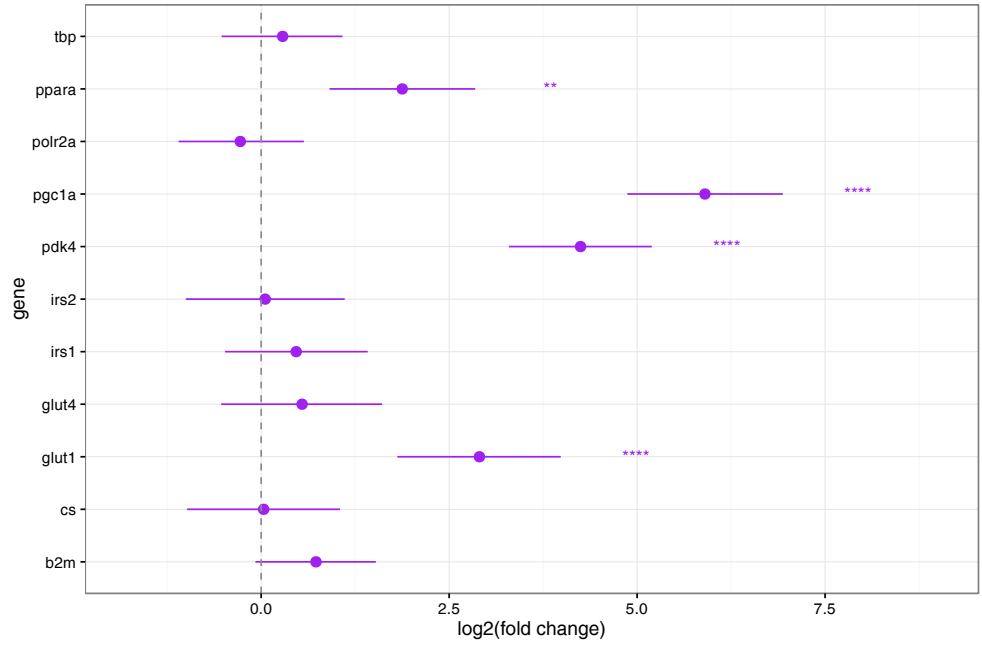


Figure 3.9: hiPS and hiPS-CM gene expression of metabolic proteins The point represents the mean, and the line the 95% credibility interval, of the gene expression fold change between iPS-CM (D31, $n = 3$) and iPS ($n = 4$). '*' denotes $p \leq 0.05$, '**' $p \leq 0.01$, '***' $p \leq 0.001$ and '****' $p \leq 0.0001$.

3.2.3.2 Medium glucose consumption and lactate production

iPS cells have a very glycolytic metabolism (Table 3.3). In a day, the cells consumed 21.8 μmoles of glucose and produced 35.6 μmoles of lactate, which is 1.6 moles of lactate per mole of glucose. Glycolysis can produce at maximum two moles of lactate for each mole of glucose (Section 1.4.3). However, glutamine metabolism also gives rise to lactate secretion. The culture medium of the iPS-CM cells underwent changes in both the glucose and produced lactate concentration (Table 3.3). However, since CMs can also consume lactate, the interpretation of the data is less straight forward.

Table 3.3: hiPS and hiPS-CM glucose and lactate concentration in the culture medium The iPS cells were cultured in six well plates, with daily medium changes (2 mL) and grown to confluency. The iPS-CM cells were cultured in T25 flasks plates, with medium changes every other day (11 mL). Glucose and lactate were measured in the tissue culture media at the day of confluency using the Horiba ABX Pentra 400 serum analyser. Data is expressed as mean ± standard deviation.

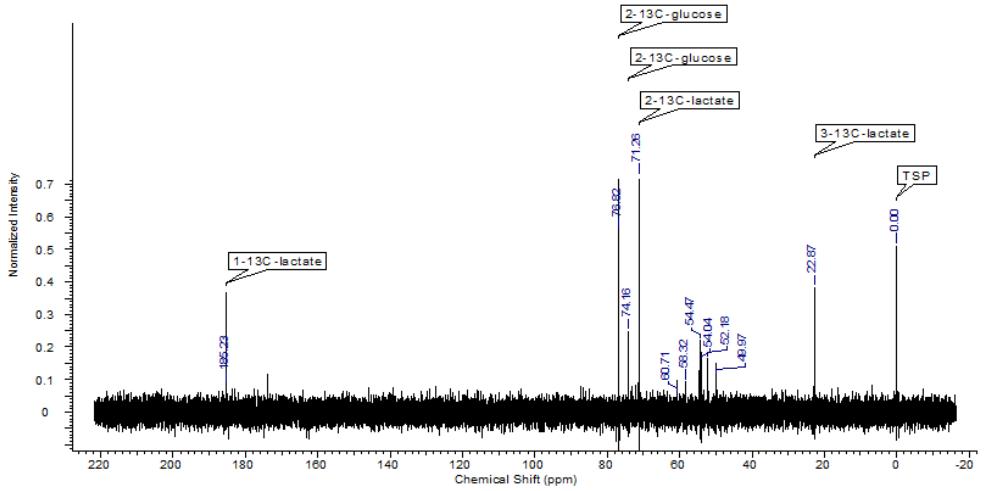
Cell type	Treatment	Glucose (mM)	Lactate (mM)
iPS	mTeSR^{TM}1 media	15.6 ± 0.3	0.0 ± 0.0
	1 Day confluent culture	4.7 ± 0.1	17.8 ± 0.3
iPS-CM	RPMI/B27complete media	12.3 ± 0.1	0.0 ± 0.0
	2 days culture	0.25 ± 0.19	19.3 ± 0.3

3.2.3.3 NMR Metabolomics

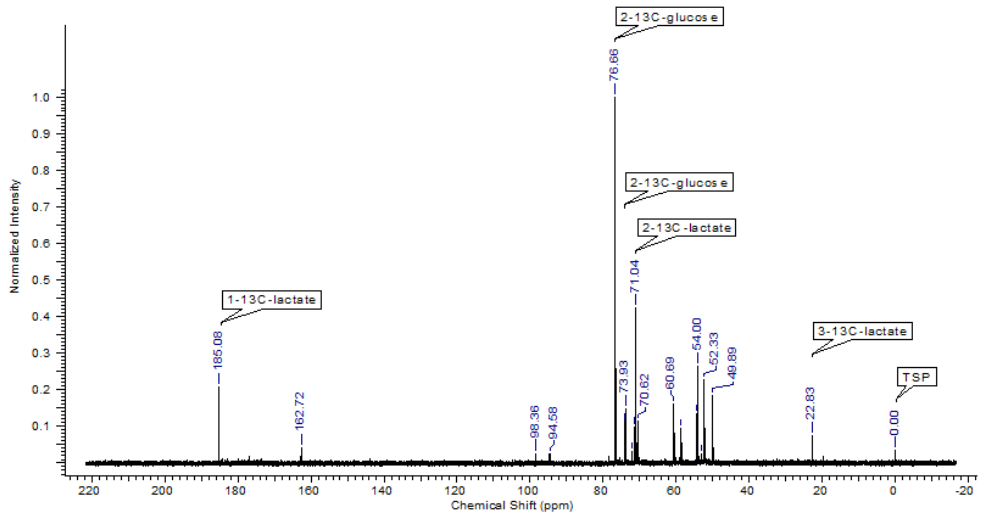
Intracellular relative substrate concentrations may shed more light on the metabolic profile of the generated cells. For this purpose, cells were fed 2-^{13}C glucose, so that ^{13}C NMR could be used to assess how the labelled glucose was processed. Additionally, ^{1}H NMR spectroscopy was used to quantify total metabolite content in the cells. Given the relative insensitivity of NMR, only the most abundant metabolites can be identified and quantified.

Culture media The most intense peaks on the ^{13}C 1D NMR were identified as the labelled glucose and both labelled and unlabelled lactate (Figure 3.10), suggesting that the lactate produced by the cells originated at least in part from the glucose in the medium. This is not unexpected given the medium concentration of lactate, as described in Table 3.3.

Cell content Pyruvate is a central molecule in both glycolysis and glucose oxidation, and can either go into the TCA cycle or can be converted into lactate or alanine. The lactate/alanine (Lac/Ala) ratio, can be quantified from ^{1}H NMR spectroscopy (Figure 3.11), and reflects the NADH/NAD+ equilibrium, since alanine is in rapid equilibrium with



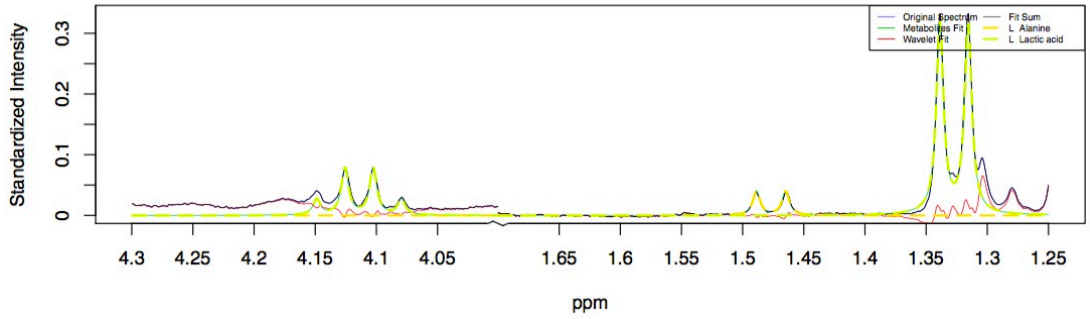
(a)



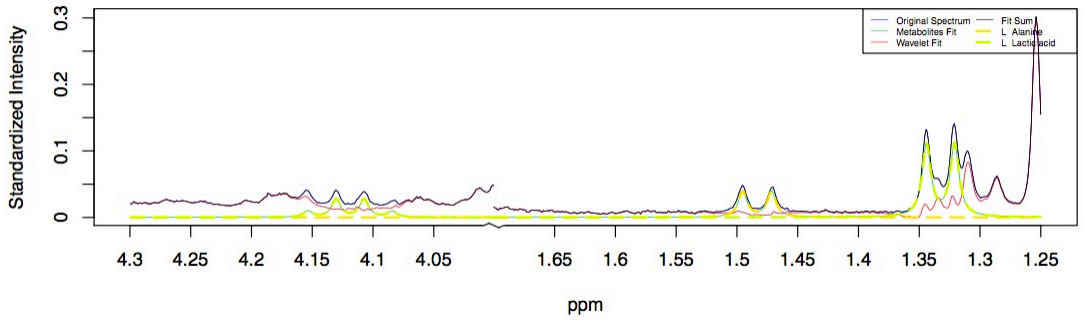
(b)

Figure 3.10: hiPS and hiPS-CM NMR metabolomics: cell media supplemented with 2-^{13}C glucose ^{13}C NMR spectroscopy was used the determine the media composition. The typical 2-^{13}C-glucose resonance peaks are located at 74 ppm and 77 ppm (α and β-D-glucose), whereas the 2-^{13}C-lactate peak is located at 71 ppm. (a) hiPS cells, (b) hiPS-CM cells.

pyruvate via a transamination reaction (278, 279). The Lac/Ala ratio was significantly lower in iPS-CMs compared to iPS cells (Figure 3.12).



(a)



(b)

Figure 3.11: hiPS and hiPS-CM NMR metabolomics: intracellular metabolites ^{1}H NMR spectroscopy was used the quantify total metabolite content in the cells. Peak integrals relate to product mass, the analysis software used here (*batman*, (244)) applied Lorentzian curve fitting. The doublet at 1.32 ppm and the quartet at 4.1 ppm refer to L-lactate (green), whereas the doublet at 1.46 ppm belongs to L-alanine (yellow). L-alanine has an additional quartet at 3.67 ppm, however given the small quantities of L-alanine fitting of this multiplet was omitted. (a) hiPS cells, (b) hiPS-CMs.

3.2.4 Culture of iPS-CMs on different ECM substrates

iPS cells are typically differentiated on RF-M, since standard Matrigel contains a variety of growth factors that prevent or limit differentiation. However, to translate the iPS-CMs to collagen scaffolds or decellularised hearts, Matrigel is not appropriate. Hence, the feasibility of subculturing beating iPS-CMs on other ECM substrates, such as collagen I, gelatin, fibronectin or mixtures of these, was studied (Table 2.2).

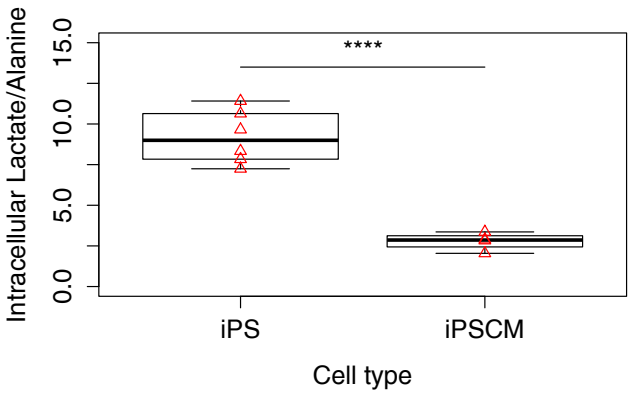


Figure 3.12: hiPS and hiPS-CM NMR metabolomics: intracellular Lactate to Alanine ratio Cells were washed with DPBS, lysed and extracted with chloroform-methanol-water. The water fraction was freeze dried and the metabolites quantified using NMR (244). The data was analysed using the Welch Two Sample t-test (245). '*' denotes $p \leq 0.05$, '**' $p \leq 0.01$, '***' $p \leq 0.001$ and '****' $p \leq 0.0001$.

3.2.4.1 All ECM conditions are able to support the culture of beating iPS-CMs

Beating iPS-CM were harvested from a five independent batches of differentiated iPS cells and replated on ECM coated surfaces. iPS-CM were able to form beating clusters in all ECM conditions (Figure 3.13).

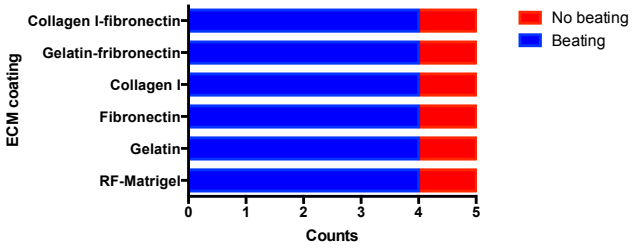


Figure 3.13: Culture of hiPS-CMs on ECM substrates: success rate of forming beating cells The reseeding experiment was repeated five times with independent batches, and the success rate of replating beating cells was counted and graphically represented. Counts are the number of independent experiments that led to either beating (blue) or no beating cells (red).

3.2.4.2 Gene expression of hiPS-CMs on different ECM substrates

The cells were harvested for RNA extraction five days post replating on the different ECM substrates. qPCR analysis was performed for the expression of *POLR2A*, *TBP*, *MYH6*, *MYH7* and *TNNT2*, and the groups were compared using the aforementioned Bayesian model for qPCR analysis (241) (Figure 3.14). There were no significant differences between the different groups post seeding, although most groups did have increased *MYH7* and *TNNT2* expression, compared to before reseeding.

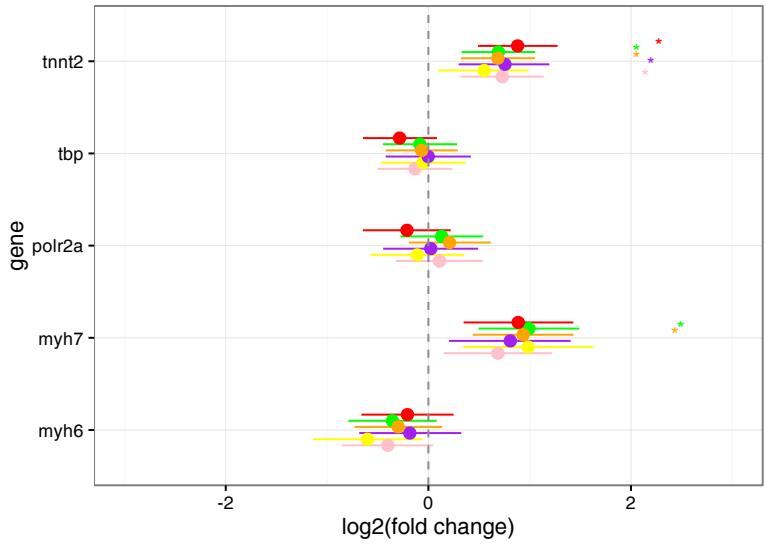


Figure 3.14: Gene expression of hiPS-CMs cultured on a variety of ECM substrates The point represents the mean, and the line the 95% credibility interval, of the gene expression fold change between iPS-CM cultured on a variety of ECM substrates and the cells before seeding. Colour coding: Gelatin-Fibronectin: green, Gelatin: orange, Fibronectin: purple, RF-Matrigel: red, Collagen: pink, Collagen-Fibronectin: yellow. Gene expression is expressed relative to the cells of the same batch before seeding on the various ECM substrates. '*' denotes $p \leq 0.05$, '**' $p \leq 0.01$, '***' $p \leq 0.001$ and '****' $p \leq 0.0001$ versus the cells of the same batch before seeding on the various ECM substrates.

3.2.5 Culture of iPS-CMs on collagen scaffolds

Since it was feasible to culture beating iPS-CM on ECM substrates other than RF-M, the possibility to culture the iPS-CM cells on cup-shaped or disc-shaped collagen scaffolds

was investigated. Collagen was chosen as ECM material since it is the most abundant ECM protein in the heart. Biventricular cup-shaped collagen scaffolds (Figure 2.3(a)) were designed as a primer or alternative to decellularised hearts (Chapter 4) to develop the humanised Langendorff setup, and in an attempt to make cell seeding more efficient as the seeded cells are largely confined to the inside of the cup.

Beating iPS-derived cardiomyocytes from three independent differentiation batches were harvested using the collagenase-trypsin method as described above and seeded on collagen scaffolds (cup or disc-shaped) or gelatin-fibronectin coated well plates. Histological analysis revealed that the cardiomyocytes formed small clusters, predominantly on the surface of the scaffold, and occasionally throughout the entire thickness of the scaffold (Figure 3.15(a) and 3.15(b)). Contractile clusters could be identified by light microscopy at the scaffold edges.

Four to seven days post seeding, the scaffolds were harvested and RNA extracted for qPCR analysis (Figure 3.15). Unfortunately, scaffolds prohibit the visual inspection of the cells seeded and not all seeded scaffolds yielded sufficient RNA to allow qPCR analysis. Nonetheless, *MCMC.qpcr* was used to analyse the gene expression data using mixed-effect Bayesian inference of those scaffolds that allowed further analysis (241). Since iPS differentiation may suffer from considerable batch to batch variability in differentiation efficacy, the batch was used as random effect in the qPCR analysis. The housekeeping genes were used as priors in the model. No significant difference in gene expression of the contractile proteins *MYH6*, *MYH7* and *TNNT2* were observed in iPS-CMs cultured on gelatin-fibronectin coated plates or collagen scaffolds, compared to the harvested differentiated cells (Figure 3.15(c)), suggesting the feasibility of maintaining iPS-CMs on collagen scaffolds, albeit possibly at lower efficacy compared to gelatin-fibronectin coated plates.

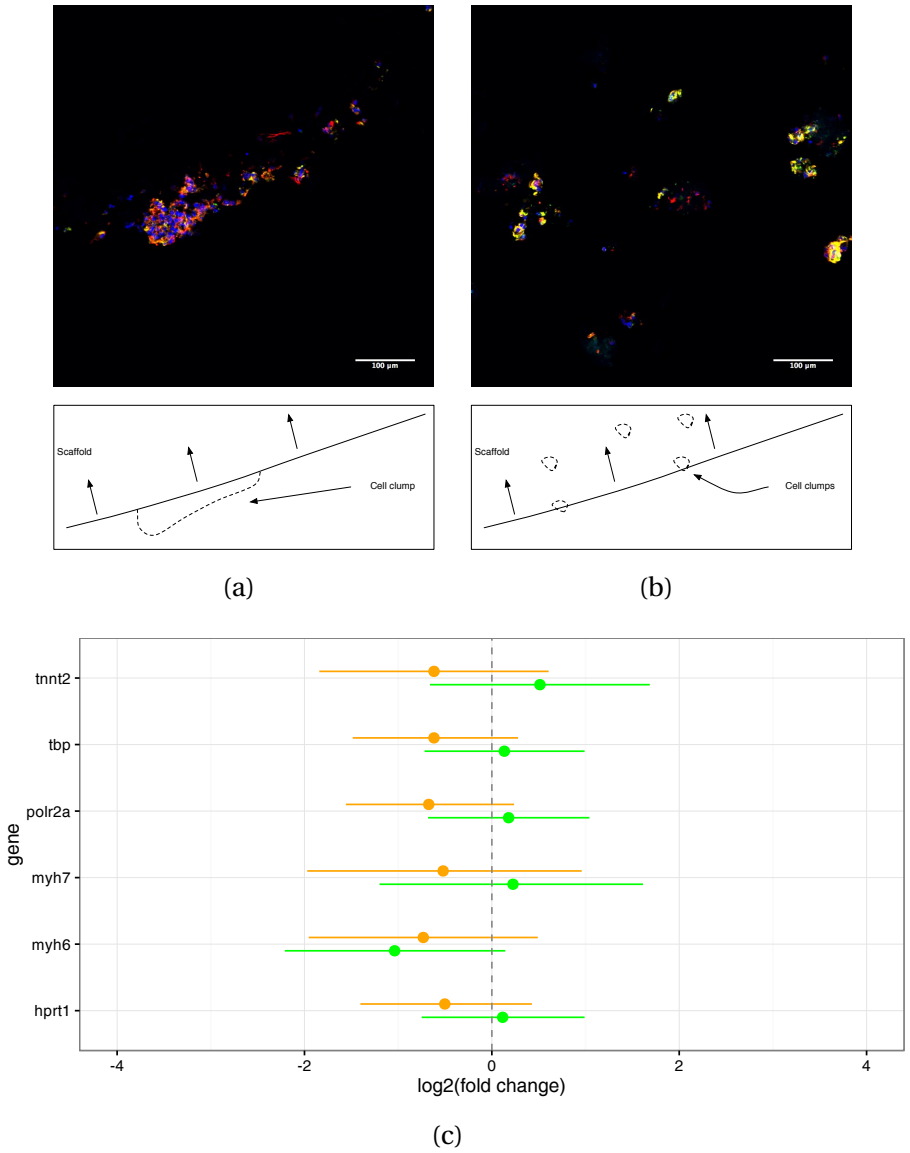


Figure 3.15: iPS-CMs on collagen scaffolds: histology and qPCR (a,b) Cross-sectional histology on a 15 day old iPS-CM-seeded disc-shaped collagen scaffold. The sample was fixed in PFA, equilibrated in 30 % sucrose, embedded in OCT and cryosectioned (10 µm). The slices were stained for nuclei (DAPI, blue), cardiac troponin-T (green), and filamentous actin (Rhodamine Phalloidin, red). The cardiomyocytes grew in small clumps predominantly on the surface of the scaffold (a), but in some instances also in deeper layers of the scaffold (b). Scale bar: 100 µm. (c) qPCR analysis of iPS-CM cultured on collagen scaffolds or gelatin-fibronectin coated wells plates, compared to the differentiated cells pre-seeding, using Bayesian mixed effect inference. The point represents the mean, and the line the 95% credibility interval of the posterior distribution. Green represents the gelatin-fibronectin group, whereas orange represents the scaffolds group.

3.3 Discussion

iPS cells and their differentiated derivatives have been proposed as models for human disease or as potential strategies for regeneration. In this Chapter, human iPS cells were differentiated to beating cardiomyocytes and their gene expression was assessed using qPCR. First, we investigated the effect of prolonged culture on gene expression and whether genetic maturation could be induced by prolonged culture. Second, the metabolic phenotype of the cells was determined using $^{1}H/^{13}C$ NMR metabolomics. Finally, the cells ability to grow on a variety of ECM substrates and collagen scaffolds was determined.

3.3.1 Cardiac differentiation of iPS cells and maturation by long-term culture

We successfully generated beating cardiomyocytes, but did observe considerable variability between different batches, and not every batch generated beating cells. This was not unexpected, since it is well known that iPS differentiation efficacy and gene expression profile varies between different cell lines and between batches of the same cell line (280). However, this factor of unexplained noise does complicate the analysis and interpretation of the acquired data. For this reason, we performed qPCR analysis on iPS-CMs derived from two independent batches to assess maturation of the gene expression profile. However, for further studies we propose to use more technical and biological replicates and mixed-effects models to more adequately take into consideration batch-to-batch variability. In addition, the proportion of cardiomyocytes within the batch, as determined by flow cytometry, could be taken into account when assessing the total gene expression by qPCR. Or alternatively, methods to purify cardiomyocytes may be applied (123, 124).

From both the clustering analysis and the gene expression analysis, it is clear that in

batch B the effect on gene expression of gaining a contractile phenotype is the largest. Nonetheless, there is little difference between the early (12 – 15 days) and late (31 days) contractile phenotype in terms of gene expression, which confirms the hypothesis that iPS-CMs have an immature phenotype and undergo little maturation. Similarly, Piccini *et al.* (281) performed transcriptome analysis on human pluripotent stem cell derived CMs and only observed marginal differences between 4 weeks and 8 week-old CMs, suggesting that indeed long-term culture induced maturation is minimal. Kehat *et al.* (266) observed more organisation in the sarcomeres when the EB get older. We did not perform any sub-cellular resolution analysis of the maturing cardiomyocytes, but did observe the formation of clusters. The observation that the cells form contracting clusters during the differentiation process, correlates with the upregulation of *COL3A1*.

RyR2 controls the SR Ca^{2+} during contraction, and is key to CICR from the SR. Whereas, in human adult myocardium, the SR is the main intracellular Ca^{2+} store, in the fetal heart, the SR is structurally and functionally underdeveloped. Hence, fetal cardiomyocytes are mostly dependent on L-type calcium channels and transsarcolemmal Ca^{2+} influx for contraction (282). This suggests that RyR2 could be a target for maturation. The expression of *RYR2* was unchanged in batch A, but upregulated after gaining a contractile phenotype in batch B, and there was no difference between day 12 – 15 and 31.

CASQ2, is also involved in CICR, and has been linked to maturation (283). Jung *et al.* (284) generated cardiomyocytes using the EB method, matured them for a couple of months *in vitro*, and observed nearly undetectable levels of *CASQ2*, when compared with adult and fetal human heart, normalised to *TNNT2*. In this study, upregulation of *CASQ2* was only observed in batch B, but there was no difference between day 12 – 15 and 31.

The gap junction protein connexin 43 (Cx43) helps to mediate the exchange of low-molecular-weight metabolites and ions between contacting cells (285) and Cx43 is the main connexin expressed by cardiomyocytes. Connexin 40 (Cx40) and connexin 45

(Cx45) are also expressed by some cardiomyocytes (286). Indeed, ventricular cardiomyocytes typically lack Cx40, whereas atrial cardiomyocytes express Cx40. Pacemaker cells such as these of the sinoatrial or atrioventricular node express Cx45, whereas the cardiomyocytes of the His-Purkinje conduction system express Cx40. Here, we were predominantly interested in ventricular cardiomyocytes and hence only Cx43 was quantified. In batch A of the study no alterations in *CX43* were observed, whereas in batch B a significant reduction was present. Although Cx43 has been linked to maturation of cardiomyocytes by electrical coupling of cells, it is important to note that cardiomyocytes are not the only cells that express Cx43. In particular, Cx43 has been linked to pluripotency since it acts downstream of Oct4, Sox2 and Nanog (287). Additionally, ectopic expression of Cx43 enhances the reprogramming efficiency, whereas RNAi knockdown of Cx43 reduces the efficiency (288).

Insulin signalling plays a dominant role in both the differentiation for iPS to cardiomyocytes (289) and in the regulation of glucose metabolism, hence the gene expression of IRS1 and IRS2 was determined during maturation of iPS-CMs. IRS1 and IRS2 play important roles in both skeletal and heart muscle growth and metabolism (290). Cardiac double knock-out of IRS1 and IRS2 causes heart failure (291). No alteration of the level of *IRS1* and *IRS2* expression was observed upon addition of insulin to the medium or with maturation of cardiomyocytes in either of our batches of cells. The GLUTs play an important role in glucose metabolism since they transport glucose across the cell membrane. GLUT1 is always present, whereas GLUT4 is insulin-dependent. The gene expression of GLUT1 and GLUT4 was unaffected by insulin supplementation and maturation of the cells.

In terms of mitochondrial metabolism, the gene expression of PPARA, PGC1A, PDK4, and CS were assessed. PPARA binds to and is activated by numerous fatty acids and fatty acid-derived compounds, and altering the expression of a large number of target genes (292, 293). PGC1A is a transcription co-activator involved in mitochandrial biogenesis.

PDK4 is a regulator of glucose oxidation, and can inhibit the pyruvate dehydrogenase (PDH) complex by phosphorylating, and hence reducing the conversion of pyruvate to acetyl-CoA. In batch A, the gene expression of none of these proteins was affected, whereas in batch B, the expression of the transcription factors *PPARA* and *PGC1A* was upregulated. *CS* was unaffected, whereas *PDK4* was also upregulated. *CS* expression is a common marker of mitochondrial biosynthesis. Hence, there was no evidence to suggest that mitochondrial proliferation occurred, even though *PPARA* and *PGC1A* were expressed. However, no fatty acids were supplemented to the culture media in the current study, hence it is possible that fat supplementation would activate PPARA signalling and give the cells a more significant metabolic phenotype.

Lundy *et al.* (294) assessed long term culture induced maturation by comparing ES and iPS cardiomyocytes after $20-40$ days or $80-120$ days of differentiation, which is considerably longer than this study. The aged cells were considerably larger, less spherical, and more likely to be multi-nucleated. In terms of gene expression, *MYH6*, *MYH7*, and *SERCA2A* were upregulated, whereas the expression of the K^+ inward rectifier *KCNJ2* showed no difference.

Chemical methods have been proposed for iPS-CM maturation. T3 treated cardiomyocytes were larger and generated more force after one week of T3 treatment (295). Moreover, the gene expression of MYH6 and SERCA2A was increased, whereas the expression of MYH7 was decreased. In terms of metabolism, no increase in total mitochondrial mitochondrial genome was observed, nonetheless the maximal mitochondrial respiratory capacity and respiratory reserve capability were significantly increased after T3 treatment.

To summarise, from the point of gene expression, gaining a contractile phenotype coincided with significant increases in multiple contractile proteins. However, little maturation was observed when day 31 cells were compared with day 12-15 cells. Moreover, it is clear that batch A and B were very different. The difference can be explained by

differences in yield per batch and hence the ratio of cardiomyocytes to non-cardiomyocytes. For this reason, we believe that cardiomyocyte differentiation efficacy may be a confounder in any experiment. Hence, strategies for optimising differentation consistency are required. In the meanwhile, we believe it is paramount to look at data from multiple independent batches of experiments, rather than at only multiple biological replicates of the same batch to identify true differences, which are valid not only within, but also across different batches.

3.3.2 Metabolism

Given the importance of a mature and functional metabolism in iPS-CMs, the gene expression of a variety of transcripts involved in cell metabolism was quantified and the metabolic phenotype determined using biochemical metabolite analysis and $^{13}C/^{1}H$ NMR.

The expression of *PPARA*, *PGC1A*, *PDK4* and *GLUT1* was higher in iPS-CMs compared to iPS cells. The expression of *IRS1*, *IRS2*, *GLUT4* and *CS* was unaffected. This suggest that the required factors for mitochondrial biosynthesis and OXPHOS were upregulated. However, the lack of any change in *CS* expression suggests that mitochondrial number was likely to be unaffected, and the lack of alterations in *IRS1/2* and *GLUT4* suggests that the iPS-CMs were insensitive to insulin-dependent regulation.

The culture metabolite results also suggested that lactate was the main export product of glucose metabolism. However, the ^{1}H NMR metabolics experiment suggested that intracellular lactate to alanine was reduced in iPS-CMs compared to iPS cells, which can imply that less pyruvate was converted into lactate to regenerate NAD+, and that glycolysis was less dominant in the metabolism of the cell. Pereira *et al.* (296) also observed a reduction in the Lac/Ala ratio upon differentiation of the H9c2 skeletal myoblast cell line. Rana *et al.* (213) determined the relative contributions of OXPHOS and glycolysis to ATP production in iPS-CMs using the Seahorse extracellular flux analyser, and con-

cluded that in glucose media with or without fatty acid (FA) supplementation, the cells mainly relied on glycolysis for ATP generation. Whereas, iPS-CMs cultured in galactose media with or without FA supplementation relied primarily on OXPHOS. Further experiments, such as metabolic flux analysis using radio-labelled substrates, are required to more accurately determine the contribution of glycolysis and OXPHOS to ATP generation.

Metabolism has also been shown to be involved in the differentiation potential of ES cells to form cardiomyocytes. Chung *et al.* (122) demonstrated that switching from merely anaerobic glycolytic metabolism into a mitochondrial oxidative metabolism is essential for cardiac specification and excitation-contraction coupling. Cardiomyocytes had upregulated expression of mitochondrial respiratory chain-associated, lipolysis and fatty acid oxidation related genes (122). Unfortunately, the authors did not assess CS, PPARA and PGC1A gene expression levels.

To summarise, the gene expression data suggests that the expression of two transcription factors involved in OXPHOS, *PPARA* and *PGC1A*, were upregulated. However, metabolic experiments suggest that anaerobic glycolysis still remained the main consumer of glucose, albeit potentially to a lesser degree in iPS-CMs.

3.3.3 ECM and scaffolds

iPS cells are cultured and differentiated on matrigel, a biological and ill-defined substrate. For translation to 3D structures, such as scaffolds and decellularised heart, the cells would have to be either differentiated within the 3D organoid, or seeded onto the scaffold before the differentiated phenotype has been acquired.

In some studies stem cells have been differentiated into CMs within the scaffold or decellularised heart (297). However, given the batch to batch variability and the limited capability to monitor the cells within the scaffolds, pre-differentiation and reseeding was chosen rather than *in situ* differentiation. We demonstrated that iPS-CMs can be

dissociated and replated on a variety of substrates, including collagen scaffolds. There was a significant, but small, increase in *TNNT2* and *MYH7* expression after replating the cells into new plates, suggesting that either maturation or selection took place when the cells were replated. The major hurdle in this experiment was setting up a suitable dissociation protocol, however we determined that a combination of collagenase and diluted trypsin allowed the dissociation of the cells into small clumps, enabling them to be reseeded. It was already well understood that the ECM proteins that we studied can be used for the culture of immature CMs (298).

Solid porous scaffolds were chosen here as material as they closely mimic the decellularised heart, proposed to develop a perfusable contractile heart *in vitro* testbed, in structure and seeding technique. Histological analysis revealed that the cardiomyocytes seem to adopt a similar morphology on the collagen scaffolds as they do initially in monolayer culture: the formation of small contractile clumps. The observation that mainly the surface was covered with cells is not unanticipated since we acquired similar results with CDCs (178). Moreover, it is well established that deeper layer cell seeding of solid preformed scaffolds is inefficient, and depends on both the pore size and the interconnectivity of the pores of the scaffold (201). However, cells secrete enzymes capable of remodeling the ECM, such that over time the innoculated scaffold will be degraded and replaced by cell-secreted matrix, suggesting that with time deeper layers may be colonised.

3.4 Conclusion

In this Chapter, the gene expression changes in iPS-CMs with prolonged culture and the feasibility to culture the cells on other ECM substrates and collagen scaffolds was assessed, as a primer to the recellularisation of decellularised hearts. Using qPCR and NMR-based metabolomics, we found that the iPS-CM cultures show little gene expres-

sion maturation with prolonged time in culture. Secondly, protocols were developed to subculture beating iPS-CMs which made it feasible to culture beating cells on a variety of ECM substrates, including collagen scaffolds.

CHAPTER 4

DECELLULARISATION OF ISOLATED RAT HEARTS

4.1 Introduction

Decellularisation offers great potential to the field of tissue engineering since it allows the generation of scaffold material with native organ structure and vasculature by washing out the cellular material and retaining the ECM. Hence, this technology was chosen here to provide scaffold material for generating humanised Langendorff perfused hearts as an *in vitro* model system for studying stem cell derived cardiomyocytes in 3D. In addition, it is believed that residual ECM proteins may stimulate seeded cells and aid in their differentiation and maturation (299, 300).

4.1.1 Decellularisation methods

Even though only decellularised matrices from hollow or tube shaped organs have started to enter the clinic, protocols to generate decellularised ECM matrices from almost any organ have been published (182, 301). The methods vary hugely in complexity and length. In general, physical, chemical and enzymatic methods can be distinguished,

and the solutions used for decellularisation are either perfused into the vasculature, or the tissues are merely submerged into the solvent (182, 301). Perfusion through the vascular circuit of the organ is a neat and effective approach for many organs given the widespread distribution of capillaries within the organ, and is superior to submerged agitation (302). For an organ or tissue to be considered decellularised, the criteria of absence of nuclei (< 50 ng double stranded (ds) DNA per mg ECM dry weight, < 200 base pairs (bp) DNA fragment length, lack of visible nuclear material in histological sections) is typically applied (182). However, there is considerable variability in literature with respect to the degree of decellularisation obtained, and this criterion is not always met.

4.1.1.1 Physical methods

Physical methods do not immediately lead to the removal of cellular material, but they do aid in the lysis and dislodgment of the remnants (182, 301). Rapid freezing results in intracellular ice crystals formation and causes cell disruption and lysis. High hydrostatic pressure has been shown to lyse cells (303). In addition, mechanical agitation and sonication also aids in cell lysis and removal (304).

4.1.1.2 Chemical methods

Chemical treatments form the most important part of the decellularisation and may lead to cell removal by different mechanisms.

First, detergents are the predominant class of chemicals used in decellularisation, three types of detergents are typically distinguished: ionic, non-ionic and zwitterionic detergents (305). Ionic detergents (i. e. SDS and sodium deoxycholate) are the most effective for solubilising cell membranes, but also cause damage to the ECM. Non-ionic detergents (i. e. TX-100) are considerably milder for the tissue and are also commonly used. Secondly, alternation of hypotonic and hypertonic treatment leads to cell lysis by osmotic shock and has been reported to be appropriate for decellularisation of some

tissues (306, 307). Third, alkalis and acids solubilise cellular material, but are also capable of causing considerable damage to the ECM. As a result, these are infrequently used, with the exception of peracetic acid (PAA), which is frequently used to disinfect decellularised tissue (182, 308).

4.1.1.3 Enzymatic methods

Enzymes have very high specificity in degrading certain components. Proteases can be used, but may lead to cleavage of collagen and other ECM components (182, 301). Some decellularisation protocols utilise protease inhibitors to limit ECM damage as a result of proteases released by the tissue. Nucleases, on the other hand, catalyse the hydrolysis of DNA and RNA, and are frequently used in the final step of the process.

4.1.2 The mechanism of decellularisation

The underlying physical mechanism of decellularisation is not well characterised, but can be considered a fluidic dynamic process in which typically a detergent solvent is used to extract soluble cellular matter from the tissue by diffusive/convective mass transfer (Figure 4.1).

Mass transfer is crucial in decellularisation. Alteration in mass content ($\frac{\partial y_i}{\partial t}$) in a voxel is determined by the sum of the amount of new mass generated, the amount transferred by diffusion and the amount transferred by convection:

$$\frac{\partial y_i}{\partial t} = \underbrace{\frac{w_i}{\rho}}_{\text{production}} + \overbrace{D_i \bigtriangledown^2 y_i}^{\text{diffusion}} - \underbrace{\bigtriangledown \cdot (y_i \vec{v})}_{\text{convection}}, \tag{4.1}$$

with w_i the mass-production rate per unit volume by chemical reaction, and D_i is species diffusivity. Hence, fluid flow might considerable contribute to the efficiency of decellularisation. Generally speaking, fluid flow is proportional to a driving force and inversely proportional to the flow resistance. Bernoulli's equation explains flow across a

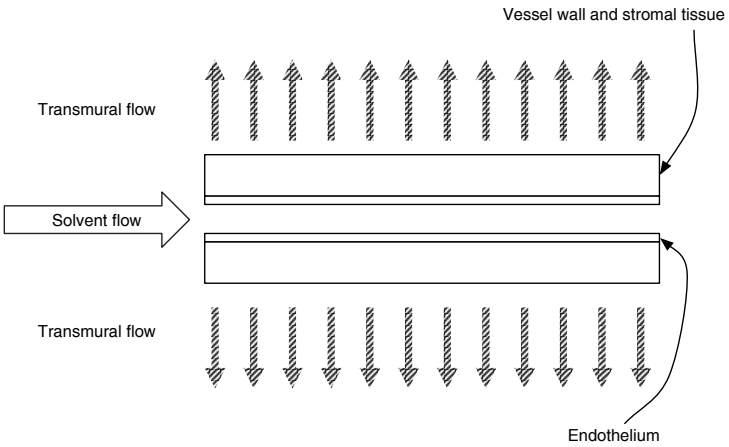


Figure 4.1: Convective flow in decellularisation: vessel model. The pressure difference across the vessel wall leads to the development of convective flow from the lumen to ablumen side. The transmural flow acts as the carrier of soluble compounds out of the vessel wall. Adapted from Villegas-Montoya & McFetridge (302).

network of pipes appropriately (Equation 4.2). The equation is based on the principles of conservation of energy: the sum of all forms of energy in a fluid along a streamline is the same at all points on that streamline (Equation 4.2, point a and b).

$$\frac{1}{2}\rho v_a^2 + \rho g h_a + p_a = \frac{1}{2}\rho v_b^2 + \rho g h_b + p_b + \Delta p_{\text{loss}}, \tag{4.2}$$

with ρ the density, h the elevation, p the pressure, v the flow and Δp_{loss} a friction loss term.

Blood or in case of decellularisation, detergent solutions, do not only flow through the blood vessels in organs and tissue, but they also permeate through the vessel walls (309) (capillary filtration $Q_{\text{filtration}}$, Equation 4.3):

$$Q_{\text{filtration}} = L_p S \Delta P, \tag{4.3}$$

with S the total membrane surface area and L_p the hydraulic conductance (inverse of flow resistance). Flow across capillary walls or porous semipermeable membranes is driven by pressure, both hydrodynamic (P) or osmotic (π) in the capillaries (C) and the

interstitial fluid (IF):

$$\Delta P = [(P_C - P_{IF}) - (\pi_C - \pi_{IF})], \tag{4.4}$$

The hydraulic conductance L_p describes how amenable a unit of membrane surface area is to fluid flow (Equation 4.5), and is a function of A_p the total cross-sectional area of the pores, t_m the capillary or membrane thickness, μ the viscosity (Pa s), τ the tortuosity and R the pore radius (309). The pore length (through the membrane wall) equals to the product of the tortuosity (τ) and the wall thickness (t_m).

$$L_p = (\frac{A_p}{S})\frac{R^2}{8\mu\tau t_m}, \tag{4.5}$$

Alternatively, flow through porous media can be studied more generally using Darcy's law (Equation 4.6a). This model is typically applied to describe the scenario where a fluid perfuses through a porous substrate. To maintain the same volumetric flow, the interstitial velocity will we much higher than superficial (empty tube) velocity. The ratio by which the flow rate will increase depends on the free volume fraction of the bed ϵ

$$Q = \frac{kA}{\mu L}\Delta P, \tag{4.6a}$$

$$k = \frac{\epsilon^3}{K(1-\epsilon)^2 S_v^2} \tag{4.6b}$$

with Q, the total discharge (m^3/s), k the permeability (m^2), A the cross sectional area to flow (in m^2), ΔP the pressure drop (Pa), the viscosity μ (Pa s), L (m) the length across the pressure drop occurs. The permeability k can be derived based on the void fraction, the specific surface area per volume S_v of the particulate matter in the porous bed, and K the Kozeny coefficient.

The underlying mass extraction mechanism during decellularisation is likely rather complex in large solid organs, given the multitude of possible flow paths (vasculature)

within the tissue. Indeed, Ott *et al.* (238) observed that the clearing of the heart followed a particular pattern: first right ventricle, then the atria and finally the left ventricle. It is well established that flow *per se* is beneficial compared to the stagnant case, as in the absence of flow, tissue permeation with detergents and protein extraction is governed solely by diffusion. On the other hand, it is unclear whether increased perfusion pressure leads to an increase of decellularisation efficiency because higher hydrostatic pressure may lead to compression of the matrix (302).

4.1.3 Aims

In this Chapter, the aim was to establish a protocol to generate decellularised tissue to use in subsequent experiments. First, we compared different methodologies for assessing decellularised tissue composition, because discrepancies in literature were observed. Second, since very few studies performed an in-dept comparison of the factors that contribute to decellularisation efficacy, a study comparing different flow conditions and permeabilisation strategies was initiated, for further optimisation of the decellularisation process.

4.2 Results and discussion

4.2.1 Decellularisation reactor design

Large solid organs are typically decellularised using perfusion, as submersion and/or agitation in decellularisation buffers is typically insufficient for thicker tissues. In fact, the heart, which comprises a large vascular bed to provide nutrients and oxygen to the muscle tissue during contraction, can efficiently be decellularised using retrograde perfusion (238), such as in the Langendorff perfused heart (Figure 4.2). In retrograde flow mode, the buffer flows in the opposite direction as it would *in vivo*. Indeed, buffers are

perfused into the heart through the ascending aorta. The pressure causes the leaflets of the aortic valve to close and as a result the perfusate enters the coronary arteries at the aortic root and eventually drains into the right atrium via the coronary sinus. In order to accommodate decellularisation using retrograde flow, a perfusion device was constructed. Two different decellularisation devices were manufactured, enabling either constant flow or constant pressure.

Under constant pressure decellularisation the flow is not constant and is allowed to fluctuate (Equation 4.2). In fact, when the organ is transferred from PBS perfusion to a decellularisation buffer, vascular resistance increases 10-fold by accumulation of cell debris (310). Hence, the initial flow rate is very low, and it slowly increases because decellularising agents strip out tissue components (Darcy's law increase in porosity: Equations 4.6a). Hence, the avenue of using constant flow decellularisation (which is from a technological perspective easier to implement) was abandoned, because constant flow would have to be modulated to be effective: tissue pressure could be too high at the initial stages and too low in the end. Similarly, decellularisation bioreactors that modulate pressure and flow in real time, to keep both flow and pressure exerted to the tissue at physiological levels, have been proposed (310). But for the purpose of this work, a device was constructed that allows constant pressure perfusion at different pressure levels, set by adjusting the height of a hydrostatic column (Equation 4.2).

4.2.2 Decellularisation of isolated rat hearts

In order to validate the decellularisation reactor and perform proof of principle experiments, rat hearts were decellularised by overnight retrograde perfusion with 1 % SDS. The hearts became increasingly paler with time during the decellularisation period. Similarly to Ott *et al.* (238), the right ventricle (RV) cleared before the LV (Figure 4.3(b)), and eventually entirely white hearts were obtained (Figure 4.3(c)). In addition, the aortic valve and large blood vessels retained structure after decellularisation, enabling the de-

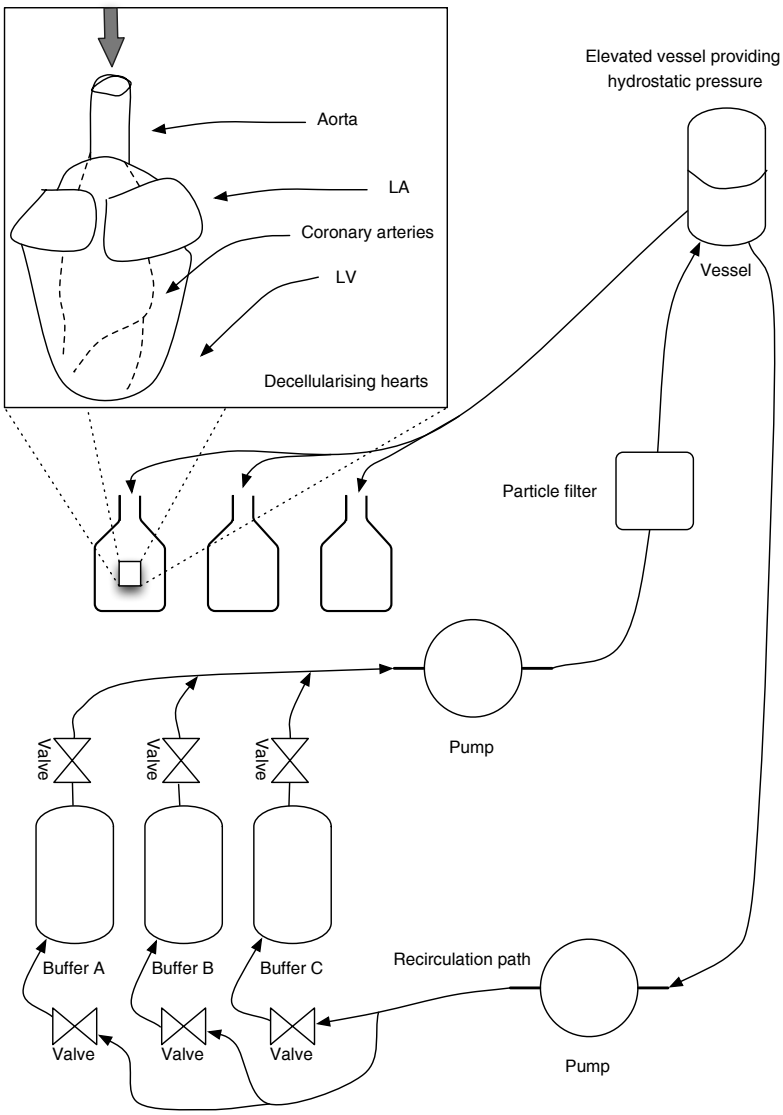


Figure 4.2: Decellularisation of rat hearts: methodology and reactor configuration. Decellularisation buffers were stored in bottles equipped with inlet and outlet tubing fittings. The coordinated action of two pumps (Masterflex®, Cole-Parmer) maintained a constant fluid level in the elevated vessel to enable constant pressure perfusion of the hearts. The perfusion pressure can be modified by altering the height of the elevated reservoir. Particulate filters were placed inline with in the inlet to the reservoir to prevent salt or detergent crystals or contaminants to enter to the samples. Up to three hearts could be decellularised simultaneously. The aorta of the hearts was cannulated for retrograde perfusion of decellularisation buffers into the coronary arteries. Eventually, the spent buffers will drain out of the heart through the coronary sinus into the bottle. To prevent overflowing, the waste stream was collected and directly discarded (not shown in diagram).

cellularised heart to be perfused (Figure 4.3(d) and 4.3(f)).

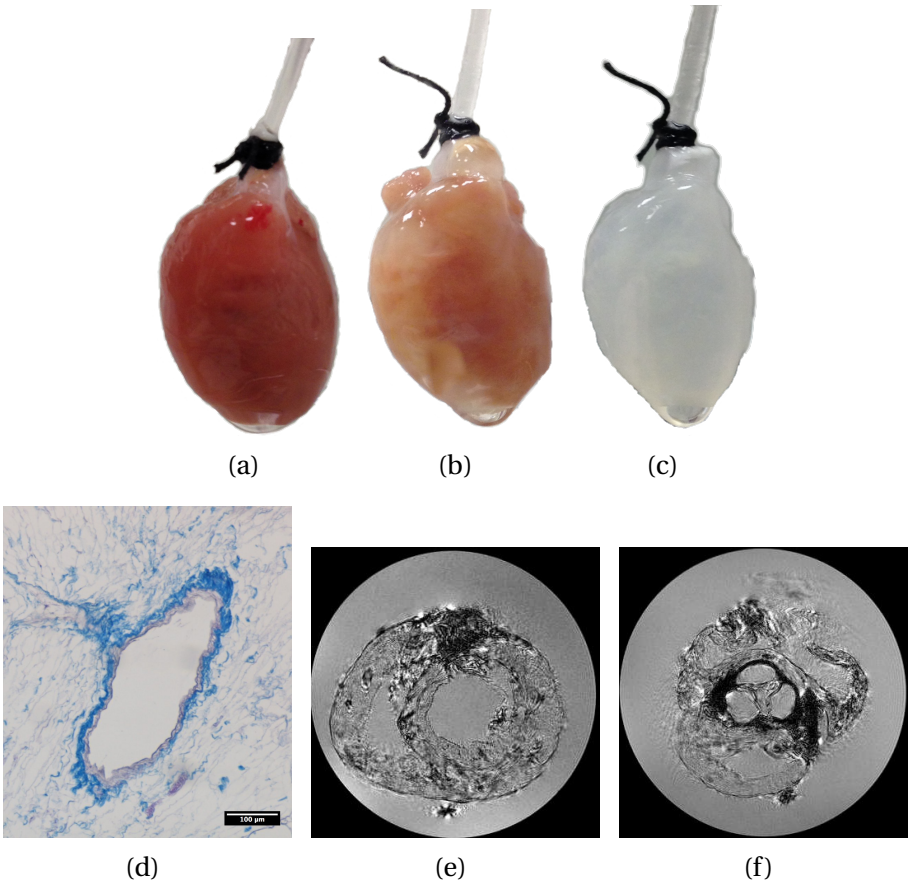


Figure 4.3: Decellularised hearts retain gross anatomy morphology. Isolated rat hearts were decellularised by overnight retrograde perfusion with 1 % SDS and photographed for assessing whole organ morphology. (a) Freshly cannulated heart before detergent perfusion, (b) Partly decellularised heart: the RV has cleared partly in contrast to the LV, (c) Fully decellularised heart. Decellularised isolated rat hearts were fixed, embedded in wax, sectioned and stained with MT to visualise blood vessel ECM (d, scale bar: 100 µm). High resolution cine-MRI microscopy of the decellularised heart. RV and LV cavities (e) and aortic valve morphology were retained (f). MRI data courtesy of Dr. Lien-Cheng Hsiao (D.Phil thesis 2012, Oxford).

4.2.3 Normalisation strategies for decellularisation

Decellularisation requires total removal of DNA, but retention of collagen and GAG are also often reported. Collagen is the major structural component of the ECM and GAGs

are polysaccharide ECM components that play a role in water retention and growth factor sequestering (311, 312).

Many parameters may affect decellularisation efficacy and ECM retention, and therefore, decellularisation protocols need to be optimised for specific needs. This requires robust methods for comparison of decellularised tissue composition. Accurate quantification by using sensitive detection techniques is essential, but the normalisation strategy used might also affect the relative and absolute magnitudes of certain parameter values and their relative comparability, since both the numerator and the denominator might be affected by the treatment. We believe that the quantification of the GAG content might be most confounded by incorrect normalisation, which is especially worrying since GAGs plays important roles in the ECM both from a mechanical and biochemical point of view (311, 313).

As a result, to optimise the decellularisation successfully, appropriate comparison and analysis methods are paramount. In this study, we decellularised rat hearts with two detergents of markedly different efficiencies, SDS, an ionic detergent, or POETE, a non-ionic detergent, to demonstrate the effect of different methods for normalisation and assess their confounding effect on quantitative component qualification.

4.2.3.1 Literature review

Papers analysed included editorials (1%), reviews (14%) and experimental studies (72%, Figure 4.4(a)). The literature search also returned papers, which were not available or not relevant. A large proportion of experimental studies did not perform any quantification of the retained ECM (48%), or only assessed DNA content (22%). When no quantitative measurements were made, qualitative histology was usually presented. For those papers that quantified multiple components (DNA, collagen, GAG, elastin, and protein), the majority of published work used a consistent approach across all analyses (Figure 4.4(b), 41%), although some did not specify enough information to determine

which method was used or whether it was used in a consistent manner (Figure 4.4(b), 6%). Some authors (Figure 4.4(b), 7%) used different normalisation strategies for different components they quantified.

We were able to determine eleven different normalisation strategies. (i) wet tissue weight, (ii) dry tissue weight, (iii) volume, (iv) whole tissue, (v) both wet and dry weight, (vi) protein content, (vii) initial tissue weight, (viii) initial dry weight, (ix) equilibrium swollen state, (x) area, and (xi) uncertain. In a significant proportion of papers, there was some ambiguity (Figure 4.4(d), 4.4(f), 4.4(h)). However, in most cases, even if the method section or the graphs failed to explicitly mention the strategy used, the surrounding text suggested the most likely used strategy. The classifier 'uncertain', was only used if multiple possible strategies were likely.

In general, normalisation to wet or dry weight was the most common (Figure 4.4(c), 4.4(e), 4.4(g)). Most papers reported reductions in DNA content. We observed that 65 % of the papers used normalisation to dry weight for GAG quantification and 50 % for collagen quantification and mostly observed comparable or reduced GAG and collagen content, although a some papers observed counter-intuitive increases in GAG and collagen content (314–317), which most likely arose from inappropriate normalisation. Papers using normalisation to wet weight predominantly observed reductions or unchanged levels of GAG content. Very few papers normalised to whole organ weight and similarly these observed comparable or reduced levels of GAG, depending on the harshness of the decellularisation protocol (318). No papers using wet weight or whole tissue weight observed increases in GAG content.

To study the confounding effect of normalisation, rat hearts were decellularised either with SDS or POETE in this study. SDS is an ionic detergent and has been reported to decellularise organs fully (182, 301). POETE, on the other hand, belongs to the class of non-ionic detergents and is ineffective at stripping tissue from cellular material. Hence, these decellularisation strategies are likely to differentially affect both numerator and

denominator in the quantification of residual DNA, collagen and GAG.

4.2.3.2 Decellularisation of isolated rat hearts

Hearts from rats of comparable body weight were decellularised with either SDS or POETE as detergent by constant pressure perfusion (Figure 4.5). Histological staining indicated that SDS treatment resulted in full decellularisation, whereas POETE treatment only partly decellularised the tissue (Figure 4.6).

4.2.3.3 Dry matter content of decellularised tissue

Decellularisation washes out cellular material from the collagen matrix and, as would be expected, total dry content decreased with decellularisation. Similarly, total wet mass decreased in SDS treated samples compared to control and POETE. Moreover, the wet to dry ratio increased with decellularisation efficacy: SDS > POETE > Control (Figure 4.7), suggesting that during decellularisation cellular material had been replaced by water. As a result, we postulate that different normalisation strategies, that relate content to either dry or final wet weight, will not necessarily result in the same data interpretation.

4.2.3.4 Analysis of retained material and comparison of normalisation strategies

The collagen, DNA and GAG content of the decellularised tissue were measured. Normalisation to wet or dry weight are the most commonly used strategies for expressing composition of decellularised tissue (Figure 4.4(c), 4.4(e), 4.4(g)), therefore we compared normalisation to initial and final wet weight, and final dry weight (Figure 4.8). Both initial and final wet weights were compared since the water absorption is different in different decellularisation protocols.

In general, different values, relative differences and distinct conclusions were reached depending on the normalisation strategy used. Collagen content was maintained after decellularisation when normalised to initial wet weight, whereas when normalised

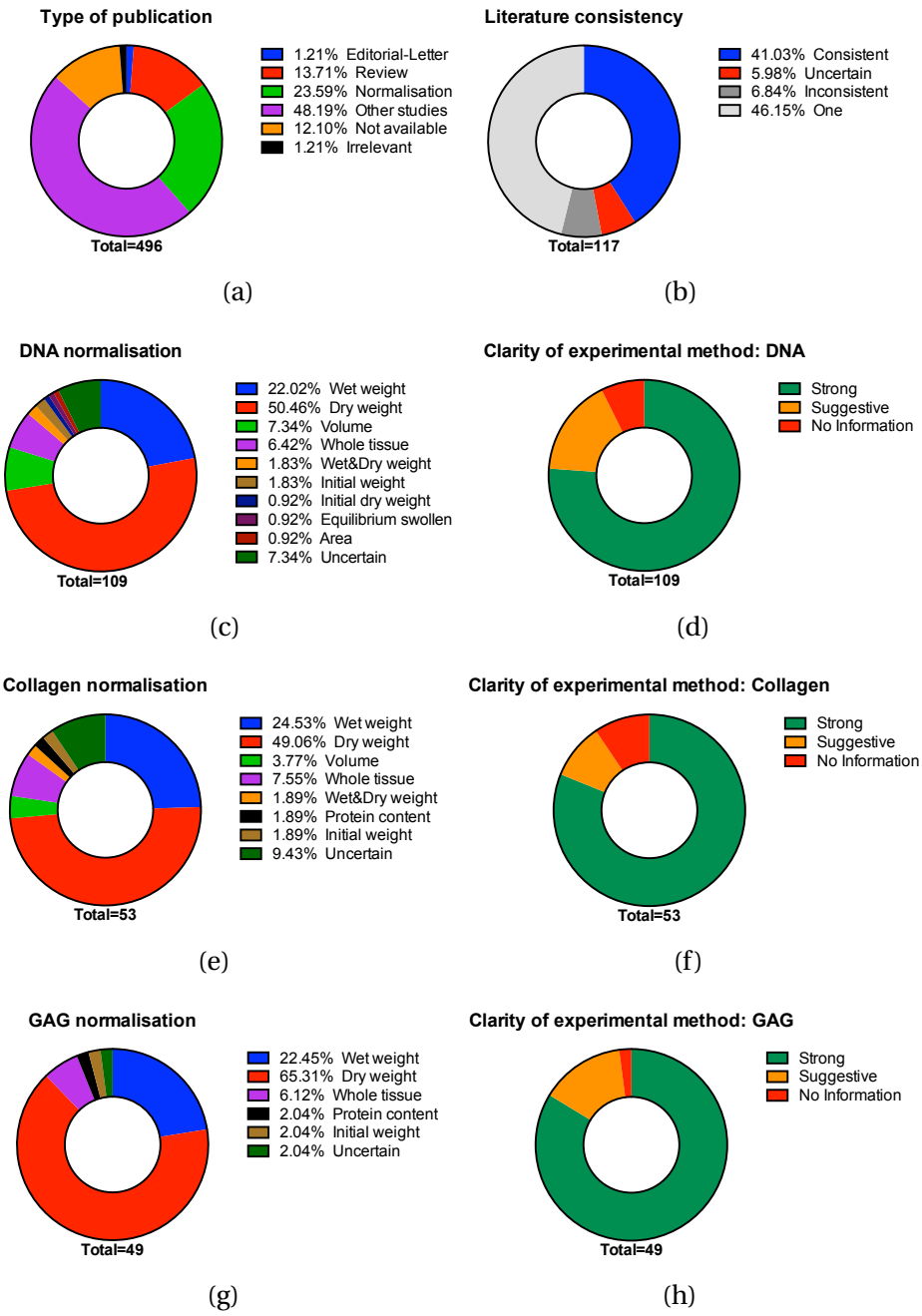
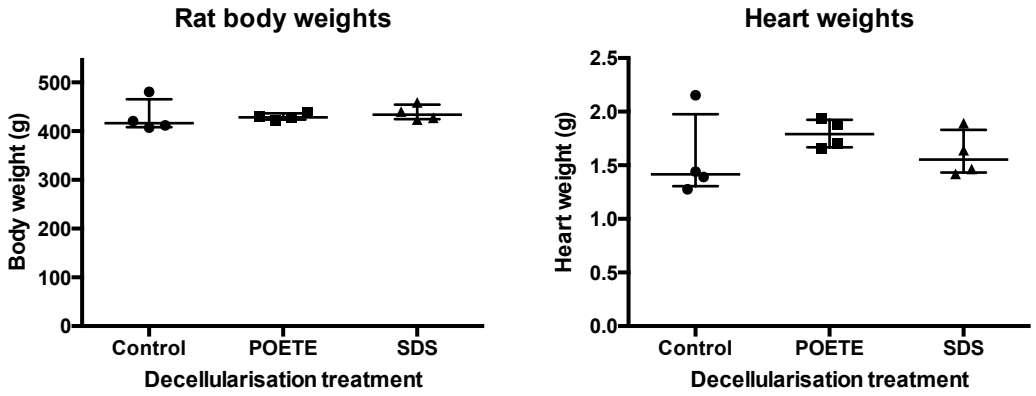


Figure 4.4: Usage of normalisation strategies in literature. (a) Overview of the types of publications retrieved from PubMed, (b) within paper consistency of used normalisation strategies, (c) distribution of strategies used for DNA content normalisation, (d) clarity of methods describing DNA content normalisation strategies, (e) distribution of strategies used for collagen content normalisation, (f) clarity of methods describing collagen content normalisation strategies, (g) distribution of strategies used for GAG content normalisation, (h) clarity of methods describing GAG content normalisation strategies.



(a) (b)

Figure 4.5: Normalisation study: heart and body weights Rat body and heart weights were recorded before decellularisation and were comparable between groups. Data is expressed as median with interquartile range. Symbols: •: Control tissue (non-decellularised rat heart), ■: POETE decellularised heart, ▲: SDS decellularised heart.

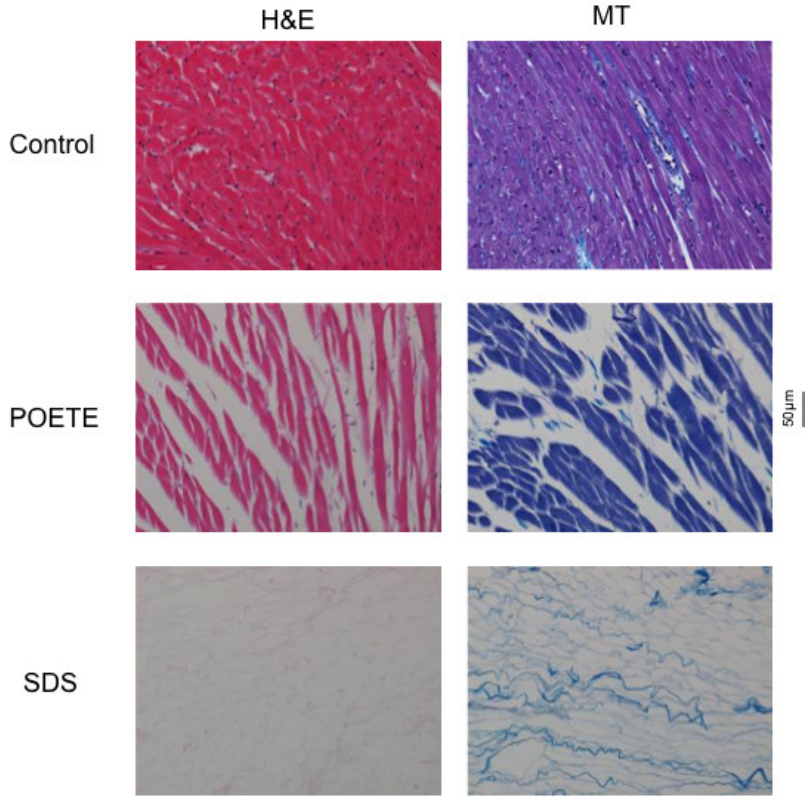


Figure 4.6: Normalisation study: histology. Control and decellularised isolated rat hearts were fixed, embedded in wax, sectioned and stained with H&E or MT. Scale bar: 50 µm.

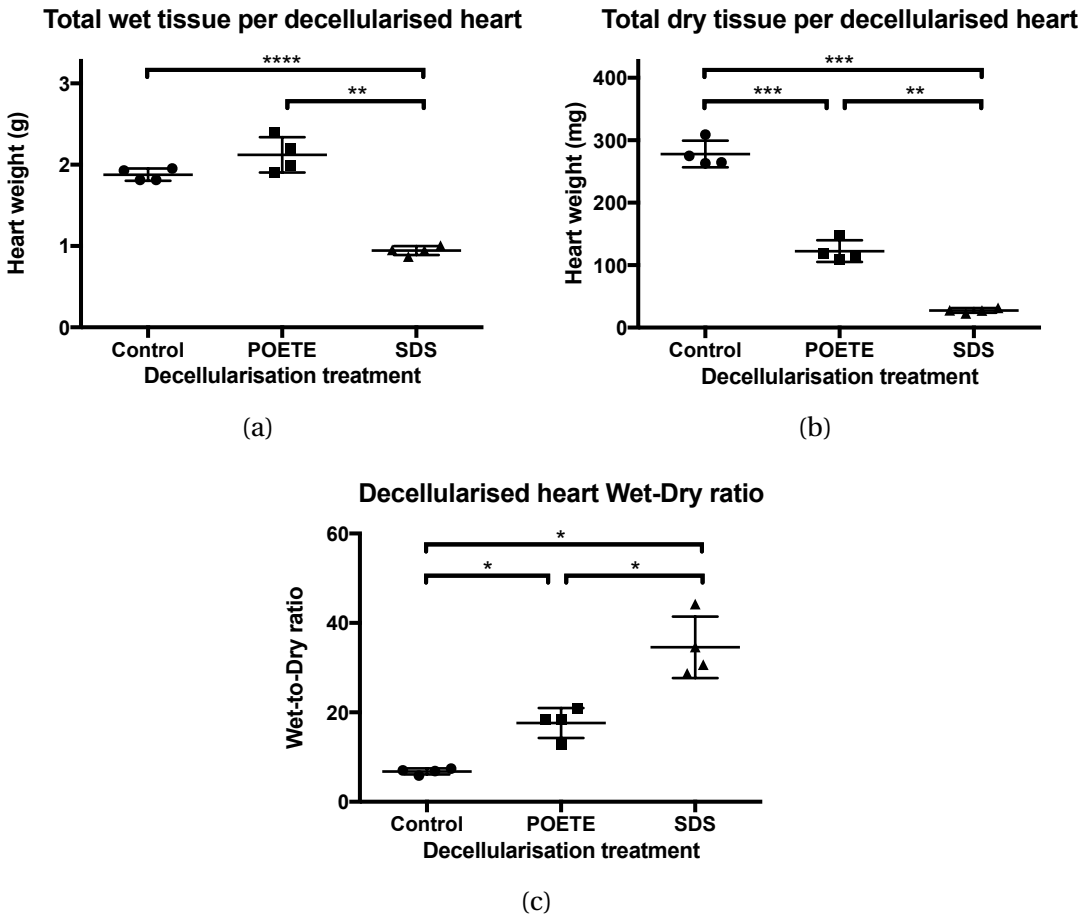


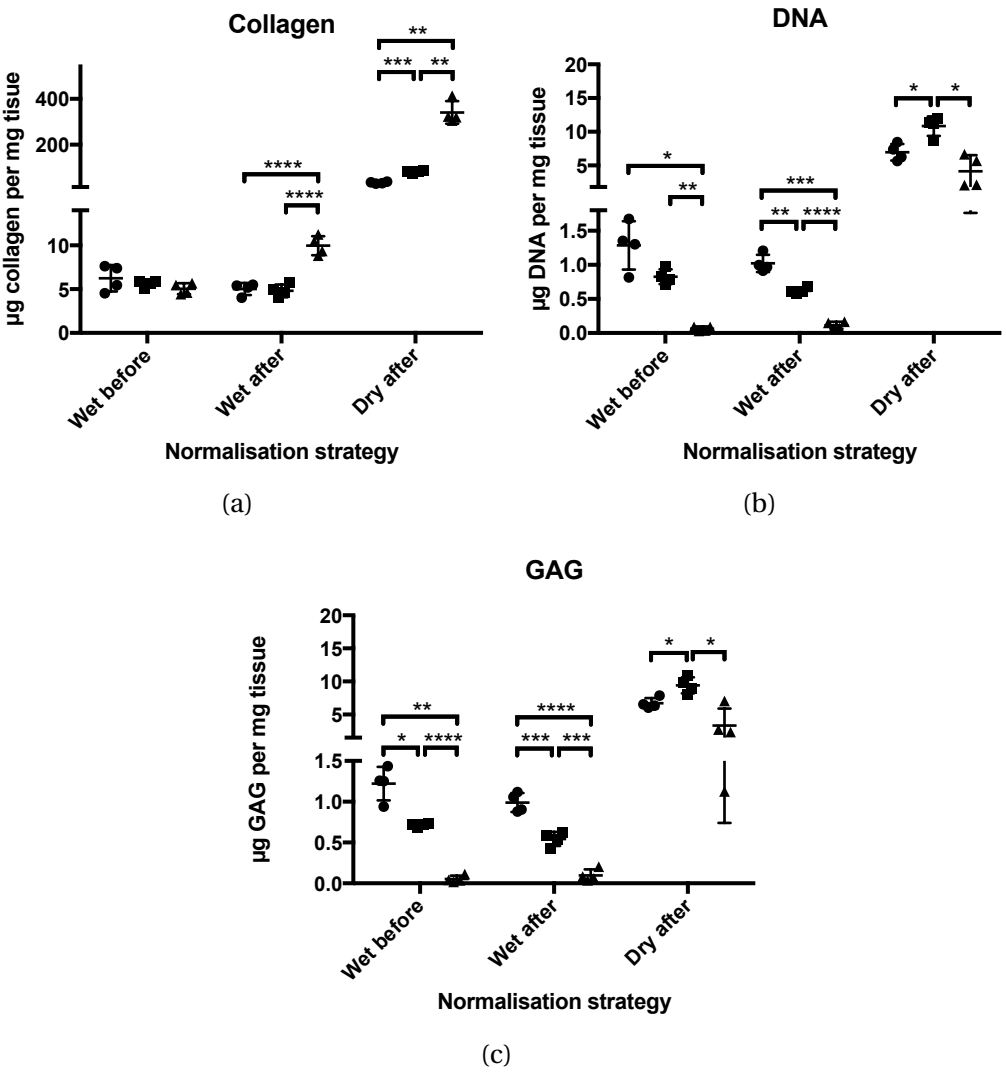
Figure 4.7: Normalisation study: tissue and water content of decellularised tissue. (a) Wet weight after decellularisation. (b) Total dry tissue per heart. (c) Wet-Dry ratio. Data was analysed using the Welch's one-way test (Holm multiple testing correction) and is expressed as mean ± standard deviation. '*' denotes $p \leq 0.05$, '**' $p \leq 0.01$, '***' $p \leq 0.001$ and '****' $p \leq 0.0001$. Symbols: •: Control tissue (non-decellularised rat heart), ■: POETE decellularised heart, ▲: SDS decellularised heart.

to final wet weight or final dry weight, the collagen content was significantly higher in the SDS decellularised hearts compared to both control and POETE treated hearts (Figure 4.8(a)). DNA content in SDS decellularised hearts was significantly reduced compared to control for both final and initial wet weight. However, when normalised to dry weight, DNA content in POETE decellularised samples was higher than control or SDS decellularised hearts (Figure 4.8(b)). Even though both normalisation to initial and final wet weight report a significant reduction in DNA content, the extent of the reduction (Control vs. SDS) is different: showing a reduction to 5 or 10%, for initial wet weight and final wet weight respectively. GAG content was significantly reduced by decellularisation, with SDS treated samples having almost undetectable levels, when normalised to final or initial wet weight. Comparable to the DNA results, the extent of the GAG content reduction is different depending on the normalization strategy: a reduction to 4 or 10%, for initial wet weight and final wet weight respectively. When normalised to final dry weight, GAG content in SDS decellularised hearts was not significantly less than control (Figure 4.8(c)).

Alternatively, components can be expressed as the total amount in the whole organ (Figure 4.9). This method gives results that are comparable to those obtained by normalisation to initial wet weight, although it is likely to be differently affected by variation.

4.2.3.5 Discussion

Most tissues contain between 65 and 85% (by mass) water, although adipose tissue contains considerably less (10−30%). Fat accounts for 0−10% of most tissues and protein for 15 to 25% (319). After decellularisation, the tissue will contain considerably less protein material by definition since cellular material is washed out. The decellularised material still contains a considerable amount of water. This water is present in cavities and/or bound by the material. In the literature, water binding ratios for collagen of about 20 gram water per gram collagen sponge have been reported (320, 321). However, collagen



(a) (b)

(c)

Figure 4.8: Normalisation study: wet and dry weight normalisation. Tissue composition (collagen, DNA, and GAG) was normalised to initial wet weight, final wet weight and final dry weight. (a) Collagen, (b) DNA, (c) GAG. Data was analysed using the Welch's one-way test (Holm multiple testing correction), in case of heteroscedasticity, and using one-way ANOVA (Tukey multiple testing correction), in case of homoscedasticity. '*' denotes $p \leq 0.05$, '**' $p \leq 0.01$, '***' $p \leq 0.001$ and '****' $p \leq 0.0001$. Symbols: •: Control tissue (non-decellularised rat heart), ■: POETE decellularised heart, ▲: SDS decellularised heart.

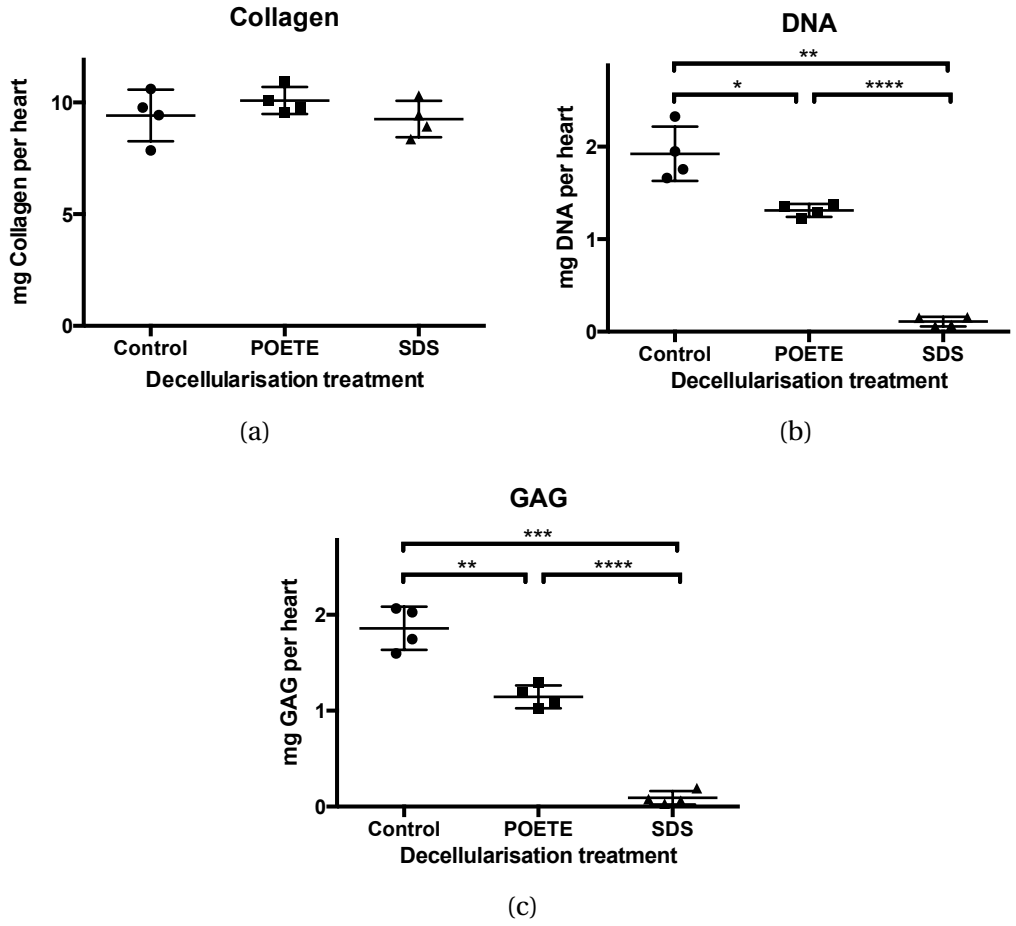


Figure 4.9: Normalisation study: whole heart normalisation. Tissue composition (collagen, DNA, and GAG) was normalised to whole heart weight. (a) Collagen, (b) DNA, (c) GAG. Data was analysed using the Welch's one-way test (Holm multiple testing correction), in case of heteroscedasticity, and using one-way ANOVA (Tukey multiple testing correction), in case of homoscedasticity. Data is expressed as mean ± standard deviation. '*' denotes $p \leq 0.05$, '**' $p \leq 0.01$, '***' $p \leq 0.001$ and '****' $p \leq 0.0001$. Symbols: •: Control tissue (non-decellularised rat heart), ■: POETE decellularised heart, ▲: SDS decellularised heart.

sponges with GAG (chondroitin sulphate) have significantly higher water binding capacity, depending on which crosslinking method was utilized. Importantly, water binding capacity correlated positively with GAG content (320, 322).

Since different decellularisation protocols might extract various ECM constituents with different efficacies, they might differently affect water-binding capacity. Indeed, the efficiency of decellularisation will in fact affect both numerator and denominator. Hence, normalisation to final wet weight is confounding, since it is unclear whether the amount of water present in the tissue is determined by the equilibrium swollen state (323), at random or arbitrarily. Importantly, since water retention is determined by material composition, materials that contain more GAG, will contain more water, and therefore might appear to have comparable GAG content per wet weight, to a material that contains considerably less GAG and less water (but identical dry weight).

Secondly, when normalising to final dry weight, one expresses the amount of any compound of interest within a unit of dry matter. Therefore, very strong decellularisation treatments might appear to have good retention of ECM components when expressed to dry weight, however when expressed to total organ it is possible there is hardly anything left, implying a low yield of the treatment. Indeed, it is expected that many of the ECM constituents might appear enriched/unchanged when expressed relative to dry weight (314, 324, 325). In our study, we did not observe a reduction in DNA or GAG content when normalised to dry weight. This interpretation is clearly flawed and emphasizes the misconceptions that could be induced by normalisation to dry weight, since whole heart measurements suggest the opposite and total dry content is substantially different between groups. Nonetheless, for demonstrating the lack of DNA in a material it is arguably very useful to express the content per mg of dry tissue, as this is the most sensitive measurement. Indeed, it might even be appropriate to compare different materials with each other in such a fashion. However, it is incorrect to compare it with native tissue or with other decellularisation protocols and look at the ratio as a measure

of DNA washout since decellularisation affects total dry matter as well.

Many authors prefer to use expressions as *% of control*, although these appear to be easy to interpret, they might also be confounded since they could have been derived from any normalisation strategy. In fact, the optimal approach is research question dependent and results should not be extrapolated to other conclusions without taking into account any of the other contributing factors.

It was recently suggested that the FDA and Conformité Européenne (CE) are jeopardising safety by allowing fast commercialisation of decellularised tissue for clinical application in humans and that there is an urgent need for legislation to deal with quality control and safety of decellularised tissue (326). We believe the authors are rightly worried; we have demonstrated that comparisons based on final dry or wet weight, which are the most commonly used, could be misleading, as the reader has no information on the total amount of material left and the loss of material by decellularisation, which renders these measures meaningless. As a result we believe it is crucial that generalised safety and quality control guidelines are issued by drug regulatory agencies such as the FDA, with legislation that is compatible with both the further development of this technology and the safety of the patients undergoing these experimental therapies.

4.2.4 Pre-treatment strategies for decellularisation

As discussed above, the normalisation strategy used had an substantial impact in both the parameter estimation and the conclusions reached. We argue that for different research questions, different normalisation strategies might be optimal. Indeed, when considering ECM retention, it is most ideal to normalise to whole tissue. Whereas for DNA washout, normalisation to dry weight is superior since that more appropriately quantifies the potential immunological burden of the tissue post-transplantation. Additionally, the criteria < 50 ng ds DNA per mg ECM dry weight was proposed as safe threshold, albeit with very little or no supporting evidence (182).

In our normalisation study, we observed no difference between control and SDS treated with respect to DNA content per mg of dry tissue. This rather conservative conclusion is likely mainly the result of the fact that the experiment was not powered to adequately quantify such difference, given the large variability in dry weight DNA content and small samples size.

Since decellularisation is a mass transfer phenomenon, is likely to be limited by tissue perfusion. We hypothesised that by manipulating tissue permeabilisation and perfusion pressure, we would be able to reduce DNA content further. Hence, two levels of physiological perfusion pressure (L: 58 and H: 72 mm Hg, or 7.7 kPa and 9.6 kPa) and three types of permeabilisation strategy (freeze-thaw cycle, Krebs-Henseleit buffer perfusion, PBS-adenosine perfusion (238)) were compared. Perfusion with Krebs-Henseleit buffer allows the hearts to contract and hence results in blood wash-out, perfusion with adenosine on the other hand results in vasodilation which may also improve blood wash-out. Finally, a freeze-thaw cycle result in cell lysis by ice-crystal formation.

4.2.4.1 Decellularisation of isolated rat hearts

Hearts from SD rats of comparable body weight (Table 4.1), were randomly assigned in groups of two to either high or low pressure and to a certain permeabilisation strategy, and were decellularised with 1% SDS as detergent by constant pressure perfusion.

4.2.4.2 Effect of perfusion pressure and permeabilisation strategy on detergent use and permeability

Detergent volume was measured before and after decellularisation. However, since two hearts were decellularised simultaneously, only cumulative information is available. Decellularisation at high pressure seemed to consume more detergent than decellularisation at low pressure (Figure 4.10(a)). Moreover, PBS/adenosine at higher pressure also seemed to consume more detergent than both freeze-thaw and Krebs permeabilisa-

Table 4.1: Heart and body weights of SD rats used to assess the effect of pressure and permeabilisation technique on decellularisation performance Values are expressed as mean ± standard deviation. There was no significant difference across groups in terms of body weight, heart weight or heart-body weight ratio, as determined by one-way ANOVA.

Group	Body weight (g)	Heart weight (g)	Heart-Body weight ratio	n
Control	374.2 ± 23.9	1.62 ± 0.19	0.432 ± 0.045	6
Frozen SDS H	387.8 ± 39.6	1.81 ± 0.26	0.467 ± 0.046	6
Frozen SDS L	381.7 ± 30.9	1.73 ± 0.15	0.454 ± 0.047	5
Krebs SDS H	367.5 ± 14.2	1.69 ± 0.13	0.459 ± 0.025	6
Krebs SDS L	367.5 ± 17.1	1.83 ± 0.27	0.498 ± 0.078	6
PBS SDS H	374.4 ± 20.6	1.79 ± 0.16	0.479 ± 0.035	6
PBS SDS L	366.0 ± 25.5	1.65 ± 0.16	0.450 ± 0.027	6

tion at high pressure. However, the end-stage flow rates and tissue permeability (Equation 2.8) were unaffected by decellularisation treatment (Figure 4.10(b) and 4.10(c)).

In additional experiments, we observed that detergent usage was quite variable and not necessarily reproducible (hence no statistical conclusion are made from this data). This might be explained by the multiple parallel flow paths in the hearts. Indeed, sample-dependent time-variable profiles of decellularisation flow, may lead to different total detergent consumption, whilst having comparable end-of-cycle flow and decellularisation efficacy.

4.2.4.3 Effect of decellularisation on dry matter content

After decellularisation, the total organ weight was reduced, as reported previously in the normalisation study (Table 4.2). There was no significant difference between groups in terms of wet or dry weight or wet-to-dry weight ratio post decellularisation.

4.2.4.4 Effect of perfusion pressure and permeabilisation strategy on DNA content

DNA content in decellularised hearts was significantly lower than in control hearts (Figure 4.11). Within the decellularised groups, perfusion pressure did not have a signifi-

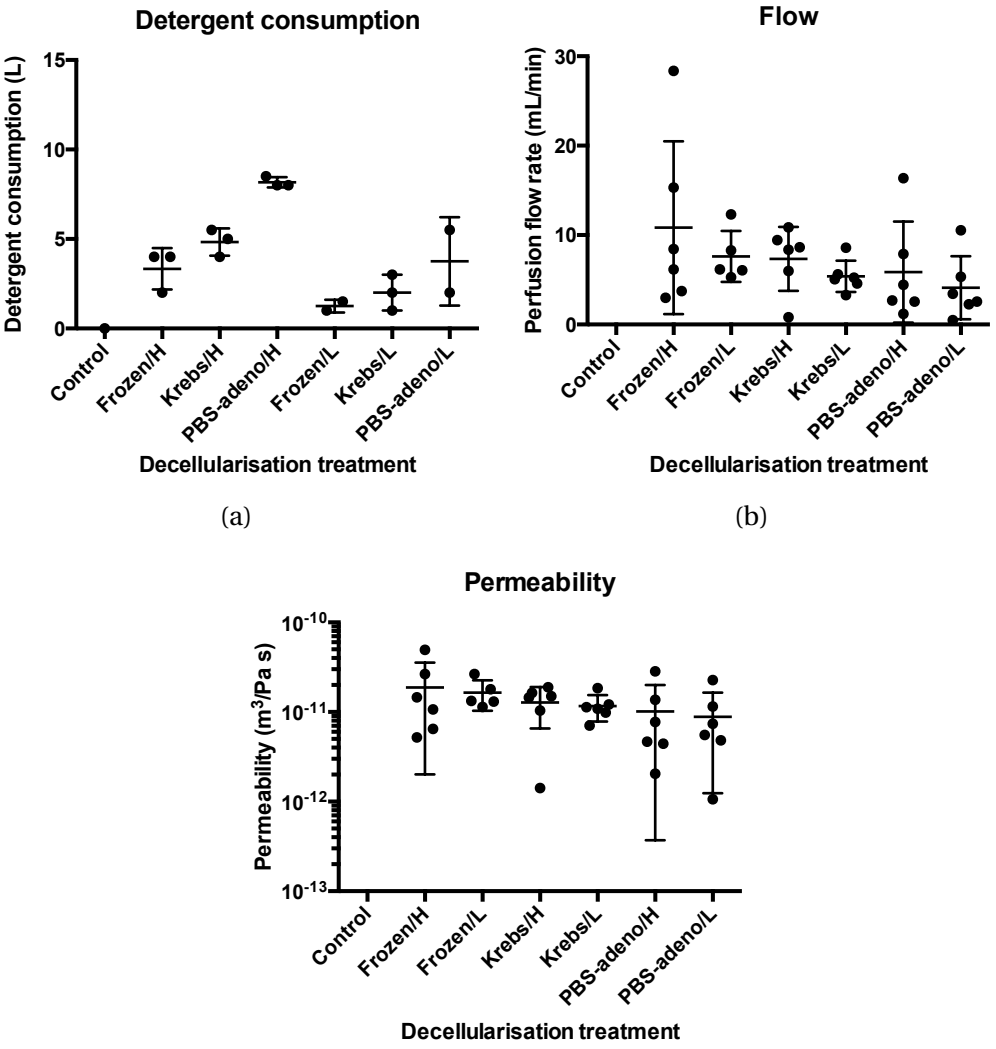


Figure 4.10: Effect of perfusion pressure and permeabilisation strategy on detergent use and permeability (a) Detergent consumption data suggest that high pressure decellularisation consumed more detergent, and PBS-Adenosine consumed more than frozen and Krebs permeabilised hearts. (b) Perfusion flow rate and (c) permeability at the end of the ddH_2O washing step. There was no significant difference between decellularisation groups (Welch's one-way test). Data is expressed as mean ± standard deviation.

Table 4.2: Wet weight of the hearts after decellularisation Weights are expressed as mean ± standard deviation. Control was significantly different from pooled decellularised, as determined by t-test or Kruskal-Wallis Rank Sum Test. There was no significant difference amongst decellularisation treatments as determined by one or two-way ANOVA. '*' denotes $p \leq 0.05$, '**' $p \leq 0.01$, '***' $p \leq 0.001$ and '****' $p \leq 0.0001$.

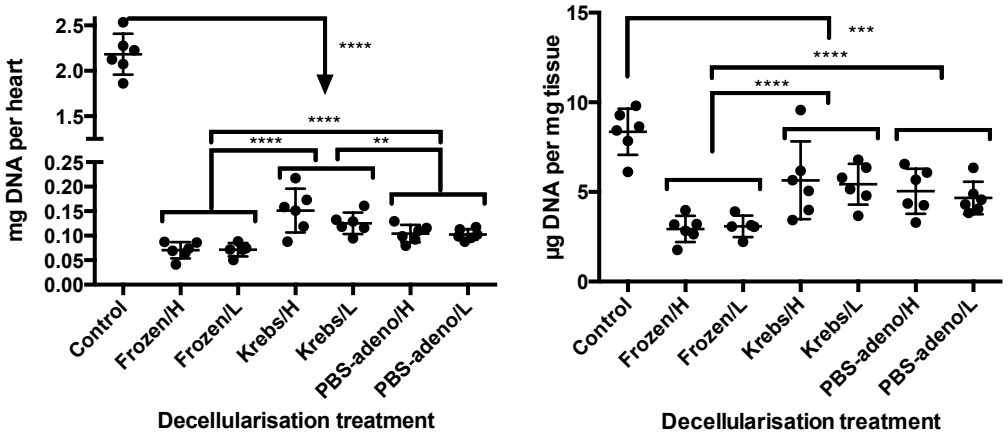
Group	Wet weight (g)	Dry weight (g)	Wet-Dry ratio
Control	1.62 ± 0.18 (****)	0.2640 ± 0.024 (****)	6.16 ± 0.59 (***)
Frozen SDS H	0.66 ± 0.13	0.0241 ± 0.003	27.38 ± 4.69
Frozen SDS L	0.68 ± 0.12	0.0233 ± 0.003	29.29 ± 5.20
Krebs SDS H	0.79 ± 0.17	0.0276 ± 0.005	29.04 ± 5.66
Krebs SDS L	0.78 ± 0.13	0.0234 ± 0.003	34.05 ± 8.39
PBS SDS H	0.82 ± 0.17	0.0213 ± 0.004	39.34 ± 10.56
PBS SDS L	0.72 ± 0.08	0.0224 ± 0.003	32.77 ± 7.61

cant effect on DNA content, whereas the permeabilisation technique did contribute to further reductions in DNA content: Krebs perfused hearts contained significantly more DNA than PBS/adenosine perfused hearts, and these contained significantly more DNA than hearts that underwent a freeze-thaw cycle, if normalised to whole organ weight (Figure 4.11(a)).

Since the criteria < 50 ng dsDNA per mg ECM dry weight was proposed as safe threshold (182), the retained DNA was also normalised to final dry weight. The results were compatible with those obtained using whole organ weight normalisation, as freeze-thaw treated hearts still had the lowest DNA concentrations. All values were considerable higher than 50 ng dsDNA per mg ECM dry weight, however the method applied for DNA quantification in this study does not discriminate between ds and single stranded (ss) DNA.

4.2.4.5 Effect of perfusion pressure and permeabilisation strategy on GAG content

GAG content per heart was significantly reduced post decellularisation (Figure 4.12). The GAG levels were in general very low. Indeed, for some of the samples the GAG content was below the level at which GAG can efficiently be quantified. Hence, no further



(a) (b)

Figure 4.11: Effect of pressure and permeabilisation technique on the DNA content of decellularised tissue (a) Normalised to whole heart weight. Tissue DNA content was significantly reduced by decellularisation (Welch's One-Way test). The effect of perfusion pressure and permeabilisation strategy were assessed using general linear models. Since small variation is heart weight might confound total organ DNA content, the full model, using generalised linear least squares (GLS) fitting, was defined as: DNA ~ Pressure + Permeabilisation + Pressure:Permeabilisation + Heart weight. Akaike information criterion (AIC) based stepwise model selection suggested the model: DNA ~ Permeabilisation as best suited for the data. Post-hoc testing (Holm correction) within the permabilisation factor argues that retained DNA content is highest in Krebs decellularisation, and lowest in freeze-thaw hearts. (b) Normalised to dry weight. GLS fitting using AIC optimisation resulted in the same model as for normalisation to whole organ weight. Data is expressed as mean ± standard deviation. '*' denotes $p \leq 0.05$, '**' $p \leq 0.01$, '***' $p \leq 0.001$ and '****' $p \leq 0.0001$.

statistical assessment of GAG content was conducted.

4.2.4.6 Effect of perfusion pressure and permeabilisation strategy on collagen content

Collagen content was unchanged after decellularisation (Figure 4.13(a)). Not unexpectedly, collagen content correlated with heart weight before (Figure 4.13(b)), which demonstrates the sensitivity of the assay. GLMs allow one to segregate the effect of heart weight from the the decellularisation treatment effect in predicting the collagen content. Additionally, as shown above, heart weight was comparable between groups (Table 4.1).

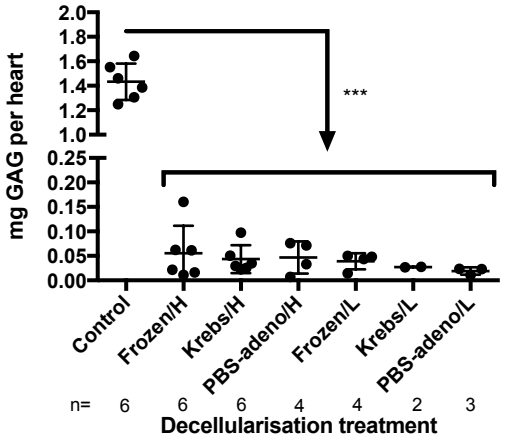


Figure 4.12: Effect of pressure and permeabilisation technique on the GAG content of decellularised tissue Tissue GAG content was significantly reduced by decellularisation (Kruskal-Wallis rank sum test). Data is expressed as mean ± standard deviation. Samples sizes were added of the samples used in this analysis, since not possible to detect sufficient GAG in all samples in this experiment. '*' denotes $p \leq 0.05$, '**' $p \leq 0.01$, '***' $p \leq 0.001$ and '****' $p \leq 0.0001$.

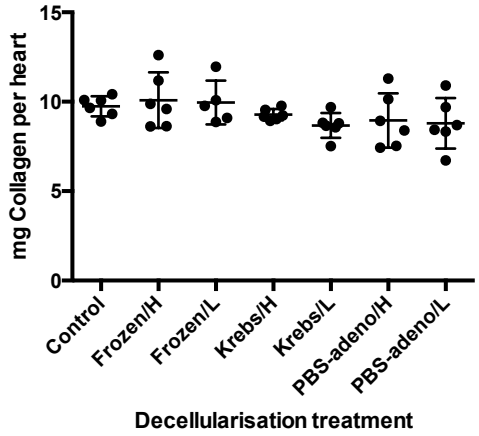
However, when only considering the decellularised groups and correcting for variability in heart weight between groups, no significant difference between groups was observed.

4.2.4.7 Discussion

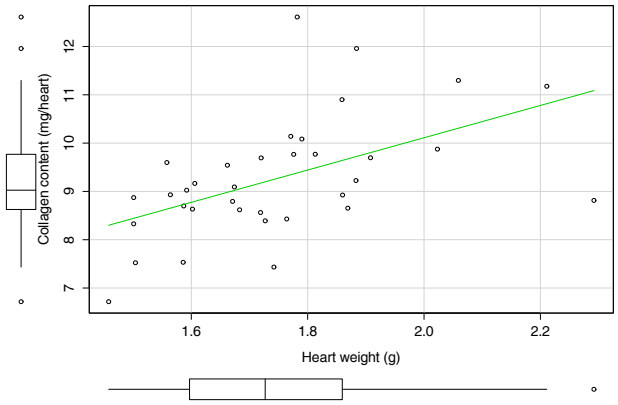
In most published work, complex protocols for decellularisation, comprised of many steps, are compared. Hence, it is difficult to extract mechanistic understanding of the underlying principles.

Given that pressure drives fluid flow through tissues (Equation 4.3), many studies have attempted to improve efficacy by modulating pressure. Firstly, Momtahan *et al.* (327) developed a bioreactor with the possibility to modulate perfusion pressure in each step of the protocol. This allowed the reduction of detergent exposure, whilst still yielding complete removal of cell debris. Secondly, Struecker *et al.* (325) suggested that the use of oscillating pressure in decellularisation showed more homogenous washout of cell remnants in liver.

In this study, marginal differences between the different pressure and permeabili-



(a)



(b)

Figure 4.13: Effect of pressure and permeabilisation technique on the collagen content of decellularised tissue (a) The collagen content in decellularised hearts is not significantly lower than control hearts (p-value = 0.30445). Within the decellularised groups, AIC based stepwise model selection suggested that the full model defined as: Collagen ~ Pressure + Permeabilisation + Pressure:Permeabilisation + Heart weight, minimalises the criteria, and was withheld. Hence, there is some evidence to suggest confounding by heart weight. Pressure and the pressure-permeabilisation interaction did not significantly affect collagen content (p-value = 0.31 and 0.186 respectively), but permeabilisation strategy, heart weight were significant (p-value = 0.0188 and 0.0015 respectively). Multiple comparison testing within the permeabilisation strategy factor found none of the groups significantly different. (b) Correlation between total collagen and heart weight: $\rho = 0.518$ (p-value = 0.001). Data is expressed as mean ± standard deviation.

sation strategies were observed. Collagen content was unaffected by decellularisation and all decellularisation treatments resulted in near complete removal of DNA and GAG from the heart. Pressure did not affect DNA content, but permeabilisation strategy did. Hearts that underwent a freeze-thaw cycle had the lowest DNA content, Krebs-buffer perfused hearts the highest and hearts treated with PBS-adenosine had intermediate levels. Perfusion with warmed Krebs-Henseleit buffer lead to contraction and washout of blood. However, the buffer was not bubbled with carbogen for technical reasons and this might have contributed to the poor performance of Krebs-Henseleit as perfusate, since O_2 and CO_2 are required for buffering and to prevent degradation of the solution (328). Nonetheless, inter-group differences were quite small and the statistical significance is likely driven by the large sample size and small variability, rather than a meaningful difference. Indeed, it seems, when taking the data from the POETE decellularisation experiments into consideration, that the choice of detergent plays a far greater role.

In none of the decellularisation protocols, values below 50 ng dsDNA per mg dry weight were achieved. However, two factors potentially contributed to this observation. Firstly, it is not inconceivable that there are hotspots of residual cell debris which succeeded in not being washed out. Indeed, it is expected that the detergent will flow via the path of lowest resistance (Equation 4.2), and would not necessarily result in homogenous decellularisation (329). Secondly, many researchers use the PicoGreen® (Invitrogen™) assay for the quantification of DNA content. This assay is specific for dsDNA, whereas spectrophotometric measurements do not discriminate between DNA and RNA and also enumerate ssDNA, oligonucleotides and free nucleotides. Given that the aforementioned safety threshold is far from evidence based (182) and ssDNA can also induce inflammatory responses (330, 331), it seems inappropriate to only quantify dsDNA. But more importantly, the level of fragmentation is a confounder in the quantification of DNA as determined by the PicoGreen® assay, but not by spectrophotometry,

with the PicoGreen® assay underestimating the true DNA content in case of fragmentation (332). Nonetheless, although the integrity of results obtained using this frequently utilised method is severely compromised, it does not mean that the tissue obtained by our protocols is sufficiently void of DNA and hence further post-treatment strategies are required to further reduce the residual DNA burden.

4.2.5 Post-treatment strategies for decellularisation

Many published decellularisation protocols have additional steps post-detergent treatment. These steps are aimed to (a) further reduce cellular content, (b) make the tissue more biocompatible. This can be accommodated by additional enzyme, detergent, acid or hyper-hypotonic steps (182, 301).

4.2.5.1 Nuclease treatment to reduce DNA content

Nucleases are enzymes capable of cleaving the bonds between subsequent nucleotide subunits, and have been suggested as agents to reduced the DNA burden of decellularised tissue. Decellularised hearts treated with DNase had significantly less DNA compared to standard SDS decellularised hearts (Figure 4.14).

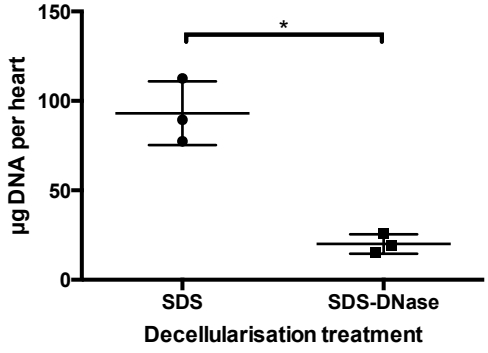


Figure 4.14: The effect of DNase treatment of the DNA content of decellularised hearts SDS decellularisation was compared with SDS decellularisation followed by DNase treatment using the unpaired *t*-test with Welch's correction. Data is expressed as mean ± standard deviation. '*' denotes $p \leq 0.05$.

4.2.5.2 Cytocompatibility and TX-100 to attenuate the residual SDS burden

The observation that mild non-ionic detergents, such as TX-100, remove SDS from protein-SDS complexes and sequester it into micelles that no longer interfere with DNA binding (333, 334), led some researchers to use TX-100 after SDS decellularisation (335).

Preliminary data suggests that indeed the SDS tissue burden can be attenuated by TX-100 perfusion (Figure 4.15). However, although methods are available for SDS quantification, the determination of the residual TX-100 content is far more difficult and rarely performed (336).

Hence, in order to assess the need and feasibility of using TX-100 perfusion in our recellularisation experiments, differentiated iPS (non-beating iPS-CMs) were utilised to quantify the toxicity of SDS and TX-100 using the AlamarBlue® metabolic activity assay (Figure 4.16). AlamarBlue® activity was comparable between the detergent and detergent plus serum treated samples within the TX-100 group, with the exception of cells treated with either 25 or 50 $mg\,L^{-1}$, where serum treated samples had significantly higher AlamarBlue® reduction. In contrast, the difference with or without serum was only significant in the SDS group for the highest dose where the serum treated groups had slightly lower AlamarBlue® reduction (Welch Two Sample t-test, Bonferroni corrected). However, all groups retained more than 80 % reduction, suggesting that the SDS was well tolerated at these concentrations. In addition, non-linear fitting was applied to determine the lethal dose 50 (LD50) value for both detergents using a four-parameter log-logistic model. No LD50 value could be determined based on the serial dilution of SDS used in this experiment, suggesting that mild concentrations of SDS are well tolerated. The LD50 value of TX-100 was 22.1 $mg\,L^{-1}$ and could be doubled by serum supplementation (Table 4.3). The uncertainty on the determination of the LD50 of TX-100 with FBS is the result of the difficulty of determining the lower asymptote since the curve only reaches the lower asymptote around 100 $mg\,L^{-1}$ and no biological data was obtained for higher detergent concentrations.

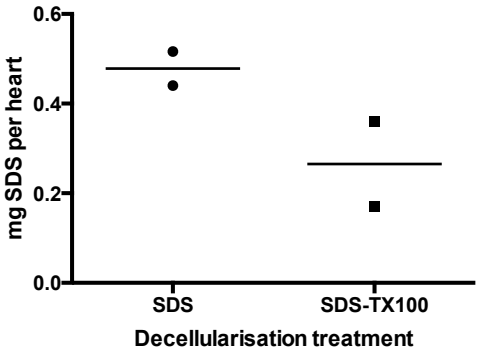


Figure 4.15: SDS content of decellularised hearts after treatment with TX-100 Data of a small trial study to assess the feasibility of using TX-100 to washout SDS during decellularisation. Isolated rat hearts were decellularised using SDS, with or without subsequent TX-100 wash step. Then, the hearts were washed with ddH_2O and finally flash frozen in liquid nitrogen for tissue analysis. Horizontal line indicates the mean, no statistics were performed given the small sample size ($n = 2$).

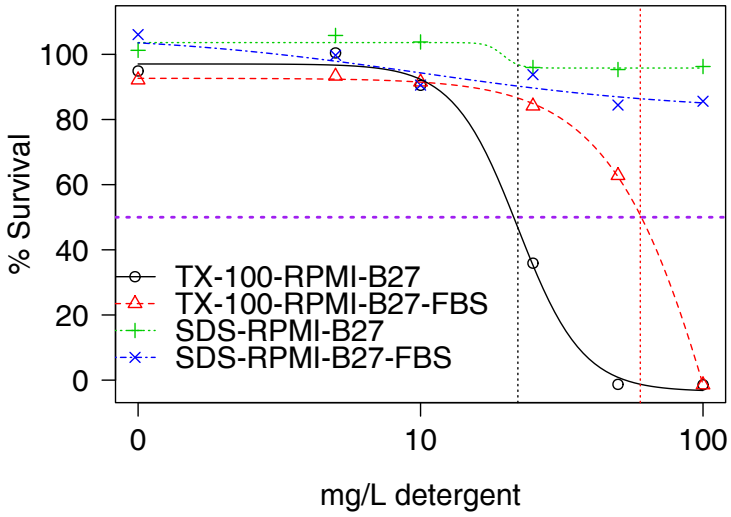


Figure 4.16: Toxic effect of SDS and TX-100 A four-parameter log-logistic function was fitted to the viability data obtained by the AlamarBlue® assay using Matlab and plotted using R (261, 264). For simplicity, the points on the plot relate to the average of four measurements. The purple line indicates the LD50 range, and its intersection with the AlamarBlue viability data is indicated by black and red lines for TX-100 without and with FBS, respectively.

Table 4.3: LD50 of SDS and TX-100 A four-parameter log-logistic function was fitted to the viability data obtained by the AlamarBlue® assay using Matlab (261). The LD50 value, the amount of a given substance required to kill half the members of a tested population, is one of the four parameters in the model and is expressed as mean and 95 % confidence limits.

Cell type	Detergent	Serum	LD50 (mg/L)
iPS-CM	SDS	-	> 100
iPS-CM	SDS	+	> 100
iPS-CM	TX-100	-	22.12 (13.19, 31.05)
iPS-CM	TX-100	+	59.97 (-15.28, 135.2)

4.2.5.3 Discussion

Ott *et al.* (238) proposed in their seminal work to utilise TX-100 to washout residual SDS (334) and this was rapidly applied by others (257, 337). Our proof of principle study confirms the appropriateness of TX-100 for SDS depletion from decellularised tissue, however toxic effects of TX-100 were observed in cell culture experiments. For this experiment, the samples were analysed for SDS content immediately after ddH_2O wash, whereas for subsequent recellularisation experiments, an ethanol sterilisation cycle precedes the cell seeding, which has been shown to reduce the SDS content even further (338). Hence, it is likely, that the true SDS content in decellularised heart post-sterilisation is considerably lower.

With respect to using TX-100 to reduce SDS content even further, there are contradicting reports in literature with respect to which detergent is most toxic (Table 4.4), which is likely partly explained by the variability in quantification techniques applied. Our data using the AlamarBlue® assay with human iPS-derived cells suggests that TX-100 is far more toxic than SDS, although the toxicity can at least partly be rescued by FBS supplementation. Similarly, Andree *et al.* (337) demonstrated that the media composition significantly affected the susceptibility of cells to detergents. Indeed, they reported SDS levels with unchanged metabolic activity up to 200 $mg L^{-1}$ for medium sup-

plemented with FBS or BSA. The standard media used here, RPMI with B27 supplement, contains BSA and this might explain why little toxicity for SDS treated cells was observed.

A potential limitation of the current study is that differentiated iPS rather than iPS-CMs were used and that the effect on CM survival in particular was not studied. However, detergents are likely to affect cells similarly irrespective of the cell type used because the main mechanism leading to death is likely cell membrane permeabilisation. Indeed, literature values are in general comparable for different cell types (337, 339) and it is not excluded some of the variability results from the differences in methodology, cell media used or the amount of ECM secretion by the cells, because medium protein or ECM proteins might act as detergent scavengers. Nonetheless, it seems contra-indicated to use a severely toxic detergent of which it is difficult (and rarely quantified in decellularisation papers) to determine the residual content present in the tissue, to remove a mildly toxic detergent of which the residual content can be routinely measured and monitored.

Table 4.4: Literature toxicity levels for SDS and TX-100. Reported or estimated SDS or TX-100 concentration for 50 % reduction in the reported viability measure.

Cell type	Method	SDS (%)	TX-100 (%)	Reference
3T3	Mitogenic	0.003	0.0005	Matuo *et al.* (340)
Endothelial cells	XTT	0.0018	0.0038	Andree *et al.* (337)
Endothelial cells + BSA	XTT	> 0.02	> 0.02	Andree *et al.* (337)
Endothelial cells + FBS	XTT	0.02	0.02	Andree *et al.* (337)
Differentiated iPS	AlamarBlue®	> 0.01	0.0022	This thesis
Differentiated iPS + FBS	AlamarBlue®	> 0.01	0.0060	This thesis

4.3 Conclusion

In this Chapter the design and development of a decellularisation setup for isolated rat hearts was introduced. Proof of principle decellularisation experiments confirmed that the decellularised hearts retained their anatomy and at least some of the vascular net-

work. Next, normalisation strategies for ECM composition of decellularised tissues were compared and discussed. In order to study and optimise the mechanism of decellularisation, a study assessing the role of pressure and permeabilisation was performed. Finally, two post treatment strategies to either reduce DNA or SDS content were discussed.

The major conclusions of this Chapter were that rat hearts can easily be decellularised using coronary perfusing with detergents. The notion that decellularisation retains GAG was refuted and the reason for the heterogeneity in published GAG contents was attributed to data analysis and normalisation methods. Indeed, > 95% of published literature wrongly concludes that GAG is retained or significantly overestimates GAG content, by failing to take into consideration the retained water as confounding factor.

Decellularisation at two levels of physiological pressure and with permeabilisation by perfusion with physiological Krebs buffer, freeze-thaw cycle or vasodilation only had minimal effect on the decellularisation efficacy after overnight decellularisation. It is not unreasonable to expect that there might be differences in kinetics, whilst obtaining the same plateau value when allowed to saturate.

The need and appropriateness to washout SDS using TX-100 was also assessed. Although there is sufficient evidence to accept that SDS levels can be reduced using TX-100, we felt uneasy about using a second detergent that is toxic and cannot easily be quantified.

CHAPTER 5

DEVELOPMENT OF A BIOMIMETIC CULTURE PLATFORM FOR RECELLULARISATION OF DECELLULARISED RAT HEARTS WITH SYNCHRONISED MECHANICAL AND ELECTRICAL STIMULATION

5.1 Introduction

For the repopulation of decellularisation matrixes, as described in the previous Chapter, a suitable culture system is typically required (341, 342). There are very few options for commercial bioreactors and they are typically very expensive (>100000€, (343)), hence the development of a bioreactor from scratch was initiated. The design of such a bioreactor, and protocols to use the bioreactor will be discussed in this Chapter. The bioreactor presented here was equipped with basic electrical and mechanical stimulation capabilities which can be applied to expose the growing organoid to biomimetic stimuli to attempt to drive cardiac maturation. The mechanical stimulation was applied by stretching a balloon within either the LV or RV, whereas the electrical stimulation was applied by electrically triggering the atrioventricular interface, to induce a contraction wave spreading synchronised with the mechanical cycle (Figure 5.1).

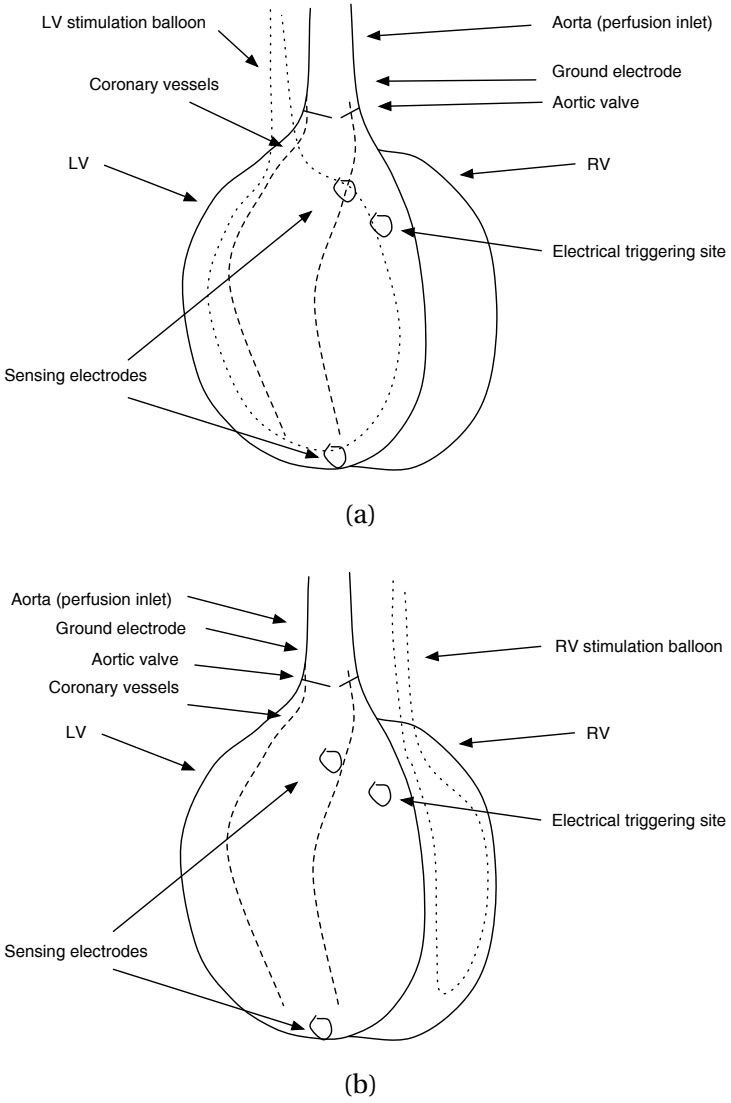


Figure 5.1: Schematic of the biomimetic stimulation features of the bioreactor. The aorta of the decellularised heart was cannulated, enabling perfusion through the innate vasculature. Pacing wires were attached to the atrioventricular interface to induced contraction, synchronised with the mechanical stretching applied to the ventricles via a latex balloon. Sensing leads were located at the top and bottom of the heart. Mechanical stimulation was either directly applied to the LV (a) or the RV (b).

5.2 Development of a recellularisation bioreactor

The bioreactor comprised a fluidics system and a regulation unit, which each comprise multiple components. In summary, the components and functions of the bioreactor

presented in this Chapter are:

1. Heated chamber (Temperature and humidity are monitored, but not controlled by the regulation unit/PC)
2. Plastic tubing, pharmaceutical grade, for fluid handling. Can be sterilised by autoclaving
3. Two pumps: one for feeding and one for waste collection (configuration set by dials on the pump-units, not monitored or controlled by the regulation unit/PC)
4. Carbogen (95 % O_2, 5 % CO_2) supply (valve opening frequency controlled by the regulation unit/PC)
5. Electrical stimulation (controlled by the regulation unit/PC)
6. Linear actuator connected to a syringe capable of filling and emptying a latex balloon placed in the LV or RV (controlled by the regulation unit/PC)
7. Two fluid pressure sensors, to measure both perfusion and stimulation pressure (controlled by the regulation unit/PC)
8. ECG sensing (controlled by the regulation unit/PC)

A detailed description of all of these functionalities will be presented below.

5.2.1 Fluidics

A circular closed-circuit consisting of medical or pharmaceutical grade Tygon® S-50-HL and 2275 tubing (Saint-Gobain) was used to deliver medium from the medium bottle to the lung-oxygenator, and then to the recellularising heart (Figure 5.2). In a second circuit, the waste medium from the heart was collected and returned to the medium bottle. The lung-oxygenator was comprised of wound Silastic™ (Dow Corning™) tubing, given its excellent O_2/CO_2 gas exchange coefficients, enclosed in an air tight box.

The entire fluid path, excluding the pumps, was enclosed in a heated chamber (Stuart incubator S160D, UK) to provide the appropriate temperature for cell culture. Peristaltic pumps were used for the fluid handling (Gilson, Inc, Minipuls® 3, USA).

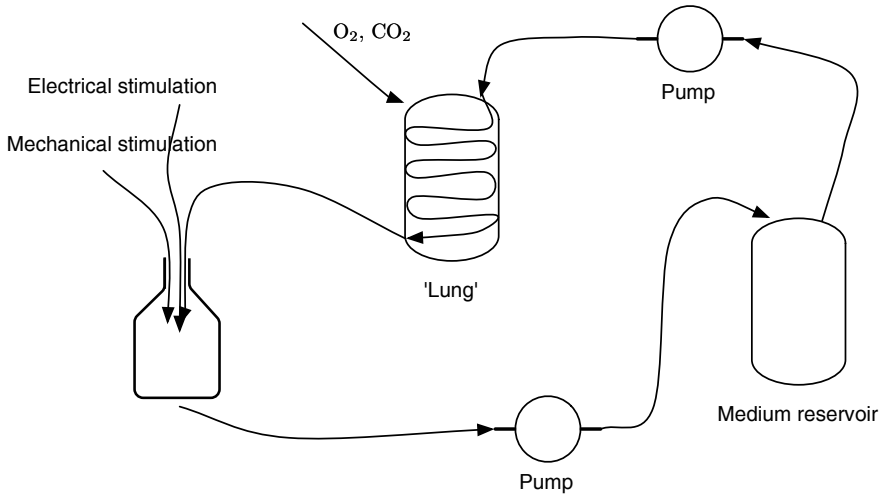
The fluid path was composed of shorter leads which can be assembled using the Luer-Lok™ system (Becton Dickinson) and Duran® bottles fitted with tubing connections were used for holding the medium and the heart. The entire fluid path can be disassembled, washed, and autoclaved to allow sterile operation.

5.2.2 Biomimetic mechano-electrical stimulation

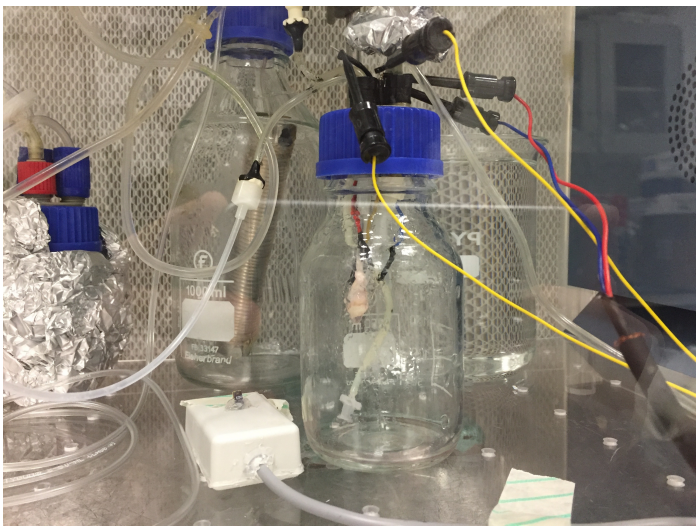
During the cardiac cycle, the atria and ventricles undergo dramatic changes in pressure and volume as a result of synchronised contraction of cardiomyocytes (Figure 5.3). As a way to provide the recellularising heart with biomimetic stimulation that might be beneficial for stem cell differentiation and cardiomyocyte maturation, the bioreactor was equipped with electrodes to pulse the top of the LV as a pacemaker, and with an inflatable latex balloon that could be fitted inside the RV or LV. The balloon was connected with tubing to a glass syringe (Hamilton® Gastight 2.5 mL) filled with sterile DPBS containing antibiotics (100 U mL^{-1} penicillin, 0.1 mg mL^{-1} streptomycin and 0.25 µg mL^{-1} amphotericin B, Sigma-Aldrich®, UK), attached to a linear actuator (Figure 5.4). The action of both the electrical pacing wires and the linear actuator can be controlled by the bioreactor controller, and any reasonable wave form can be constructed.

5.2.3 Electronics

The circuits, responsible for monitoring and regulation, were split across four boards. The first panel provides and stabilises the power supply for the device at different voltages: GND, ± 5 and ± 9 V (Section 5.2.3.1). The second panel contains the circuits for communication to a PC and is responsible for the high frequency tasks such as data acquisition (Section 5.2.3.2). The third panel contains the signal amplifiers and filters



(a)



(b)

Figure 5.2: Schematic and photo of the bioreactor fluidics path. (a) Cell culture medium was pumped using a peristaltic pump from the medium reservoir to the oxygenator, where oxygen and CO_2 were exchanged. Then, the medium was perfused into the cannulated aorta (retrograde perfusion). The heart was also equipped with pacing wires and a latex balloon to induce electrical and mechanical stimulation, respectively. Spent media was collected and pumped back into the medium reservoir to enable recirculation. (b) The bottle at the left is the medium reservoir, the bottle in the middle the lung-oxygenator, and the bottle on the right contains the recellularised heart. The yellow wires connect to the pacing electrodes and the red/blue wire connect to the sensing electrodes.

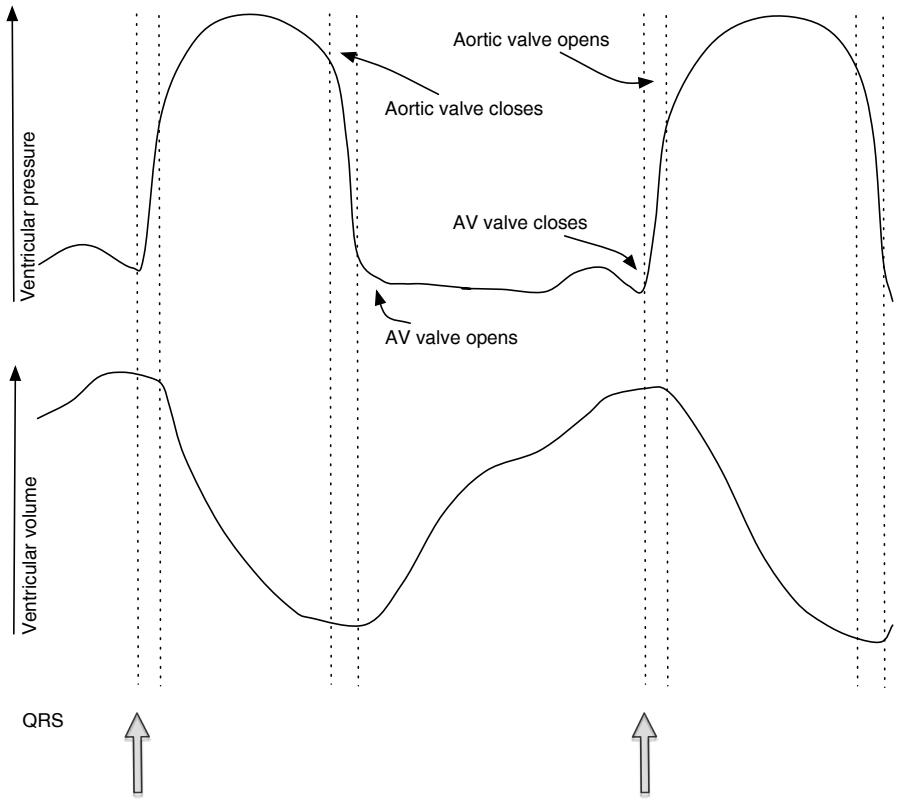


Figure 5.3: Ventricular pressure and volume during the cardiac cycle. During diastole, the pulmonary valve and the aortic valve are closed, and the atrioventricular (AV) valves are opened, allowing the ventricles and atria to passively fill during ventricular filling. Then, during atrial systole, additional blood is pumped from atria into the ventricles, and at this stage, the ventricles reach their maximum volume. Next, during isovolumic contraction, the ventricles begin to contract, and when both AV and semilunar valves are closed there is no change in volume. Whereas during ventricular ejection, when the ventricles are contracting, the semilunar valves open allowing the ventricles to eject part of their volume. Next, during isovolumic relaxation, ventricular contraction stops and the semilunar valves close.

(Section 5.2.3.3). The last panel contains the climate and stimulation controller and reports directly to the master controller (Section 5.2.3.4).

5.2.3.1 Power supply board

The bioreactor was powered using the mains supply and the AC mains was converted into DC voltage $V_{out} = \pm 12, +48$ V, using two Traco Power supplies (Table 5.1). Both the mains and the low voltage outputs of these supplies were fitted with fuses. An isolated

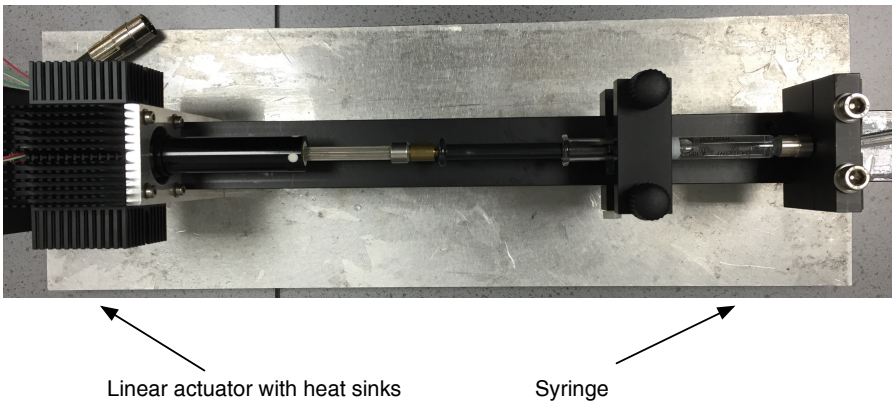


Figure 5.4: Linear actuator fitted with syringe for inducing mechanical stimulation. A linear actuator was fitted on a aluminium stand. The lead of the actuator was connected to a glass syringe. Heat sinks and a fan (not visible on photograph) were used to provide additional cooling of the actuator.

DC-DC converter, to provide power to the isolated circuit of the ECG amplifier and the electrical stimulation unit, was supplied with power from the +48 V supply. Most of the electrical circuits within the bioreactor controller unit were powered at +5 V. Regulated ±5 and ±9 V were provided from ±12 V using linear voltage regulators. Schematics and outlines of the PCB of the power board can be found in Figure 5.5 and B.1.

Table 5.1: Bioreactor design: Power supplies. List of power supplies used in the bioreactor controller, to provide power to the different boards, the valve and the actuator.

Supply	Type	Input	Output(s)
Traco® Power TXL 035-1212D	AC-DC	Mains	±12 V
Traco® Power TXH 120-148	AC-DC	Mains	+48 V
Traco® Power TEL 3-4822	Isolated DC-DC	36 – 75 V DC	±12 V

5.2.3.2 The master controller board

The digital circuits in the bioreactor controller were regulated by PIC® MCUs. The software operating the actions of MCUs can be programmed in a variety of programming languages, most commonly ASM and C, which are subsequently compiled into machine code, and loaded onto the MCU using a programming device. PIC® MCUs contain

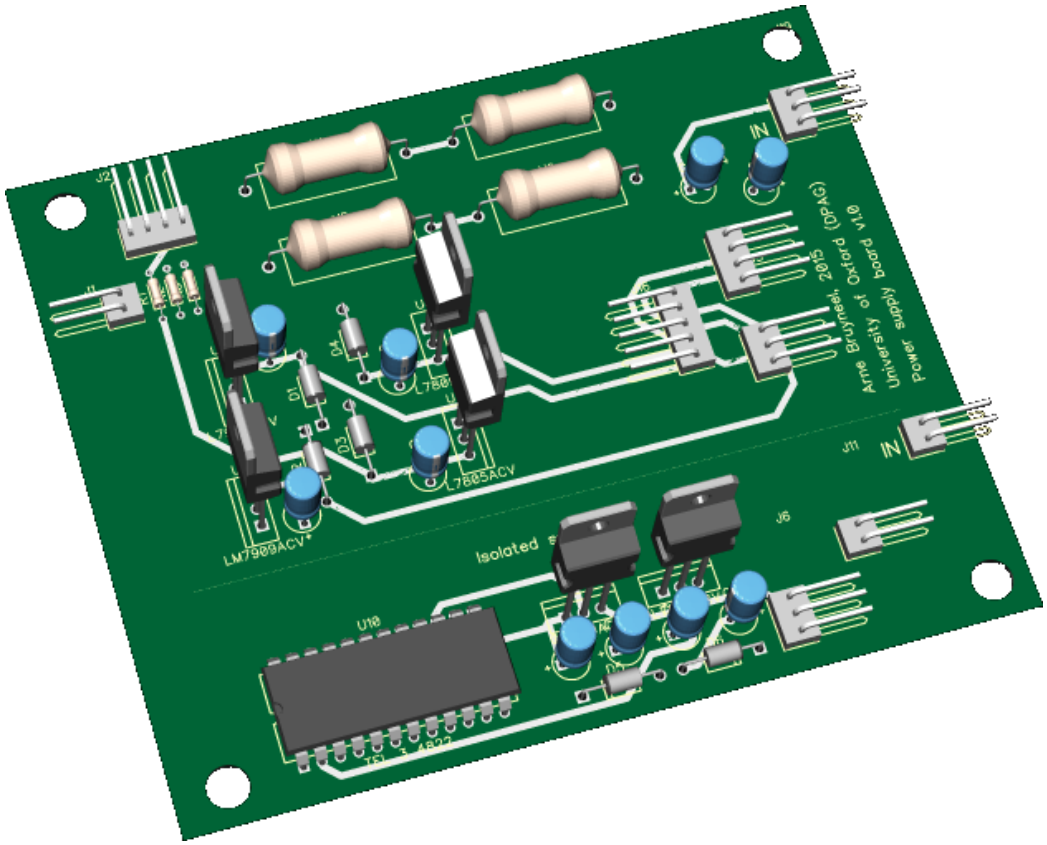


Figure 5.5: Bioreactor power supply board: PCB. 3D model of the power board PCB. This board received ± 12 V from the Traco® power supply to provide regulated ± 5 V and ± 9 V to the other boards. In addition, this board powers an isolated power supply, used to isolate the ECG amplifier and the electrical stimulation unit.

flash read-only memory (ROM) program memory that can be erased and reprogrammed many times.

The PIC® 18F4550 MCU (Microchip) was used as main processor in the bioreactor controller unit and was used to communicate to the computer using a serial interface (RS-232), and to all other major regulating chips using inter-integrated circuit (I^2C). The MCU panel also had a second MCU, a PIC® 16F887 (Microchip), which was able to display status messages on the liquid crystal display (LCD). Analog signals amplified on the amplifier board (Section 5.2.3.3) were digitalised on this board using a MAX118 analog-to-digital convertor (ADC) (Maxim Integrated™). The ADC was separated from the digital circuits by using separate power lines and the digitalised output was fed through a

digital buffer (74F244) before being fed into the MCU. Since serial data transmission is too slow to allow acquired data to be transmitted in real-time at an appropriate rate, the board was also equipped with additional external static random-access memory (SRAM) (1 Mbit Serial SRAM, 23LC1024, Microchip) for data storage and a buffered acquisition sequence was implemented (Figure 5.7). Briefly, the user configures the acquisition system by setting the sample rate (0.5 , 1 or 2 kHz). Upon starting the acquisition sequence, the MCU starts an internal timer which will call an interrupt upon timer overflow. The interrupt handler will then execute the ADC function and write the result to the SRAM. The timer/interrupt sequence will continue to run until the required number of samples has been completed. Next, the MCU will inform the PC that the acquisition has been completed and will transmit the data across. Schematics and outlines of the PCB of the MCU board can be found in Figure 5.6 and B.2.

5.2.3.3 Amplifier board

The four layer amplifier board contained three different amplifiers, to monitor pressure and electrical activity as a result of cell activity and biomimetic stimulation. The schematics and an outline of the PCB can be found in Figure 5.8 and B.3.

ECG amplifier The difference between both signal lines (E- and E+) was amplified 100× using an instrumentation amplifier (INA118P, Texas Instruments). In order to provide safety the inputs were protected with diodes and the amplified signal from the instrumentation amplifier was fed through an isolation amplifier (ISO124P, Texas Instruments). The resulting signal was low pass filtered (f_c = 1 kHz) in order to remove the high frequency ripple superimposed on the signal by the isolation amplifier. The resulting signal was high pass filtered (f_c = 0.05 Hz) to remove any DC-offset and was then further amplified using two software programmable gain amplifiers (SPGAs) in series (AD526, Analog Devices) that each provided gains of $1, 2, 4, 8$ and $16\times$. The board

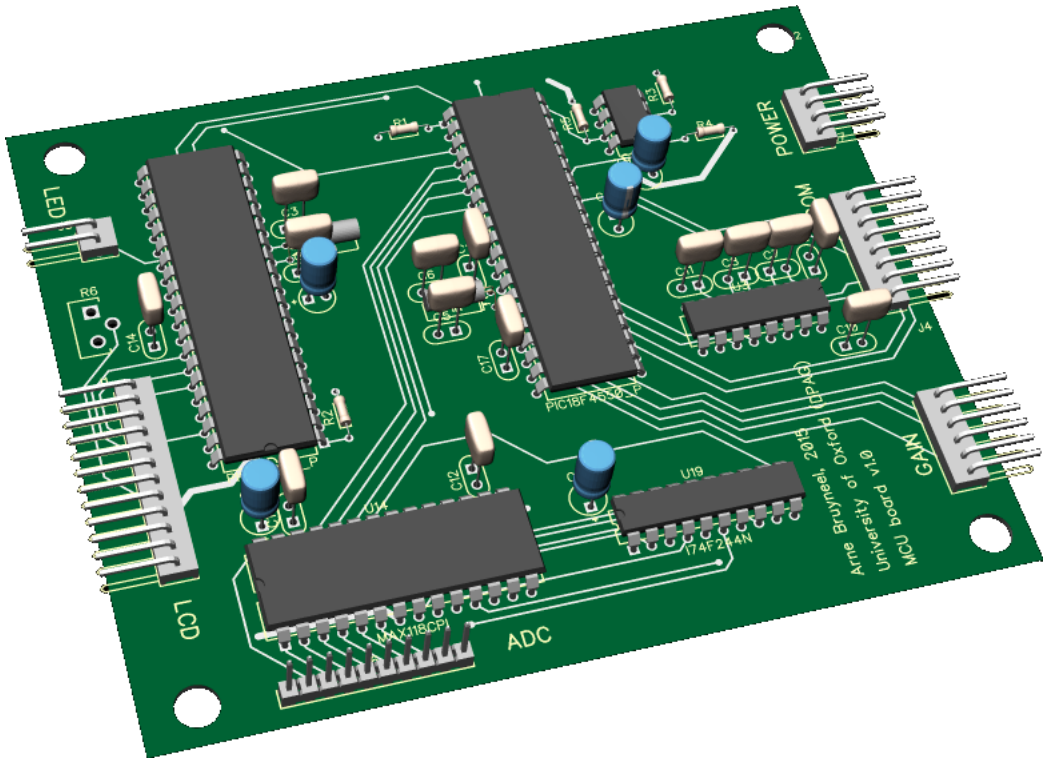


Figure 5.6: Bioreactor MCU board: PCB. 3D model of the MCU board PCB. This board controls all other boards and is responsible for the communication with the PC. The PIC® 18F4550 MCU (Microchip) acted as master controller. This board was in addition equipped with a PIC® 16F887 slave MCU (Microchip), a MAX118 ADC (Maxim Integrated™), additional SRAM (23LC1024, Microchip) memory, and an RS-232 interphase to communicate to a PC. The ADC and SRAM were used to enable high frequency acquisition and data storage of pressure and electrical activity data.

was also equipped with a socket to fit an active 50/60 Hz active band elimination filter (SD-1BE, NF) which can be switched on/off using a digital high/low signal, in case the 50 Hz noise would not be a problem or if it would be distorting the original signal too much. The AD526 requires a four bit parallel digital signal to set the gain. Both SPGA were controlled by the 18F4550 master MCU using a 3-bit serial interface which was subsequently converted to a 8-bit parallel interface using a Parallel-Out/Serial-In Shift Register (SN74LS164N, Texas Instruments). Next, the resulting amplified signal was centred around 2.5 V (valid signal range: $[0,5]$ V, no difference between E- and E+ results in a 2.5V signal), and low pass filtered (f_c = 150 Hz) using a 5^{th} order active lowpass filter (LTC1062, Linear Technology) as an anti-aliasing filter. Taken together, the resulting sig-

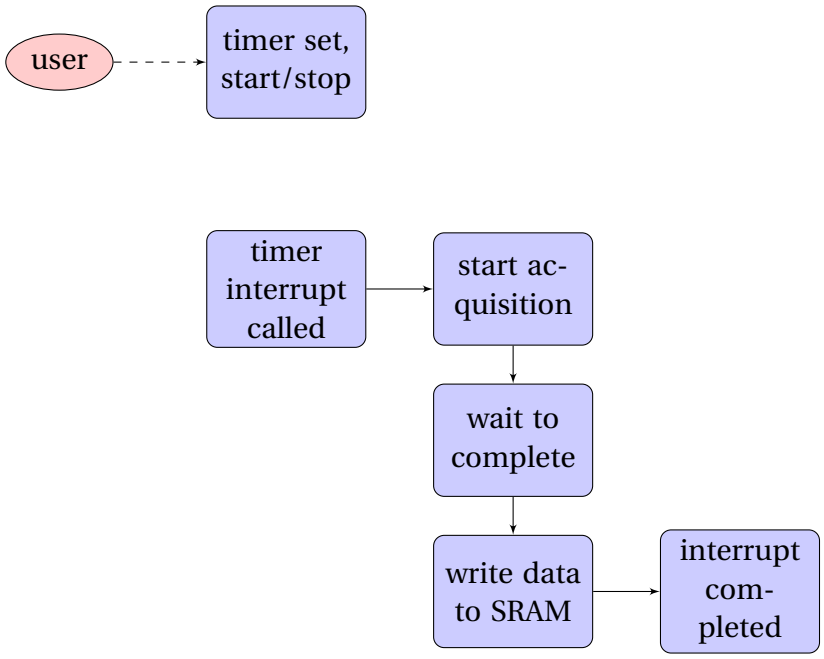


Figure 5.7: SRAM buffered digitalisation algorithm The user sets the sampling frequency and initiates the acquisition sequence. Starting the sequence starts a hardware timer module which subsequently calls interrupts upon time-out. When the interrupt is called, the MCU halts its current process and initiates a ADC conversion which is read out and written to external SRAM memory using the serial peripheral interface (SPI) bus. When all samples are recorded and stored in memory, the computer can request the measurements to be transferred across the serial link.

nal had a total gain of $\{1,2,4,8,16,32,64,128,256\} \times 100$ with a $[0.05,150]$ Hz frequency bandwidth.

Pressure amplifiers The signal origination from the pressure transducers (MLT1199, AD Instruments) was pre-amplified (RS 846-171, RS Components) before being processed by the amplifier panel. Briefly, the pressure signals were low-pass filtered and centred around a preset variable offset voltage (valid signal range: $[0,5]$ V).

5.2.3.4 Climate and stimulation board

The climate and stimulation controller tasks are (a) to monitor temperature and humidity in both the room and inside the incubator, (b) to control the oxygen valve which regulated the oxygen gas supply to the bioreactor and (c) to regulate both mechanical

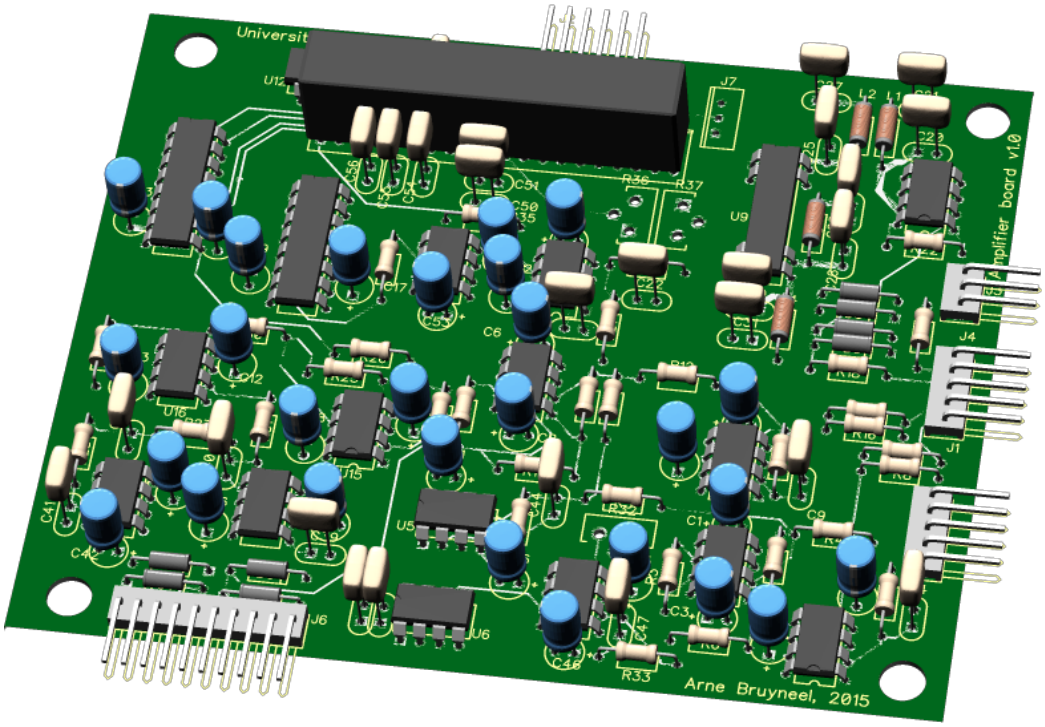


Figure 5.8: Bioreactor amplifier board: PCB. 3D model of the amplifier PCB. This four layer board comprises three independent amplifier units, two for pressure and one for electrical activity. Pressure signals were low-pass filtered and centred around a preset variable offset voltage. ECG signals underwent multiple stages of amplification. First, the difference between the input signals was amplified using an instrumentation amplifier, then the signal was passed through an isolation amplifier before being filtered and amplified further.

and electrical stimulation of the recellularising heart.

Temperature and humidity are measured approximately every five to 30 seconds, and displayed on the LCD. Moreover, the values are transmitted to the master bioreactor module, which passes it on the the PC. The duty cycle of the oxygen valve is set by the PC and transmitted to the slave unit which will open/close the valve as appropriately.

The PIC®18F4520 MCU (Microchip) was used as processor in the climate circuit board and communication to the master board was accommodated by the I^2C protocol. Both opening and closing of the valve and measurements of temperature and humidity are triggered by the timer module in the PIC®18F4520. The schematics and an outline of the PCB for the mechano-electrical stimulation board can be found in Figure B.4 and 5.9.

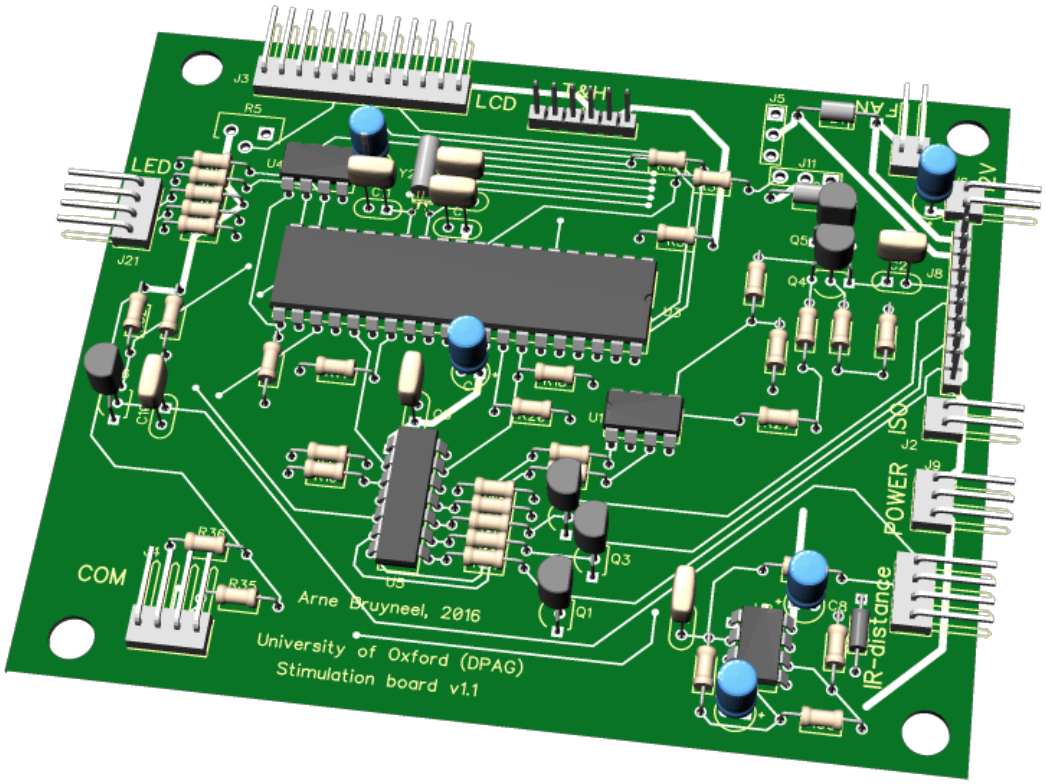


Figure 5.9: Bioreactor Stimulation board: PCB. 3D model of the Stimulation board PCB. This board controls the temperature and humidity measurements, the valve regulating the flow of O_2 and CO_2, and electrical and mechanical stimulation. In addition, it contains an amplifier for the determination of the linear position of the actuator.

Temperature and humidity sensors In contrast to the ECG and pressure recorders, the temperature and humidity were sampled less frequently (every 5 – 30 seconds). Digital sensors were utilised (SHT75 sensors, Sensirion) to measure both parameters which were transmitted to the climate controller module through a serial interface.

Oxygenation of the perfusate The perfusion buffer was provided with CO_2 and O_2 by diffusion through gas permeable tubing. A solenoid valve (Asco 411 series, 12 V DC, 0.65 W, 100 psi, normally closed) was installed in-line with the gas supply to the membrane oxygenator in order to allow the regulating system to limit the supply.

Synchronised electrical and bio-mechanical stimulation A digitally controllable linear actuator was used for the filling and emptying of the latex balloon within the ven-

tricle. Linear actuators are a type of motor that propel movement in a straight line: forwards or backwards. One way of obtaining linear motion is using the rotary power of a stepper motor and a nut and lead-screw. The stepper motor is composed of a stator and rotor and operates by sequentially energising stator coils. This makes it possible to move a predefined distance for every electrical pulse. Such engines need a specialised driving circuit to be operated, such as L/R or chopper drives. L/R drives operate at constant voltage, whereas chopper drives work at constant current. Chopper drives can maintain higher torque or forces at higher speeds than L/R drives. Many common stepper motors do 1.8° steps (200 steps/rev), but can be operated with microstepping drives to allow smaller displacements and smoother operation by dividing steps even further (up to 51200 steps/rev).

Linear actuators are bespoke engines with a large variety of features that can be set at the stage of manufacturing. In order to determine what type of actuator would be most appropriate for our purposes, design estimates and calculations were made. We estimated that the linear actuator should be able to move loads with a force up to 25 N. The displacement required to perform the stimulation cycle depends on the diameter or the syringe used, with larger diameters requiring shorter travel distances. However, larger travel distances also enable more fine-tuning (with step size <<< travel distance). As a result, we determined that a 2 to 5 mL syringe was most appropriate and that the actuator should be capable of doing displacements ranging from 100 µm to 1 cm within the time span of a stimulation cycle.

Even though the most appropriate stimulation frequency is arguably 1 Hz, we decided that the device should be able to operate up to 2.5 Hz, to make it comparable to published devices (343). This means that at maximum speed the actuator should be able to fill or empty the balloon in the LVRV in 50 to 100 ms. Based on Equation 5.1, a power up to 5 W was estimate to be required for such displacements (Equation 5.3).

$$P_{linear} = \frac{\text{distance travelled [meter]} \times \text{force [N]}}{\text{time of travel [s]}} \tag{5.1}$$

$$P_{linear,min} = \frac{0.002 \times 25}{0.1} = 0.5\ \text{W} \tag{5.2}$$

$$P_{linear,max} = \frac{0.01 \times 25}{0.05} = 5\ \text{W} \tag{5.3}$$

By taking into consideration a safety margin, a linear actuator (Haydon-Kerk, 43M4Y-05-825ENG, Table 5.2) with 5 V windings, 0.0636 mm step^{-1} and 1.8° step size was chosen that can deliver up to 100 N of force at the required speeds. A 1.8° step means that 200 full steps are required to do one full rotation around the threaded column.

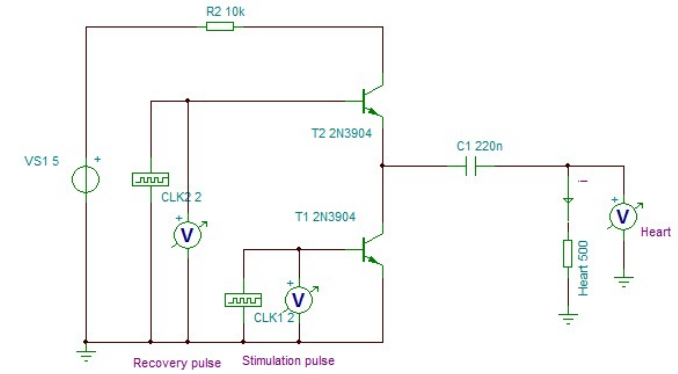
Table 5.2: Linear actuator characteristics

Parameter	Description
Manufacturer	Haydon-Kerk
Model series	43000 series
Motor design	Bipolar, 4 wires
Stack	1.8° double stack, captive
Step size	0.0636 mm step^{-1} (resolution)
Maximum force	100 N at 400 steps s^{-1}
Maximum speed	3 cm s^{-1} at 100 N, 10 cm s^{-1} unloaded
Voltage	5 V
Current	1.3 A
Power	14 W
Stroke	825ENG

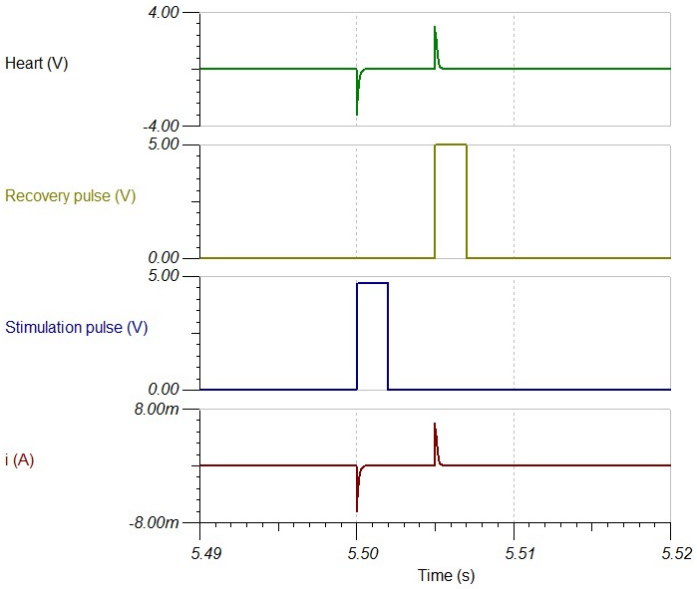
In terms of software control, the actuator was connected to a chopper drive provided by the manufacturer (DCM8027, Haydon-Kerk) which exposes the actuator's copper windings to appropriate current/voltage for it to move in a certain direction and speed. The drive acts on digital pulses from the MCU in the bioreactor controller (PUL/DIR method). Briefly, the the drive is connected to the MCU by three digital channels: ENABLE, PUL and DIR. ENABLE is used to switch the device on or off. DIR determines the direction of travel and PUL makes to actuator move one step. In addition, the board was equipped with circuitry to do basic position measurements of the actuator.

Cells in the body and *in vitro* are surrounded by a media with high electrical conductivity ($3-15\ \mathrm{mS\,cm^{-1}}$) and endogenous electrical field gradients are $0.1-10\ \mathrm{V\,cm^{-1}}$ (234, 344, 345). For the heart, the contractive activity is synchronised by the pacemaker cells and conductive system, and the beating frequency depends on the species (60 bpm for human and 360 bpm for rat). Exogenous pulse may be applied to trigger contraction, durations of $0.3-2$ ms are considered sufficiently long to excite cardiac tissue depending on the voltage applied. Indeed, larger stimulation durations are required when applying smaller stimulation voltages (346, 347). Electrical stimulation of the tissue culture medium results in charge transfer by different chemical mechanisms. Some of these transfer mechanisms may result in the degradation of the electrode and toxic products that might affect the cells, as a result the application of biphasic pulses have been proposed to limit this effect (234). In fact, biphasic field stimulation has been shown to be superior to monophasic stimulation for the differentiation of human cardiac progenitor cells and the culture of rat neonatal cardiomyocytes (348, 349). The bioreactor was equipped with a simple biphasic pulse obtained by charge dumping, as described by Laudon (346) (Figure 5.10). The voltage across the load, charge deposited and the pulse characteristics depend on the capacitor (C_1) and resistor (R_{Heart}) values, and the timing (discharge period). In this simulation, the capacitor discharged very quickly, using a larger capacitor on the other hand could keep the voltage higher and more constant during the stimulation pulse. In addition, the resistance of the tissue/medium also contributes to the time constant of the discharge, however, this is more difficult to modify. Platinum wires were used as inert electrodes to transfer the charge. The isolated voltage source was used to power the stimulation, and the digital signals driving the triggering were optically isolated in order to ensure isolation.

A basic combined mechano-electrical stimulation sequence goes as follows (a) inflate the balloon: the heart dilates and is in diastole, (b) trigger the heart: initiate systole, (c) deflate the balloon: the heart is in systole, (d) Goto step 1. Two basic stimu-



(a)

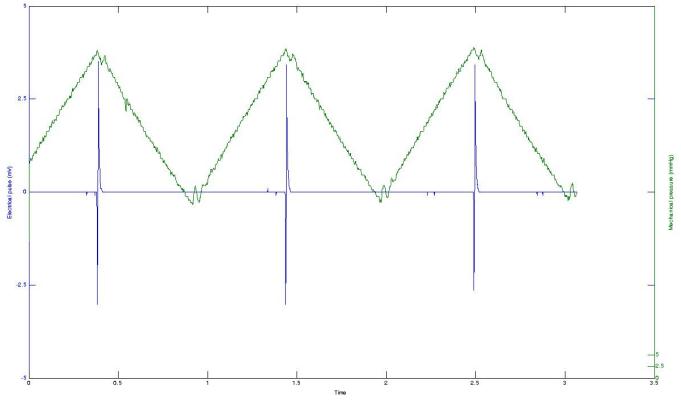


(b)

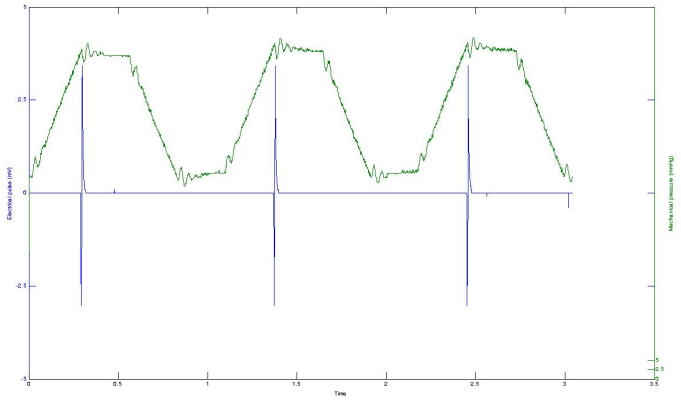
Figure 5.10: Biphasic electrical stimulation pulse by charge dumping (a) Circuit diagram of the electrical stimulation component, (b) Example of the electrical stimulation pulse, with $C_1 = 220\,\text{nF}$, $R_{\text{Heart}} = 500\,\Omega$ and a 1 ms pulse width (Simulation using Tina 10).

lation pulses were programmed into the bioreactor controller: a *triangluar* wave, and a *trapezoidal* wave (Figure 5.11). The triangular wave mimics the ventricular volume, whereas the the trapezoidal wave mimics the ventricular pressure during the cardiac cycle (Figure 5.3). The latter is arguably more relevant as mechanical stimulation pulse as it stretches the cardiomyocytes and makes them contract against a load (Frank-Starling

mechanism) (350).



(a)



(b)

Figure 5.11: Synchronised mechanical and electrical stimulation: triangular or trapezoidal pulse. Example pressure and electrical pulse time course recorded by compression/decompression of a mixture of water and air in a syringe at ~ 1 Hz synchronised with a biphasic pulse exerted across a 470 Ω resistor. The ECG signal was amplified 200× and both pressure and ECG were recorded at a 1 kHz sampling rate. The data was save by the bioreactor GUI as a comma-separated value (CSV) file, and subsequently post-processed for noise and plotted in Matlab. The pressure wave profile can be modulated to represent either a triangle (a) or trapezoid (b) wave, mimicking respectively the volume or the pressure within the contractile ventricle.

5.2.3.5 Communication with computer

The PC software allows the configuration of various settings, which are transmitted to the bioreactor controller as characters (Table B.1, B.2, B.3, and B.4). Conversely, raw measurements from various sensors are transmitted to the PC for processing and analysis. The desktop computer was connected to the master controller device with a nine-pin serial cable (RS-232). The PIC®18F4550 MCU, which is the main processing core in the master unit, has a hardware module for serial communication. However, the serial signals originating from the hardware module use 0,5 V logic, whereas the serial bus in the computer requires $-[3,15], +[3,15]$ V logic, hence for this conversion, a MAX232 dual driver/receiver (Maxim Integrated) was utilised. The PCB and the 18F4550 master controller were equipped with the required hardware to enable computer-MCU communication using universal serial bus (USB). However, the current software only allows serial communication.

5.2.3.6 Inter-MCU communication

Communication between the many MCUs, both within the master controller and between MCUs in the master controller and the stimulation controller, are organised by the I^2C protocol. All slave MCUs had hardware I^2C implemented, whereas for the master MCU I^2C was bit-banged, as the hardware module was used for SPI communication to the SRAM external memory. The communication to the oxygenation and stimulation controller occurred using a parallel communication protocol (Table B.5 and B.6). In order to validate communication, and to prevent corrupted transmissions to affect the function of the bioreactor, a two-step validation algorithm was implemented.

5.2.4 Computer client software

The PC software was developed with the aim of monitoring the ongoing recellularisation process and to modify stimulation parameters. The program was coded in C++/Qt and compiled on a Linux PC.

The program was implemented as a dual threaded application, which means that the software operates as two independent tasks. One thread was used to render the GUI, and a second *worker* thread provided the means to communicate with the bioreactor and for computation and data processing. Communication between the two parallel running threads utilised the signal-slot strategy embedded in Qt.

The software allows the configuration of the mechanical and electrical stimulation parameters, and allow the monitoring of pressure, electrical activity, temperature and humidity. The data is plotted on the screen, the raw data is saved as a CSV file and the graphical output directly save as portable document format (PDF).

5.3 Recellularisation of decellularised hearts

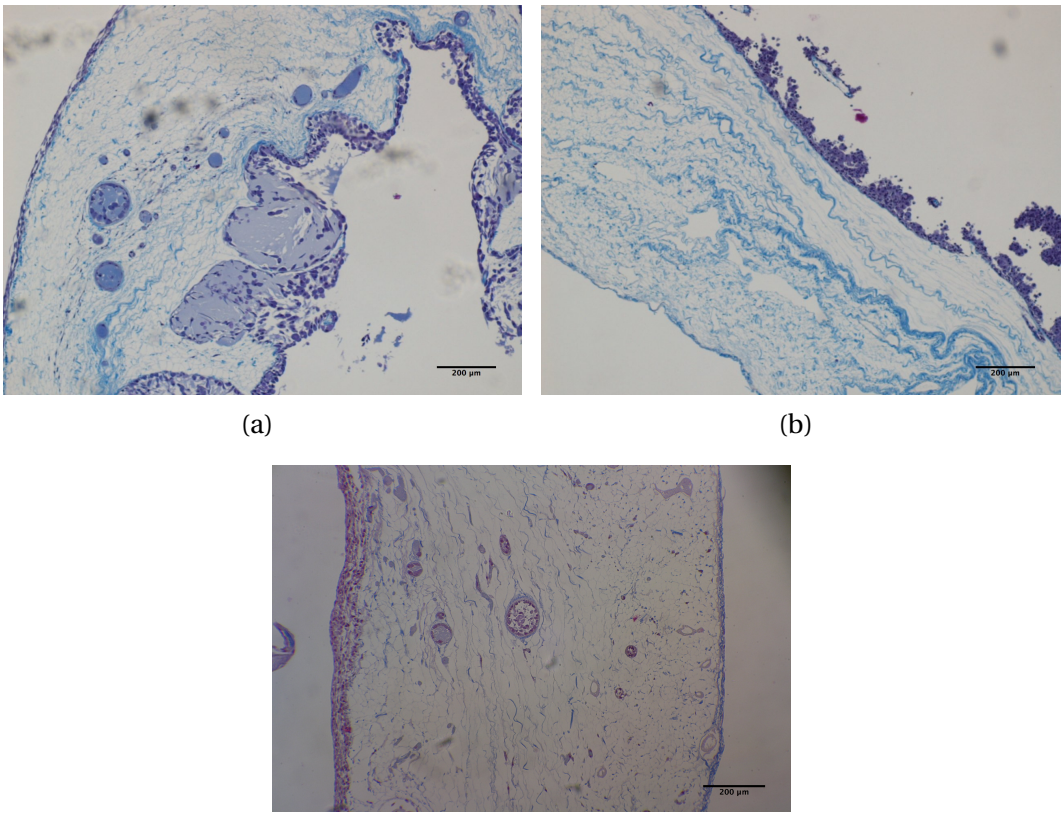
Preliminary studies were performed to establish proof of principle culturing techniques for decellularised hearts. These experiments were performed using the bioreactor at various stages of its development, as success or failure provided useful feedback for the further development and optimising of the device and the technique as a whole. CDCs were used in initial experiments, whereas iPS-CMs were the actual target cells for developing the humanised Langendorff perfused heart model.

5.3.1 Infused cells populate the vasculature and cavities, but fail to populate the full thickness of the construct

Isolated rat hearts were canulated via the ascending aorta and perfused briefly with PBS-adenosine (10 μM), and decellularised by constant pressure perfusion (72 mmHg) for about 18 hours with 1% SDS in ddH_2O and finally thoroughly washed using ddH_2O. Decellularised hearts were sterilised with ethanol, washed with PBS and seeded with CDCs and cultured in the bioreactor without mechano-electrical stimulation. Recellularised hearts were subjected to histological staining to assess where coronary-infused cells were located (Figure 5.12). Most cells were either located on the cavity walls or within the coronary vessels. Static culture in a standard incubator resulted in inhomogeneous seeding of the LV cavity, whereas cell infusion into the coronaries and bioreactor culture allowed the cells the cover most of the cavity and vascular bed. Very few cells seemed to have extravasated and migrated into the tissue.

5.3.2 Cells are viable and metabolically active within the recellularised heart

Decellularised hearts were sterilised with ethanol, washed with PBS and seeded with CDCs or iPS-CMs and cultured in the bioreactor. Media samples were collected every couple of days for the CDCs experiments or at harvest for the iPS-CM experiments to determine the lactate concentration (Figure 5.13). Lactate concentration increased with time, suggesting that recellularised hearts survived up to eight days and were metabolically active. Interestingly, lactate efflux from hearts recellularised with iPS-CMs was lower than those with CDCs, which might be due to differences in seeding efficiency, mechano-electrical stimulation, cell survival and proliferation or effective recirculating volume.



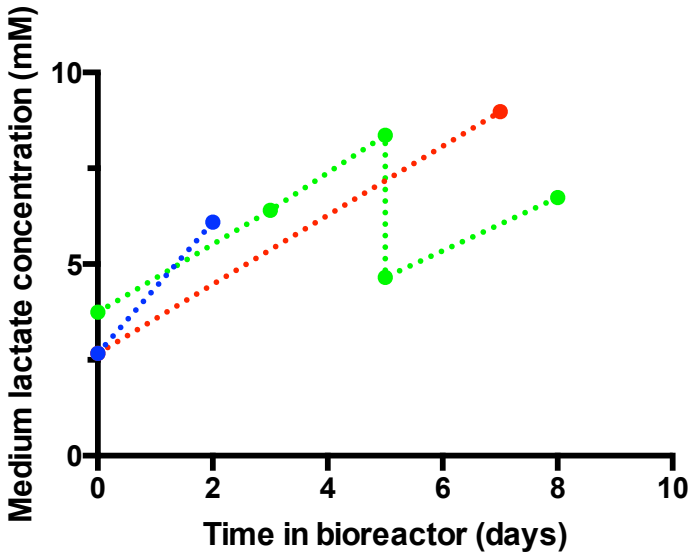
(a) (b)

(c)

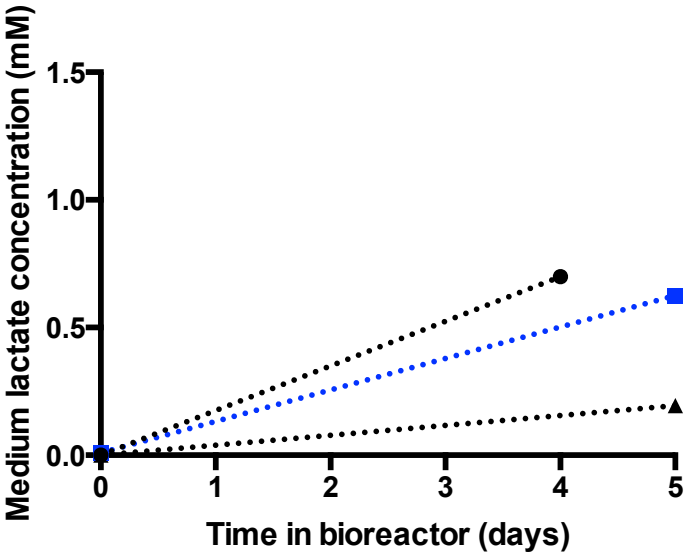
Figure 5.12: Histology on decellularised hearts reseeded with CDCs The recellularised heart was fixed in 4 % PFA and embedded in wax for sectioning. Slides were stained with MT and imaged using ordinary light microscopy. (a,c) Bioreactor culture, (b) Static culture. Scale bar: 200 µm.

5.3.3 Effect of biomimetic stimulation on gene expression of iPS-CMs

iPS cells were differentiated into iPS-CMs and seeded onto decellularised hearts in order to assess the maturation induced by mechano-electrical stimulation. The balloon was placed in the RV, rather than the LV, to limit cell loss as a result of mechanical friction. As control treatment, cells were cultured on collagen scaffolds and gelatin-fibronectin coated flasks. Contracting cells were observed in the gelatin-fibronectin coated dishes and at the edges of some of the collagen scaffolds. qPCR analysis suggested that cardiomyocytes were retained within the recellularised heart, as the gene expression of *TNNT2*, *MYH6* and *MYH7* was unchanged compared to the harvest cells used for seed-



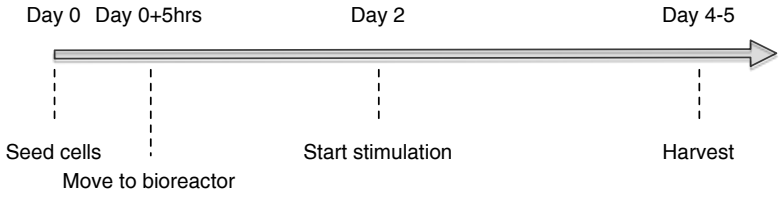
(a)



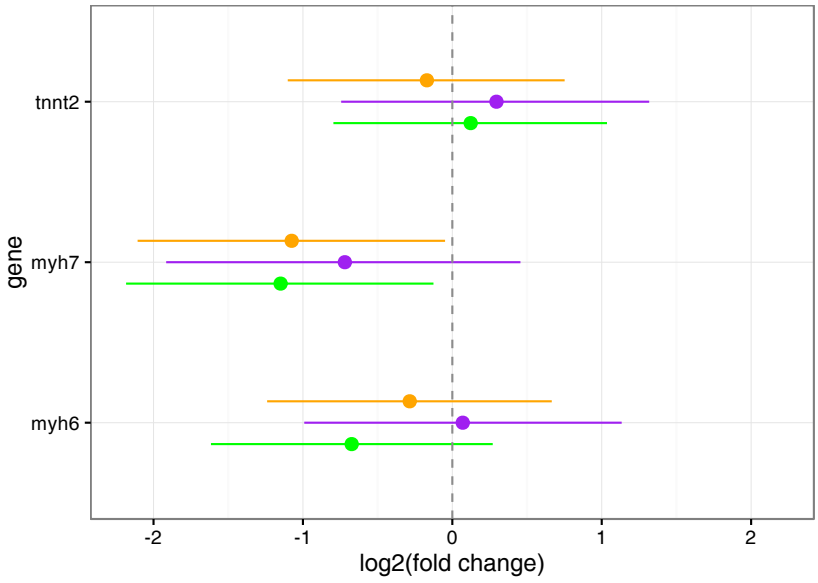
(b)

Figure 5.13: Metabolic activity of recellularised hearts: CDCs and hiPS-CMs Decellularised hearts were sterilised, seeded with cells and cultured in the bioreactor. (a) Decellularised hearts reseeded with CDCs. These hearts were under biomimetic conditions, but without mechano-electrical stimulation ($n = 3$). (b) Decellularised hearts reseeded with iPS-CMs. These hearts were under biomimetic conditions with mechano-electrical stimulation (ME: $n = 2$, M only: $n = 1$). Medium samples were collected every couple of days and analysed for lactate concentration on a Pentra ABX 400 blood and serum analyser.

ing, or any other group (Figure 5.14).



(a)



(b)

Figure 5.14: iPS-CMs on collagen scaffolds and decellularised hearts (a) Time line expressing the experimental outline of the recellularisation experiment. (b) Point represents the mean, and the line the 95% credibility interval of the fold-change in expression relative to the cells used for seeding. Gene expression was normalised to the expression of the housekeeping genes. Green represents the gelatin-fibronectin group ($n = 3$), whereas orange represents the scaffolds group ($n = 3$) and purple the recellularised group ($n = 2$: ME: $n = 1$, M only: $n = 1$).

5.4 Discussion

The design and development of a bioreactor setup for cardiac recellularisation enabling coronary perfusion and mechano-electrical stimulation was described in this Chapter. Few commercial alternatives are available and hence a bioreactor was designed and

manufactured. In fact, the development of bioreactors for tissue engineering is an active area of research (341, 342).

Recellularised hearts are considered too big to be adequately supplied with nutrients and oxygen in static culture, and hence the development of a perfusion device is required for their culture. Furthermore, mechanical and electrical stimulation have been shown to have beneficial effects on CM maturation and hence these stimuli were implemented in the bioreactor setup. In addition, in this Chapter we described the results of our attempts to recellularise whole rat hearts with both CDCs and iPS-CMs. The CDCs were used as a stepping stone for setting up the protocols, whereas the iPS-CMs were the actual target cells for developing the humanised Langendorff perfused heart.

Multiple different ways of seeding and culturing recellularised hearts have been proposed. Ott *et al.* (238) mounted the heart suspended in air, seeded by perfusion and injection, and perfused the heart in working heart mode. Whereas Hülsmann *et al.* (343) injected cells into the heart, cultured it submerged in cell culture medium, and applied retrograde perfusion. Lu *et al.* (297) on the other hand, did not continuously perfuse their recellularised mouse hearts as they observed washout of most of the cells within the first five days.

In our bioreactor, the hearts were suspended in air, and perfused via the aorta (retrograde). We demonstrated that it is possible to culture cells within the decellularised heart, but showed that coronary infusion with cells does not lead to homogenous seeding, since most cells were located on the capillary walls and within the cavities of the heart. Injection into the LV wall was attempted, but abandoned given that most cells were observed dripping out of the injection site, and since injection through a very fine bore needle resulted in significant lethality in control seeded cells (351). Cell infusion and direct cavity seeding was then attempted and used for the qPCR data presented in this Chapter. Given that most cells are likely to reside on the intracardial surface, the mechanical stimulation balloon was placed in the RV. Stimulation of the RV will hence

reduce mechanical rubbing of the cells, but limits the mechanically stimulated area to the septum in between both ventricles. By the time of submission, we failed to acquire sufficient samples for a more thorough qPCR analysis, hence we are only able to confirm the CM fate of the seeded cells. It was difficult to obtain sufficient quantities of high quality RNA, hence normalisation to housekeeping genes was applied to correct for differences in sample quality. Cell culture in the decellularised heart is challenging. First of all, handling of seeded decellularised hearts as they are transferred to the bioreactor might result in cell damage. It would clearly be beneficial to optimise the process further to make it more user friendly. With respect to cell seeding, dispersion of cells within the matrix of the decellularised tissue would be the most ideal scenario. The problematic nature of seeding was already reported by Ott *et al.* (238) in 2008, but unfortunately, little progress has been made in improving seeding efficacy so far. Secondly, the iPS-CMs in contrast to CDCs do not proliferate at a significant level by the time they form the larger contractile networks. In addition, the iPS-CMs are quite sensitive to digestion methods to prepare cells for reseeding. Hence, it might be beneficial to use the cells at a more immature stage, when there are more flexible, resilient and proliferate. Thirdly, decellularised matrixes may not be entirely biocompatible and might limit cell activity to a certain extent. It remains unclear whether this is due to residual detergent bound to the matrix, or due to matrix alterations caused by the decellularisation process (338).

The bioreactor was enclosed within a heated chamber, and not a standard CO_2 incubator. The atmosphere within a CO_2 incubator is kept at 5 % CO_2 for buffering the tissue culture medium. Whereas, in the heated chamber used here, the tissue culture medium was gassed with CO_2 and O_2, using gas permeable tubing, before it enters the bubble trap above the heart. This means that only part of the perfusion loop would be adequately buffered. Depending on the rate of CO_2 escaping from the medium, the pH may or may not be optimal for the cells. In addition, CO_2 incubators are superior in maintaining humidity, compared to the heated chamber which uses convective flow to

maintain temperature. Having the heart submerged in medium, rather than air, might make it easier to provide the cells with the optimal pH, oxygen content and temperature.

There is considerable variation in electrical and mechanical configurations described in literature, and since recellularisation is a low-throughput method and iteration through device configuration is difficult, standard stimulation conditions were utilised in this device as a starting condition. Various methods have been proposed to induce mechanical stimulation (224), such as *inter alia* compressive loading, longitudinal stretch, and substrate bending. Uniaxial longitudinal elongation of 5−20% is the most frequently used given its simplicity (Table 5.3). For whole heart mechanical stimulation, either pulsatile flow (238) or balloon inflation have been applied (343, 352). When using a flat deformable substrate, the percentage stretch can easily be computed, however in the present 3D scenario this is not as straightforward. Hülsmann *et al.* (343) applied surface scanning microscopy techniques to determine the elongation, whereas Guyette *et al.* (352) did not provide any information with respect to the used configuration. We propose to use a simplified model, assuming that the RV or LV cavity is a sphere and that the default volume is known (inflation of the balloon that leads to swelling but not stretching). Hence, assuming that the ventricular cavity deforms in all directions equally, the percentage stretching can be determined by the ratio of the surface areas.

Similarly, there is little uniformity in the use of AC signals to electrically stimulate tissues (Table 5.4). First, bidirectional electrical fields are typically generated using either direct contact between metal electrode and the medium or tissue or by capacitive or inductive coupling. Secondly, either mono-phasic or biphasic pulses are applied. Biphasic pulses have the advantage that they recover more of the deposited charge, however, a second stimulation pulse, too soon after the first, might limit the efficacy of depolatisation and hence ablate the effect of stimulation (234). In the present bioreactor design, it was not the aim to expose all cells to a fluctuating electrical field. Indeed, the aim here was the trigger some cells at the atrioventricular interface to contract such that

the excitation wave would spread across the entire ventricle at the right phase of the mechanical cycle.

It is currently unresolved whether the triangular or trapezoidal mechanical pulse is more potent in maturing iPS-CMs by mechanical stimulation. In addition, it is also unclear whether the profile of the electrical pulse is able to induce contraction of the cells within the recellularising heart. However, for testing and eventually optimising these parameters, successful culture of cells within the organoid is required first. If one is interested in deviating from either a triangular or trapezoidal wave, the mechanical waveform can be modified in the source code in the MCUs. Similarly, the stimulation duration and the delay between stimulation and recovery can be altered in the source code. for manipulating the electrical pulse, modification can be made to alter the amplitude of the stimulation pulse and the slope during discharge (leading and trailing edge). Alternatively, the stimulation board can be rewired to trigger an external cardiac stimulator (354).

Cell monitoring is problematic in 3D constructs, in contrast to 2D monolayers cultured on transparent plastics. The bioreactor described here lacks direct cell monitoring capacities, because they are very difficult to implement. However, the bioreactor is able to measure electrical activity, both arising from the stimulation pulse or potential cell activity, with sufficient dynamic range to detect ECG signals (356). Currently, we have not been able to detect an ECG signal from recellularised hearts. However, it is likely that further improvements are required in terms of cell culture strategy. In addition, it would be beneficial to mount the bioreactor within a Faraday cage and provide additional earthing to limit noise and mains interference which hinders the detection of small amplitude signals. The easiest method to get some idea of cell activity is to measure metabolite concentrations in the culture media. Alternatively, dyes can be perfused into the construct which change colour depending on the cell activity (357). However, more ingenious approaches are currently being developed to allow real-time

non-invasive monitoring of the 3D constructs (358).

The optimal medium volume within the setup may be an important parameter to consider. On the one hand, media is a source of nutrients and a too small recirculating volume may require medium changes too often. On the other hand, a too large volume will result in dilution of the paracrine factors secreted by the cells (222). There is some indication that paracrine signalling plays significant roles in iPS-CM differentiation. In addition, the flow rate at which the medium is perfused through the tissue is of considerable importance. If the flow rate is too high, cells may be washout out, whereas if the flow rate is too low, the supply of essential nutrients may be restricted. In addition, shear stress induced by flow may aid in the differentiation and development of vasculature (359).

Notwithstanding our difficulties with recellularisation, most solid organs have been decellularised/recellularised since the seminal work by Ott *et al.* (238) was published in 2008. However, most evidence provided is restricted to histology and/or is anecdotical (Table 5.5), and no significant progress has been made in either the throughput or quality of the presented data. For example, the work presented by Ren *et al.* (357) and Guyette *et al.* (352) contained data with standard deviation larger than the mean for metrics that are positive-definite, suggesting high batch-to-batch variability. Hence, it is clear that additional work or alternative strategies will be required to develop this technique further.

Few studies to our knowledge have attempted to make a comparison between differentially treated recellularised tissues. Only Robertson *et al.* (360) performed such a study and demonstrated that the average maximal rate of change in pressure was significantly higher in re-endothelialised compared to non-endothelialised neonatal CM reseeded decellularised hearts. Ott *et al.* (238) applied both electrical and mechanical stimulation (pulsatile flow), whereas in the follow-up study from the same group (352) only mechanical stimulation (balloon) was used. The likely reason for the limited amount of

comparative studies is the low throughput nature of this work, and the high variability. In our study, the qPCR data, at least for the genes we investigated, was consistent. This is not unsurprising since qPCR data is normalised and corrected for differences in cell seeding efficacy and quality of the samples. However, the more interesting parameters, in particular those relevant to the development of the humanised Langendorff model, such as function, are most likely burdened the most by variability.

In the development of a bioreactor setup, it seems advised to iteratively improve the current setup and associated culture methods based on experience gained from attempting to use the current prototype. As a result, the bioreactor described in this thesis has a modular design, which allows the user to upgrade part of the device, without the need to modify other aspects.

5.5 Conclusion

In this Chapter, a modular bioreactor setup that enables perfused culture of recellularised hearts under mechanical and electrical biomimetic stimulation and protocols for the culture of recellularised hearts in the bioreactor were described. The fluidic part of the device enables perfusion and oxygenation of the organoid, and can be autoclaved to acquire sterility. Mechanical stimulation is achieved by inflating and deflating a balloon located within the RV or LV, whereas electrical stimulation is exerted using biphasic pulses delivered via platinum electrodes attached to the surface of the heart. In addition, the feasibility of culturing cells within the recellularised hearts under biomimetic conditions in a bioreactor was investigated and recommendations were made for further development of this technique.

In summary, this device and associated protocols form a framework for the generation of human Langendorff perfused hearts for *in vitro* testing. However, further development and optimisation is required before this technique can be applied.

Table 5.3: Overview of mechanical stimulation parameters used in literature Abbreviations: human umbilical vein endothelial cells (HUVECs).

Culture system	Cell type	Stimulation profile	Outcome	Reference
Recellularisation	Neonatal CMs	Pulsatile flow	Contraction	Ott *et al.* (238)
Recellularisation	iPS-CMs	Balloon inflation	Contraction	Guyette *et al.* (352)
Recellularisation	C2C12	0 – 2.5 Hz, 10% elongation (balloon)	Alignment	Hülsmann *et al.* (343)
Chamber-sheet	HUVECs	1 Hz, 10%	Alignment	Lu *et al.* (353)
Silicon sheets	BM-MSCs	0.17 Hz, 10%	Marker upregulation	Egusa *et al.* (225)
FlexCell	iPS-CMs, ES-CMs	1 Hz, 5%	Alignment, hypertrophy	Tulloch *et al.* (226)
Silicon chamber	CDCs	1 Hz, 20%	Differentiation	Kurazumi *et al.* (227)

Table 5.4: Overview of electrical stimulation parameters used in literature

Culture system	Cell type	Stimulation profile	Outcome	Reference
Microfluidic	NIH3T3	6 V/cm, DC, 3 mA	Alignment	Tandon *et al.* (234)
Recellularisation	Neonatal	5 – 20 V, 1 Hz, 2 ms	Contraction	Ott *et al.* (238)
Chamber-sheet	Neonatal	7 V/cm, 1 – 2 Hz, 4 ms	Contraction	Lu *et al.* (353)
C-Pace (Ion-Optics Co.)	ES-CM	6.6 V/cm, 1 Hz, 2 ms	Gene expression, maturation (Ventricular, Ca^{2+})	Chan *et al.* (355)

Table 5.5: Overview of whole organ recellularisation studies Abbreviations: Western blot (WB), rat aortic endothelial cells (RAECs), fetal lung cells (FLCs), neonatal kidney cells (NKCs).

Organ	Seeding	Cell type	Phenotypical characterisation					Reference
			Histology	WB	qPCR	Function	*In Vivo*	
Heart	Infusion/injection	Neonatal CMs, RAECs	+	-	-	+	heterotopic (decell.)	Ott *et al.* (238)
Lung	Infusion	HUVECs, epithelial cells, FLCs	+	+	-	+	heterotopic (recell.)	Ott *et al.* (361)
Liver	Infusion/injection	Primary rat hepatocytes	+	-	+	+	heterotopic (recell.)	Uygun *et al.* (362)
Kidney	Infusion	HUVECs, rat NKCs	+	-	-	+	heterotopic (recell.)	Song *et al.* (363)
Heart	Infusion	iPS-CM	+	-	+	+	-	Lu *et al.* (297)
Heart	Injection	iPS-CM	+	-	-	+	-	Guyette *et al.* (352)
Heart	Infusion/injection	Neonatal CMs, RAECs	+	-	-	+	heterotopic (recell.)	Robertson *et al.* (360)

CHAPTER 6

THERAPEUTIC EFFECT OF TRANSPLANTATION OF BILAYER COLLAGEN SCAFFOLDS SEEDED WITH HYPOXIC-PRECONDITIONED CARDIOSPHERE-DERIVED STEM CELLS AFTER MYOCARDIAL INFARCTION IN AN EXPERIMENTAL RAT MODEL

6.1 Introduction

Current therapeutic strategies for AMI, although they prolong life, offer only temporary relief. Since, dead muscle tissue will be replaced by scar tissue, which is maladaptive and leads to the development of HF. Hence, stem cell and tissue engineering approaches were proposed as these might give rise to the development of new muscle.

6.1.1 Stem cell therapy and tissue engineering for the heart

Clinical trials using adult stem cells have demonstrated safety, but only limited efficacy (107). It is believed that low cell retention, low cell survival, lack of cellular effect, failure to establish mechanical and electrical coupling, or low rates of cardiac differentiaton are key to the limited beneficial effect seen in patients (364). As a result, tissue engineering strategies were proposed, which may offer a plausible rebuttal.

Cardiosphere-derived cells The ideal source for cardiac cell therapy still remains to be elucidated. Many exogenous stem cells or progenitors (BM (65), myoblasts (78), adipose-derived stem cell (ADSC) (365), iPS-CM (87), ES) and endogenous CSC have been investigated (c-kit (58), Sca-1 (90), ALDH (91), side population (92), epicardial (93, 94) and cardiospheres (95)). A recent meta-regression of pre-clinical animal studies revealed that different cell types had different therapeutic effects in terms of EF post-MI (366). Indeed, CDCs had the largest therapeutic effect, which was significantly higher than the effect seen by Sca-1 positive cells.

In the current study CDCs were used (95), which can be isolated from small cardiac biopsies, allowing the production of patient-specific stem cells without the risk of rejection. The CDCs isolation is a multistep procedure, which enables the purification of the stem cells from the fibroblasts present in the cultures (95, 100). CDCs have been shown to have beneficial effects after transplantation in experimental infarction models (101, 105, 106). A phase-I clinical trial demonstrate safety but limited therapeutic effect (102, 107).

The exact mechanism by which CSCs induce their beneficial effects on cardiac function is not well understood as multiple signalling pathways are possible. However, a recent study by Chimenti *et al.* (135) suggested that paracrine effects are the most likely cause. Nonetheless, CDCs have been shown to differentiate into CMs and endothelial cells *in vitro*, suggesting that direct differentiation can also aid in regeneration post-MI

(103, 104). Given the importance of paracrine signalling, the CDCs in this study were exposed to hypoxia before implantation, as previous research has shown that hypoxia increases stemness and growth factor secretion (143).

Scaffolds as vehicle Tissue engineered constructs, such as scaffolds can provide a biomimetic environment suitable for cell engraftment and proliferation, or can deliver suitable growth factors, such as VEGF to steer the regenerative process.

In this study, collagen type I scaffolds were used. Collagen is the most abundant protein in the mammalian ECM. An advantage of using natural scaffolds is that by default these materials are biocompatible and biodegradable, in contrast to many synthetic materials.

6.1.2 Mechanical considerations of scaffolds

Mechano-compatibility is essential for tissue engineered strategies for the heart, as incompatible materials may cause additional damage by hindering contraction (367).

The following model for mechano-compatibility can be derived, by considering the heart as a spherical thin-walled pressure vessel. In such vessels no bending occurs, only tensile forces are present. The stress in the circumferential direction (σ_θ) and the stress in the longitudinal direction (σ_{long}), are defined as:

$$\sigma_\theta = \sigma_{long} = \frac{PR}{2t}, \tag{6.1}$$

with, P the internal pressure, R the inner radius of the curvature and t the wall thickness. This model holds if $R/t > 10$.

For a material attached to the epicardium to be 'mechano-compatibile', the heart and patch should undergo same strain (ϵ):

$$\epsilon_{heart} = \epsilon_{patch} \tag{6.2a}$$

$$\frac{\sigma_{heart}}{E_{heart}} = \frac{\sigma_{patch}}{E_{patch}} \tag{6.2b}$$

$$\frac{PR}{2t_{heart}E_{heart}} = \frac{PR}{2t_{patch}E_{patch}} \tag{6.2c}$$

$$t_{heart}E_{heart} = t_{patch}E_{patch} \tag{6.2d}$$

The product of the Young's modulus (E) with the thickness of the layer (t), has been named the 'structural modulus, Ω' (367):

$$\Omega = Et \tag{6.3}$$

Defining Equation 6.2d as the requirement for mechanocompatiblity implies that the mechanotherapeutic effect is optimal when the injured area and the patch material carry the same straining. As a result if the LV, as a result of infarction would weaken, the patch would still ensure the straining is limited and dilation would not occur.

Stuckey *et al.* (367) determined that a structural modulus of $0.1\,\mathrm{N\,mm^{-1}}$ would be ideal for a rat heart, considering the Young's modulus E_{heart} of heart muscle is 0.05 MPa and rat heart wall thickness at end diastole, t_{heart}, is 2 mm. The heart patch thickness t_{patch} should be $0.2-0.5$ mm to prevent tearing during attachment, and adhesion to or pressure on the chest wall (368), this implies that a 0.33 mm-thick patch should have a Young's modulus of 0.3 MPa to be structurally compatible (Equation 6.3).

Alternatively, Engler *et al.* (369) demonstrated that a considerable softer material than the adult myocardium or scar tissue is superior to achieve maximum myocyte contractility and development of immature cardiomyocytes ($E = 1-14$ kPa).

However, these calculations do not take into account the fact that the material properties are dynamic, as degradation and cellular activity is very likely going to affect the mechanical properties.

6.1.3 Host response to scaffolds

Foreign objects, including transplanted scaffolds, are recognised by the body and activate the immune system. Key to any inflammatory response are the macrophages, and these mononuclear cells have the ability to secrete a wide variety of inflammatory molecules, including cytokines and chemokines, by which they can steer the local inflammatory response.

Different types of macrophages can be distinguished by distinct functional properties, surface markers, and the cytokine profile (370). Polarised macrophages are referred to as either M1 or M2 cells, although they are loosely defined and on a spectrum. The role of the classically activated (M1) macrophage is pro-inflammatory, whereas the alternatively activated (M2) macrophages are involved in immunosuppression and tissue repair. Hence, in normal tissue repair, at early stages macrophages exhibit an M1 phenotype and at later stages a pro-healing phenotype M2.

6.1.4 Aims

The hypothesis under investigation in this Chapter is whether collagen scaffolds are a suitable vehicle for CDC stem cell delivery to the heart post MI. To study this hypothesis, we aimed to develop a collagen scaffold suitable for use in cardiac surgery in rats. Since, hypoxia had been shown to increase the stemness and paracrine secretome of stem cells, we aimed to culture CDCs in hypoxia and to culture these cells on the collagen scaffolds in preparation for the surgery. Next, we aimed to use these scaffolds in a rat *in vivo* model of MI to assess the potential beneficial effect of collagen scaffolds versus collagen scaffolds with CDCs.

6.2 Results

6.2.1 Design and manufacture of a bilayer collagen scaffold

Collagen type-I, accounting for 91 % of all collagen, is the most abundant collagen isoform in the heart. Collagen type-III, on the other hand accounts for 6 % (371). Moreover, extracted and purified type I collagen is biocompatible and processable (177). Hence, collagen type-I was chosen as scaffold material to develop cardiac patches.

Initial attempts to place collagen type-I scaffolds (circular, $r = 13$ mm, $h = 4$ mm, as described in (178, 249)) on rat hearts were not very successful for two reasons: (a) upon hydration, the scaffolds easily folded making is hard to place the scaffold on the heart, (b) adhesions between the scaffold and the chest wall were a very common complication of the surgery.

As a result, a bilayer scaffold was developed in order to improve handling and limit adhesions (Figure 6.1), based on earlier developments (372, 373). Imaging by scanning electron microscopy (SEM) confirmed that the scaffold is comprised of a porous layer and a solid film layer (Figure 6.1(c) and 6.1(d)).

6.2.2 Host response to the transplantation of collagen scaffolds

In order to assess the *in vivo* behaviour of collagen scaffolds, in terms of engraftement, degradation and colonisation, a time course experiment was performed. Collagen scaffolds were sterilised with ethanol and rinsed with DPBS, before being transplanted onto infarcted rat hearts. The hearts were surgically removed after two or six weeks, and prepared for histological analysis.

At time of tissue collection, scaffold remnants were clearly visible at two weeks post surgery (Figure 6.2(a) and 6.2(c)). Whereas at six weeks, for the majority of hearts no scaffold remains were visible, at least by visual inspection. Histological analysis revealed

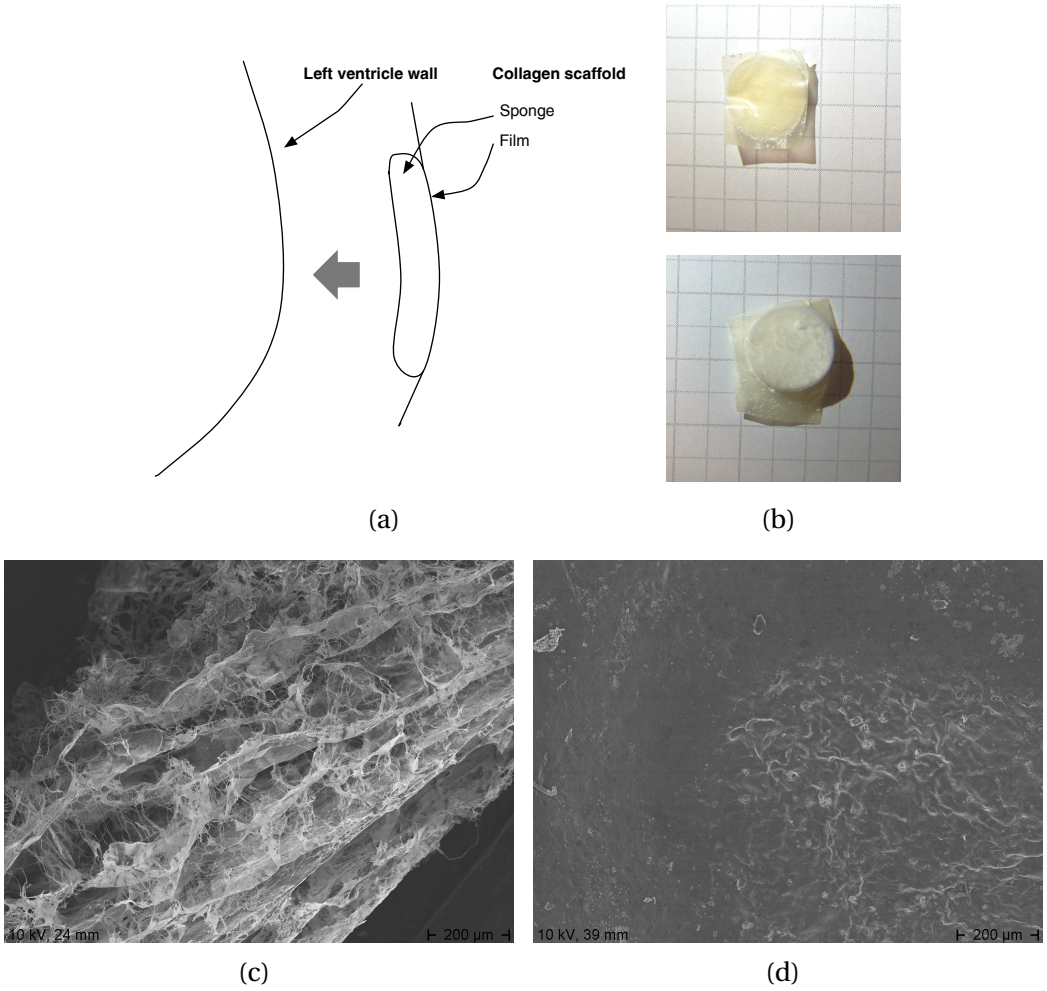


Figure 6.1: Design of bilayer collagen scaffold for implantation on the LV wall post-MI (a) Diagram of the scaffolds and attachment to the heart. (b) Photograph of the top and bottom of scaffolds on 5 mm graph paper: film on top (top), sponge on top (bottom). SEM imaging of the bilayer scaffold (scale bar: 200 µm): (c) Collagen sponge, (d) Collagen film. SEM images courtesy of Rabia Nazir (Dept. Materials, Oxford).

that the scaffold-attachment was incomplete at two weeks (Figure 6.2(d) and 6.2(e)), whereas integration was near complete at six weeks (Figure 6.2(f) and 6.2(g)).

Immunohistochemistry analysis was performed to assess macrophage recruitment and blood vessel formation (Figure 6.3). Macrophages were stained using an antibody for CD68 (pan-macrophage), which revealed that macrophages were present in the scaffold both at two weeks and at six weeks post-implantation (Figure 6.3(a) and 6.3(b)). Additionally, von Willebrand factor (vWF) positive blood vessels could be identified within

the scaffolds (Figure 6.3(c)).

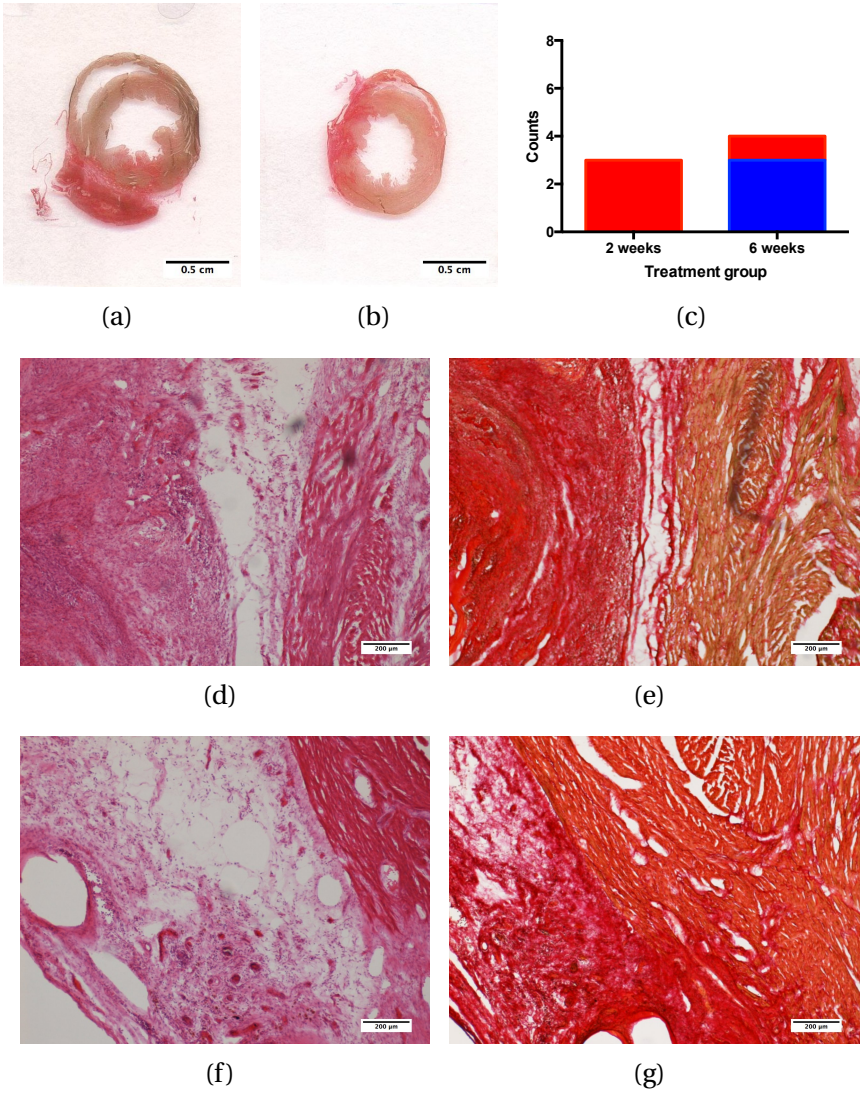
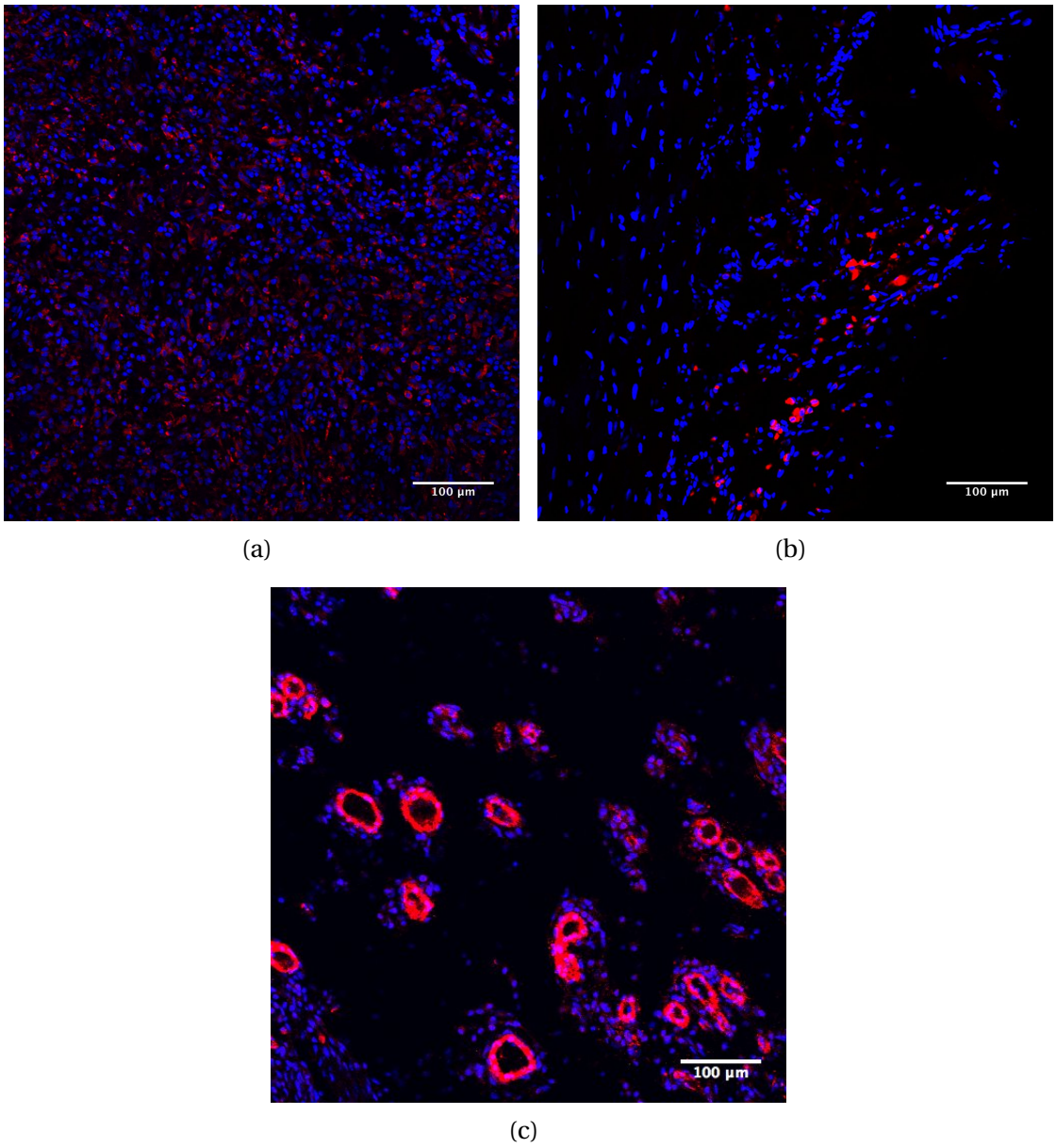


Figure 6.2: Retention and integration of collagen scaffolds to the heart two and six weeks post surgery H&E and SR staining of tissue cryosections. Whole section SR staining at (a) two weeks or (b) six weeks post surgery. (c) Quantification of scaffold visibility at two or six weeks post surgery (Red: visible, Blue: not visible by eye, both $n = 3-4$). H&E (d,f) and SR (e,g) staining of the scaffold-heart interface at two (d,e) and six (f,g) weeks post-surgery. Scale bar: 200 µm.



(a) (b)

(c)

Figure 6.3: Scaffold colonisation by macrophages *in vivo* Macrophages two (a) and six (b) weeks post-implantation (Red: CD68, Blue: DAPI). (c) Blood vessels within the scaffold two weeks post-implantation (Red: vWF, Blue: DAPI). Scale bar: 100 µm.

6.2.3 Cardiosphere-Derived Cells

6.2.3.1 Harvest

CDCs were extracted from the apex and atrial appendices of six-week old male SD rats (body weight 158 ± 3 g, $n = 10$), by mincing the tissue and plating the fragments on fi-

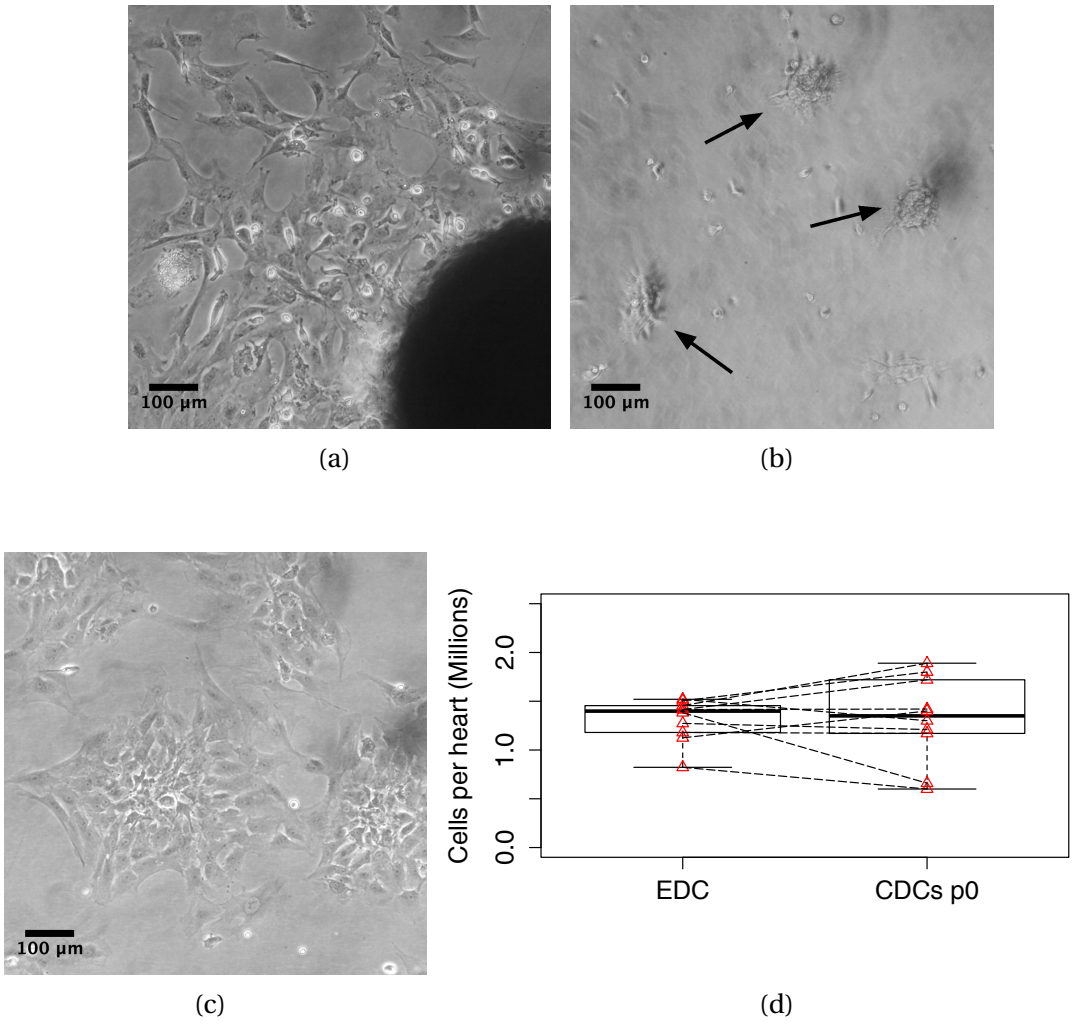
bronectin coated plates. After nine days of culture, EDCs were harvested from the explants yielding $1.3 \pm 0.1 \times 10^6$ cells per heart (Figure 6.4(a), Figure 6.4(d)), which were subsequently cultured for four days on poly-d-lysine plates in CGM media to form cardiospheres (Figure 6.4(b)). These spheres were harvested to form passage zero CDCs (Figure 6.4(c)). After three days in culture, the plates were confluent and the cells harvested for cryopreservation, yielding $1.3 \pm 0.1 \times 10^6$ cells per heart (Figure 6.4(d)).

6.2.3.2 Characterisation of colony formation potential of Cardiosphere-Derived Cells cultured in normoxia and hypoxia

CDCs form colonies in both normoxia and hypoxia. However, the colony forming efficiency was higher in hypoxia (Figure 6.6(a), paired t-test: p-value < 0.001) and different types of colonies could be distinguished (Figure 6.5).

Interestingly, the relative abundance of the different types of colonies appeared to be different between normoxia and hypoxia. Indeed, in normoxia two types could be distinguished (a, b), whereas in hypoxia four types were present. Colony types a and b are the most prevalent. Mixed effect models were fitted to compare colony sizes (Figure 6.6(b)). As the data was not-normally distributed (upward skewness), the data was log transformed. When considering only the hypoxic colonies, colony type b had a significant negative effect-size compared to type a. In addition, multiple testing within all types, revealed only the difference a-b as significant (p-value $< 1 \times 10^{-3}$). This is most likely the result of the higher power in those groups. When only considering the normoxic colonies, type b colonies were significantly smaller than type a colonies (p-value= 0.001). When only considering colony types a and b, but both hypoxia and normoxia, colonies of type b were significantly smaller (p-value $< 1 \times 10^{-4}$), independent of the oxygen tension.

In summary, hypoxic treatment increased colony forming potential and the different colony types present. The colony size is colony type dependent, and independent of

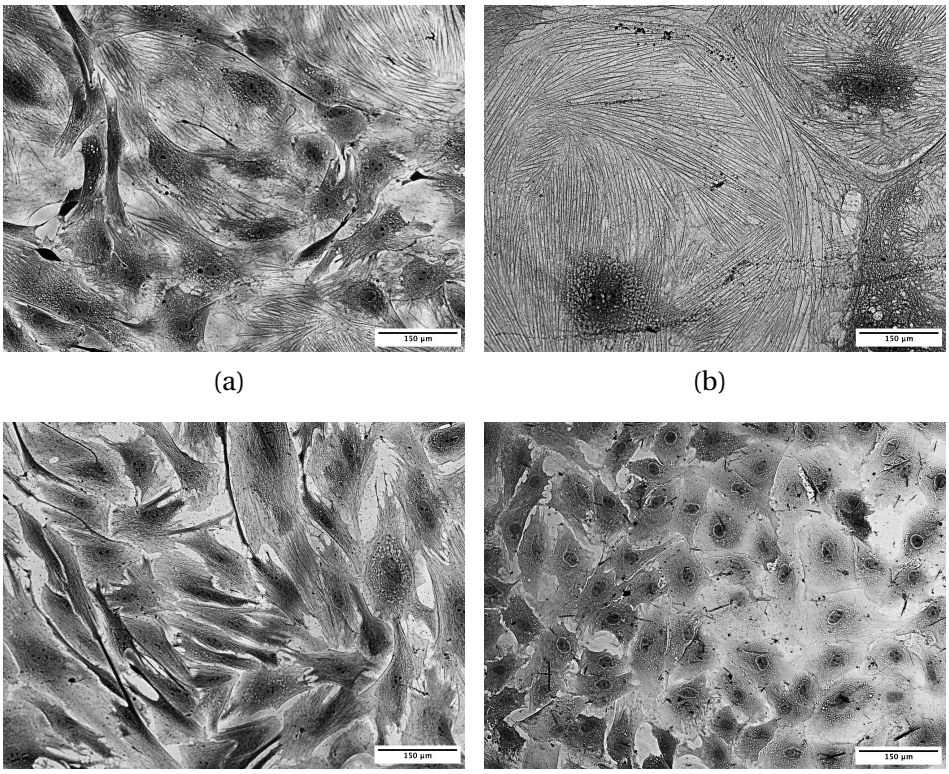


(a) (b)

(c) (d)

Figure 6.4: Cell morphology during the cell isolation protocol CDCs are generated using a three-step procedure. First, explant tissue from the apex and atria was cultured on fibronectin coated dishes, and a mixed population of cells migrates out of the tissue: explant-derived cells (a). Then, these cells were harvested and replated on poly-d-lysine coated plates, which allows them to form spheres (b). After four days, the sphere were harvested and the resulting cells cultured on fibronection, these cells were named p0 cardiosphere-derived cells (c). Yield of cells at different stages of the stem cell isolation process (d). The cell yield did not differ between the EDCs and CDCs (p0) stage.

oxygen tension.



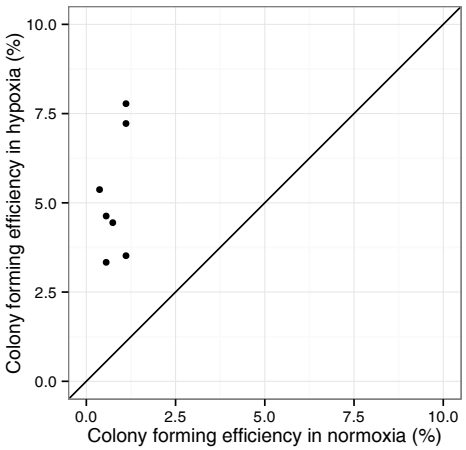
(a) (b)

(c) (d)

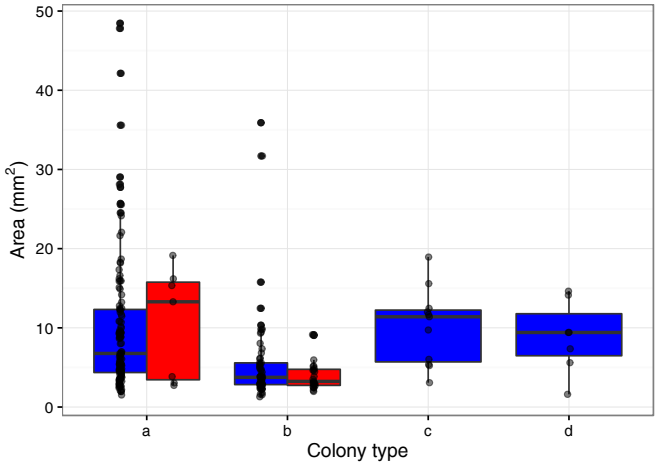
Figure 6.5: CDC colony types under normoxic and hypoxic culture conditions. The cells were fixed in cold ethanol, dried and stained with crystal violet. Four different colony types could be distinguished: (a) large heterogenous cells, (b) large homogenous cells, (c) spindle-like cells, (d) small homogenous cells, cobblestone shaped. Scale bar: 150 µm.

6.2.3.3 Cardiosphere-derived cell culture on collagen scaffolds in normoxia and hypoxia

In parallel to the scaffolds prepared for implantation, scaffolds were also cultured to measure and compare metabolic activity and VEGF secretion (Figure 6.7). The scaffolds were cultured for a week, and at the sixth day, the medium was changed to fresh media, and then the next day the media was collected for VEGF analysis by ELISA and metabolite analysis. CDCs seeded onto collagen scaffolds and cultured in normoxia or hypoxia, secreted VEGF, however in hypoxia the amount of VEGF secreted per scaffold was significantly higher than from scaffolds cultured in normoxia (Figure 6.7(a)). Additionally,



(a)



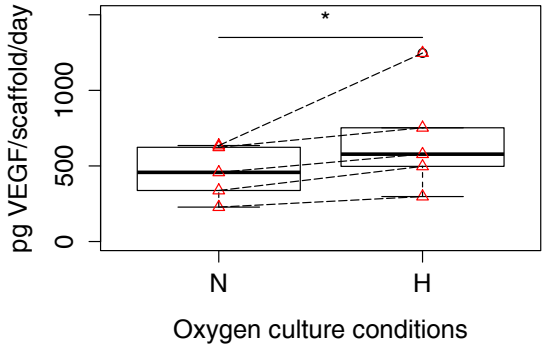
(b)

Figure 6.6: CFU potential in normoxia and hypoxia. (a) Colony forming potential in hypoxia and normoxia. (b) Colony area as a factor of colony type and oxygen tension (Blue: hypoxia, red: normoxia).

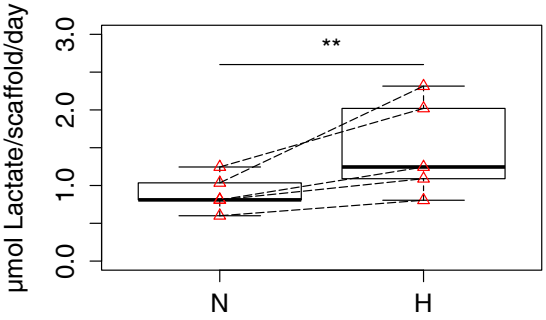
scaffolds cultured in hypoxia secreted more lactate compared to scaffolds cultured in normoxia (Figure 6.7(b)).

6.2.4 Effect of scaffold transplantation with or without cells on cardiac function

In order to assess the therapeutic effect of collagen scaffolds with or without hypoxic preconditioned CDCs, an *in vivo* trial was setup using the rat MI model with four groups



(a)



(b)

Figure 6.7: VEGF and lactate secretion by CDC-seeded scaffolds in normoxia (N) and hypoxia (H). (a) VEGF secretion in hypoxia and normoxia was compared using mixed effect linear models (374, 375), (b) Lactate secretion in hypoxia and normoxia, statistical comparison using the ratio paired t-test. '*' denotes $p \leq 0.05$ and '**' $p \leq 0.01$.

($n = 6-10$ in each group). Female rats were randomly assigned to either sham (open-chest surgery, no infarct, no scaffold), I/R-scaffold, I/R-scaffold-CDCs, or I/R. Cardiac I/R was induced by occluding the LAD for 40 min, followed by reperfusion. I/R damage was chosen, rather than permanent occlusion, since the former is more representative to the human disease state. For the cell seeded scaffolds, scaffolds were seeded with 100 kcells scaffold^{-1} (male CDCs) seven days before the surgery, and cultured in hypoxia

(5 % O_2).

The rats were scanned one, six, and twelve weeks post surgery using cine-MRI to determine cardiac function and LV remodeling (Figure 6.8). This technique enables the quantification of a variety of parameters describing LV cardiac function: end diastolic LV mass (mg), end systolic LV mass (mg), average LV mass (mg), end systolic lumen (ESL) (µL), end diastolic lumen (EDL) (µL), stroke volume (SV) (µL), relative infarct size (%), absolute infarct size (mm^2), EF (%), heart rate (bpm), and cardiac output (CO) (mL/min).

The obtained data was analysed using both descriptive and inferential statistics, and as cardiac function and LV remodeling was studied across time, both cross-sectional and longitudinal analysis was performed.



Figure 6.8: Experimental overview scaffold surgery study. Rats were randomly assigned to one of the four treatment groups (sham, I/R-scaffold, I/R-scaffold-CDCs, or I/R). MI was induced by a 40 minute period of I/R. Where a subject was assigned to scaffold treatment, the scaffold was transplanted epicardially using sutures immediately after the ischaemic period. The cardiac function was determined by cine-MRI, one, six and twelve weeks post surgery.

6.2.4.1 Cine-MRI: Descriptive statistics

Evidently, some of the factors quantified by cine-MRI will be highly correlated and not particularly descriptive. Before delving into applying inferential statistics to study the effect of scaffold transplantation on cardiac function, descriptive statistics were utilised to visualise the data and to assess which factors explain most variability between samples and treatment groups. PCA analysis is particularly useful for this purpose, as it looks

at the variability within the data irrespective of the groups and can indicate whether groups cluster together (Figure 6.9). The first two principle components generated from all data (all time points) explained about 80 % of the variability within the data. Most factors are present in both dimension one and two.

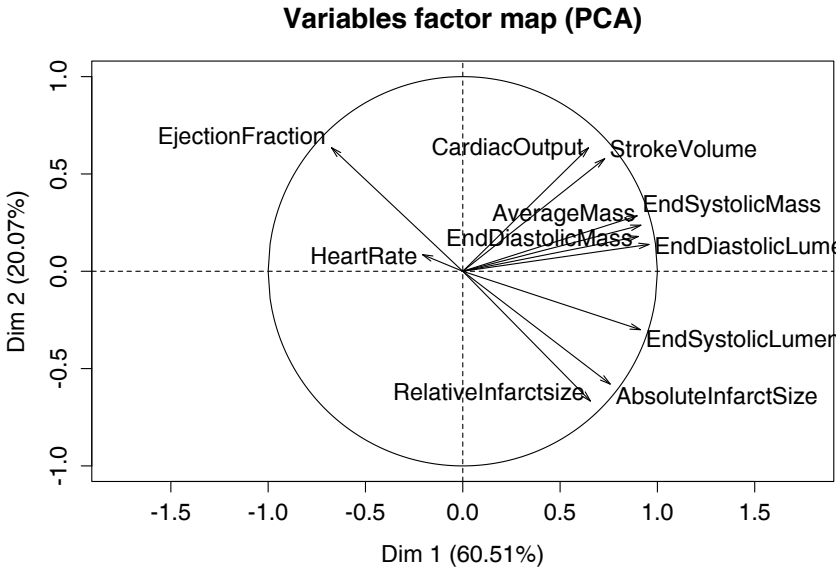
When the different time points are visualised within these two dimensions by different colours (Figure 6.9(b), left), it is clear that the main effect of time is an increase in heart mass, because the clusters move in the direction indicated by the mass and volume vectors (Figure 6.9(a)). Alternatively, when the treatment groups are colour-coded (Figure 6.9(b), right), it becomes obvious that the means of all infarcted and treated groups cluster around the origin and that the sham group is located in the upper left quadrant, suggesting that the sham group differed from the others by having a higher EF and smaller ESL and infarct size (Figure 6.9(a)). It is not a surprise that EF and ESL have an opposite direction as this follows from the definition of EF. Secondly, CO and SV, and end systolic, end diastolic and average mass are highly correlated, this also follows from the definition of the parameters.

It is important to note that the PCA dimensions are calculated without taking the different groups into consideration. In other words, although the dimensions are determined in such a way to maximise explanatory power in explaining the data, it relates to between samples and not between groups. In this case, the graphs suggest that the infarcted and treatment groups have comparable cardiac function. Nonetheless, hypothesis driven statistical testing is required to assess this properly.

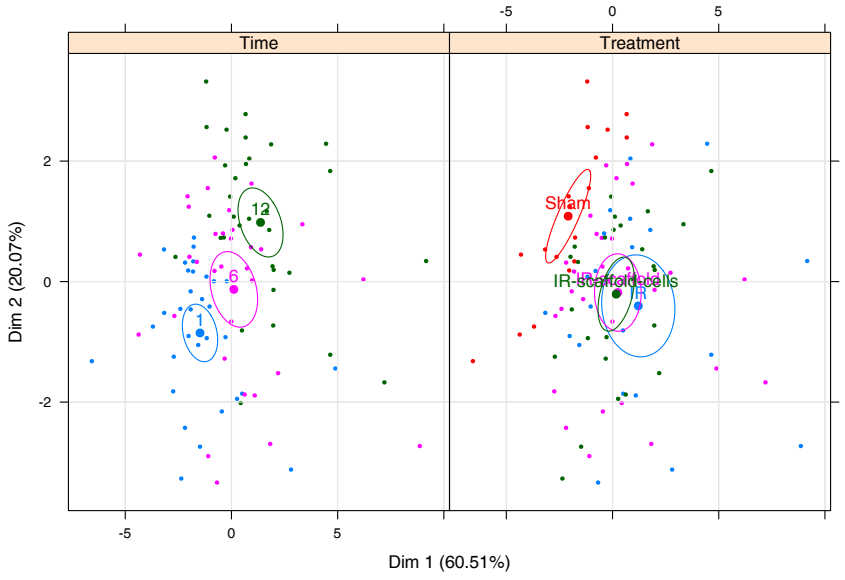
6.2.4.2 Cine-MRI: Inferential statistics

Heart and body weight The rats had comparable body weight at the beginning of the study and continued to gain weight during the study. There was no significant difference in body weight between the groups at either of the time points (Figure 6.10(c)).

In terms of LV mass, both end diastolic mass and end systolic mass were determined



(a)



(b)

Figure 6.9: Descriptive statistics: PCA on MRI data. Descriptive statistics were performed on the cine-MRI data to determine the most variable features. (a) PCA, variables vector map (b) 95% confidence limits around sample cluster means: (left) colour-coded for time, blue: one week, pink: six weeks, green: twelve weeks, (right) colour-coded for group, red: sham, pink: IR-scaffold, green: IR-scaffold-cells, blue: IR.

using MRI, and average mass was used for further comparison to account for potential differences in precision of measurement (Figure 6.10(a)). Longitudinal analysis revealed that average LV mass was not different between groups and was 669 ± 40 mg at week one and increased with time at a rate of 21 ± 3 mg week^{-1} (p-value $< 1 \times 10^{-4}$). There was a significant interaction between time and treatment in this model, suggesting that scaffold-treated (with or without cells) increase less with time, compared to sham or I/R animals. The difference between sham and I/R was also significant, when averaged across interaction effects (p-value = 0.02). However, cross-sectional analysis found no difference between the groups at the various time points. The ratio between LV mass and body weight is arguably more relevant, since it reduces the variability originating from varying body weights. Longitudinal analysis revealed that the average LV mass to body weight ratio did not change in time and was for the ischeamia and treatment groups 2.79 ± 0.12 mg g^{-1}, whereas for the sham group it was 0.44 ± 0.16 mg g^{-1} smaller (p-value 0.01, Figure 6.10(b)), suggesting that the hearts undergo hypertrophy post-I/R. Cross-sectional analysis at one week and twelve weeks found no difference between the groups (p-value = 0.13 and 0.077, respectively). Whereas, at six weeks, the difference sham vs. I/R was significant (p-value= 0.041).

Ejection fraction, stroke volume, heart rate and cardiac output EF, SV, heart rate and CO were measured as indices of cardiac function (Figure 6.11). The EF is defined as the fraction of blood in diastole that is pumped out in systole. The total ejected blood volume per cycle is called the SV, and the CO is the product of heart rate and stroke volume.

Longitudinal analysis of the EF suggests that the EF was significantly different between the sham group, on the one hand and the infarcted and treated groups, on the other hand (ANOVA, p-value = 0.0003). In addition, there was a small increase in average EF with time in the sham group (0.68 ± 0.29 % week^{-1}, p-value = 0.023). Cross-sectional

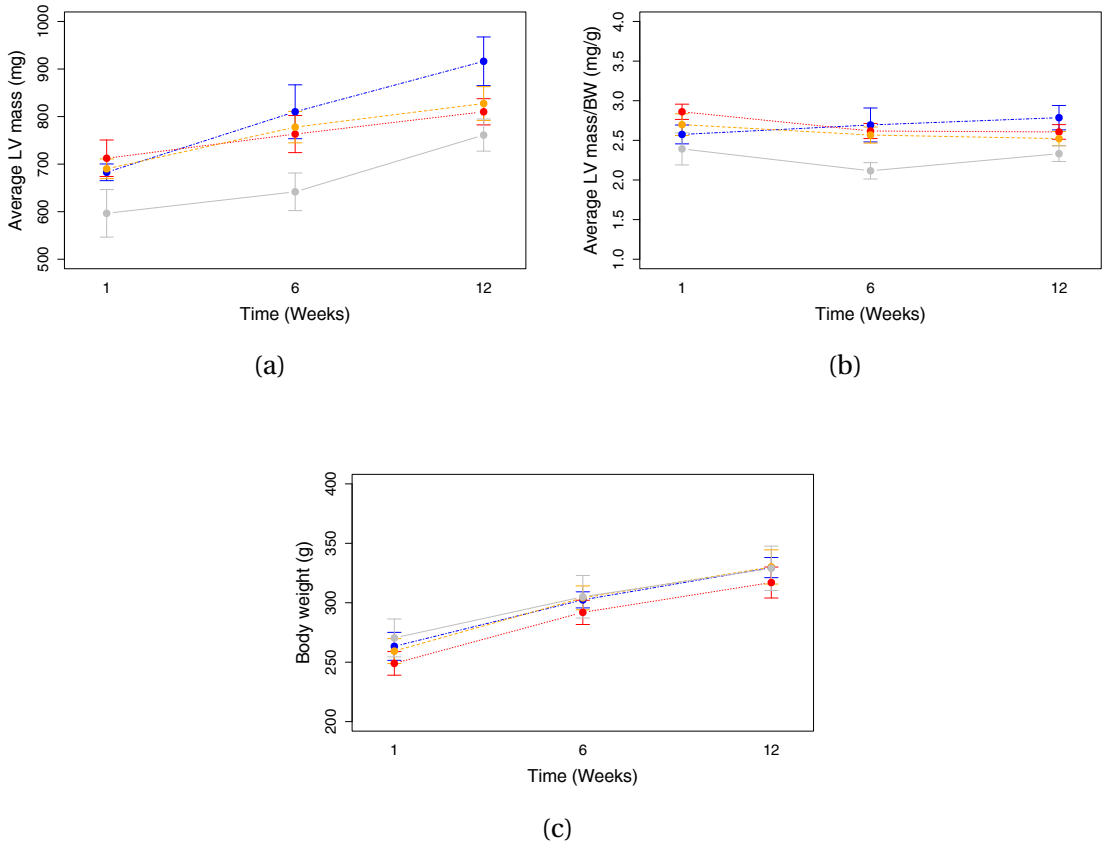


Figure 6.10: Effect of MI and scaffold treatment on LV mass. LV mass was determined using cine-MRI and the rats were weighted each time point to determine body weight. (a) Average LV mass, (b) Average LV-to-body-weight ratio, (c) Body weight. Grey: sham, red: IR-scaffold, orange: IR-scaffold-cells, blue: IR. The error bars represent the standard error.

data analysis revealed no difference in EF at one week post surgery (ANOVA, p-value = 0.10), whereas at six and twelve weeks post surgery all infarcted and treated groups had significantly lower EF compared to sham (ANOVA, Tukey multiple testing), apart from the comparison sham versus I/R-scaffold at twelve weeks (p-value = 0.07). However, the treatment groups were not significantly different, and not significantly higher than the I/R group.

The heart rate decreased with time at a rate of 2.50 ± 0.57 bpm week^{-1}. Additionally, the difference sham vs. I/R-scaffold was also significant. Similarly, cross-sectional analy-

sis revealed no differences between the groups at one and six weeks post-MI, whereas at twelve week the difference I/R-scaffold versus sham was significant. The cardiac output was not different between groups, but increased with time (2.70 ± 0.31 mL min^{-1} week^{-1}). Cross-sectional analysis revealed no differences between the groups at the different time points. Similarly, the stroke volume was comparable between groups, but increased with time: 9.40 ± 0.66 µL week^{-1}.

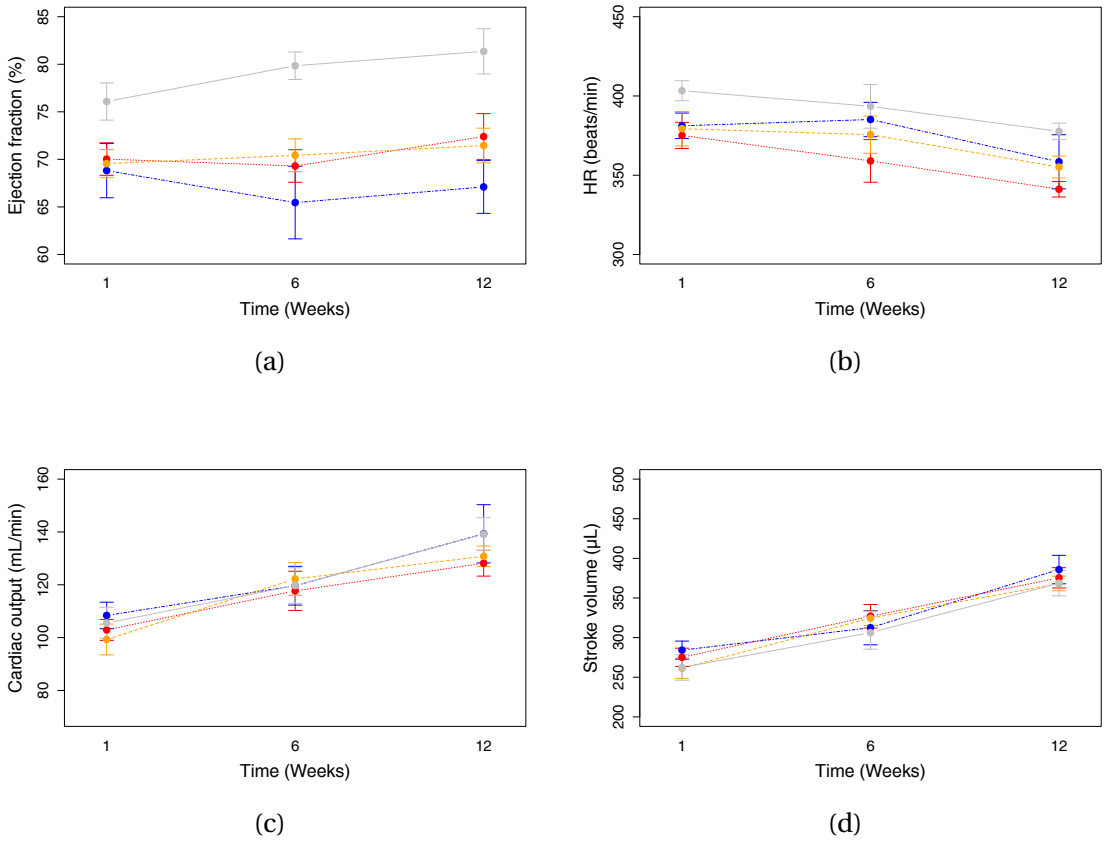
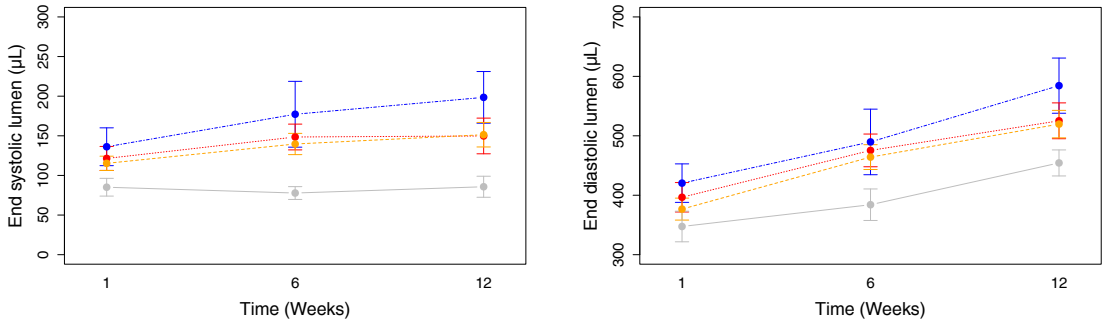


Figure 6.11: Effect of MI and scaffold treatment on heart rate and cardiac output. EF, SV, heart rate and CO were measured using cine-MRI. (a) Ejection fraction, (b) Heart rate, (c) Cardiac output, (d) Stroke volume. Grey: sham, red: IR-scaffold, orange: IR-scaffold-cells, blue: IR. The error bars represent the standard error.

Lumen The blood volume at the end of diastole and systole was determined using cine-MRI as a measure of LV dilation (Figure 6.12). Cross-sectional analysis suggested

comparable ESL at one week post surgery, whereas at six and twelve weeks, the sham group had a significantly lower ESL compared to the I/R group (Kruskal-Wallis Rank Sum Test, p-value < 0.05). At six weeks, the comparison scaffolds with or without cells vs. sham was also significant. Cross-sectional analysis of the EDL revealed no differences between the groups (Kruskal-Wallis Rank Sum Test).



(a) (b)

Figure 6.12: Effect of MI and scaffold treatment on end systolic and diastolic lumen The end systolic and diastolic lumen volumes were determined using cine-MRI, by measuring the blood volumes within the ventricle at systole and diastole. (a) End systolic lumen (b) End diastolic lumen. Grey: sham, red: IR/scaffold, orange: IR-scaffold-cells, blue: IR. The error bars represent the standard error.

Infarct size Infarct size was determined by quantifying the akinetic region in diastole on the MRI recordings (Figure 6.13). The sham group was excluded for statistical analysis. Both the relative and absolute infarct size were unaffected by treatment (Kruskal-Wallis Rank Sum Test).

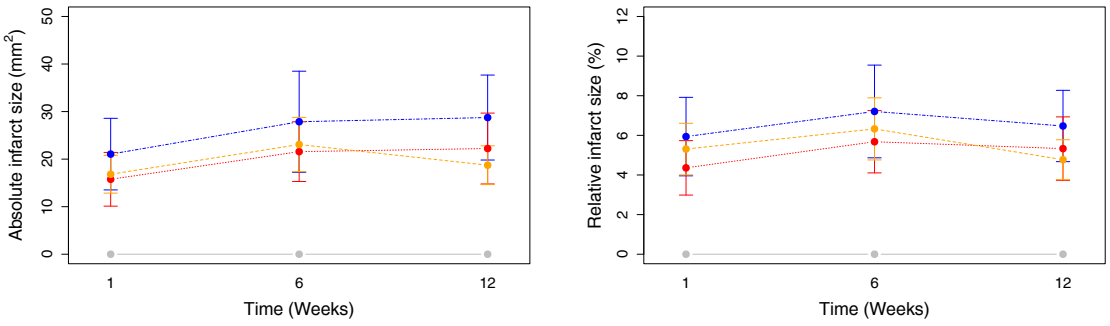
In summary, both acellular scaffolds and scaffolds loaded with CDCs failed to show any significant benefit post-MI.

6.2.4.3 *Ex vivo analysis*: scaffold degradation and scarring of the heart

After twelve weeks the hearts were explanted and processed for histological analysis. In the majority of cases, no remnants of the scaffold could be detected, at least by visual

Table 6.1: Overview of the cine-MRI data Values are expressed as mean ± standard deviation. The sample size was 7 for the I/R group, 10 for the I/R-scaffold group, 9 for the I/R-scaffold-cells group and 6 for the shams. '*': p-value < 0.05 versus sham. No comparison was made with sham for relative and absolute infarct size.

	One week				Six weeks				Twelve weeks			
	Sham	I/R-S	I/R-SC	I/R	Sham	I/R-S	I/R-SC	I/R	Sham	I/R-S	I/R-SC	I/R
BW (g)	270 ± 36	249 ± 31	259 ± 31	263 ± 29	305 ± 44	292 ± 32	304 ± 30	302 ± 18	329 ± 46	317 ± 39	330 ± 43	330 ± 22
HR (bpm)	403 ± 15	375 ± 26	379 ± 33	381 ± 21	393 ± 34	359 ± 43	375 ± 35	385 ± 29	378 ± 13	341 ± 15 *	355 ± 21	358 ± 45
EF (%)	76 ± 5	70 ± 5	70 ± 4	69 ± 8	80 ± 4	69 ± 5 *	70 ± 5 *	65 ± 10 *	81 ± 6	72 ± 8	71 ± 5 *	67 ± 7 *
SV (µL)	262 ± 39	275 ± 36	261 ± 39	284 ± 30	306 ± 51	327 ± 47	325 ± 27	312 ± 57	369 ± 39	375 ± 41	368 ± 28	386 ± 47
CO ($mL\,min^{-1}$)	106 ± 15	103 ± 13	99 ± 18	108 ± 13	120 ± 16	118 ± 23	122 ± 19	120 ± 19	139 ± 15	128 ± 15	131 ± 12	139 ± 29
ESL (µL)	85 ± 27	121 ± 48	115 ± 27	136 ± 63	78 ± 20	149 ± 51 *	140 ± 40 *	177 ± 110 *	86 ± 33	150 ± 71	151 ± 46	199 ± 86 *
EDL (µL)	347 ± 63	397 ± 78	377 ± 55	420 ± 86	384 ± 65	475 ± 87	464 ± 63	490 ± 146	454 ± 54	525 ± 95	520 ± 69	584 ± 123
Av Mass (mg)	597 ± 122	712 ± 121	690 ± 62	683 ± 46	642 ± 97	763 ± 123	778 ± 99	810 ± 150	761 ± 83	810 ± 87	827 ± 106	916 ± 135
Av Mass/BW ($mg\,g^{-1}$)	2.4 ± 0.5	2.9 ± 0.3	2.7 ± 0.4	2.6 ± 0.3	2.1 ± 0.3	2.6 ± 0.3	2.6 ± 0.3	2.7 ± 0.6*	2.3 ± 0.2	2.6 ± 0.3	2.5 ± 0.3	2.8 ± 0.4
Rel MI (%)	0 ± 0	4.4 ± 4.3	5.3 ± 3.9	5.9 ± 5.2	0 ± 0	5.7 ± 5.0	6.3 ± 4.7	7.2 ± 6.2	0 ± 0	5.3 ± 5.1	4.7 ± 3.0	6.5 ± 4.8
Abs MI (mm^2)	0 ± 0	15.8 ± 18.0	16.8 ± 11.9	21.1 ± 19.9	0 ± 0	21.6 ± 19.9	23.1 ± 17	27.9 ± 28.1	0 ± 0	22.2 ± 23.6	18.7 ± 12.2	28.7 ± 23.6



(a) (b)

Figure 6.13: Effect of MI and scaffold treatment on infarct size The infarcted area was quantified using cine-MRI by determining the akinetic region. (a) Absolute infarct size (b) Relative infarct size. Grey: sham, red: IR-scaffold, orange: IR-scaffold-cells, blue: IR. The error bars represent the standard error.

inspection *ex vivo* (Figure 6.14).

The hearts were embedded for cryosectioning and sections were collected roughly every 2 mm, to match with the MRI analysis. Scarred area and minimal LV wall thickness was determined by staining the tissue with SR (Figure 6.15). The total area and minimal LV wall thickness were unchanged across groups. The percentage scarred and total scarred area, were analysed after exclusion of the sham group, and no significant difference between the I/R and treated groups was detected (Welch's one-way test or Kruskal-Wallis rank sum test).

6.3 Discussion

Cell therapy has been proposed as a potential therapeutic strategy for AMI and HF. However, clinical translation has not yet fulfilled its promise, at least in part thought to be due to low cell retention and survival. Scaffolds enable the immobilisation of cells and hence limit the cell washout seen in cell injection. Secondly, pretreatment or conditioning strategies have been shown to aid cells in the survival of harsh milieus.

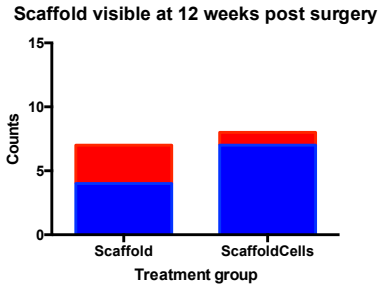


Figure 6.14: Scaffold degradation *in vivo* Degradation of the scaffolds transplanted into the rats with or without cells at the twelve week time point. There was no significant difference in visibility between scaffolds with and without cells at the twelve week time point (Fisher's exact test, p-value = 0.2821). Values represent the counts of individual rats belonging to a certain category (Red: not entirely degraded, Blue: no remnants visible by the naked eye).

In this Chapter, we assessed the therapeutic benefit of scaffolds loaded with CDCs on cardiac function post-MI. A collagen bilayer scaffold was designed and its biocompatibility demonstrated. Secondly, CDCs were harvested and characterised both in hypoxia and normoxia. Finally, both cell-loaded and acellular scaffolds were implanted onto infarcted rat hearts, and cardiac function measured using cine-MRI.

6.3.1 Scaffold design and biocompatibility

A bilayer collagen scaffold was designed in this project to limit adhesions to the chest and to limit folding. Roelofs *et al.* (372) applied a similar bilayer scaffold for fetal abdominal wall repair and observed reduced adhesions (372, 373). Biocompatibility of CDCs with collagen scaffolds was determined previously (178, 249).

Mechanical properties The mechanical properties of the scaffolds were not determined in this study. In fact, the material properties are very likely to be dynamic throughout the course of the materials lifetime both *in vitro* and *in vivo*. Indeed, hydration, degradation and cellular activity all affect the mechanical properties. Nonetheless, it is possible to roughly estimate the modulus from previous work and the literature. Chen *et al.* (178) reported a Young's modulus of 0.35 MPa for the 100 % dry collagen foam scaf-

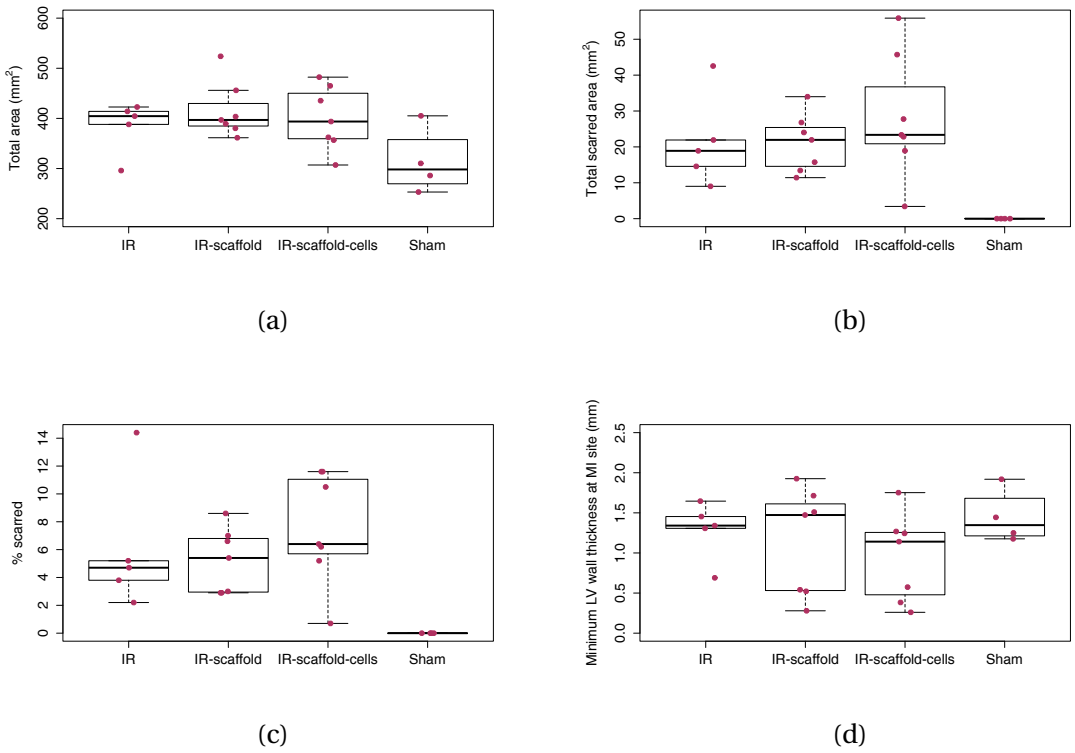


Figure 6.15: Histological quantification of scarred area The scarred and healthy areas within the heart were visualised using SR staining and quantified in ImageJ using the freehand selection tool. (a) Total area, (b) Total infarcted area, (c) Percentage infarcted area, (d) Minimal LV wall thickness at infarction site. There was no significant difference between groups (Welch's one-way test or Kruskal-Wallis rank sum test).

folds, identical to those used in this trial (excluding the film). Additionally, hydration will reduce the modulus of the scaffold to about $\frac{1}{150}$ of the value in dry status (376). Moreover, cell contraction will most likely at least triple the modulus (377). In vivo, the scaffold will be colonised and degraded, and both processes are likely to change the modulus further.

Based on the aforementioned estimates, a modulus of 7 kPa is obtained at baseline, which is in line with the range (1 – 14 kPa) known to achieve maximum myocyte contractility and development of immature cardiomyocytes (369). This is considerably less than what would be required for mechanocompatibility as defined by Equation 6.2d, where scaffold and LV undergo the same strain. However, it remains to be elucidated what stiffness has the best response *in vivo* in combination with cells.

Adhesion, integration and host response Integration of the scaffold and the host response to the scaffold were assessed by applying the collagen scaffold onto the epicardial surface of infarcted hearts and harvesting the heart at either two or six weeks post-implantation.

Initially, the scaffolds were mainly attached and adhered to the heart at the suture points, whereas after a couple of weeks, full integration took place (Figure 6.2). Araña *et al.* (378) studied the adhesion of collagen scaffolds with varying degrees of cross-linking to the heart by explanting the tissue two, seven or 30 days post implantation. Complete adhesion was observed in the non-crosslinked scaffolds as soon as two days post-surgery. The cross-linked scaffolds failed to adhere properly, even after one month. In comparison it took the scaffolds in our study longer to fully integrate. However, this may in part be explained by the fact that Araña *et al.* (378) applied five sutures, whereas only one or two were applied in this study. The additional suture points in their study might have aided in the faster adhesion and integration. Delayed integration might hinder the tissue repair and regeneration since effectively a barrier between the host and the graft is formed. Hence, it is paramount that integration in thoroughly investigated and optimised.

The scaffolds degraded over time in the present study. At two weeks post-implantation scaffolds remnants were visible on all hearts, whereas at six weeks post-implantation in the majority of cases no or only very small scaffold remnants could be identified. Similarly, Araña *et al.* (378) reported that their non-crosslined scaffolds were nearly totally degraded one month post-transplantation.

Histological analysis of the hearts revealed an influx of host cells into the scaffolds, including the recruitment of macrophages and the formation of new blood vessels within the scaffolds, as was also found by Serpooshan *et al.* (379). Blackburn *et al.* (380) cultured BM-derived macrophages on a collagen matrix and compared it with culture in polystyrene flasks to study the induction of cytokine secretion, and observed a decrease

in pro-inflammatory cytokines and an increase in anti-inflammatory cytokines, suggesting that collagen scaffolds alone can modulate the local inflammatory response.

M1 macrophages have a pro-inflammatory role, whereas the M2 macrophage is involved in immunosuppression and tissue repair. Hence, in normal tissue repair both M1 and M2 are typically present, in the initial stages mainly M1 and in the later stages mainly M2. Interestingly, both M1 and M2 macrophages contribute to angiogenesis. It was suggested that M1 macrophages promote sprouting of blood vessels via secretion of factors such as VEGF, whereas M2a macrophages promote fusion of blood vessels (381, 382). In this study we did not quantify macrophage numbers. It is important to note that polarised macrophages are loosely defined and on a spectrum. Additionally, many of the polarisation markers are also expressed by other cells. We attempted to differentiate between M1 and M2, but were unable to because two antibodies we assessed for detecting M1 polarisation had aspecific behaviour. Nonetheless, our macrophage staining and material behaviour *in vivo* were compatible with beneficial remodeling and integration, as described by Brown *et al.* (370), who demonstrated that there is a strong correlation between the early macrophage response to scaffold materials and the outcome of tissue remodeling.

6.3.2 Characterisation of CDCs

The ideal cell source for cardiac cell therapy remains to be elucidated. Endogenous cardiac progenitors such as CDCs have several benefits. First, they can be isolated from the target patient and are hence non-immunogenic. Secondly, they can give rise to cardiomyocytes and blood vessels *in vivo* and *in vitro* and secrete a range of growth factors (101, 143).

A previous student in the lab, Tan *et al.* (143) demonstrated that hypoxia culture increased the stemness of the CDCs. The colony forming capacity data presented here supports this theory, since an increased colony forming capacity and more diverse colony

types were observed in hypoxia.

It is well known that CDCs secrete many growth and anti-apoptotic factors both *in vivo* and *in vitro*, and the beneficial effect seen in MI-treatment has been contributed in part to this phenomena (135). In the present study we observed an increase in VEGF secretion per scaffold in hypoxia. Although, the cell density was not determined here, Tan *et al.* (143) reported increased proliferation in hypoxia. Hence, it is not clear at present whether VEGF production per cell is upregulated, or whether more cells were present in scaffolds cultured in hypoxia. Nonetheless, Hosoyama *et al.* (383) reported increased VEGF secretion as a result of hypoxic stimulation in cell sheets loaded with CDCs.

6.3.3 Effect of scaffold transplantation on cardiac function and adverse remodeling

In the currect study we failed to observe any difference in cardiac function between infarcted rat hearts and those treated with scaffolds with or without cells post-MI. In general, for most parameters investigated the main significant difference was sham versus I/R, or sham versus all I/R and treated groups. However, in several parameters there was a small but not significant improvement in cardiac function between the treated groups and the I/R group, suggesting that the current study might have been underpowered for measuring this difference. Indeed, intra-group variability was quite large for some features which makes powerful statistical analysis difficult.

In fact most published studies using collagen scaffolds had a positive beneficial effect post-MI (Table 6.2). This is not unexpected and results in part from the publication bias (384). Although publication bias is mainly studied in the context of large clinical trials, it clearly plays a role in experimental medicine too. Indeed, Sena *et al.* (385) demonstrated that publication bias might account for one-third in the efficacy reported in systematic reviews for stroke animal studies. In fact, some consider this an underestimate. A recent preclinical meta-analysis on cardiac stem cell therapy, on the other hand,

found evidence for publication bias, but it did not result in major changes in adjusted effect size (366). Moreover, many animal studies are underpowered, meaning that they are not likely to identify small effect sizes. But more importantly, underpowered studies have the additional disadvantage that they frequently inaccurately estimate (overestimate) the effect size.

Nonetheless, absence of evidence is not evidence of absence, and hence the study limitations of the present experiment will be discussed in detail.

MI models and time point of delivery Permanent occlusion of the LAD artery is the most popular approach to inducing MI in rodents. It is however the least clinically relevant approach, since most surviving patients undergo reperfusion post-MI. Hence, we applied a 40 min I/R protocol in our study, which led to moderate infarct sizes (5 % of LV). Riegler *et al.* (386) also performed I/R in their study, but waited 60 min before reperfusion and had slightly larger infarct sizes (10 % of LV). Indeed, Riegler *et al.* (386) observed a reduction in EF to 55 % in infarcted groups one month post-I/R, whereas in the current study the EF only reached 66 % in the infarcted group. It is unclear whether total occlusion is more likely to give rise to beneficial effects post cell or scaffold therapy. Total occlusion tends to give larger infarct sizes and a more pronounced reduction in EF, and it might be possible that insufficient damage was caused in the current study to enable appropriate investigation of the potential therapeutic effect of scaffolds loaded with CDCs. In fact, it seems more likely that too much rather than insufficient damage would be more detrimental to observe improvement post-MI. However, a tighter variance or larger sample size is likely required in case of small infarct sizes. Interestingly, a recent meta-analysis of pre-clinical data seems to suggest that there is no difference in average beneficial effect seen in stem cell treated versus placebo between studies using permanent occlusion or I/R (366).

Most animal studies deliver the therapeutic agent immediately after induction of MI,

which most likely does not represent the potential future clinical scenario. In fact, in studies investigating delayed implantation, less or no beneficial effects were observed (380, 386). Blackburn *et al.* (380) injected collagen gel post-MI at either three hours, one or two weeks after MI, and demonstrated that the earlier delivery of treatment better prevented deterioration of cardiac function. The study of Riegler *et al.* (386) also failed to meet its primary end point. However, this study implanted the scaffold both one month after MI and used an I/R protocol.

Infarct sizes are quite variable when performing total occlusion or I/R in the rat heart (387). This stems in part from the technical challenge of occluding the coronary at exactly the same anatomical location in all animals, and from anatomic variations between animals. Interestingly, Zornoff *et al.* (388) suggested that the rat total occlusion AMI model is inadequate for assessing the therapeutic benefit of interventions, since differences in the infarction size observed may relate to inherent variability of the method. We are currently investigating the possibility of using the LV cryoinjury model, in which an area of the LV is frozen for a brief amount of time using a liquid nitrogen cooled probe (389). Even though this method is not entirely physiological, there is evidence to suggest that it might be more reproducible and that it does mimic similar healing and disease progression features as seen in perfusion occlusion models.

Determination of cardiac function Cardiac cine-MRI and echocardiography are the two main techniques to non-invasively determine cardiac function. Even though echocardiography is the most commonly used technique, it is considered the least reliable (390). Indeed, it was recently shown in a meta-analysis that cardiac cell therapy clinical trials using echocardiography were far more likely to establish significance, compared to trials using MRI to determine cardiac function. In fact, subgroup analysis revealed that there was no significant effect on cardiac function after bone marrow-derived mononuclear cell (BMMNC) infusion when only trials using MRI were analysed (391).

Cell number and cell retention Cell retention has been shown to be problematic in cell therapy. For example, Pons *et al.* (392) reported that 90 % of the injected stem cells were lost within the first day, and 99 % in the first week. There are many mechanisms leading to poor cell survival and retention (393). First, as a result of the continuous compressive mechanical stress in the heart, cells are pushed outwards from the injection sites; secondly, as a result of cell death in the harsh microenvironment of hypoxia, inflammation, and oxidative stress; thirdly, as a result of loss attributed to the limited self-renewal in the harsh *in vivo* conditions.

Under the hypothesis that the implanted cells are primarily responsible for the therapeutic effect, more cells would most likely result in more benefit, up to a certain point, as is seen for all therapeutic agents following the typical dose response curve. Very few studies compare multiple doses of cells, and in literature there is considerable heterogeneity in cells quantities used. Moreover, in case of tissue engineered constructs that undergo a lengthly *in vitro* culture period, the assessment of therapeutic dose is far more complex.

In the current study, CDCs were seeded at a density of 100 kcells scaffold^{-1} and the scaffolds were cultured for seven days before implantation. Cheng *et al.* (394) injected 150 kcells suspended in hydrogel into the border zone of the infarct in mice. Araña *et al.* (365), on the other hand, seeded ADSC at a density of 500 kcells cm^{-2} onto 1 cm^2 scaffolds, and kept them in culture for 24 h before the implantation. It is hard to tell whether comparable cell numbers were used in our study and the study by Araña *et al.* (365), however it is likely that they are reasonably comparable. Moreover, the authors compared injection of ADSC with transplantation of collagen scaffolds loaded with ADSC four weeks post-MI. Araña *et al.* (365) observed improvement in EF in the scaffold-ADSC group, but not in the ADSC-alone group, in contrast to many other papers which observed beneficial effects with ADSC injection or infusion post-MI (395).

Many strategies have been suggested and tested to improve cell retention and sur-

vival, such as alternative delivery routes and/or mechanisms, biomaterials, preconditioning of the cells, genetic modification of the cells, transplantation of mixed cell populations and administration of drugs (393). The use of scaffolds immobilises the cells, and hence limits washout. The type of scaffolds and how they retain the cells might be a significant contributing factor to beneficial effects seen. Cheng *et al.* (394) applied an *in situ* polymerisable hyaluronan-gelatin hydrogel loaded with CDCs and observed remarkable increases in EF post-treatment. Similarly, Hosoyama *et al.* (383) observed a significant therapeutic effect after transplantation of CDCs-loaded cell sheets. In the present study, a collagen sponge was used, in which the majority of the cells will inevitably be located on the scaffold surface. Intramyocardial injection of a gel containing cells might be superior to our collagen scaffold as it directly delivers and retains cells within the border zone of the infarct area. Conversely, the collagen scaffolds presented here are applied epicardially and require time to fully integrate, by which point the cells might have been lost.

The vulnerability to the local inflammatory milieu is likely not reduced even if a biomaterial is utilised to retain and immobilise the cells. Indeed, Holladay *et al.* (396) reported a loss of 95 % of the MSC seeded in a collagen scaffold after one week, and demonstrated that the supplementation with complexed-IL-10 or by genetically inducing the MSC to over express IL-10, can lead to prolonged cell retention. This suggests that modulation of the local inflammatory response can aid in the survival of the transplanted cells. Holladay *et al.* (397) did not see increased LV recovery in collagen scaffold plus MSC treated hearts one month post-MI. However, in the scaffolds loaded with IL-10 and MSC, a marked recovery was visible, suggesting that improved survival of the cells was induced by IL-10. Unfortunately, the authors did not study the effect of IL-10-loaded scaffolds alone. Araña *et al.* (378) could recover 25.3 ± 7.0 % of the seeded cells in the scaffolds one week after cell transplantation, whereas in cell-injected control animals, no cells could be recovered. In the present study, the cells were preconditioned

with hypoxia, which increased the stemness and VEGF expression, comparable to previous literature. Cell retention was not determined in the present study. Although, we used sex-mismatched cells especially for this purpose, we have not performed these experiments due to time constraints. However, taking into consideration that the scaffolds degrade almost entirely and that most literature describes low cell retention, we expect to detect very few cells twelve weeks post implantation.

Cell (in)action Alternatively, the CDCs used in the current study could have lacked the potential to induce a beneficial response. In the study of Carr *et al.* (101) which showed beneficial effects when using CDCs as cell therapy, neonatal CDCs were used, and considerable more cells were delivered both by intramyocardial injection and intravenous infusion. Alternatively, the delayed scaffold engraftment might have hindered migration of the cells or paracrine factor diffusion. On the other hand, similarly to Serpooshan *et al.* (379) we observed neovascularisation with the scaffolds, suggesting that the biomaterial alone might be capable of inducing a beneficial response. Indeed, the latter authors did observe a beneficial effect of acellular scaffold implantation of cardiac function post-MI. Interestingly, in the same study, the recruitment of epicardial derived progenitor cells and cardiac fibroblasts to the scaffold was also observed, which may also play a role in the regeneration seen post-MI. In the current study, we did not stain for endogenous progenitors, although in future work this would be of considerable interest.

6.4 Conclusion

In summary, in this Chapter we described a bilayer collagen scaffold as potential therapeutic strategy for the treatment of AMI. Secondly, CDCs were harvested and characterised in normoxia and hypoxia, as we proposed to use hypoxic preconditioning as a method for enhancing the stemness of this cardiac progenitor population. The ef-

fect of implantation of collagen scaffolds with or without hypoxic pretreated-CDCs was assessed in a rat cardiac I/R model using cine-MRI. The study failed to observe any significant difference between treated and untreated infarcted hearts.

Table 6.2: Overview of *in vivo* studies using collagen scaffolds with or without cells post-MI Abbreviations: fractional shortening (FS), left ventricle internal diameter at end diastole (LVIDd), left ventricle internal diameter at end systole (LVIDs), left ventricle posterior wall dimension at end diastole (LVPWDd), left ventricle posterior wall dimension at end systole (LVPWDs), granulocyte-colony stimulating factor (G-CSF).

Scaffold	Cells or GFs	MI model	Cardiac function & outcome	Reference
Compressed collagen-I gel	-	Mouse, permanent occlusion	Echo: EF ↑, FS↑, LVIDd ↓, LVIDs ↓, LVPWDd ↑, LVPWDs ↑	Serpooshan *et al.* (379)
Injectable collagen gel	-	Mouse, permanent occlusion	Echo: CO↑, SV ↑ ESL↓. Scarring↓	Blackburn *et al.* (380)
Collagen-I foam	G-CSF	Rat	LV dilation↓, neo-angiognesis↑	Gaballa *et al.* (398)
Collagen foam	IL-10	Rat, permanent occlusion		Holladay *et al.* (397)
Collagen-I	ADSC	Rat, permanent occlusion	Degradation and integration	Araña *et al.* (378)
Collagen-I	ADSC	Rat, pig, permanent occlusion	EF↑, fibrosis↓, vascularisation↑	Araña *et al.* (365)
Collagen-I	ES-CM	Rat, I/R (60 min)	No cell-dependent effect, ΔEF↓	Riegler *et al.* (386)

CHAPTER 7

CONCLUSIONS AND FUTURE PERSPECTIVES

The overarching hypothesis of this thesis was that the 3D environment plays an important role in cardiomyocyte cell behaviour and maturation, and that taking the 3D environment into consideration might be beneficial for *in vitro* modelling of cardiac physiology or pathology on the one hand, or for the delivery of therapeutic agents to the heart post-MI on the other hand.

A humanised Langendorff perfused heart was proposed to model the heart *in vitro*. Whereas the *in vivo* arm of the hypothesis was assessed by developing a bilayer scaffold for the delivery of CDCs to heart post-MI.

7.1 Development of a humanised Langendorff perfused heart

The Langendorff perfused heart pioneered by Oskar Langendorff in 1898 played a predominant role in the unraveling of cardiac physiology (212). Notwithstanding the fact that this technology is more than 100 year old, it is still applied on a daily basis in academia

and the pharmaceutic industry. In this thesis, we attempted to develop a humanised variant of the most commonly used rat model by reseeding the isolated decellularised rat heart with human iPS-CMs.

iPS cells were chosen as cell type to generate the CMs, because human iPS cells can be non-invasively generated and cultured. This is in strong contrast to ES cells, for which there are considerable ethical concerns, in particular for the generation of new cell lines. It is paramount to the development of this technique that the cells can easily be generated, since this enables the study of patients with a particular genotype (for example disease causing mutations in relevant cardiac genes). In Chapter 3, iPS cells were differentiated into iPS-CMs and basic protocols for culturing the iPS-CMs on collagen based scaffolds were developed and discussed. In addition, the study of long term culture of iPS-CMs on gene expression revealed that the cells displayed little maturation in terms of gene expression after obtaining a contractile phenotype.

To generate the 3D scaffold for developing the humanised Langendorff model, the native rat heart was chosen. Indeed, decellularisation allows the generation of cell free scaffolds from whole organs by washing out the cellular content and by retaining as much of the ECM as possible. In Chapter 4, we demonstrated that whole organ morphology and major vasculature is maintained post decellularisation. To address the confusion is the field concerning the retention of ECM composition and the observation that there was no gold standard for quantifying this, the potential bias of normalisation strategies on decellularised tissue composition was determined. We concluded that $>$ 95% of published literature wrongly concludes that GAG is retained or significantly overestimates GAG content, by failing to take into consideration the retained water as confounding factor. In addition, in order to improve our understanding of the underlying mechanisms leading to effective decellularisation, the effect of perfusion pressure and pretreatment strategy was determined. Modulation of pressure or permeabilisation strategy affected DNA washout or GAG retention only minimally, suggesting that the

choice of detergent is the most dominant factor leading to efficient decellularisation.

The culture of 3D constructs is complicated by their dimensions since oxygen and nutrient diffusion is limited to about 200 µm. Hence, a bioreactor setup was designed and constructed for culturing the decellularised hearts *in vitro* (Chapter 5). The bioreactor was equipped with the capability to stimulate the organoids with biomimetic electrical and mechanical stimulation. The bioreactor followed a modular approach such that in future it can easily be upgraded. Many of the bioreactor parameters can be modified using a custom developed computer program, which also provides monitoring functionality.

In addition, we aimed to seed the decellularised hearts described in Chapter 4 with either CDCs or iPS-CMs and culture them in the bioreactor setup described in Chapter 5. The feasibility of culturing the recellularised hearts under biomimetic conditions in a bioreactor was demonstrated by both metabolic activity measurements, histology and qPCR. However, inhomogenous seeding and survival seems to be the major limiting factor currently in the further development of this technique. Indeed, additional experiments and further optimisation will be needed before the constructs can be used as humanised Langendorff perfused hearts.

7.1.1 Limitations and future work aimed towards developing the humanised Langendorff perfused heart

The major limiting factor in developing the humanised Langendorff perfused heart from a decellularised heart is the difficulty in obtaining homogenous seeding. Injection of cells into the heart is unlikely to be sustainable and is technically challenging. Hence, we resorted to surface seeding with pre-differentiated iPS-CMs. In contrast, Lu *et al.* (297) differentiated stem cells *in situ* to cardiomyocytes. Although, this is arguably a neater system, it is not robust given the current batch to batch variability in iPS differentiation.

In addition, decellularised matrices may not be sufficiently biocompatible. A ma-

jor concern is residual detergent content, however some research shows that matrix alterations, such as degradation of collagen structure, has a dominant effect on cell behaviour post-decellularisation (338).

The bi-ventricular collagen scaffold presented in this thesis already aimed to resolve some of the potential limitations of the decellularised heart model, but is restricted to seeding after construction. As an alternative, we propose to engineer the humanised Langendorff perfused heart, not using the decellularised heart, but using a cast hydrogel (Figure 7.1). This implementation would resolve any issues with respect to toxicity of the decellularised matrix (structural damage or residual detergent), and the problem of surface seeding. Indeed, pure ECM suspensions could be moulded mixed with cells allowing the generation of a homogenous suspension. With careful design of the moulds, it might be possible to increase the throughput of the method (compared to decellularisation) by reducing the number of processing steps, making the technique more user-friendly and leading to increased consistency and reproducibility. In order to provide perfusion, channels can be implemented within the hydrogel biomaterial using subtractive or additive fabrication technologies (399, 400). In the former, a template defining the vascular bed (sacrificial template) is encased in the bulk material and subsequently removed to create void space (401, 402), whereas in the latter, channels are created by either stacking multiple patterned layers (403) or bioprinting (404).

These hydrogel-based artificial ventricles would also be compatible with the bioreactor described in this thesis and the biomimetic stimulation regimes. Similarly, the method could allow the high density culture of the contractile cardiomyocytes working against a load, a requirement for making sensible contractile force and metabolic measurements.

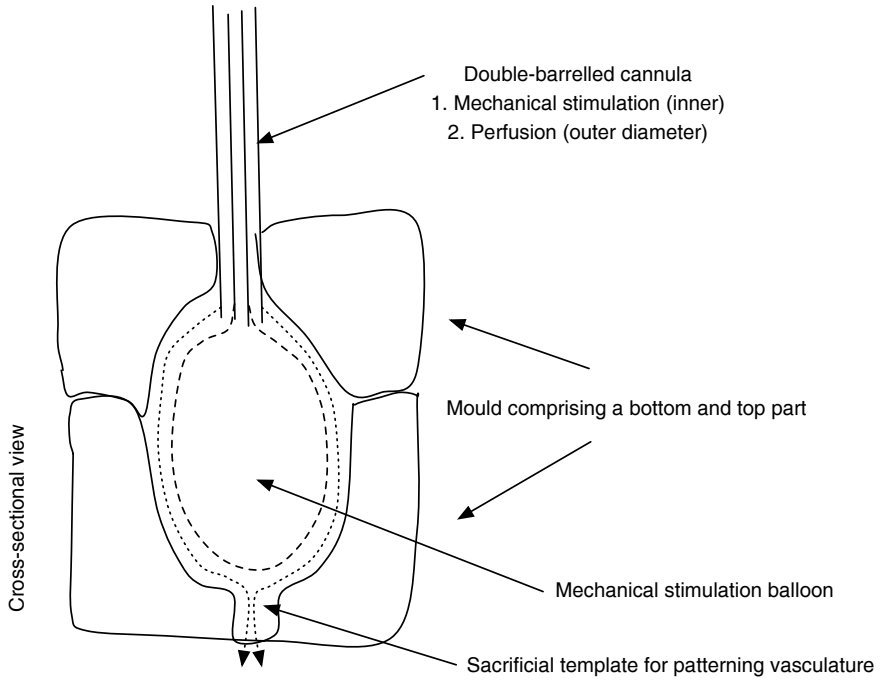


Figure 7.1: A vascularised hydrogel as a humanised Langendorff perfused heart. A mould comprising a bottom and a top part would allow a hydrogel layer to be casted around the mechanical stimulation balloon. Sacrificial templates may be included to enable the formation of a vascular bed within the artificial ventricle model. A double-barrelled cannula would enable the perfusion of the embedded vascular bed, and the mechanical stimulation of the artificial ventricle.

7.2 Development of a cardiac patch for preventing adverse remodelling post-MI

Clinical trials using adult stem cells as treatment strategy for either AMI or HF have so far failed to deliver clinically relevant therapeutic outcomes. One of the possible reasons for the difficulty in translation may be the lack of cell retention within the infarct area. As a result, the application of *delivery vehicles* was proposed.

In the current study we used a bi-layer collagen scaffold for cell delivery, which was designed to restrict chest wall adhesions and make the surgical procedure more straightforward. The scaffolds degraded within weeks upon engraftment onto the LV, most likely

as a result of the recruitment of macrophages. However, no encapsulation of the scaffolds was observed, suggesting that the vehicle was biocompatible. In addition, blood vessel formation within the scaffold was observed. The therapeutic benefit of the scaffold in combination with CDCs was determined by applying scaffolds with or without CDCs onto the LV epicardial surface after a 40-minute I/R period. CDCs-loaded scaffolds were preconditioned with hypoxia for seven days before the surgery in order to increase the stemness of the cells and their intrinsic paracrine factor secretion. Cardiac function was measured over a twelve week time period using cardiac cine-MRI and but no significant effect of scaffold or cells-loaded scaffold was observed.

Interestingly, others observed beneficial effects after direct injection of CDCs (95, 101) or when applying CDCs incapsulated in scaffolds (383, 394). Hence, additional research is required to establish the contributing factors to efficient translation or to the failure of this study. This understanding could help in establishing the essential characteristics of clinically beneficial cell-loaded scaffold transplantation post-MI. This is important since the first clinical trials using cell bearing scaffolds have started[1]. First, it is important to establish the cell retention within the scaffolds post-implantation. Male CDCs were used in female rats, with the aim to use fluorescence in situ hybridisation (FISH) or polymerase chain reaction (PCR) to detect and quantify cell retention. Due to time limitations, we have not yet been able to assess this. Nonetheless, rapid cell loss from within scaffolds has been reported by others and might be detrimental to the therapeutic effect. Secondly, we are investigating more potent cell sources or scaffolds for implantation. The *modus operandi* of CDCs is predominantly paracrine signalling, which may contribute to reduced damage if infused immediately after MI. However, for the more clinically relevant scenario where significant tissue damage and scaring has already developed, remuscularisation strategies may be more appropriate. Indeed, alternative stem cell sources such as iPS or ES cells might be an appropriate source of

[1] `http://www.clinicaltrials.gov`, ID: NCT02057900

new cardiomyocytes. Integration of new cardiomyocytes might be problematic though, given the complex nature of the cardiomyocyte organisation within the heart. With respect to the development of alternative scaffolds, a potential limitation to the current scaffold is likely that it takes a couple of weeks before the scaffold is properly integrated. Cells within the scaffold might suffer from perfusion limitations within this interim period. Cells were exposed to hypoxia for a week in the present study to increase their stemness and paracrine factor secretions, in order to accommodate the transition to the ischaemic heart. Pre-vascularisation strategies have been proposed to aid cell loaded scaffolds in their survival (405). Nonetheless, the scaffolds were rapidly colonised by macrophages and blood vessels. Hence, stimulation of the intrinsic pathways that lead to this vascularisation may also be a potential avenue. Taken together, further developments in both cell source and scaffold material will be required to further translate this technology.

7.3 Conclusion

The central hypothesis of this thesis was that exploiting the 3D environment may be beneficial for both the further development of *in vitro* models for cardiac disease, and to improve the efficacy of cardiac stem cell treatment.

The *in vitro* arm of this hypothesis was addressed by working towards developing a humanised Langendorff perfused heart model. The decellularised heart was chosen as biomaterial because the heart retains its gross anatomy and part of its vasculature post-decellularisation. Secondly, a bioreactor was developed to enable the culture of cells on decellularised hearts under biomimetic mechano-electrical stimulation. This stimulation regime was chosen, since iPS-CMs have an immature phenotype when compared to the adult heart, and previous research had shown that both mechanical and electrical stimulation contribute to the phenotypical maturation of stem cell derived cardio-

myocytes. Although, we managed to grow cells on the decellularised heart within the bioreactor, the quality of the humanised Langendorff hearts were currently insufficient for measuring contractile or metabolic function. Hence, additional research will be required to address the shortcomings of the current work.

The *in vivo* arm of this hypothesis was investigated by constructing a cell delivering bi-layer scaffold for epicardial implantation post-MI. Neither scaffolds alone or scaffolds loaded with CDCs showed a significant beneficial effect post-implantation, whereas infusion of CDCs had previously shown beneficial effects. As a result, additional research will be required to determine the factors contributing to the negative result seen here, and to make recommendations for further improvement of cardiac tissue engineering as a therapeutic strategy for MI or HF.

BIBLIOGRAPHY

1. WHO (2011). *Cardiovascular diseases Fact Sheet*. World Health Organization.

2. Fuster, V., Kelly, B.B., & Vedanthan, R. (2011). Promoting Global Cardiovascular Health: Moving Forward. *Circulation*, 123(15), 1671–1678. doi: 10.1161/CIRCULATIONAHA.110.009522.

3. Mackay, J. & Mensah, G., eds. (2004). *The Atlas of Heart Disease and Stroke*. World Health Organization.

4. Fuster, V. (2014). Global Burden of Cardiovascular Disease: Time to Implement Feasible Strategies and to Monitor Results. *Journal of the American College of Cardiology*, 64(5), 520–522. doi: 10.1016/j.jacc.2014.06.1151.

5. Townsend, N., Bhatnagar, P., Wilkins, E., Wickramasinghe, K., & Rayner, M. (2015). *Cardiovascular Disease Statistics, 2015*. Britisch Heart Foundation, London.

6. Jacobs, M.L. (2014). Pediatric Cardiac Surgery: The Long View. *Circulation*, 131(4), 328–330. doi: 10.1161/CIRCULATIONAHA.114.014318.

7. Mitchell, S.C., Korones, S.B., & Berendes, H.W. (1971). Congenital Heart Disease in 56,109 Births Incidence and Natural History. *Circulation*, 43(3), 323–332. doi: 10.1161/01.CIR.43.3.323.

8. Hoffman, J.I.E. & Kaplan, S. (2002). The incidence of congenital heart disease. *Journal of the American College of Cardiology*, 39(12), 1890–1900. doi: 10.1016/S0735-1097(02)01886-7.

9. Cannon, C.P. (1999). *Management of acute coronary syndromes*. Contemporary Cardiology. Humana Press, Totowa, N.J.

10. White, H.D. & Chew, D.P. (2008). Acute myocardial infarction. *The Lancet*, 372(9638), 570–584. doi: 10.1016/S0140-6736(08)61237-4.

11. Kumar, A. & Cannon, C.P. (2009). Acute coronary syndromes: diagnosis and management, part I. *Mayo Clinic Proceedings*, 84(10), 917–938. doi: 10.1016/S0025-6196(11)60509-0.

12. Kumar, A. & Cannon, C.P. (2009). Acute Coronary Syndromes: Diagnosis and Management, Part II. *Mayo Clinic Proceedings*, 84(11), 1021–1036. doi: 10.1016/S0025-6196(11)60674-5.

13. Grech, E.D. & Ramsdale, D.R. (2003). Acute coronary syndrome: ST segment elevation myocardial infarction. *BMJ (Clinical research ed.)*, 326(7403), 1379–1381. doi: 10.1136/bmj.326.7403.1379.

14. Liao, J.K. (2002). Beyond lipid lowering: the role of statins in vascular protection. *International journal of cardiology*, 86(1), 5–18.

15. Kolansky, D.M. (2009). Acute coronary syndromes: morbidity, mortality, and pharmacoeconomic burden. *The American journal of managed care*, 15(2 Suppl), S36–41.

16. Chatterjee, K. (2002). Congestive heart failure: what should be the initial therapy and why? *American journal of cardiovascular drugs : drugs, devices, and other interventions*, 2(1), 1–6.

17. Roger, V.L., Weston, S.A., Redfield, M.M., Hellermann-Homan, J.P., Killian, J., Yawn, B.P., & Jacobsen, S.J. (2004). Trends in Heart Failure Incidence and Survival in a Community-Based Population. *Journal of the American Medical Association*, 292(3), 344–350. doi: 10.1001/jama.292.3.344.

18. Braunwald, E. (2013). Heart Failure. *JACC. Heart failure*, 1(1), 1–20. doi: 10.1016/j.jchf.2012.10.002.

19. Mosterd, A. & Hoes, A.W. (2007). Clinical epidemiology of heart failure. *Heart*, 93(9), 1137–1146. doi: 10.1136/hrt.2003.025270.

20. Zannad, F. (2015). Pharmacotherapy in heart failure with reduced ejection fraction during the last 20 years, and the way ahead for precision medicine. *European Heart Journal - Cardiovascular Pharmacotherapy*, 1(1), 10–12. doi: 10.1093/ehjcvp/pvu006.

21. Tonsho, M., Michel, S., Ahmed, Z., Alessandrini, A., & Madsen, J.C. (2014). Heart Transplantation: Challenges Facing the Field. *Cold Spring Harbor Perspectives in Medicine*, 4(5), a015636–a015636. doi: 10.1101/cshperspect.a015636.

22. Anyanwu, A. & Treasure, T. (2003). Prognosis after heart transplantation. *BMJ (Clinical research ed.)*, 326(7388), 509–510. doi: 10.1136/bmj.326.7388.509.

23. DeRose, J.J., Argenziano, M., Sun, B.C., Reemtsma, K., Oz, M.C., & Rose, E.A. (1997). Implantable left ventricular assist devices: an evolving long-term cardiac replacement therapy. *Annals of surgery*, 226(4), 461–470.

24. Kyo, S., Minami, T., Nishimura, T., Gojo, S., & Ono, M. (2012). New era for therapeutic strategy for heart failure: Destination therapy by left ventricular assist device. *Journal of Cardiology*, 59(2), 101–109. doi: 10.1016/j.jjcc.2012.01.001.

25. Shipton, B. & Wahba, H. (2001). Valvular heart disease: review and update. *American family physician*, 63(11), 2201–2208.

26. Mickell, J.J., Mathews, R.A., Park, S.C., Lenox, C.C., Fricker, F.J., Neches, W.H., & Zuberbuhler, J.R. (1980). Left atrioventricular valve atresia: clinical management. *Circulation*, 61(1), 123–127.

27. Manji, R.A., Lee, W., & Cooper, D.K.C. (2015). Xenograft bioprosthetic heart valves: Past, present and future. *International Journal of Surgery*. doi: 10.1016/j.ijsu.2015.07.009.

28. Lasser, K.E., Allen, P.D., Woolhandler, S.J., Himmelstein, D.U., Wolfe, S.M., & Bor, D.H. (2002). Timing of New Black Box Warnings and Withdrawals for Prescription Medications. *Journal of the American Medical Association*, 287(17), 2215–2220. doi: 10.1001/jama.287.17.2215.

29. Lazarou, J., Pomeranz, B.H., & Corey, P.N. (1998). Incidence of Adverse Drug Reactions in Hospitalized Patients: A Meta-analysis of Prospective Studies. *Journal of the American Medical Association*, 279(15), 1200–1205. doi: 10.1001/jama.279.15.1200.

30. Force, T. & Kolaja, K.L. (2011). Cardiotoxicity of kinase inhibitors: the prediction and translation of preclinical models to clinical outcomes. *Nature Reviews Drug*

Discovery, 10(2), 111–126. doi: 10.1038/nrd3252.

31. Giorgi, M., Bolanos, R., Gonzalez, C., & Di Girolamo, G. (2010). QT Interval Prolongation: Preclinical and Clinical Testing Arrhythmogenesis in Drugs and Regulatory Implications. *Current Drug Safety*, 5(1), 54–57. doi: 10.2174/157488610789869148.

32. Ahmad, T., Yin, P., Saffitz, J., Pockros, P.J., Lalezari, J., Shiffman, M., Freilich, B., Zamparo, J., Brown, K., Dimitrova, D., Kumar, M., Manion, D., Heath-Chiozzi, M., Wolf, R., Hughes, E., Muir, A.J., & Hernandez, A.F. (2015). Cardiac dysfunction associated with a nucleotide polymerase inhibitor for treatment of hepatitis C. *Hepatology (Baltimore, Md.)*, 62(2), 409–416. doi: 10.1002/hep.27488.

33. Perricone, A.J. & Vander Heide, R.S. (2014). Novel therapeutic strategies for ischemic heart disease. *Pharmacological research*, 89, 36–45. doi: 10.1016/j.phrs.2014.08.004.

34. Frangogiannis, N.G. (2015). Pathophysiology of Myocardial Infarction. *Comprehensive Physiology*, 5(4), 1841–1875. doi: 10.1002/cphy.c150006.

35. Liu, X., Kim, C.N., Yang, J., Jemmerson, R., & Wang, X. (1996). Induction of Apoptotic Program in Cell-Free Extracts: Requirement for dATP and Cytochrome c. *Cell*, 86(1), 147–157. doi: 10.1016/S0092-8674(00)80085-9.

36. Orrenius, S., Gogvadze, V., & Zhivotovsky, B. (2015). Calcium and mitochondria in the regulation of cell death. *Biochemical and Biophysical Research Communications*, 460(1), 72–81. doi: 10.1016/j.bbrc.2015.01.137.

37. Hausenloy, D.J. & Yellon, D.M. (2013). Myocardial ischemia-reperfusion injury: a neglected therapeutic target. *Journal of Clinical Investigation*, 123(1), 92–100. doi: 10.1172/JCI62874.

38. Zeymer, U., Suryapranata, H., Monassier, J.P., Opolski, G., Davies, J., Rasmanis, G., Linssen, G., Tebbe, U., Schröder, R., Tiemann, R., Machnig, T., Neuhaus, K.L., & ESCAMI Investigators (2001). The Na(+)/H(+) exchange inhibitor eniporide as an adjunct to early reperfusion therapy for acute myocardial infarction. Results of the evaluation of the safety and cardioprotective effects of eniporide in acute myocardial infarction (ESCAMI) trial. *Journal of the American College of Cardiology*, 38(6), 1644–1650.

39. Mentzer, R.M., Bartels, C., Bolli, R., Boyce, S., Buckberg, G.D., Chaitman, B., Haverich, A., Knight, J., Menasché, P., Myers, M.L., Nicolau, J., Simoons, M., Thulin, L., Weisel, R.D., & EXPEDITION Study Investigators (2008). Sodium-hydrogen exchange inhibition by cariporide to reduce the risk of ischemic cardiac events in patients undergoing coronary artery bypass grafting: results of the EXPEDITION study. *The Annals of thoracic surgery*, 85(4), 1261–1270. doi: 10.1016/j.athoracsur.2007.10.054.

40. Bär, F.W., Tzivoni, D., Dirksen, M.T., Fernández-Ortiz, A., Heyndrickx, G.R., Brachmann, J., Reiber, J.H.C., Avasthy, N., Tatsuno, J., Davies, M., Hibberd, M.G., Krucoff, M.W., & CASTEMI Study Group (2006). Results of the first clinical study of adjunctive CAldaret (MCC-135) in patients undergoing primary percutaneous coronary intervention for ST-Elevation Myocardial Infarction: the randomized multicentre CASTEMI study. *European Heart Journal*, 27(21), 2516–2523. doi: 10.1093/eurheartj/ehl304.

41. Ye, Y., Li, J., & Yuan, Z. (2013). Effect of antioxidant vitamin supplementation on cardiovascular outcomes: a meta-analysis of randomized controlled trials.

PloS one, 8(2), e56803. doi: 10.1371/journal.pone.0056803.

42. Meybohm, P., Bein, B., Brosteanu, O., Cremer, J., Gruenewald, M., Stoppe, C., Coburn, M., Schaelte, G., Böning, A., Niemann, B., Roesner, J., Kletzin, F., Strouhal, U., Reyher, C., Laufenberg-Feldmann, R., Ferner, M., Brandes, I.F., Bauer, M., Stehr, S.N., Kortgen, A., Wittmann, M., Baumgarten, G., Meyer-Treschan, T., Kienbaum, P., Heringlake, M., Schön, J., Sander, M., Treskatsch, S., Smul, T., Wolwender, E., Schilling, T., Fuernau, G., Hasenclever, D., & Zacharowski, K. (2015). A Multicenter Trial of Remote Ischemic Preconditioning for Heart Surgery. *New England Journal of Medicine*, 373(15), 1397–1407. doi: 10.1056/NEJMoa1413579.

43. Simons, M. & Ware, J.A. (2003). Therapeutic angiogenesis in cardiovascular disease. *Nature Reviews Drug Discovery*, 2(11), 863–872. doi: 10.1038/nrd1226.

44. Henry, T.D., Annex, B.H., McKendall, G.R., Azrin, M.A., Lopez, J.J., Giordano, F.J., Shah, P.K., Willerson, J.T., Benza, R.L., Berman, D.S., Gibson, C.M., Bajamonde, A., Rundle, A.C., Fine, J., McCluskey, E.R., & VIVA Investigators (2003). The VIVA trial: Vascular endothelial growth factor in Ischemia for Vascular Angiogenesis. *Circulation*, 107(10), 1359–1365. doi: 10.1038/cr.2015.143.

45. Simons, M., Annex, B.H., Laham, R.J., Kleiman, N., Henry, T., Dauerman, H., Udelson, J.E., Gervino, E.V., Pike, M., Whitehouse, M.J., Moon, T., & Chronos, N.A. (2002). Pharmacological treatment of coronary artery disease with recombinant fibroblast growth factor-2: double-blind, randomized, controlled clinical trial. *Circulation*, 105(7), 788–793.

46. Ylä-Herttuala, S., Rissanen, T.T., Vajanto, I., & Hartikainen, J. (2007). Vascular Endothelial Growth Factors. *Journal of the American College of Cardiology*, 49(10), 1015–1026. doi: 10.1016/j.jacc.2006.09.053.

47. Maillet, M., van Berlo, J.H., & Molkentin, J.D. (2013). Molecular basis of physiological heart growth: fundamental concepts and new players. *Nature reviews. Molecular cell biology*, 14(1), 38–48. doi: 10.1038/nrm3495.

48. Butany, J., Nair, V., Naseemuddin, A., Nair, G.M., Catton, C., & Yau, T. (2005). Cardiac tumours: diagnosis and management. *The Lancet. Oncology*, 6(4), 219–228. doi: 10.1016/S1470-2045(05)70093-0.

49. Ertl, G. & Frantz, S. (2005). Healing after myocardial infarction. *Cardiovascular research*, 66(1), 22–32. doi: 10.1016/j.cardiores.2005.01.011.

50. Quaini, F., Cigola, E., Lagrasta, C., Saccani, G., Quaini, E., Rossi, C., Olivetti, G., & Anversa, P. (1994). End-stage cardiac failure in humans is coupled with the induction of proliferating cell nuclear antigen and nuclear mitotic division in ventricular myocytes. *Circulation research*, 75(6), 1050–1063.

51. Kajstura, J., Leri, A., Finato, N., Di Loreto, C., Beltrami, C.A., & Anversa, P. (1998). Myocyte proliferation in end-stage cardiac failure in humans. *Proceedings of the National Academy of Sciences*, 95(15), 8801–8805.

52. Beltrami, A.P., Urbanek, K., Kajstura, J., Yan, S.M., Finato, N., Bussani, R., Nadal-Ginard, B., Silvestri, F., Leri, A., Beltrami, C.A., & Anversa, P. (2001). Evidence that human cardiac myocytes divide after myocardial infarction. *New England Journal of Medicine*, 344(23), 1750–1757. doi: 10.1056/NEJM200106073442303.

53. Senyo, S.E., Steinhauser, M.L., Pizzimenti, C.L., Yang, V.K., Cai, L., Wang, M., Wu, T.D., Guerquin-Kern, J.L., Lechene,

C.P., & Lee, R.T. (2013). Mammalian heart renewal by pre-existing cardiomyocytes. *Nature*, 493(7432), 433–436. doi: 10.1038/nature11682.

54. Kajstura, J., Gurusamy, N., Ogórek, B., Goichberg, P., Clavo-Rondon, C., Hosoda, T., D'Amario, D., Bardelli, S., Beltrami, A.P., Cesselli, D., Bussani, R., del Monte, F., Quaini, F., Rota, M., Beltrami, C.A., Buchholz, B.A., Leri, A., & Anversa, P. (2010). Myocyte turnover in the aging human heart. *Circulation research*, 107(11), 1374–1386. doi: 10.1161/CIRCRESAHA.110.231498.

55. Bergmann, O., Bhardwaj, R.D., Bernard, S., Zdunek, S., Barnabé-Heider, F., Walsh, S., Zupicich, J., Alkass, K., Buchholz, B.A., Druid, H., Jovinge, S., & Frisén, J. (2009). Evidence for cardiomyocyte renewal in humans. *Science*, 324(5923), 98–102. doi: 10.1126/science.1164680.

56. Mollova, M., Bersell, K., Walsh, S., Savla, J., Das, L.T., Park, S.Y., Silberstein, L.E., dos Remedios, C.G., Graham, D., Colan, S., & Kuhn, B. (2013). Cardiomyocyte proliferation contributes to heart growth in young humans. *Proceedings of the National Academy of Sciences*, 110(4), 1446–1451. doi: 10.1073/pnas.1214608110.

57. Kikuchi, K., Holdway, J.E., Werdich, A.A., Anderson, R.M., Fang, Y., Egnaczyk, G.F., Evans, T., MacRae, C.A., Stainier, D.Y.R., & Poss, K.D. (2010). Primary contribution to zebrafish heart regeneration by gata4+ cardiomyocytes. *Nature*, 464(7288), 601–605. doi: 10.1038/nature08804.

58. Beltrami, A.P., Barlucchi, L., Torella, D., Baker, M., Limana, F., Chimenti, S., Kasahara, H., Rota, M., Musso, E., Urbanek, K., Leri, A., Kajstura, J., Nadal-Ginard, B., & Anversa, P. (2003). Adult cardiac stem cells are multipotent and support myocardial regeneration. *Cell*, 114(6), 763–776.

59. Ellison, G.M., Vicinanza, C., Smith, A.J., Aquila, I., Leone, A., Waring, C.D., Henning, B.J., Stirparo, G.G., Papait, R., Scarfò, M., Agosti, V., Viglietto, G., Condorelli, G., Indolfi, C., Ottolenghi, S., Torella, D., & Nadal-Ginard, B. (2013). Adult c-kit(pos) cardiac stem cells are necessary and sufficient for functional cardiac regeneration and repair. *Cell*, 154(4), 827–842. doi: 10.1016/j.cell.2013.07.039.

60. Martello, G. & Smith, A. (2014). The Nature of Embryonic Stem Cells. *Annual review of cell and developmental biology*, 30(1), 647–675. doi: 10.1146/annurev-cellbio-100913-013116.

61. Zipori, D. (2009). Multipotency and Tissue-Specific Stem Cells. In *Biology of Stem Cells and the Molecular Basis of the Stem State*. Humana Press, Totowa, NJ, (pp. 39–55). doi: 10.1007/978-1-60761-130-1_2.

62. Mafi, P., Hindocha, S., Mafi, R., Griffin, M., & Khan, W.S. (2011). Adult mesenchymal stem cells and cell surface characterization - a systematic review of the literature. *The open orthopaedics journal*, 5(Suppl 2), 253–260. doi: 10.2174/1874325001105010253.

63. Hoffman, L.M. & Carpenter, M.K. (2005). Characterization and culture of human embryonic stem cells. *Nature biotechnology*, 23(6), 699–708. doi: 10.1038/nbt1102.

64. Tomita, S., Li, R.K., Weisel, R.D., Mickle, D.A., Kim, E.J., Sakai, T., & Jia, Z.Q. (1999). Autologous transplantation of bone marrow cells improves damaged heart function. *Circulation*, 100(19 Suppl), II247–56. doi: 10.1161/01.CIR.100.suppl_2.II-247.

65. Orlic, D., Kajstura, J., Chimenti, S., Jakoniuk, I., Anderson, S.M., Li, B., Pickel, J., McKay, R., Nadal-Ginard, B., Bodine, D.M., Leri, A., & Anversa, P. (2001). Bone

marrow cells regenerate infarcted myocardium. *Nature*, 410(6829), 701–705. doi: 10.1038/35070587.

66. Makino, S., Fukuda, K., Miyoshi, S., Konishi, F., Kodama, H., Pan, J., Sano, M., Takahashi, T., Hori, S., Abe, H., Hata, J.i., Umezawa, A., & Ogawa, S. (1999). Cardiomyocytes can be generated from marrow stromal cells in vitro. *Journal of Clinical Investigation*, 103(5), 697–705. doi: 10.1172/JCI5298.

67. Murry, C.E., Soonpaa, M.H., Reinecke, H., Nakajima, H., Nakajima, H.O., Rubart, M., Pasumarthi, K.B.S., Virag, J.I., Bartelmez, S.H., Poppa, V., Bradford, G., Dowell, J.D., Williams, D.A., & Field, L.J. (2004). Haematopoietic stem cells do not transdifferentiate into cardiac myocytes in myocardial infarcts. *Nature*, 428(6983), 664–668. doi: 10.1038/nature02446.

68. Balsam, L.B., Wagers, A.J., Christensen, J.L., Kofidis, T., Weissman, I.L., & Robbins, R.C. (2004). Haematopoietic stem cells adopt mature haematopoietic fates in ischaemic myocardium. *Nature*, 428(6983), 668–673. doi: 10.1038/nature02460.

69. Jeevanantham, V., Butler, M., Saad, A., Abdel-Latif, A., Zuba-Surma, E.K., & Dawn, B. (2012). Adult bone marrow cell therapy improves survival and induces long-term improvement in cardiac parameters: a systematic review and meta-analysis. *Circulation*, 126(5), 551–568. doi: 10.1161/CIRCULATIONAHA.111.086074.

70. Delewi, R., Andriessen, A., Tijssen, J.G.P., Zijlstra, F., Piek, J.J., & Hirsch, A. (2013). Impact of intracoronary cell therapy on left ventricular function in the setting of acute myocardial infarction: a meta-analysis of randomised controlled clinical trials. *Heart*, 99(4), 225–232. doi: 10.1136/heartjnl-2012-302230.

71. Francis, D.P., Mielewczik, M., Zargaran, D., & Cole, G.D. (2013). Autologous bone marrow-derived stem cell therapy in heart disease: discrepancies and contradictions. *International journal of cardiology*, 168(4), 3381–3403. doi: 10.1016/j.ijcard.2013.04.152.

72. Nowbar, A.N., Mielewczik, M., Karavassilis, M., Dehbi, H.M., Shun-Shin, M.J., Jones, S., Howard, J.P., Cole, G.D., Francis, D.P., & DAMASCENE writing group (2014). Discrepancies in autologous bone marrow stem cell trials and enhancement of ejection fraction (DAMASCENE): weighted regression and meta-analysis. *BMJ (Clinical research ed.)*, 348, g2688. doi: 10.1136/bmj.g2688.

73. Fisher, S.A., Zhang, H., Doree, C., Mathur, A., & Martin-Rendon, E. (2015). Stem cell treatment for acute myocardial infarction. *Cochrane database of systematic reviews (Online)*, 9, CD006536. doi: 10.1002/14651858.CD006536.pub4.

74. Fisher, S.A., Doree, C., Taggart, D.P., Mathur, A., & Martin-Rendon, E. (2016). Cell therapy for heart disease: Trial sequential analyses of two cochrane reviews. *Clinical Pharmacology & Therapeutics*, n/a–n/a. doi: 10.1002/cpt.344.

75. Murry, C.E., Wiseman, R.W., Schwartz, S.M., & Hauschka, S.D. (1996). Skeletal myoblast transplantation for repair of myocardial necrosis. *The Journal of clinical investigation*, 98(11), 2512–2523. doi: 10.1172/JCI119070.

76. Taylor, D.A., Atkins, B.Z., Hungspreugs, P., Jones, T.R., Reedy, M.C., Hutcheson, K.A., Glower, D.D., & Kraus, W.E. (1998). Regenerating functional myocardium: Improved performance after skeletal myoblast transplantation. *Nature Medicine*, 4(8), 929–933.

77. Chiu, R., Zibaitis, A., & Kao, R.L. (1995). Cellular Cardiomyoplasty - Myocardial

Regeneration with Satellite Cell Implantation. *The Annals of Thoracic Surgery*, 60(1), 12–18.

78. Menasché, P., Hagege, A.A., Scorsin, M., Pouzet, B., Desnos, M., Duboc, D., Schwartz, K., Vilquin, J.T., & Marolleau, J.P. (2001). Myoblast transplantation for heart failure. *The Lancet*, 357(9252), 279–280. doi: 10.1016/S0140-6736(00)03617-5.

79. Menasché, P., Hagege, A.A., Vilquin, J.T., Desnos, M., Abergel, E., Pouzet, B., Bel, A., Sarateanu, S., Scorsin, M., Schwartz, K., Bruneval, P., Benbunan, M., Marolleau, J.P., & Duboc, D. (2003). Autologous skeletal myoblast transplantation for severe postinfarction left ventricular dysfunction. *Journal of the American College of Cardiology*, 41(7), 1078–1083. doi: 10.1016/S0735-1097(03)00092-5.

80. Herreros, J., Prosper, F., Perez, A., Gavira, J.J., Garcia-Velloso, M.J., Barba, J., Sanchez, P.L., Caniz, C., Rabago, G., Marti-Climent, J.M., Hernandez, M., Lopez-Holgado, N., Gonzalez-Santos, J.M., Martin-Luengo, C., & Alegria, E. (2003). Autologous intramyocardial injection of cultured skeletal muscle-derived stem cells in patients with non-acute myocardial infarction. *European Heart Journal*, 24(22), 2012–2020. doi: 10.1016/j.ehj.2003.09.012.

81. Menasché, P., Alfieri, O., Janssens, S., McKenna, W., Reichenspurner, H., Trinquart, L., Vilquin, J.T., Marolleau, J.P., Seymour, B., Larghero, J., Lake, S., Chatellier, G., Solomon, S., Desnos, M., & Hagege, A.A. (2008). The Myoblast Autologous Grafting in Ischemic Cardiomyopathy (MAGIC) Trial: First Randomized Placebo-Controlled Study of Myoblast Transplantation. *Circulation*, 117(9), 1189–1200. doi: 10.1161/CIRCULATIONAHA.107.734103.

82. Lipinski, M.J., Biondi-Zoccai, G.G.L., Abbate, A., Khianey, R., Sheiban, I., Bartunek, J., Vanderheyden, M., Kim, H.S., Kang, H.J., Strauer, B.E., & Vetrovec, G.W. (2007). Impact of intracoronary cell therapy on left ventricular function in the setting of acute myocardial infarction: a collaborative systematic review and meta-analysis of controlled clinical trials. *Journal of the American College of Cardiology*, 50(18), 1761–1767. doi: 10.1016/j.jacc.2007.07.041.

83. Léobon, B., Garcin, I., Menasché, P., Vilquin, J.T., Audinat, E., & Charpak, S. (2003). Myoblasts transplanted into rat infarcted myocardium are functionally isolated from their host. *Proceedings of the National Academy of Sciences*, 100(13), 7808–7811. doi: 10.1073/pnas.1232447100.

84. Takahashi, K. & Yamanaka, S. (2006). Induction of pluripotent stem cells from mouse embryonic and adult fibroblast cultures by defined factors. *Cell*, 126(4), 663–676. doi: 10.1016/j.cell.2006.07.024.

85. Takahashi, K., Tanabe, K., Ohnuki, M., Narita, M., Ichisaka, T., Tomoda, K., & Yamanaka, S. (2007). Induction of pluripotent stem cells from adult human fibroblasts by defined factors. *Cell*, 131(5), 861–872. doi: 10.1016/j.cell.2007.11.019.

86. González, F., Boue, S., & Belmonte, J.C.I. (2011). Methods for making induced pluripotent stem cells: reprogramming à la carte. *Nature Reviews Genetics*, 12(4), 231–242. doi: 10.1038/nrg2937.

87. Carpenter, L., Carr, C.A., Yang, C.T., Stuckey, D.J., Clarke, K., & Watt, S.M. (2012). Efficient differentiation of human induced pluripotent stem cells generates cardiac cells that provide protection following myocardial infarction in the rat. *Stem Cells and Development*, 21(6), 977–986. doi: 10.1089/scd.2011.0075.

88. Schwartz, S.D., Regillo, C.D., Lam, B.L., Eliott, D., Rosenfeld, P.J., Gregori, N.Z., Hubschman, J.P., Davis, J.L., Heilwell, G., Spirn, M., Maguire, J., Gay, R., Bateman, J., Ostrick, R.M., Morris, D., Vincent, M., Anglade, E., Del Priore, L.V., & Lanza, R. (2015). Human embryonic stem cell-derived retinal pigment epithelium in patients with age-related macular degeneration and Stargardt's macular dystrophy: follow-up of two open-label phase 1/2 studies. *The Lancet*, 385(9967), 509–516. doi: 10.1016/S0140-6736(14)61376-3.

89. Chong, J.J.H., Yang, X., Don, C.W., Minami, E., Liu, Y.W., Weyers, J.J., Mahoney, W.M., Van Biber, B., Cook, S.M., Palpant, N.J., Gantz, J.A., Fugate, J.A., Muskheli, V., Gough, G.M., Vogel, K.W., Astley, C.A., Hotchkiss, C.E., Baldessari, A., Pabon, L., Reinecke, H., Gill, E.A., Nelson, V., Kiem, H.P., Laflamme, M.A., & Murry, C.E. (2014). Human embryonic-stem-cell-derived cardiomyocytes regenerate non-human primate hearts. *Nature*, 510(7504), 273–277. doi: 10.1038/nature13233.

90. Oh, H., Bradfute, S.B., Gallardo, T.D., Nakamura, T., Gaussin, V., Mishina, Y., Pocius, J., Michael, L.H., Behringer, R.R., Garry, D.J., Entman, M.L., & Schneider, M.D. (2003). Cardiac progenitor cells from adult myocardium: homing, differentiation, and fusion after infarction. *Proceedings of the National Academy of Sciences*, 100(21), 12313–12318. doi: 10.1073/pnas.2132126100.

91. Koninckx, R., Daniëls, A., Windmolders, S., Mees, U., Macianskiene, R., Mubagwa, K., Steels, P., Jamaer, L., Dubois, J., Robic, B., Hendrikx, M., Rummens, J.L., & Hensen, K. (2013). The cardiac atrial appendage stem cell: a new and promising candidate for myocardial repair. *Cardiovascular research*, 97(3), 413–423. doi: 10.1093/cvr/cvs427.

92. Hierlihy, A.M., Seale, P., Lobe, C.G., Rudnicki, M.A., & Megeney, L.A. (2002). The post-natal heart contains a myocardial stem cell population. *FEBS letters*, 530(1-3), 239–243. doi: 10.1016/S0014-5793(02)03477-4.

93. Smart, N., Bollini, S., Dubé, K.N., Vieira, J.M., Zhou, B., Davidson, S., Yellon, D., Riegler, J., Price, A.N., Lythgoe, M.F., Pu, W.T., & Riley, P.R. (2011). De novo cardiomyocytes from within the activated adult heart after injury. *Nature*, 474(7353), 640–644. doi: 10.1038/nature10188.

94. Smart, N., Risebro, C.A., Melville, A.A.D., Moses, K., Schwartz, R.J., Chien, K.R., & Riley, P.R. (2006). Thymosin β4 induces adult epicardial progenitor mobilization and neovascularization. *Nature*, 445(7124), 177–182. doi: 10.1038/nature05383.

95. Messina, E., De Angelis, L., Frati, G., Morrone, S., Chimenti, S., Fiordaliso, F., Salio, M., Battaglia, M., Latronico, M.V.G., Coletta, M., Vivarelli, E., Frati, L., Cossu, G., & Giacomello, A. (2004). Isolation and expansion of adult cardiac stem cells from human and murine heart. *Circulation research*, 95(9), 911–921. doi: 10.1161/01.RES.0000147315.71699.51.

96. Bolli, R., Chugh, A.R., D'Amario, D., Loughran, J.H., Stoddard, M.F., Ikram, S., Beache, G.M., Wagner, S.G., Leri, A., Hosoda, T., Sanada, F., Elmore, J.B., Goichberg, P., Cappetta, D., Solankhi, N.K., Fahsah, I., Rokosh, D.G., Slaughter, M.S., Kajstura, J., & Anversa, P. (2011). Cardiac stem cells in patients with ischaemic cardiomyopathy (SCIPIO): initial results of a randomised phase 1 trial. *The Lancet*, 378(9806), 1847–1857. doi: 10.1016/S0140-6736(11)61590-0.

97. The Lancet Editors (2014). Expression of concern: the SCIPIO trial. *The Lancet*, 383(9925), 1279. doi: 10.1016/S0140-6736(14)60608-5.

98. Sultana, N., Zhang, L., Yan, J., Chen, J., Cai, W., Razzaque, S., Jeong, D., Sheng, W., Bu, L., Xu, M., Huang, G.Y., Hajjar, R.J., Zhou, B., Moon, A., & Cai, C.L. (2015). Resident c-kit+ cells in the heart are not cardiac stem cells. *Nature Communications*, 6, 8701. doi: 10.1038/ncomms9701.

99. van Berlo, J.H., Kanisicak, O., Maillet, M., Vagnozzi, R.J., Karch, J., Lin, S.C.J., Middleton, R.C., Marbán, E., & Molkentin, J.D. (2014). c-kit+ cells minimally contribute cardiomyocytes to the heart. *Nature*, 509(7500), 337–341. doi: 10.1038/nature13309.

100. Tan, J.J., Carr, C.A., Stuckey, D.J., Ellison, G.M., Messina, E., Giacomello, A., & Clarke, K. (2007). *Isolation and Expansion of Cardiosphere-Derived Stem Cells*. John Wiley & Sons, Inc., Hoboken, NJ, USA. doi: 10.1002/9780470151808.sc02c03s16.

101. Carr, C.A., Stuckey, D.J., Tan, J.J., Tan, S.C., Gomes, R.S.M., Camelliti, P., Messina, E., Giacomello, A., Ellison, G.M., & Clarke, K. (2011). Cardiosphere-derived cells improve function in the infarcted rat heart for at least 16 weeks–an MRI study. *PloS one*, 6(10), e25669. doi: 10.1371/journal.pone.0025669.

102. Malliaras, K., Makkar, R.R., Smith, R.R., Cheng, K., Wu, E., Bonow, R.O., Marbán, L., Mendizabal, A., Cingolani, E., Johnston, P.V., Gerstenblith, G., Schuleri, K.H., Lardo, A.C., & Marbán, E. (2014). Intracoronary Cardiosphere-Derived Cells After Myocardial Infarction. *Journal of the American College of Cardiology*, 63(2), 110–122. doi: 10.1016/j.jacc.2013.08.724.

103. Heng, B.C., Haider, H.K., Sim, E.K.W., Cao, T., & Ng, S.C. (2004). Strategies for directing the differentiation of stem cells into the cardiomyogenic lineage in vitro. *Cardiovascular research*, 62(1), 34–42. doi: 10.1016/j.cardiores.2003.12.022.

104. Smits, A.M., van Vliet, P., Metz, C.H., Korfage, T., Sluijter, J.P., Doevendans, P.A., & Goumans, M.J. (2009). Human cardiomyocyte progenitor cells differentiate into functional mature cardiomyocytes: an in vitro model for studying human cardiac physiology and pathophysiology. *Nature Protocols*, 4(2), 232–243. doi: 10.1038/nprot.2008.229.

105. Smith, R.R., Barile, L., Cho, H.C., Leppo, M.K., Hare, J.M., Messina, E., Giacomello, A., Abraham, M.R., & Marbán, E. (2007). Regenerative potential of cardiosphere-derived cells expanded from percutaneous endomyocardial biopsy specimens. *Circulation*, 115(7), 896–908. doi: 10.1161/CIRCULATIONAHA.106.655209.

106. Lee, S.T., White, A.J., Matsushita, S., Malliaras, K., Steenbergen, C., Zhang, Y., Li, T.S., Terrovitis, J., Yee, K., Simsir, S., Makkar, R., & Marbán, E. (2011). Intramyocardial injection of autologous cardiospheres or cardiosphere-derived cells preserves function and minimizes adverse ventricular remodeling in pigs with heart failure post-myocardial infarction. *Journal of the American College of Cardiology*, 57(4), 455–465. doi: 10.1016/j.jacc.2010.07.049.

107. Makkar, R.R., Smith, R.R., Cheng, K., Malliaras, K., Thomson, L.E.J., Berman, D., Czer, L.S.C., Marbán, L., Mendizabal, A., Johnston, P.V., Russell, S.D., Schuleri, K.H., Lardo, A.C., Gerstenblith, G., & Marbán, E. (2012). Intracoronary cardiosphere-derived cells for heart regeneration after myocardial infarction (CADUCEUS): a prospective, randomised phase 1 trial. *The Lancet*, 379(9819), 895–904. doi: 10.1016/S0140-6736(12)60195-0.

108. O'Farrell, P.H. (2015). Growing an Embryo from a Single Cell: A Hurdle in Animal Life. *Cold Spring Harbor Perspectives*

in Biology, 7(11), a019042. doi: 10.1101/cshperspect.a019042.

109. Miquerol, L. & Kelly, R.G. (2012). Organogenesis of the vertebrate heart. *Wiley Interdisciplinary Reviews: Developmental Biology*, 2(1), 17–29. doi: 10.1002/wdev.68.

110. Rajala, K., Pekkanen-Mattila, M., & Aalto-Setälä, K. (2011). Cardiac differentiation of pluripotent stem cells. *Stem cells international*, 2011(21), 383709–12. doi: 10.4061/2011/383709.

111. Gessert, S. & Kühl, M. (2010). The multiple phases and faces of wnt signaling during cardiac differentiation and development. *Circulation research*, 107(2), 186–199. doi: 10.1161/CIRCRESAHA.110.221531.

112. van Wijk, B., Moorman, A.F.M., & van den Hoff, M.J.B. (2007). Role of bone morphogenetic proteins in cardiac differentiation. *Cardiovascular research*, 74(2), 244–255. doi: 10.1016/j.cardiores.2006.11.022.

113. Kattman, S.J., Witty, A.D., Gagliardi, M., Dubois, N.C., Niapour, M., Hotta, A., Ellis, J., & Keller, G. (2011). Stage-Specific Optimization of Activin/Nodal and BMP Signaling Promotes Cardiac Differentiation of Mouse and Human Pluripotent Stem Cell Lines. *Stem Cell*, 8(2), 228–240. doi: 10.1016/j.stem.2010.12.008.

114. Ueno, S., Weidinger, G., Osugi, T., Kohn, A.D., Golob, J.L., Pabon, L., Reinecke, H., Moon, R.T., & Murry, C.E. (2007). Biphasic role for Wnt/beta-catenin signaling in cardiac specification in zebrafish and embryonic stem cells. *Proceedings of the National Academy of Sciences*, 104(23), 9685–9690. doi: 10.1073/pnas.0702859104.

115. Smits, A.M., van Vliet, P., Metz, C.H., Korfage, T., Sluijter, J.P., Doevendans, P.A., & Goumans, M.J. (2009). Human cardiomyocyte progenitor cells differentiate into functional mature cardiomyocytes: an in vitro model for studying human cardiac physiology and pathophysiology. *Nature Protocols*, 4(2), 232–243. doi: 10.1038/nprot.2008.229.

116. Xu, X.Q., Soo, S.Y., Sun, W., & Zweigerdt, R. (2009). Global Expression Profile of Highly Enriched Cardiomyocytes Derived from Human Embryonic Stem Cells. *Stem Cells*, 27(9), 2163–2174. doi: 10.1002/stem.166.

117. Evans, R.D. & Clarke, K. (2012). Myocardial substrate metabolism in heart disease. *Frontiers in bioscience (Scholar edition)*, 4, 556–580.

118. Neubauer, S. (2007). Mechanisms of disease - The failing heart - An engine out of fuel. *New England Journal of Medicine*, 356(11), 1140–1151. doi: 10.1056/NEJMra063052.

119. Lopaschuk, G.D., Ussher, J.R., Folmes, C.D.L., Jaswal, J.S., & Stanley, W.C. (2010). Myocardial fatty acid metabolism in health and disease. *Physiological Reviews*, 90(1), 207–258. doi: 10.1152/physrev.00015.2009.

120. Vander Heiden, M.G., Cantley, L.C., & Thompson, C.B. (2009). Understanding the Warburg effect: the metabolic requirements of cell proliferation. *Science*, 324(5930), 1029–1033. doi: 10.1126/science.1160809.

121. Varum, S., Rodrigues, A.S., Moura, M.B., Momcilovic, O., Easley IV, C.A., Ramalho-Santos, J., Van Houten, B., & Schatten, G. (2011). Energy Metabolism in Human Pluripotent Stem Cells and Their Differentiated Counterparts. *PloS one*, 6(6), e20914. doi: 10.1371/journal.pone.0020914.

122. Chung, S., Dzeja, P.P., Faustino, R.S., Perez-Terzic, C., Behfar, A., & Terzic, A. (2007). Mitochondrial oxidative metabolism is required for the cardiac differentiation of stem cells. *Nature clinical practice. Cardiovascular medicine*, 4 Suppl 1, S60–7. doi: 10.1038/ncpcardio0766.

123. Tohyama, S., Hattori, F., Sano, M., Hishiki, T., Nagahata, Y., Matsuura, T., Hashimoto, H., Suzuki, T., Yamashita, H., Satoh, Y., Egashira, T., Seki, T., Muraoka, N., Yamakawa, H., Ohgino, Y., Tanaka, T., Yoichi, M., Yuasa, S., Murata, M., Suematsu, M., & Fukuda, K. (2013). Distinct metabolic flow enables large-scale purification of mouse and human pluripotent stem cell-derived cardiomyocytes. *Cell Stem Cell*, 12(1), 127–137. doi: 10.1016/j.stem.2012.09.013.

124. Kadari, A., Mekala, S., Wagner, N., Malan, D., Köth, J., Doll, K., Stappert, L., Eckert, D., Peitz, M., Matthes, J., Sasse, P., Herzig, S., Brüstle, O., Ergün, S., & Edenhofer, F. (2014). Robust Generation of Cardiomyocytes from Human iPS Cells Requires Precise Modulation of BMP and WNT Signaling. *Stem Cell Reviews and Reports*, 1–10. doi: 10.1007/s12015-014-9564-6.

125. Knollmann, B.C. & Roden, D.M. (2008). A genetic framework for improving arrhythmia therapy. *Nature*, 451(7181), 929–936. doi: 10.1038/nature06799.

126. van den Berg, C.W., Okawa, S., Chuva de Sousa Lopes, S.M., van Iperen, L., Passier, R., Braam, S.R., Tertoolen, L.G., del Sol, A., Davis, R.P., & Mummery, C.L. (2015). Transcriptome of human foetal heart compared with cardiomyocytes from pluripotent stem cells. *Development*, 142(18), 3231–3238. doi: 10.1242/dev.123810.

127. Fijnvandraat, A.C., van Ginneken, A.C.G., de Boer, P.A.J., Ruijter, J.M., Christoffels, V.M., Moorman, A.F.M., & Lekanne Deprez, R.H. (2003). Cardiomyocytes derived from embryonic stem cells resemble cardiomyocytes of the embryonic heart tube. *Cardiovascular research*, 58(2), 399–409.

128. Novak, A., Barad, L., Zeevi-Levin, N., Shick, R., Shtrichman, R., Lorber, A., Itskovitz-Eldor, J., & Binah, O. (2012). Cardiomyocytes generated from CPVTD307H patients are arrhythmogenic in response to β-adrenergic stimulation. *Journal of cellular and molecular medicine*, 16(3), 468–482. doi: 10.1111/j.1582-4934.2011.01476.x.

129. Robertson, C., Tran, D.D., & George, S.C. (2013). Concise Review: Maturation Phases of Human Pluripotent Stem Cell-Derived Cardiomyocytes. *Stem Cells*, 31(5), 829–837. doi: 10.1002/stem.1331.

130. Desvergne, B., Michalik, L., & Wahli, W. (2006). Transcriptional regulation of metabolism. *Physiological Reviews*, 86(2), 465–514. doi: 10.1152/physrev.00025.2005.

131. Dimmeler, S., Zeiher, A.M., & Schneider, M.D. (2005). Unchain my heart: the scientific foundations of cardiac repair. *Journal of Clinical Investigation*, 115(3), 572–583. doi: 10.1172/JCI24283.

132. Cheng, K., Ibrahim, A., Hensley, M.T., Shen, D., Sun, B., Middleton, R., Liu, W., Smith, R.R., & Marban, E. (2014). Relative Roles of CD90 and c-Kit to the Regenerative Efficacy of Cardiosphere-Derived Cells in Humans and in a Mouse Model of Myocardial Infarction. *Journal of the American Heart Association*, 3(5), e001260. doi: 10.1161/JAHA.114.001260.

133. Vrtovec, B., Poglajen, G., Lezaic, L., Sever, M., Domanovic, D., Cernelc, P., Socan, A., Schrepfer, S., Torre-Amione, G., Haddad, F., & Wu, J.C. (2013). Effects of in-

tracoronary CD34+ stem cell transplantation in nonischemic dilated cardiomyopathy patients: 5-year follow-up. *Circulation research*, 112(1), 165–173. doi: 10.1161/CIRCRESAHA.112.276519.

134. Bartunek, J., Sherman, W., Vanderheyden, M., Fernandez-Aviles, F., Wijns, W., & Terzic, A. (2009). Delivery of Biologics in Cardiovascular Regenerative Medicine. *Clinical Pharmacology & Therapeutics*, 85(5), 548–552. doi: 10.1038/clpt.2008.295.

135. Chimenti, I., Smith, R.R., Li, T.S., Gerstenblith, G., Messina, E., Giacomello, A., & Marbán, E. (2010). Relative roles of direct regeneration versus paracrine effects of human cardiosphere-derived cells transplanted into infarcted mice. *Circulation research*, 106(5), 971–980. doi: 10.1161/CIRCRESAHA.109.210682.

136. Gnecchi, M., Zhang, Z., Ni, A., & Dzau, V.J. (2008). Paracrine mechanisms in adult stem cell signaling and therapy. *Circulation research*, 103(11), 1204–1219. doi: 10.1161/CIRCRESAHA.108.176826.

137. He, A., Jiang, Y., Gui, C., Sun, Y., Li, J., & Wang, J.a. (2009). The antiapoptotic effect of mesenchymal stem cell transplantation on ischemic myocardium is enhanced by anoxic preconditioning. *The Canadian journal of cardiology*, 25(6), 353–358.

138. Fujio, Y., Nguyen, T., Wencker, D., Kitsis, R.N., & Walsh, K. (2000). Akt promotes survival of cardiomyocytes in vitro and protects against ischemia-reperfusion injury in mouse heart. *Circulation*, 101(6), 660–667.

139. D'Amario, D., Cabral-Da-Silva, M.C., Zheng, H., Fiorini, C., Goichberg, P., Steadman, E., Ferreira-Martins, J., Sanada, F., Piccoli, M., Cappetta, D., D'Alessandro, D.A., Michler, R.E., Hosoda, T., Anastasia, L., Rota, M., Leri, A., Anversa, P., & Kajstura, J. (2011). Insulin-Like Growth Factor-1 Receptor Identifies a Pool of Human Cardiac Stem Cells With Superior Therapeutic Potential for Myocardial Regeneration. *Circulation research*, 108(12), 1467–1481. doi: 10.1161/CIRCRESAHA.111.240648.

140. Du, Y.Y., Zhou, S.H., Zhou, T., Su, H., Pan, H.W., Du, W.H., Liu, B., & Liu, Q.M. (2008). Immuno-inflammatory regulation effect of mesenchymal stem cell transplantation in a rat model of myocardial infarction. *Cytotherapy*, 10(5), 469–478. doi: 10.1080/14653240802129893.

141. Ohnishi, S., Sumiyoshi, H., Kitamura, S., & Nagaya, N. (2007). Mesenchymal stem cells attenuate cardiac fibroblast proliferation and collagen synthesis through paracrine actions. *FEBS letters*, 581(21), 3961–3966. doi: 10.1016/j.febslet.2007.07.028.

142. Kinnaird, T., Stabile, E., Burnett, M.S., Lee, C.W., Barr, S., Fuchs, S., & Epstein, S.E. (2004). Marrow-derived stromal cells express genes encoding a broad spectrum of arteriogenic cytokines and promote in vitro and in vivo arteriogenesis through paracrine mechanisms. *Circulation research*, 94(5), 678–685. doi: 10.1161/01.RES.0000118601.37875.AC.

143. Tan, S.C., Gomes, R.S.M., Yeoh, K.K., Perbellini, F., Malandraki-Miller, S., Ambrose, L., Heather, L.C., Faggian, G., Schofield, C.J., Davies, K.E., Clarke, K., & Carr, C.A. (2016). Preconditioning of Cardiosphere-Derived Cells With Hypoxia or Prolyl-4-Hydroxylase Inhibitors Increases Stemness and Decreases Reliance on Oxidative Metabolism. *Cell transplantation*, 25(1), 35–53. doi: 10.3727/096368915X687697.

144. Linke, A., Müller, P., Nurzynska, D., Casarsa, C., Torella, D., Nascimbene, A.,

Castaldo, C., Cascapera, S., Böhm, M., Quaini, F., Urbanek, K., Leri, A., Hintze, T.H., Kajstura, J., & Anversa, P. (2005). Stem cells in the dog heart are self-renewing, clonogenic, and multipotent and regenerate infarcted myocardium, improving cardiac function. *Proceedings of the National Academy of Sciences*, 102(25), 8966–8971. doi: 10.1073/pnas.0502678102.

145. Yoon, Y.S., Wecker, A., Heyd, L., Park, J.S., Tkebuchava, T., Kusano, K., Hanley, A., Scadova, H., Qin, G., Cha, D.H., Johnson, K.L., Aikawa, R., Asahara, T., & Losordo, D.W. (2005). Clonally expanded novel multipotent stem cells from human bone marrow regenerate myocardium after myocardial infarction. *Journal of Clinical Investigation*, 115(2), 326–338. doi: 10.1172/JCI22326.

146. Jang, Y.H., Kim, J.H., Ban, C., Ahn, K., Cheong, J.H., Kim, H.H., Kim, J.S., Park, Y.H., Kim, J., Chun, K.J., Lee, G.H., Kim, M., Kim, C., & Xu, Z. (2012). Stromal cell derived factor-1 (SDF-1) targeting reperfusion reduces myocardial infarction in isolated rat hearts. *Cardiovascular therapeutics*, 30(5), 264–272. doi: 10.1111/j.1755-5922.2011.00301.x.

147. Davidson, S.M., Selvaraj, P., He, D., Boi-Doku, C., Yellon, R.L., Vicencio, J.M., & Yellon, D.M. (2013). Remote ischaemic preconditioning involves signalling through the SDF-1α/CXCR4 signalling axis. *Basic research in cardiology*, 108(5), 377–10. doi: 10.1007/s00395-013-0377-6.

148. Haider, H.K., Jiang, S., Idris, N.M., & Ashraf, M. (2008). IGF-1-overexpressing mesenchymal stem cells accelerate bone marrow stem cell mobilization via paracrine activation of SDF-1alpha/CXCR4 signaling to promote myocardial repair. *Circulation research*, 103(11), 1300–1308. doi: 10.1161/CIRCRESAHA.108.186742.

149. Chung, E.S., Miller, L., Patel, A.N., Anderson, R.D., Mendelsohn, F.O., Traverse, J.H., Silver, K.H., Shin, J., Ewald, G., Farr, M.J., Anwaruddin, S., Plat, F., Fisher, S.J., AuWerter, A.T., Pastore, J.M., Aras, R., & Penn, M.S. (2015). Changes in ventricular remodelling and clinical status during the year following a single administration of stromal cell-derived factor-1 non-viral gene therapy in chronic ischaemic heart failure patients: the STOP-HF randomized Phase II trial. *European Heart Journal*, 36(33), 2228–2238. doi: 10.1093/eurheartj/ehv254.

150. Thum, T., Bauersachs, J., Poole-Wilson, P.A., Volk, H.D., & Anker, S.D. (2005). The dying stem cell hypothesis: immune modulation as a novel mechanism for progenitor cell therapy in cardiac muscle. *Journal of the American College of Cardiology*, 46(10), 1799–1802. doi: 10.1016/j.jacc.2005.07.053.

151. Krijnen, P.A.J., Nijmeijer, R., Meijer, C.J.L.M., Visser, C.A., Hack, C.E., & Niessen, H.W.M. (2002). Apoptosis in myocardial ischaemia and infarction. *Journal of clinical pathology*, 55(11), 801–811.

152. McCully, J.D., Wakiyama, H., Hsieh, Y.J., Jones, M., & Levitsky, S. (2004). Differential contribution of necrosis and apoptosis in myocardial ischemia-reperfusion injury. *American journal of physiology. Heart and circulatory physiology*, 286(5), H1923–35. doi: 10.1152/ajpheart.00935.2003.

153. Yu, L., Wang, L., & Chen, S. (2010). Endogenous toll-like receptor ligands and their biological significance. *Journal of cellular and molecular medicine*, 14(11), 2592–2603. doi: 10.1111/j.1582-4934.2010.01127.x.

154. Gallucci, S., Lolkema, M., & Matzinger, P. (1999). Natural adjuvants: endogenous activators of dendritic cells. *Nature*

Medicine, 5(11), 1249–1255. doi: 10.1038/15200.

155. Henson, P.M. & Bratton, D.L. (2013). Antiinflammatory effects of apoptotic cells. *Journal of Clinical Investigation*, 123(7), 2773–2774. doi: 10.1172/JCI69344.

156. Ankersmit, H.J., Hoetzenecker, K., Dietl, W., Soleiman, A., Horvat, R., Wolfsberger, M., Gerner, C., Hacker, S., Mildner, M., Moser, B., Lichtenauer, M., & Podesser, B.K. (2009). Irradiated cultured apoptotic peripheral blood mononuclear cells regenerate infarcted myocardium. *European Journal of Clinical Investigation*, 39(6), 445–456. doi: 10.1111/j.1365-2362.2009.02111.x.

157. Beer, L., Zimmermann, M., Mitterbauer, A., Ellinger, A., Gruber, F., Narzt, M.S., Zellner, M., Gyöngyösi, M., Madlener, S., Simader, E., Gabriel, C., Mildner, M., & Ankersmit, H.J. (2015). Analysis of the Secretome of Apoptotic Peripheral Blood Mononuclear Cells: Impact of Released Proteins and Exosomes for Tissue Regeneration. *Scientific Reports*, 5, 16662. doi: 10.1038/srep16662.

158. Burt, R.K., Chen, Y.h., Verda, L., Lucena, C., Navale, S., Johnson, J., Han, X., Lomasney, J., Baker, J.M., Ngai, K.L., Kino, A., Carr, J., Kajstura, J., & Anversa, P. (2012). Mitotically inactivated embryonic stem cells can be used as an in vivo feeder layer to nurse damaged myocardium after acute myocardial infarction: a preclinical study. *Circulation research*, 111(10), 1286–1296. doi: 10.1161/CIRCRESAHA.111.262584.

159. McIntire, L.V., ed. (2003). *WTEC Panel Report on Tissue Engineering Research*. Academic Press.

160. Langer, R. & Vacanti, J.P. (1993). Tissue engineering. *Science*, 260(5110), 920–926.

161. Groeber, F., Holeiter, M., Hampel, M., Hinderer, S., & Schenke-Layland, K. (2011). Skin tissue engineering — In vivo and in vitro applications. *Advanced Drug Delivery Reviews*, 63(4-5), 352–366. doi: 10.1016/j.addr.2011.01.005.

162. De Philippo, R.E., Bishop, C.E., Filho, L.F., Yoo, J.J., & Atala, A. (2008). Tissue Engineering a Complete Vaginal Replacement From a Small Biopsy of Autologous Tissue. *Transplantation*, 86(2), 208–214. doi: 10.1097/TP.0b013e31817f1686.

163. Raya-Rivera, A.M., Esquiliano, D., Fierro-Pastrana, R., López-Bayghen, E., Valencia, P., Ordorica-Flores, R., Soker, S., Yoo, J.J., & Atala, A. (2014). Tissue-engineered autologous vaginal organs in patients: a pilot cohort study. *The Lancet*, 384(9940), 329–336. doi: 10.1016/S0140-6736(14)60542-0.

164. Atala, A., Bauer, S.B., Soker, S., Yoo, J.J., & Retik, A.B. (2006). Tissue-engineered autologous bladders for patients needing cystoplasty. *The Lancet*, 367(9518), 1241–1246. doi: 10.1016/S0140-6736(06)68438-9.

165. Moretti, M., Wendt, D., Dickinson, S.C., Sims, T.J., Hollander, A.P., Kelly, D.J., Prendergast, P.J., Heberer, M., & Martin, I. (2005). Effects of in Vitro Preculture on in Vivo Development of Human Engineered Cartilage in an Ectopic Model. *Tissue engineering*, 11(9-10), 1421–1428. doi: 10.1089/ten.2005.11.1421.

166. Ko, I.K., Lee, S.J., Atala, A., & Yoo, J.J. (2013). In situ tissue regeneration through host stem cell recruitment. *Experimental & molecular medicine*, 45(11), e57. doi: 10.1038/emm.2013.118.

167. Andreas, K., Sittinger, M., & Ringe, J. (2014). Toward in situ tissue engineering: chemokine-guided stem cell recruitment. *Trends in Biotechnology*, 32(9), 483–492. doi: 10.1016/j.tibtech.2014.06.008.

168. Bayrak, A., Prüger, P., Stock, U.A., & Seifert, M. (2013). Absence of immune responses with xenogeneic collagen and elastin. *Tissue Engineering Part A*, 19(13-14), 1592–1600. doi: 10.1089/ten.TEA.2012.0394.

169. Brown, B.N. & Badylak, S.F. (2013). Expanded applications, shifting paradigms and an improved understanding of host-biomaterial interactions. *Acta Biomaterialia*, 9(2), 4948–4955. doi: 10.1016/j.actbio.2012.10.025.

170. Anderson, J.M. (1988). Inflammatory response to implants. *ASAIO transactions / American Society for Artificial Internal Organs*, 34(2), 101–107.

171. Wells, R.G. (2008). The role of matrix stiffness in regulating cell behavior. *Hepatology (Baltimore, Md.)*, 47(4), 1394–1400. doi: 10.1002/hep.22193.

172. Tse, J.R. & Engler, A.J. (2011). Stiffness gradients mimicking in vivo tissue variation regulate mesenchymal stem cell fate. *PloS one*, 6(1), e15978. doi: 10.1371/journal.pone.0015978.

173. Bonnans, C., Chou, J., & Werb, Z. (2014). Remodelling the extracellular matrix in development and disease. *Nature reviews. Molecular cell biology*, 15(12), 786–801. doi: 10.1038/nrm3904.

174. Löhler, J., Timpl, R., & Jaenisch, R. (1984). Embryonic lethal mutation in mouse collagen I gene causes rupture of blood vessels and is associated with erythropoietic and mesenchymal cell death. *Cell*, 38(2), 597–607.

175. Keane, T.J., Londono, R., Turner, N.J., & Badylak, S.F. (2012). Consequences of ineffective decellularization of biologic scaffolds on the host response. *Biomaterials*, 33(6), 1771–1781. doi: 10.1016/j.biomaterials.2011.10.054.

176. Parenteau-Bareil, R., Gauvin, R., & Berthod, F. (2010). Collagen-Based Biomaterials for Tissue Engineering Applications. *Materials*, 3(3), 1863–1887. doi: 10.3390/ma3031863.

177. Glowacki, J. & Mizuno, S. (2008). Collagen scaffolds for tissue engineering. *Biopolymers*, 89(5), 338–344. doi: 10.1002/bip.20871.

178. Chen, Q., Bruyneel, A.A.N., Carr, C.A., Clarke, K., & Czernuszka, J. (2012). Collagen-Based Scaffolds for Potential Application of Heart Valve Tissue Engineering. *Journal of Tissue Science & Engineering*, S11, 003. doi: 10.4172/2157-7552.S11-003.

179. Douglas, J.F., Gaughran, E.R., Henderson, J., Lord, G.H., & Rosenberg, N. (1956). The use of segmental arterial implants prepared by enzymatic modification of heterologous blood vessels. *Surgical Forum*, 6, 242–246.

180. Rosenberg, N. (1957). The Use of Arterial Implants Prepared by Enzymatic Modification of Arterial Heterografts. *A.M.A. Archives of Surgery*, 74(1), 89–95. doi: 10.1001/archsurg.1957.01280070093011.

181. Rosenberg, N. (1958). Use of Enzyme-Digested Heterografts as Segmental Arterial Substitutes. *A.M.A. Archives of Surgery*, 76(2), 275. doi: 10.1001/archsurg.1958.01280200097011.

182. Crapo, P.M., Gilbert, T.W., & Badylak, S.F. (2011). An overview of tissue and whole organ decellularization processes. *Biomaterials*, 32(12), 3233–3243. doi: 10.1016/j.biomaterials.2011.01.057.

183. Bee, Y.S., Alonzo, B., & Ng, J.D. (2015). Review of AlloDerm Acellular Human Dermis Regenerative Tissue Matrix in Multiple Types of Oculofacial Plastic and Reconstructive Surgery. *Ophthalmic Plas-*

tic and Reconstructive Surgery, 31(5), 348–351. doi: 10.1097/IOP.0000000000000339.

184. Bloch, O., Golde, P., Dohmen, P.M., Posner, S., Konertz, W., & Erdbrügger, W. (2011). Immune Response in Patients Receiving a Bioprosthetic Heart Valve: Lack of Response with Decellularized Valves. *Tissue Engineering Part A*, 17(19-20), 2399–2405. doi: 10.1089/ten.tea.2011.0046.

185. Hilfiker, A., Ramm, R., Goecke, T., & Haverich, A. (2013). Heart valve transplantation: the urgent need for non-immunogenic porcine heart valve matrices. *Xenotransplantation*, 20(1), 56–56. doi: 10.1111/xen.12014_13.

186. Erdbrügger, W., Konertz, W., Dohmen, P.M., Posner, S., Ellerbrok, H., Brodde, O.E., Robenek, H., Modersohn, D., Pruss, A., Holinski, S., Stein-Konertz, M., & Pauli, G. (2006). Decellularized Xenogenic Heart Valves Reveal Remodeling and Growth Potential in Vivo. *Tissue engineering*, 12(8), 2059–2068. doi: 10.1089/ten.2006.12.2059.

187. Vesely, I. (2005). Heart valve tissue engineering. *Circulation research*, 97(8), 743–755. doi: 10.1161/01.RES.0000185326.04010.9f.

188. Jungebluth, P., Alici, E., Baiguera, S., Le Blanc, K., Blomberg, P., Bozoky, B., Crowley, C., Einarsson, O., Grinnemo, K.H., Gudbjartsson, T., Le Guyader, S., Henriksson, G., Hermanson, O., Juto, J.E., Leidner, B., Lilja, T., Liska, J., Luedde, T., Lundin, V., Moll, G., Nilsson, B., Roderburg, C., Stromblad, S., Sutlu, T., Teixeira, A.I., Watz, E., Seifalian, A., & Macchiarini, P. (2011). Tracheobronchial transplantation with a stem-cell-seeded bioartificial nanocomposite: a proof-of-concept study. *The Lancet*, 378(9808), 1997–2004. doi: 10.1016/S0140-6736(11)61715-7.

189. Zong, X., Bien, H., Chung, C.Y., Yin, L., Fang, D., Hsiao, B.S., Chu, B., & Entcheva, E. (2005). Electrospun fine-textured scaffolds for heart tissue constructs. *Biomaterials*, 26(26), 5330–5338. doi: 10.1016/j.biomaterials.2005.01.052.

190. Wang, Y., Liu, X.C., Zhao, J., Kong, X.R., Shi, R.F., Zhao, X.B., Song, C.X., Liu, T.J., & Lu, F. (2009). Degradable PLGA Scaffolds with Basic Fibroblast Growth Factor Experimental Studies in Myocardial Revascularization. *Texas Heart Institute Journal*, 36(2), 89–97.

191. Shimizu, T., Yamato, M., Isoi, Y., Akutsu, T., Setomaru, T., Abe, K., Kikuchi, A., Umezu, M., & Okano, T. (2002). Fabrication of pulsatile cardiac tissue grafts using a novel 3-dimensional cell sheet manipulation technique and temperature-responsive cell culture surfaces. *Circulation research*, 90(3), E40–E48. doi: 10.1161/hh0302.105722.

192. Shimizu, T., Yamato, M., Kikuchi, A., & Okano, T. (2003). Cell sheet engineering for myocardial tissue reconstruction. *Biomaterials*, 24(13), 2309–2316. doi: 10.1016/S0142-9612(03)00110-8.

193. Miyahara, Y., Nagaya, N., Kataoka, M., Yanagawa, B., Tanaka, K., Hao, H., Ishino, K., Ishida, H., Shimizu, T., Kangawa, K., Sano, S., Okano, T., Kitamura, S., & Mori, H. (2006). Monolayered mesenchymal stem cells repair scarred myocardium after myocardial infarction. *Nature Medicine*, 12(4), 459–465. doi: 10.1038/nm1391.

194. Sawa, Y., Miyagawa, S., Sakaguchi, T., Fujita, T., Matsuyama, A., Saito, A., Shimizu, T., & Okano, T. (2012). Tissue engineered myoblast sheets improved cardiac function sufficiently to discontinue LVAS in a patient with DCM: report of a case. *Surgery today*, 42(2), 181–184. doi: 10.1007/s00595-011-0106-4.

195. Zimmermann, W.H.H., Melnychenko, I., Wasmeier, G., Didié, M., Naito, H., Nixdorff, U., Hess, A., Budinsky, L., Brune, K., Michaelis, B., Dhein, S., Schwoerer, A., Ehmke, H., & Eschenhagen, T. (2006). Engineered heart tissue grafts improve systolic and diastolic function in infarcted rat hearts. *Nature Medicine*, 12(4), 452–458. doi: 10.1038/nm1394.

196. Zimmermann, W.H.H., Didié, M., Wasmeier, G.H., Nixdorff, U., Hess, A., Melnychenko, I., Boy, O., Neuhuber, W.L., Weyand, M., & Eschenhagen, T. (2002). Cardiac grafting of engineered heart tissue in syngenic rats. *Circulation*, 106(12 Suppl 1), I151–7.

197. Zimmermann, W.H.H., Schneiderbanger, K., Schubert, P., Didie, M., Munzel, F., Heubach, J.F., Kostin, S., Neuhuber, W.L., & Eschenhagen, T. (2002). Tissue engineering of a differentiated cardiac muscle construct. *Circulation research*, 90(2), 223–230.

198. Li, Z. & Guan, J. (2011). Hydrogels for Cardiac Tissue Engineering. *Polymers*, 3(4), 740–761. doi: 10.3390/polym3020740.

199. Li, R.K., Jia, Z.Q., Weisel, R.D., Mickle, D., Choi, A., & Yau, T.M. (1999). Survival and function of bioengineered cardiac grafts. *Circulation*, 100(19), 63–69.

200. Pawelec, K.M., Husmann, A., Best, S.M., & Cameron, R.E. (2013). A design protocol for tailoring ice-templated scaffold structure. *Journal of The Royal Society Interface*, 11(92), 20130958–20130958. doi: 10.1098/rsif.2013.0958.

201. Ashworth, J.C., Mehr, M., Buxton, P.G., Best, S.M., & Cameron, R.E. (2015). Cell Invasion in Collagen Scaffold Architectures Characterized by Percolation Theory. *Advanced Healthcare Materials*, 4(9), 1317–1321. doi: 10.1002/adhm.201500197.

202. Li, D. & Xia, Y.N. (2004). Electrospinning of nanofibers: Reinventing the wheel? *Advanced Materials*, 16(14), 1151–1170. doi: 10.1002/adma.200400719.

203. Dor, V., Saab, M., Coste, P., Kornaszewska, M., & Montiglio, F. (1989). Left ventricular aneurysm: a new surgical approach. *The Thoracic and Cardiovascular Surgeon*, 37(1), 11–19. doi: 10.1055/s-2007-1013899.

204. Sartipy, U., Albåge, A., & Lindblom, D. (2005). The Dor procedure for left ventricular reconstruction. Ten-year clinical experience. *European journal of cardiothoracic surgery*, 27(6), 1005–1010. doi: 10.1016/j.ejcts.2005.01.055.

205. Menicanti & Donato, D. (2003). The Dor procedure: What has changed after fifteen years of clinical practice? *Journal of Thoracic and Cardiovascular Surgery*, 125(3), 720–720.

206. Konertz, W.F., Shapland, J.E., Hotz, H., Dushe, S., Braun, J.P., Stantke, K., & Kleber, F.X. (2001). Passive containment and reverse remodeling by a novel textile cardiac support device. *Circulation*, 104(12), I270–I275.

207. Oh, J.H., Badhwar, V., Mott, B.D., Li, C.M., & CHIU, R. (1998). The effects of prosthetic cardiac binding and adynamic cardiomyoplasty in a model of dilated cardiomyopathy. *Journal of Thoracic and Cardiovascular Surgery*, 116(1), 148–153.

208. Mann, D.L., Kubo, S.H., Sabbah, H.N., Starling, R.C., Jessup, M., Oh, J.K., & Acker, M.A. (2012). Beneficial effects of the CorCap cardiac support device: five-year results from the Acorn Trial. *The Journal of Thoracic and Cardiovascular Surgery*, 143(5), 1036–1042. doi: 10.1016/j.jtcvs.2011.06.014.

209. Lin, Y.D., Luo, C.Y., Hu, Y.N., Yeh, M.L., Hsueh, Y.C., Chang, M.Y., Tsai,

D.C., Wang, J.N., Tang, M.J., Wei, E.I.H., Springer, M.L., & Hsieh, P.C.H. (2012). Instructive Nanofiber Scaffolds with VEGF Create a Microenvironment for Arteriogenesis and Cardiac Repair. *Science translational medicine*, 4(146), 146ra109–146ra109. doi: 10.1126/scitranslmed.3003841.

210. Kardami, E., Detillieux, K., Ma, X., Jiang, Z., Santiago, J.J., Jimenez, S.K., & Cattini, P.A. (2007). Fibroblast growth factor-2 and cardioprotection. *Heart failure reviews*, 12(3-4), 267–277. doi: 10.1007/s10741-007-9027-0.

211. Wei, K., Serpooshan, V., Hurtado, C., Diez-Cuñado, M., Zhao, M., Maruyama, S., Zhu, W., Fajardo, G., Noseda, M., Nakamura, K., Tian, X., Liu, Q., Wang, A., Matsuura, Y., Bushway, P., Cai, W., Savchenko, A., Mahmoudi, M., Schneider, M.D., van den Hoff, M.J.B., Butte, M.J., Yang, P.C., Walsh, K., Zhou, B., Bernstein, D., Mercola, M., & Ruiz-Lozano, P. (2015). Epicardial FSTL1 reconstitution regenerates the adult mammalian heart. *Nature*, 525(7570), 479–485. doi: 10.1038/nature15372.

212. Skrzypiec-Spring, M., Grotthus, B., Szeląg, A., & Schulz, R. (2007). Isolated heart perfusion according to Langendorff—Still viable in the new millennium. *Journal of Pharmacological and Toxicological Methods*, 55(2), 113–126. doi: 10.1016/j.vascn.2006.05.006.

213. Rana, P., Anson, B., Engle, S., & Will, Y. (2012). Characterization of human induced pluripotent stem cell derived cardiomyocytes: Bioenergetics and utilization in safety screening. *Toxicological Sciences*, 130(1), 117–131.

214. Sinnecker, D., Goedel, A., Laugwitz, K.L., & Moretti, A. (2013). Induced Pluripotent Stem Cell-Derived Cardiomyocytes A Versatile Tool for Arrhythmia Research. *Circulation research*, 112(6), 961–968. doi: 10.1161/CIRCRESAHA.112.268623.

215. Bhatia, S.N. & Ingber, D.E. (2014). Microfluidic organs-on-chips. *Nature biotechnology*, 32(8), 760–772. doi: 10.1038/nbt.2989.

216. Huh, D.D., Matthews, B.D., Mammoto, A., Montoya-Zavala, M., Hsin, H.Y., & Ingber, D.E. (2010). Reconstituting organ-level lung functions on a chip. *Science*, 328(5986), 1662–1668. doi: 10.1126/science.1188302.

217. Huh, D.D., Leslie, D.C., Matthews, B.D., Fraser, J.P., Jurek, S., Hamilton, G.A., Thorneloe, K.S., McAlexander, M.A., & Ingber, D.E. (2012). A human disease model of drug toxicity-induced pulmonary edema in a lung-on-a-chip microdevice. *Science translational medicine*, 4(159), 159ra147–159ra147. doi: 10.1126/scitranslmed.3004249.

218. Huh, D.D., Kim, H.J., Fraser, J.P., Shea, D.E., Khan, M., Bahinski, A., Hamilton, G.A., & Ingber, D.E. (2013). Microfabrication of human organs-on-chips. *Nature Protocols*, 8(11), 2135–2157. doi: 10.1038/nprot.2013.137.

219. Wang, G., McCain, M.L., Yang, L., He, A., Pasqualini, F.S., Agarwal, A., Yuan, H., Jiang, D., Zhang, D., Zangi, L., Geva, J., Roberts, A.E., Ma, Q., Ding, J., Chen, J., Wang, D.Z., Li, K., Wang, J., Wanders, R.J.A., Kulik, W., Vaz, F.M., Laflamme, M.A., Murry, C.E., Chien, K.R., Kelley, R.I., Church, G.M., Parker, K.K., & Pu, W.T. (2014). Modeling the mitochondrial cardiomyopathy of Barth syndrome with induced pluripotent stem cell and heart-on-chip technologies. *Nature Medicine*, 20(6), 616–623. doi: 10.1038/nm.3545.

220. Fink, C., Ergün, S., Kralisch, D., Remmers, U., Weil, J., & Eschenhagen, T. (2000). Chronic stretch of engineered heart tissue induces hypertrophy and functional

improvement. *The FASEB journal*, 14(5), 669–679.

221. Eschenhagen, T., Fink, C., Remmers, U., Scholz, H., Wattchow, J., Weil, J., Zimmermann, W.H.H., Dohmen, H.H., Schafer, H., Bishopric, N., Wakatsuki, T., & Elson, E.L. (1997). Three-dimensional reconstitution of embryonic cardiomyocytes in a collagen matrix: a new heart muscle model system. *The FASEB journal*, 11(8), 683–694. doi: 10.1096/fj.1530-6860.

222. Zhou, S., Cui, Z., & Urban, J.P.G. (2008). Nutrient gradients in engineered cartilage: metabolic kinetics measurement and mass transfer modeling. *Biotechnology and Bioengineering*, 101(2), 408–421. doi: 10.1002/bit.21887.

223. Kanzaki, M. (1999). Molecular Identification of a Eukaryotic, Stretch-Activated Nonselective Cation Channel. *Science*, 285(5429), 882–886. doi: 10.1126/science.285.5429.882.

224. Brown, T.D. (2000). Techniques for mechanical stimulation of cells in vitro: a review. *Journal of biomechanics*, 33(1), 3–14. doi: 10.1016/S0021-9290(99)00177-3.

225. Egusa, H., Kobayashi, M., Matsumoto, T., Sasaki, J.I., Uraguchi, S., & Yatani, H. (2013). Application of cyclic strain for accelerated skeletal myogenic differentiation of mouse bone marrow-derived mesenchymal stromal cells with cell alignment. *Tissue Engineering Part A*, 19(5-6), 770–782. doi: 10.1089/ten.TEA.2012.0164.

226. Tulloch, N.L., Muskheli, V., Razumova, M.V., Korte, F.S., Regnier, M., Hauch, K.D., Pabon, L., Reinecke, H., & Murry, C.E. (2011). Growth of engineered human myocardium with mechanical loading and vascular coculture. *Circulation research*, 109(1), 47–59. doi: 10.1161/CIRCRESAHA.110.237206.

227. Kurazumi, H., Kubo, M., Ohshima, M., Yamamoto, Y., Takemoto, Y., Suzuki, R., Ikenaga, S., Mikamo, A., Udo, K., Hamano, K., & Li, T.S. (2011). The effects of mechanical stress on the growth, differentiation, and paracrine factor production of cardiac stem cells. *PloS one*, 6(12), e28890. doi: 10.1371/journal.pone.0028890.

228. Wang, H., Riha, G.M., Yan, S., Li, M., Chai, H., Yang, H., Yao, Q., & Chen, C. (2005). Shear stress induces endothelial differentiation from a murine embryonic mesenchymal progenitor cell line. *Arteriosclerosis, Thrombosis, and Vascular Biology*, 25(9), 1817–1823. doi: 10.1161/01.ATV.0000175840.90510.a8.

229. Balint, R., Cassidy, N.J., & Cartmell, S.H. (2013). Electrical stimulation: a novel tool for tissue engineering. *Tissue Engineering Part B: Reviews*, 19(1), 48–57. doi: 10.1089/ten.TEB.2012.0183.

230. Illingworth, C.M. & Barker, A.T. (1980). Measurement of electrical currents emerging during the regeneration of amputated finger tips in children. *Clinical Physics and Physiological Measurement*, 1(1), 87–89.

231. Zhao, M. (2009). Electrical fields in wound healing-An overriding signal that directs cell migration. *Seminars in Cell & Developmental Biology*, 20(6), 674–682. doi: 10.1016/j.semcdb.2008.12.009.

232. Hronik-Tupaj, M. & Kaplan, D.L. (2012). A review of the responses of two- and three-dimensional engineered tissues to electric fields. *Tissue Engineering Part B: Reviews*, 18(3), 167–180. doi: 10.1089/ten.TEB.2011.0244.

233. Berger, H.J., Prasad, S.K., Davidoff, A.J., Pimental, D., Ellingsen, O., Marsh, J.D., Smith, T.W., & Kelly, R.A. (1994). Continual electric field stimulation preserves

contractile function of adult ventricular myocytes in primary culture. *The American journal of physiology*, 266(1 Pt 2), H341–9.

234. Tandon, N., Cannizzaro, C., Chao, P.H.G., Maidhof, R., Marsano, A., Au, H.T.H., Radisic, M., & Vunjak-Novakovic, G. (2009). Electrical stimulation systems for cardiac tissue engineering. *Nature Protocols*, 4(2), 155–173. doi: 10.1038/nprot.2008.183.

235. Barash, Y., Dvir, T., Tandeitnik, P., Ruvinov, E., Guterman, H., & Cohen, S. (2010). Electric field stimulation integrated into perfusion bioreactor for cardiac tissue engineering. *Tissue Engineering Part C: Methods*, 16(6), 1417–1426. doi: 10.1089/ten.TEC.2010.0068.

236. Radisic, M., Park, H., Shing, H., Consi, T., Schoen, F.J., Langer, R., Freed, L.E., & Vunjak-Novakovic, G. (2004). Functional assembly of engineered myocardium by electrical stimulation of cardiac myocytes cultured on scaffolds. *Proceedings of the National Academy of Sciences*, 101(52), 18129–18134. doi: 10.1073/pnas.0407817101.

237. Feng, Z., Matsumoto, T., Nomura, Y., & Nakamura, T. (2005). An electro-tensile bioreactor for 3-D culturing of cardiomyocytes. A bioreactor system that simulates the myocardium's electrical and mechanical response in vivo. *IEEE Engineering in Bedicine and Biology Magazine*, 24(4), 73–79.

238. Ott, H., Matthiesen, T.S., Goh, S.K., Black, L.D., Kren, S.M., Netoff, T.I., & Taylor, D.A. (2008). Perfusion-decellularized matrix: using nature's platform to engineer a bioartificial heart. *Nature Medicine*, 14(2), 213–221. doi: 10.1038/nm1684.

239. Kruschke, J.K. (2014). *Doing Bayesian data analysis: a tutorial with R, JAGS, and Stan*. Academic Press, 2 ed.

240. Hadfield, J.D. (2010). Mcmc methods for multi-response generalized linear mixed models: The MCMCglmm R package. *Journal of Statistical Software*, 33(2), 1–22.

241. Matz, M.V., Wright, R.M., & Scott, J.G. (2013). No Control Genes Required: Bayesian Analysis of qRT-PCR Data. *PloS one*, 8(8), e71448. doi: 10.1371/journal.pone.0071448.

242. Hao, J., Astle, W., De Iorio, M., & Ebbels, T.M.D. (2012). BATMAN–an R package for the automated quantification of metabolites from nuclear magnetic resonance spectra using a Bayesian model. *Bioinformatics*, 28(15), 2088–2090. doi: 10.1093/bioinformatics/bts308.

243. Hao, J., Liebeke, M., Astle, W., De Iorio, M., Bundy, J.G., & Ebbels, T.M.D. (2014). Bayesian deconvolution and quantification of metabolites in complex 1D NMR spectra using BATMAN. *Nature Protocols*, 9(6), 1416–1427. doi: 10.1038/nprot.2014.090.

244. Hao, J., Astle, W., Iorio, M.D., & Ebbels, T. (2014). *batman: Bayesian AuTomated Metabolite Analyser for NMR spectra*. R package version 1.2.1.03/r340.

245. R Development Core Team (2008). *R: A Language and Environment for Statistical Computing*. Vienna, Austria.

246. Michael, L.H., Entman, M.L., Hartley, C.J., Youker, K.A., Zhu, J., Hall, S.R., Hawkins, H.K., Berens, K., & Ballantyne, C.M. (1995). Myocardial ischemia and reperfusion: a murine model. *The American journal of physiology*, 269(6 Pt 2), H2147–54.

247. Schindelin, J., Arganda-Carreras, I., Frise, E., Kaynig, V., Longair, M., Pietzsch, T., Preibisch, S., Rueden, C., Saalfeld, S., Schmid, B., Tinevez, J.Y., White, D.J., Hartenstein, V., Eliceiri, K., Tomancak, P.,

& Cardona, A. (2012). Fiji: an open-source platform for biological-image analysis. *Nature Methods*, 9(7), 676–682. doi: 10.1038/nmeth.2019.

248. Schneider, C.A., Rasband, W.S., & Eliceiri, K.W. (2012). NIH Image to ImageJ: 25 years of image analysis. *Nature Methods*, 9(7), 671–675. doi: 10.1038/nmeth.2089.

249. Chen, Q., Bruyneel, A.A.N., Carr, C.A., & Czernuszka, J. (2013). Bio-mechanical Properties of Novel Bi-layer Collagen-Elastin Scaffolds for Heart Valve Tissue Engineering. *Procedia Engineering*, 59, 247–254. doi: 10.1016/j.proeng.2013.05.118.

250. Sekita, S., Katagiri, T., Sasai, Y., & Takeda, K. (1985). Studies on Collagen in the Experimental Myocardial-Infarction. *Japanese circulation journal*, 49(2), 171–178.

251. Cleutjens, J.P., Verluyten, M.J., Smiths, J.F., & Daemen, M.J. (1995). Collagen remodeling after myocardial infarction in the rat heart. *The American Journal of Pathology*, 147(2), 325–338.

252. Chiariello, M., Ambrosio, G., Cappelli-Bigazzi, M., Perrone-Filardi, P., Brigante, F., & Sifola, C. (1986). A biochemical method for the quantitation of myocardial scarring after experimental coronary artery occlusion. *Journal of Molecular and Cellular Cardiology*, 18(3), 283–290.

253. Woessner, J.F. (1961). The determination of hydroxyproline in tissue and protein samples containing small proportions of this imino acid. *Archives of biochemistry and biophysics*, 93, 440–447.

254. Edwards, C.A. & O'Brien, W.D. (1980). Modified Assay for Determination of Hydroxyproline in a Tissue Hydrolyzate. *Clinica Chimica Acta*, 104(2), 161–167.

255. Stegeman, H. & Stalder, K. (1967). Determination of Hydroxyproline. *Clinica Chimica Acta*, 18(2), 267–&.

256. Reddy, G.K. & Enwemeka, C.S. (1996). A simplified method for the analysis of hydroxyproline in biological tissues. *Clinical biochemistry*, 29(3), 225–229.

257. Wang, Y., Bao, J., Wu, Q., Zhou, Y., Li, Y., Wu, X., Shi, Y., Li, L., & Bu, H. (2015). Method for perfusion decellularization of porcine whole liver and kidney for use as a scaffold for clinical-scale bioengineering engrafts. *Xenotransplantation*, 22(1), 48–61. doi: 10.1111/xen.12141.

258. Hayashi, K. (1975). A rapid determination of sodium dodecyl sulfate with methylene blue. *Analytical Biochemistry*, 67(2), 503–506.

259. Fan, J. & Yin, C. (2012). *Methylene green SDS detection assay - Bowdish Lab, McMaster University*.

260. Rusconi, F., Valton, É., Nguyen, R., & Dufourc, E. (2001). Quantification of sodium dodecyl sulfate in microliter-volume biochemical samples by visible light spectroscopy. *Analytical Biochemistry*, 295(1), 31–37.

261. Cardillo, G. (2012). *MathWorks - File Exchange - Four parameters logistic regression - There and back again*.

262. Vandesompele, J., De Preter, K., Pattyn, F., Poppe, B., Van Roy, N., De Paepe, A., & Speleman, F. (2002). Accurate normalization of real-time quantitative RT-PCR data by geometric averaging of multiple internal control genes. *Genome Biology*, 3(7), RESEARCH0034.

263. Steibel, J.P., Poletto, R., Coussens, P.M., & Rosa, G.J.M. (2009). A powerful and flexible linear mixed model framework for the analysis of relative quantification RT-PCR data. *Genomics*, 94(2), 146–152. doi: 10.1016/j.ygeno.2009.04.008.

264. Ritz, C. & Streibig, J.C. (2005). Bioassay analysis using r. *Journal of Statistical Software*, 12.

265. Ando, I., Hirose, T., Nemoto, T., Totsune, K., Imai, Y., Takeuchi, K., & Fujiwara, M. (2010). Quantification of molecules in 1H-NMR metabolomics with formate as a concentration standard. *The Journal of Toxicological Sciences*, 35(2), 253–256. doi: 10.2131/jts.35.253.

266. Kehat, I., Kenyagin-Karsenti, D., Snir, M., Segev, H., Amit, M., Gepstein, A., Livne, E., Binah, O., Itskovitz-Eldor, J., & Gepstein, L. (2001). Human embryonic stem cells can differentiate into myocytes with structural and functional properties of cardiomyocytes. *Journal of Clinical Investigation*, 108(3), 407–414. doi: 10.1172/JCI12131.

267. Zhang, J., Wilson, G.F., Soerens, A.G., Koonce, C.H., Yu, J., Palecek, S.P., Thomson, J.A., & Kamp, T.J. (2009). Functional cardiomyocytes derived from human induced pluripotent stem cells. *Circulation research*, 104(4), e30–41. doi: 10.1161/CIRCRESAHA.108.192237.

268. Passier, R., Oostwaard, D.W.v., Snapper, J., Kloots, J., Hassink, R.J., Kuijk, E., Roelen, B., de la Riviere, A.B., & Mummery, C. (2005). Increased cardiomyocyte differentiation from human embryonic stem cells in serum-free cultures. *Stem Cells*, 23(6), 772–780. doi: 10.1634/stemcells.2004-0184.

269. Lian, X., Zhang, J., Zhu, K., Kamp, T.J., & Palecek, S.P. (2013). Insulin Inhibits Cardiac Mesoderm, Not Mesendoderm, Formation During Cardiac Differentiation of Human Pluripotent Stem Cells and Modulation of Canonical Wnt Signaling Can Rescue This Inhibition. *Stem Cells*, 31(3), 447–457. doi: 10.1002/stem.1289.

270. Lian, X., Zhang, J., Azarin, S.M., Zhu, K., Hazeltine, L.B., Bao, X., Hsiao, C., Kamp, T.J., & Palecek, S.P. (2013). Directed cardiomyocyte differentiation from human pluripotent stem cells by modulating Wnt/β-catenin signaling under fully defined conditions. *Nature Protocols*, 8(1), 162–175. doi: 10.1038/nprot.2012.150.

271. Graichen, R., Xu, X., Braam, S.R., Balakrishnan, T., Norfiza, S., Sieh, S., Soo, S.Y., Tham, S.C., Mummery, C., Colman, A., Zweigerdt, R., & Davidson, B.P. (2008). Enhanced cardiomyogenesis of human embryonic stem cells by a small molecular inhibitor of p38 MAPK. *Differentiation*, 76(4), 357–370. doi: 10.1111/j.1432-0436.2007.00236.x.

272. Freund, C., Davis, R.P., Gkatzis, K., Ward-van Oostwaard, D., & Mummery, C.L. (2010). The first reported generation of human induced pluripotent stem cells (iPS cells) and iPS cell-derived cardiomyocytes in the Netherlands. *Netherlands Heart Journal*, 18(1), 51–54.

273. Laflamme, M.A., Chen, K.Y., Naumova, A.V., Muskheli, V., Fugate, J.A., Dupras, S.K., Reinecke, H., Xu, C., Hassanipour, M., Police, S., O'Sullivan, C., Collins, L., Chen, Y., Minami, E., Gill, E.A., Ueno, S., Yuan, C., Gold, J., & Murry, C.E. (2007). Cardiomyocytes derived from human embryonic stem cells in pro-survival factors enhance function of infarcted rat hearts. *Nature biotechnology*, 25(9), 1015–1024. doi: 10.1038/nbt1327.

274. Yang, L., Soonpaa, M.H., Adler, E.D., Roepke, T.K., Kattman, S.J., Kennedy, M., Henckaerts, E., Bonham, K., Abbott, G.W., Linden, R.M., Field, L.J., & Keller, G.M. (2008). Human cardiovascular progenitor cells develop from a KDR+ embryonic-stem-cell-derived population. *Nature*, 453(7194), 524–528. doi: 10.1038/nature06894.

275. Moretti, A., Bellin, M., Welling, A., Jung, C.B., Lam, J.T., Bott-Flügel, L., Dorn, T.,

Goedel, A., Höhnke, C., Hofmann, F., Seyfarth, M., Sinnecker, D., Schömig, A., & Laugwitz, K.L. (2010). Patient-specific induced pluripotent stem-cell models for long-QT syndrome. *New England Journal of Medicine*, 363(15), 1397–1409. doi: 10.1056/NEJMoa0908679.

276. Zhang, J., Klos, M., Wilson, G.F., Herman, A.M., Lian, X., Raval, K.K., Barron, M.R., Hou, L., Soerens, A.G., Yu, J., Palecek, S.P., Lyons, G.E., Thomson, J.A., Herron, T.J., Jalife, J., & Kamp, T.J. (2012). Extracellular matrix promotes highly efficient cardiac differentiation of human pluripotent stem cells: the matrix sandwich method. *Circulation research*, 111(9), 1125–1136. doi: 10.1161/CIRCRESAHA.112.273144.

277. Husson, F., Josse, J., Le, S., & Mazet, J. (2015). *FactoMineR: Multivariate Exploratory Data Analysis and Data Mining*. R package version 1.31.3.

278. Williamson, D.H., Lund, P., & Krebs, H.A. (1967). The redox state of free nicotinamide-adenine dinucleotide in the cytoplasm and mitochondria of rat liver. *Biochemical Journal*, 103(2), 514–527.

279. Kailavasan, M., Rehman, I., Reynolds, S., Bucur, A., Tozer, G., & Paley, M. (2014). NMR-based evaluation of the metabolic profile and response to dichloroacetate of human prostate cancer cells. *NMR in biomedicine*, 27(5), 610–616. doi: 10.1002/nbm.3101.

280. Narsinh, K.H., Sun, N., Sanchez-Freire, V., Lee, A.S., Almeida, P., Hu, S., Jan, T., Wilson, K.D., Leong, D., Rosenberg, J., Yao, M., Robbins, R.C., & Wu, J.C. (2011). Single cell transcriptional profiling reveals heterogeneity of human induced pluripotent stem cells. *Journal of Clinical Investigation*, 121(3), 1217–1221. doi: 10.1172/JCI44635.

281. Piccini, I., Rao, J., Seebohm, G., & Greber, B. (2015). Human pluripotent stem cell-derived cardiomyocytes: Genome-wide expression profiling of long-term in vitro maturation in comparison to human heart tissue. *Genomics Data*, 4, 69–72. doi: 10.1016/j.gdata.2015.03.008.

282. Yee-Ki, L. & Chung-Wah, S. (2012). *Calcium Handling in hiPSC-Derived Cardiomyocytes*. SpringerBriefs in Stem Cells. Springer New York, New York, NY. doi: 10.1007/978-1-4614-4093-2.

283. Liu, J., Lieu, D.K., Siu, C.W., Fu, J.D., Tse, H.F., & Li, R.A. (2009). Facilitated maturation of Ca2+ handling properties of human embryonic stem cell-derived cardiomyocytes by calsequestrin expression. *American journal of physiology. Cell physiology*, 297(1), C152–C159. doi: 10.1152/ajpcell.00060.2009.

284. Jung, C.B., Moretti, A., Schnitzler, M.M.y., Iop, L., Storch, U., Bellin, M., Dorn, T., Ruppenthal, S., Pfeiffer, S., Goedel, A., Dirschinger, R.J., Seyfarth, M., Lam, J.T., Sinnecker, D., Gudermann, T., Lipp, P., & Laugwitz, K.L. (2012). Dantrolene rescues arrhythmogenic RYR2 defect in a patient-specific stem cell model of catecholaminergic polymorphic ventricular tachycardia. *EMBO molecular medicine*, 4(3), 180–191. doi: 10.1002/emmm.201100194.

285. Oyamada, M., Takebe, K., Endo, A., Hara, S., & Oyamada, Y. (2013). Connexin expression and gap-junctional intercellular communication in ES cells and iPS cells. *Frontiers in pharmacology*, 4. doi: 10.3389/fphar.2013.00085.

286. Severs, N.J., Coppen, S.R., Dupont, E., Yeh, H.I., Ko, Y.S., & Matsushita, T. (2004). Gap junction alterations in human cardiac disease. *Cardiovascular research*, 62(2), 368–377. doi: 10.1016/j.cardiores.2003.12.007.

287. Boyer, L.A., Lee, T.I., Cole, M.F., Johnstone, S.E., Levine, S.S., Zucker, J.P., Guenther, M.G., Kumar, R.M., Murray, H.L., Jenner, R.G., Gifford, D.K., Melton, D.A., Jaenisch, R., & Young, R.A. (2005). Core transcriptional regulatory circuitry in human embryonic stem cells. *Cell*, 122(6), 947–956. doi: 10.1016/j.cell.2005.08.020.

288. Ke, Q., Li, L., Cai, B., Liu, C., Yang, Y., Gao, Y., Huang, W., Yuan, X., Wang, T., Zhang, Q., Harris, A.L., Tao, L., & Xiang, A.P. (2013). Connexin 43 is involved in the generation of human-induced pluripotent stem cells. *Human molecular genetics*, 22(11), 2221–2233.

289. Freund, C., Ward van Oostwaard, D., Monshouwer-Kloots, J., van den Brink, S., van Rooijen, M., Xu, X., Zweigerdt, R., Mummery, C., & Passier, R. (2008). Insulin Redirects Differentiation from Cardiogenic Mesoderm and Endoderm to Neuroectoderm in Differentiating Human Embryonic Stem Cells. *Stem Cells*, 26(3), 724–733. doi: 10.1634/stemcells.2007-0617.

290. Long, Y.C., Cheng, Z., Copps, K.D., & White, M.F. (2011). Insulin receptor substrates Irs1 and Irs2 coordinate skeletal muscle growth and metabolism via the Akt and AMPK pathways. *Molecular and Cellular Biology*, 31(3), 430–441. doi: 10.1128/MCB.00983-10.

291. Qi, Y., Xu, Z., Zhu, Q., Thomas, C., Kumar, R., Feng, H., Dostal, D.E., White, M.F., Baker, K.M., & Guo, S. (2013). Myocardial loss of IRS1 and IRS2 causes heart failure and is controlled by p38α MAPK during insulin resistance. *Diabetes*, 62(11), 3887–3900. doi: 10.2337/db13-0095.

292. Rakhshandehroo, M., Knoch, B., Müller, M., Kersten, S., Rakhshandehroo, M., Knoch, B., & Kersten, S. (2010). Peroxisome Proliferator-Activated Receptor Alpha Target Genes. *PPAR Research*, 2010(5), 1–20. doi: 10.1155/2010/612089.

293. Mandard, S., M ller, M., & Kersten, S. (2004). Peroxisome proliferator-activated receptor a target genes. *Cellular and Molecular Life Sciences (CMLS)*, 61(4), 393–416. doi: 10.1007/s00018-003-3216-3.

294. Lundy, S.D., Zhu, W.Z., Regnier, M., & Laflamme, M.A. (2013). Structural and functional maturation of cardiomyocytes derived from human pluripotent stem cells. *Stem Cells and Development*, 22(14), 1991–2002. doi: 10.1089/scd.2012.0490.

295. Yang, X., Rodriguez, M., Pabon, L., Fischer, K.A., Reinecke, H., Regnier, M., Sniadecki, N.J., Ruohola-Baker, H., & Murry, C.E. (2014). Tri-iodo-l-thyronine promotes the maturation of human cardiomyocytes-derived from induced pluripotent stem cells. *Journal of Molecular and Cellular Cardiology*, 72, 296–304. doi: 10.1016/j.yjmcc.2014.04.005.

296. Pereira, S.L., Ramalho-Santos, J., Branco, A.F., Sardão, V.A., Oliveira, P.J., & Carvalho, R.A. (2011). Metabolic remodeling during H9c2 myoblast differentiation: relevance for in vitro toxicity studies. *Cardiovascular Toxicology*, 11(2), 180–190. doi: 10.1007/s12012-011-9112-4.

297. Lu, T.Y., Lin, B., Kim, J., Sullivan, M., Tobita, K., Salama, G., & Yang, L. (2013). Repopulation of decellularized mouse heart with human induced pluripotent stem cell-derived cardiovascular progenitor cells. *Nature Communications*, 4. doi: 10.1038/ncomms3307.

298. Claycomb, W.C., Lanson, N.A., Stallworth, B.S., Egeland, D.B., Delcarpio, J.B., Bahinski, A., & Izzo, N.J. (1998). HL-1 cells: a cardiac muscle cell line that contracts and retains phenotypic characteristics of the adult cardiomyocyte. *Proceedings of*

the National Academy of Sciences, 95(6), 2979–2984.

299. Carvalho, J.L., Herthel de Carvalho, P., Gomes, D.A., & Goes, A.M. (2012). Characterization of Decellularized Heart Matrices as Biomaterials for Regular and Whole Organ Tissue Engineering and Initial In-vitro Recellularization with Ips Cells. *Journal of Tissue Science & Engineering*, S11. doi: 10.4172/2157-7552.S11-002.

300. Chamberland, C., Martinez-Fernandez, A., Beraldi, R., Chamberland, C., Beraldi, R., & Nelson, T.J. (2014). Embryonic Decellularized Cardiac Scaffold Supports Embryonic Stem Cell Differentiation to Produce Beating Cardiac Tissue. *International Scholarly Research Notices*, 2014, 1–10. doi: 10.1155/2014/625164.

301. He, M. & Callanan, A. (2013). Comparison of methods for whole-organ decellularization in tissue engineering of bioartificial organs. *Tissue Engineering Part B: Reviews*, 19(3), 194–208. doi: 10.1089/ten.TEB.2012.0340.

302. Villegas-Montoya, C. & McFetridge, P.S. (2009). Preparation of ex vivo-based biomaterials using convective flow decellularization. *Tissue Engineering Part C: Methods*, 15(2), 191–200. doi: 10.1089/ten.tec.2008.0372.

303. Funamoto, S., Nam, K., Kimura, T., Murakoshi, A., Hashimoto, Y., Niwaya, K., Kitamura, S., Fujisato, T., & Kishida, A. (2010). The use of high-hydrostatic pressure treatment to decellularize blood vessels. *Biomaterials*, 31(13), 3590–3595. doi: 10.1016/j.biomaterials.2010.01.073.

304. Azhim, A., Syazwani, N., Morimoto, Y., Furukawa, K.S., & Ushida, T. (2014). The use of sonication treatment to decellularize aortic tissues for preparation of bioscaffolds. *Journal of biomaterials applications*, 29(1), 130–141. doi: 10.1177/0885328213517579.

305. Gilbert, T.W., Sellaro, T.L., & Badylak, S.F. (2006). Decellularization of tissues and organs. *Biomaterials*. doi: 10.1016/j.biomaterials.2006.02.014.

306. Elder, B.D., Eleswarapu, S.V., & Athanasiou, K.A. (2009). Extraction techniques for the decellularization of tissue engineered articular cartilage constructs. *Biomaterials*, 30(22), 3749–3756. doi: 10.1016/j.biomaterials.2009.03.050.

307. Dahl, S.L.M., Koh, J., Prabhakar, V., & Niklason, L.E. (2003). Decellularized native and engineered arterial scaffolds for transplantation. *Cell transplantation*, 12(6), 659–666.

308. Rosario, D.J., Reilly, G.C., Ali Salah, E., Glover, M., Bullock, A.J., & Macneil, S. (2008). Decellularization and sterilization of porcine urinary bladder matrix for tissue engineering in the lower urinary tract. *Regenerative medicine*, 3(2), 145–156. doi: 10.2217/17460751.3.2.145.

309. Fournier, R.L. (2012). *Basic Transport Phenomena in Biomedical Engineering*. CRC Press, 3 ed.

310. da Palma, R.K., Campillo, N., Uriarte, J.J., Oliveira, L.V.F., Navajas, D., & Farré, R. (2015). Pressure- and flow-controlled media perfusion differently modify vascular mechanics in lung decellularization. *Journal of the mechanical behavior of biomedical materials*, 49, 69–79. doi: 10.1016/j.jmbbm.2015.04.024.

311. Raman, R., Sasisekharan, V., & Sasisekharan, R. (2005). Structural insights into biological roles of protein-glycosaminoglycan interactions. *Chemistry & biology*, 12(3), 267–277. doi: 10.1016/j.chembiol.2004.11.020.

312. Frantz, C., Stewart, K.M., & Weaver, V.M. (2010). The extracellular matrix at a glance. *Journal of Cell Science*, 123(Pt 24), 4195–4200. doi: 10.1242/jcs.023820.

313. Lovekamp, J.J., Simionescu, D.T., Mercuri, J.J., Zubiate, B., Sacks, M.S., & Vyavahare, N.R. (2006). Stability and function of glycosaminoglycans in porcine bioprosthetic heart valves. *Biomaterials*, 27(8), 1507–1518. doi: 10.1016/j.biomaterials.2005.08.003.

314. Bühler, N.E.M., Schulze-Osthoff, K., Königsrainer, A., & Schenk, M. (2014). Controlled processing of a full-sized porcine liver to a decellularized matrix in 24 h. *Journal of Bioscience and Bioengineering*, 119(5), 609–613. doi: 10.1016/j.jbiosc.2014.10.019.

315. Sabetkish, S., Kajbafzadeh, A.M., Sabetkish, N., Khorramirouz, R., Akbarzadeh, A., Ladi Seyedian, S.S., Pasalar, P., Orangian, S., Beigi, R.S.H., Aryan, Z., Akbari, H., & Tavangar, S.M. (2014). Whole-Organ Tissue Engineering: Decellularization and Recellularization of Three-Dimensional Matrix Liver Scaffolds. *Journal of Biomedical Materials Research Part A*, n/a–n/a.

316. Hussein, K.H., Park, K.M., Ghim, J.H., Yang, S.R., & Woo, H.M. (2015). Three dimensional culture of HepG2 liver cells on a rat decellularized liver matrix for pharmacological studies. *Journal of biomedical materials research. Part B, Applied biomaterials*, n/a–n/a. doi: 10.1002/jbm.b.33384.

317. Baptista, P.M., Siddiqui, M.M., Lozier, G., Rodriguez, S.R., Atala, A., & Soker, S. (2011). The use of whole organ decellularization for the generation of a vascularized liver organoid. *Hepatology*, 53(2), 604–617. doi: 10.1002/hep.24067.

318. Xing, Q., Yates, K., Tahtinen, M., Shearier, E., Qian, Z., & Zhao, F. (2015). Decellularization of Fibroblast Cell Sheets for Natural Extracellular Matrix Scaffold Preparation. *Tissue Engineering Part C: Methods*, 21(1), 77–87. doi: 10.1089/ten.tec.2013.0666.

319. Woodard, H.Q. & White, D.R. (1986). The composition of body tissues. *The British Journal of Radiology*, 59(708), 1209–1218. doi: 10.1259/0007-1285-59-708-1209.

320. Pieper, J.S., Oosterhof, A., Dijkstra, P.J., Veerkamp, J.H., & van Kuppevelt, T.H. (1999). Preparation and characterization of porous crosslinked collagenous matrices containing bioavailable chondroitin sulphate. *Biomaterials*, 20, 847–858. doi: 10.1016/S0142-9612(98)00240-3.

321. Chvapil, M. (1977). Collagen sponge: theory and practice of medical applications. *Journal of Biomedical Materials Research Part A*, 11(5), 721–741. doi: 10.1002/jbm.820110508.

322. van Susante, J.L.C., Pieper, J.S., Buma, P., van Kuppevelt, T.H., van Beuningen, H., van Der Kraan, P.M., Veerkamp, J.H., van den Berg, W.B., & RPH, V. (2001). Linkage of chondroitin-sulfate to type I collagen scaffolds stimulates the bioactivity of seeded chondrocytes in vitro. *Biomaterials*, 22(17), 2359–2369. doi: 10.1016/S0142-9612(00)00423-3.

323. Mattei, G., Di Patria, V., Tirella, A., Alaimo, A., Elia, G., Corti, A., Paolicchi, A., & Ahluwalia, A. (2014). Mechanostructure and composition of highly reproducible decellularized liver matrices. *Acta Biomaterialia*, 10(2), 875–882. doi: 10.1016/j.actbio.2013.10.023.

324. Weymann, A., Patil, N.P., Sabashnikov, A., Jungebluth, P., Korkmaz, S., Li, S., Veres, G., Soós, P., Ishtok, R., Chaimow, N., Pätzold, I., Czerny, N., Schies, C., Schmack, B., Popov, A.F., Simon, A.R., Karck, M., & Szabó, G. (2014). Bioartificial heart:

a human-sized porcine model - the way ahead. *PloS one*, 9(11), e111591.

325. Struecker, B., Hillebrandt, K.H., Voitl, R., Butter, A., Schmuck, R.B., Reutzel-Selke, A., Geisel, D., Joehrens, K., Pickerodt, P.A., Raschzok, N., Puhl, G., Neuhaus, P., Pratschke, J., & Sauer, I.M. (2014). Porcine liver decellularization under oscillating pressure conditions - A technical refinement to improve the homogeneity of the decellularization process. *Tissue Engineering Part C: Methods*, 21(3), 303–313. doi: 10.1089/ten.TEC.2014.0321.

326. Naso, F., Iop, L., Spina, M., & Gerosa, G. (2014). Are FDA and CE sacrificing safety for a faster commercialization of xenogeneic tissue devices? Unavoidable need for legislation in decellularized tissue manufacturing. *Tissue antigens*, 83(3), 193–194. doi: 10.1111/tan.12275.

327. Momtahan, N., Poornejad, N., Struk, J.A., Castleton, A.A., Herrod, B.J., Vance, B.R., Eatough, J.P., Roeder, B.L., Reynolds, P.R., & Cook, A.D. (2015). Automation of Pressure Control Improves Whole Porcine Heart Decellularization. *Tissue Engineering Part C: Methods*, 150714090832003. doi: 10.1089/ten.tec.2014.0709.

328. MacConaill, M. (1985). Calcium precipitation from mammalian physiological salines (Ringer solutions) and the preparation of high [Ca] media. *Journal of pharmacological methods*, 14(2), 147–155.

329. Akhyari, P., Aubin, H., Gwanmesia, P., Barth, M., Hoffmann, S., Huelsmann, J., Preuss, K., & Lichtenberg, A. (2011). The quest for an optimized protocol for whole-heart decellularization: a comparison of three popular and a novel decellularization technique and their diverse effects on crucial extracellular matrix qualities. *Tissue Engineering Part C: Methods*, 17(9), 915–926. doi: 10.1089/ten.TEC.2011.0210.

330. Paludan, S.R. & Bowie, A.G. (2013). Immune Sensing of DNA. *Immunity*, 38(5), 870–880. doi: 10.1016/j.immuni.2013.05.004.

331. Rutz, M., Metzger, J., Gellert, T., Luppa, P., Lipford, G.B., Wagner, H., & Bauer, S. (2004). Toll-like receptor 9 binds single-stranded CpG-DNA in a sequence- and pH-dependent manner. *European journal of immunology*, 34(9), 2541–2550. doi: 10.1002/eji.200425218.

332. Sedlackova, T., Repiska, G., Celec, P., Szemes, T., & Minarik, G. (2013). Fragmentation of DNA affects the accuracy of the DNA quantitation by the commonly used methods. *Biological Procedures Online*, 15(1), 5. doi: 10.1186/1480-9222-15-5.

333. Ossipow, V., Laemmli, U.K., & Schibler, U. (1993). A Simple Method to Renature Dna-Binding Proteins Separated by Sds-Polyacrylamide Gel-Electrophoresis. *Nucleic Acids Research*, 21(25), 6040–6041.

334. Lee, L.T., Deas, J.E., & Howe, C. (1978). Removal of unbound sodium dodecyl sulfate (SDS) from proteins in solution by electrophoresis through triton X-100-agarose. *Journal of immunological methods*, 19(1), 69–75. doi: 10.1016/0022-1759(78)90009-1.

335. Crawford, B., Koshy, S.T., Jhamb, G., Woodford, C., Thompson, C.M., Levy, A.S., Rush, J.W.E., Guyette, J.P., Lillicrap, D., & Jervis, E. (2011). Cardiac decellularisation with long-term storage and repopulation with canine peripheral blood progenitor cells. *The Canadian Journal of Chemical Engineering*, 90(6), 1457–1464. doi: 10.1002/cjce.20670.

336. Guyette, J.P., Gilpin, S.E., Charest, J.M., Tapias, L.F., Ren, X., & Ott, H. (2014). Perfusion decellularization of whole organs. *Nature Protocols*, 9(6), 1451–1468. doi: 10.1038/nprot.2014.097.

337. Andree, B., Bela, K., Horvath, T., Lux, M., Ramm, R., Venturini, L., Ciubotaru, A., Zweigerdt, R., Haverich, A., & Hilfiker, A. (2014). Successful re-endothelialization of a perfusable biological vascularized matrix (BioVaM) for the generation of 3D artificial cardiac tissue. *Basic research in cardiology*, 109(6), 441. doi: 10.1007/s00395-014-0441-x.

338. Gratzer, P.F., Harrison, R.D., & Woods, T. (2006). Matrix alteration and not residual sodium dodecyl sulfate cytotoxicity affects the cellular repopulation of a decellularized matrix. *Tissue engineering*, 12(10), 2975–2983.

339. Zvarova, B., Uhl, F.E., Uriarte, J.J., Borg, Z.D., Coffey, A.L., Bonenfant, N.R., Weiss, D.J., & Wagner, D.E. (2016). Residual Detergent Detection Method for Non-Destructive Cytocompatibility Evaluation of Decellularized Whole Lung Scaffolds. *Tissue Engineering Part C: Methods*, ten.TEC.2015.0439. doi: 10.1089/ten.TEC.2015.0439.

340. Matuo, Y., Nishi, N., Muguruma, Y., Yoshitake, Y., Masuda, Y., Nishikawa, K., & Wada, F. (1988). The usefulness of CHAPS as a non-cytotoxic stabilizing agent in purification of growth factors. *Cytotechnology*, 1(4), 309–318. doi: 10.1007/BF00365076.

341. Bilodeau, K. & Mantovani, D. (2006). Bioreactors for Tissue Engineering: Focus on Mechanical Constraints. A Comparative Review. *Tissue engineering*, 12(8), 2367–2383. doi: 10.1089/ten.2006.12.2367.

342. Hansmann, J., Groeber, F., Kahlig, A., Kleinhans, C., & Walles, H. (2012). Bioreactors in tissue engineering-principles, applications and commercial constraints. *Biotechnology Journal*, 8(3), 298–307. doi: 10.1002/biot.201200162.

343. Hülsmann, J., Aubin, H., Kranz, A., Godehardt, E., Munakata, H., Kamiya, H., Barth, M., Lichtenberg, A., & Akhyari, P. (2013). A novel customizable modular bioreactor system for whole-heart cultivation under controlled 3D biomechanical stimulation. *Journal of Artificial Organs*, 16(3), 294–304. doi: 10.1007/s10047-013-0705-5.

344. Cannizzaro, C., Tandon, N., Figallo, E., Park, H., Gerecht, S., Radisic, M., Elvassore, N., & Vunjak-Novakovic, G. (2007). Practical aspects of cardiac tissue engineering with electrical stimulation. *Methods in molecular medicine*, 140, 291–307.

345. Song, B., Gu, Y., Pu, J., Reid, B., Zhao, Z., & Zhao, M. (2007). Application of direct current electric fields to cells and tissues in vitro and modulation of wound electric field in vivo. *Nature Protocols*, 2(6), 1479–1489. doi: 10.1038/nprot.2007.205.

346. Laudon, M.K. (1995). Pulse output. In J.G. Webster, ed., *Design of Cardiac Pacemakers*. IEEE Press, New York, (pp. 251–276).

347. Sanders, R.S. (2008). The Pulse Generator. In F.M. Kusumoto & N.F. Goldschlager, eds., *Cardiac Pacing for the Clinician*. Springer US, Boston, MA, (pp. 47–71). doi: 10.1007/978-0-387-72763-9_2.

348. Pietronave, S., Zamperone, A., Oltolina, F., Colangelo, D., Follenzi, A., Novelli, E., Diena, M., Pavesi, A., Consolo, F., Fiore, G.B., Soncini, M., & Prat, M. (2014). Monophasic and Biphasic Electrical Stimulation Induces a Precardiac Differentiation in Progenitor Cells Isolated from Human Heart. *Stem Cells and Development*, 23(8), 888–898. doi: 10.1089/scd.2013.0375.

349. Chiu, L.L.Y., Iyer, R.K., King, J.P., & Radisic, M. (2011). Biphasic Electrical Field Stimulation Aids in Tissue Engineering of Multicell-Type Cardiac Organoids. *Tissue*

Engineering Part A, 17(11-12), 1465–1477. doi: 10.1089/ten.tea.2007.0244.

350. Asnes, C.F., Marquez, J.P., Elson, E.L., & Wakatsuki, T. (2006). Reconstitution of the Frank-Starling Mechanism in Engineered Heart Tissues. *Biophysical journal*, 91(5), 1800–1810. doi: 10.1529/biophysj.105.065961.

351. Amer, M.H., White, L.J., & Shakesheff, K.M. (2015). The effect of injection using narrow-bore needles on mammalian cells: administration and formulation considerations for cell therapies. *Journal of Pharmacy and Pharmacology*, 67(5), 640–650. doi: 10.1111/jphp.12362.

352. Guyette, J.P., Charest, J.M., Mills, R.W., Jank, B.J., Moser, P.T., Gilpin, S.E., Gershlak, J.R., Okamoto, T., Gonzalez, G., Milan, D.J., Gaudette, G.R., & Ott, H. (2016). Bioengineering Human Myocardium on Native Extracellular Matrix. *Circulation research*, 118(1), 56–72. doi: 10.1161/CIRCRESAHA.115.306874.

353. Lu, L., Mende, M., Yang, X., Körber, H.F., Schnittler, H.J., Weinert, S., Heubach, J., Werner, C., & Ravens, U. (2013). Design and Validation of a Bioreactor for Simulating the Cardiac Niche: A System Incorporating Cyclic Stretch, Electrical Stimulation, and Constant Perfusion. *Tissue Engineering Part A*, 19(3-4), 403–414. doi: 10.1089/ten.TEA.2012.0135.

354. Sanders, J.I. & Kepecs, A. (2014). A low-cost programmable pulse generator for physiology and behavior. *Frontiers in Neuroengineering*, 7, 735. doi: 10.3389/fneng.2014.00043.

355. Chan, Y.C., Ting, S., Lee, Y.K., Ng, K.M., Zhang, J., Chen, Z., Siu, C.W., Oh, S.K.W., & Tse, H.F. (2013). Electrical stimulation promotes maturation of cardiomyocytes derived from human embryonic stem cells. *Journal of Cardiovascular Translational Research*, 6(6), 989–999. doi: 10.1007/s12265-013-9510-z.

356. Stark, G., Huber, U., Hofer, E., & Tritthart, H.A. (1987). Continuous ECG measurements of intracardiac activity from the surface of Langendorff-perfused guinea pig hearts. *Basic research in cardiology*, 82(5), 437–444.

357. Ren, X., Tapias, L.F., Jank, B.J., Mathisen, D.J., Lanuti, M., & Ott, H. (2015). Ex vivo non-invasive assessment of cell viability and proliferation in bio-engineered whole organ constructs. *Biomaterials*, 52, 103–112. doi: 10.1016/j.biomaterials.2015.01.061.

358. Lee, S.M., Han, N., Lee, R., Choi, I.H., Park, Y.B., Shin, J.S., & Yoo, K.H. (2016). Real-time monitoring of 3D cell culture using a 3D capacitance biosensor. *Biosensors and Bioelectronics*, 77, 56–61. doi: 10.1016/j.bios.2015.09.005.

359. Yamamoto, K., Sokabe, T., Watabe, T., Miyazono, K., Yamashita, J.K., Obi, S., Ohura, N., Matsushita, A., Kamiya, A., & Ando, J. (2005). Fluid shear stress induces differentiation of Flk-1-positive embryonic stem cells into vascular endothelial cells in vitro. *American journal of physiology. Heart and circulatory physiology*, 288(4), H1915–24. doi: 10.1152/ajpheart.00956.2004.

360. Robertson, M.J., Dries-Devlin, J.L., Kren, S.M., Burchfield, J.S., & Taylor, D.A. (2014). Optimizing recellularization of whole decellularized heart extracellular matrix. *PloS one*, 9(2), e90406. doi: 10.1371/journal.pone.0090406.

361. Ott, H., Clippinger, B., Conrad, C., Schuetz, C., Pomerantseva, I., Ikonomou, L., Kotton, D., & Vacanti, J.P. (2010). Regeneration and orthotopic transplantation of a bioartificial lung. *Nature Medicine*, 16(8), 927–933. doi: 10.1038/nm.2193.

362. Uygun, B.E., Soto-Gutierrez, A., Yagi, H., Izamis, M.L., Guzzardi, M.A., Shulman, C., Milwid, J., Kobayashi, N., Tilles, A., Berthiaume, F., Hertl, M., Nahmias, Y., Yarmush, M.L., & Uygun, K. (2010). Organ reengineering through development of a transplantable recellularized liver graft using decellularized liver matrix. *Nature Medicine*, 16(7), 814–820. doi: 10.1038/nm.2170.

363. Song, J.J., Guyette, J.P., Gilpin, S.E., Gonzalez, G., Vacanti, J.P., & Ott, H. (2013). Regeneration and experimental orthotopic transplantation of a bioengineered kidney. *Nature Medicine*, 19(5), 646–651. doi: 10.1038/nm.3154.

364. Perea-Gil, I., Prat-Vidal, C., & Bayes-Genis, A. (2015). In vivo experience with natural scaffolds for myocardial infarction: the times they are a-changin'. *Stem cell research & therapy*, 6(1), 248. doi: 10.1186/s13287-015-0237-4.

365. Araña, M., Gavira, J.J., Peña, E., Gonzalez, A., Abizanda, G., Cilla, M., Pérez, M.M., Albiasu, E., Aguado, N., Casado, M., López, B., González, S., Soriano, M., Moreno, C., Merino, J., Garcia-Verdugo, J.M., Díez, J., Doblaré, M., Pelacho, B., & Prósper, F. (2014). Epicardial delivery of collagen patches with adipose-derived stem cells in rat and minipig models of chronic myocardial infarction. *Biomaterials*, 35(1), 143–151. doi: 10.1016/j.biomaterials.2013.09.083.

366. Zwetsloot, P.P., Végh, A.M.D., Jansen of Lorkeers, S.J., van Hout, G.P.J., Currie, G.L., Sena, E.S., Gremmels, H., Buikema, J.W., Goumans, M.J., Macleod, M.R., Doevendans, P.A., Chamuleau, S.A.J., & Sluijter, J.P.G. (2016). Cardiac Stem Cell Treatment in Myocardial Infarction Novelty and Significance. *Circulation research*. doi: 10.1161/CIRCRESAHA.115.307676.

367. Stuckey, D.J., Ishii, H., Chen, Q.Z., Boccaccini, A.R., Hansen, U., Carr, C.A., Roether, J.A., Jawad, H., Tyler, D.J., Ali, N.N., Clarke, K., & Harding, S.E. (2010). Magnetic resonance imaging evaluation of remodeling by cardiac elastomeric tissue scaffold biomaterials in a rat model of myocardial infarction. *Tissue Engineering Part A*, 16(11), 3395–3402. doi: 10.1089/ten.TEA.2010.0213.

368. Fujimoto, K.L., Tobita, K., Merryman, W.D., Guan, J., Momoi, N., Stolz, D.B., Sacks, M.S., Keller, B.B., & Wagner, W.R. (2007). An elastic, biodegradable cardiac patch induces contractile smooth muscle and improves cardiac remodeling and function in subacute myocardial infarction. *Journal of the American College of Cardiology*, 49(23), 2292–2300. doi: 10.1016/j.jacc.2007.02.050.

369. Engler, A.J., Carag-Krieger, C., Johnson, C.P., Raab, M., Tang, H.Y., Speicher, D.W., Sanger, J.W., Sanger, J.M., & Discher, D.E. (2008). Embryonic cardiomyocytes beat best on a matrix with heart-like elasticity: scar-like rigidity inhibits beating. *Journal of Cell Science*, 121(Pt 22), 3794–3802. doi: 10.1242/jcs.029678.

370. Brown, B.N., Londono, R., Tottey, S., Zhang, L., Kukla, K.A., Wolf, M.T., Daly, K.A., Reing, J.E., & Badylak, S.F. (2012). Macrophage phenotype as a predictor of constructive remodeling following the implantation of biologically derived surgical mesh materials. *Acta Biomaterialia*, 8(3), 978–987. doi: 10.1016/j.actbio.2011.11.031.

371. Bashey, R.I., Martinez-Hernandez, A., & Jimenez, S.A. (1992). Isolation, characterization, and localization of cardiac collagen type VI. Associations with other extracellular matrix components. *Circulation research*, 70(5), 1006–1017.

372. Roelofs, L.A.J., Eggink, A.J., Hulsbergen-van de Kaa, C.A., van den Berg, P.P., van Kuppevelt, T.H., van Moerkerk, H.T.B., Crevels, A.J., Lotgering, F.K., Feitz, W.F.J.,

& Wijnen, R.M.H. (2008). Fetal abdominal wall repair with a collagen biomatrix in an experimental sheep model for gastroschisis. *Tissue Engineering Part A*, 14(12), 2033–2040. doi: 10.1089/ten.tea.2007.0191.

373. Roelofs, L.A.J., Geutjes, P.J., Hulsbergen-van de Kaa, C.A., Eggink, A.J., van Kuppevelt, T.H., Daamen, W.F., Crevels, A.J., van den Berg, P.P., Feitz, W.F.J., & Wijnen, R.M.H. (2013). Prenatal coverage of experimental gastroschisis with a collagen scaffold to protect the bowel. *Journal of pediatric surgery*, 48(3), 516–524. doi: 10.1016/j.jpedsurg.2012.07.056.

374. Pinheiro, J., Bates, D., DebRoy, S., Sarkar, D., & R Core Team (2015). *nlme: Linear and Nonlinear Mixed Effects Models*. R package version 3.1-122.

375. Bates, D., Mächler, M., Bolker, B., & Walker, S. (2015). Fitting linear mixed-effects models using lme4. *Journal of Statistical Software*, 67(1), 1–48. doi: 10.18637/jss.v067.i01.

376. Harley, B.A.C., Leung, J.H., Silva, E.C.C.M., & Gibson, L.J. (2007). Mechanical characterization of collagen-glycosaminoglycan scaffolds. *Acta Biomaterialia*, 3(4), 463–474. doi: 10.1016/j.actbio.2006.12.009.

377. Tilley, J.M.R., Chaudhury, S., Hakimi, O., Carr, A.J., & Czernuszka, J.T. (2012). Tenocyte proliferation on collagen scaffolds protects against degradation and improves scaffold properties. *Journal of Materials Science: Materials in Medicine*, 23(3), 823–833. doi: 10.1007/s10856-011-4537-7.

378. Araña, M., Peña, E., Abizanda, G., Cilla, M., Ochoa, I., Gavira, J.J., Espinosa, G., Doblaré, M., Pelacho, B., & Prósper, F. (2013). Preparation and characterization of collagen-based ADSC-carrier sheets for cardiovascular application. *Acta Biomaterialia*, 9(4), 6075–6083. doi: 10.1016/j.actbio.2012.12.014.

379. Serpooshan, V., Zhao, M., Metzler, S.A., Wei, K., Shah, P.B., Wang, A., Mahmoudi, M., Malkovskiy, A.V., Rajadas, J., Butte, M.J., Bernstein, D., & Ruiz-Lozano, P. (2013). The effect of bioengineered acellular collagen patch on cardiac remodeling and ventricular function post myocardial infarction. *Biomaterials*, 34(36), 9048–9055. doi: 10.1016/j.biomaterials.2013.08.017.

380. Blackburn, N.J.R., Sofrenovic, T., Kuraitis, D., Ahmadi, A., McNeill, B., Deng, C., Rayner, K.J., Zhong, Z., Ruel, M., & Suuronen, E.J. (2015). Timing underpins the benefits associated with injectable collagen biomaterial therapy for the treatment of myocardial infarction. *Biomaterials*, 39, 182–192. doi: 10.1016/j.biomaterials.2014.11.004.

381. Spiller, K.L., Anfang, R.R., Spiller, K.J., Ng, J., Nakazawa, K.R., Daulton, J.W., & Vunjak-Novakovic, G. (2014). The role of macrophage phenotype in vascularization of tissue engineering scaffolds. *Biomaterials*, 35(15), 4477–4488. doi: 10.1016/j.biomaterials.2014.02.012.

382. Spiller, K.L., Nassiri, S., Witherel, C.E., Anfang, R.R., Ng, J., Nakazawa, K.R., Yu, T., & Vunjak-Novakovic, G. (2015). Sequential delivery of immunomodulatory cytokines to facilitate the M1-to-M2 transition of macrophages and enhance vascularization of bone scaffolds. *Biomaterials*, 37, 194–207. doi: 10.1016/j.biomaterials.2014.10.017.

383. Hosoyama, T., Samura, M., Kudo, T., Nishimoto, A., Ueno, K., Murata, T., Ohama, T., Sato, K., Mikamo, A., Yoshimura, K., Li, T.S., & Hamano, K. (2015). Cardiosphere-derived cell sheet

primed with hypoxia improves left ventricular function of chronically infarcted heart. *American Journal of Translational Research*, 7(12), 2738–2751.

384. Dirnagl, U. & Lauritzen, M. (2010). Fighting publication bias: introducing the Negative Results section. *Journal of Cerebral Blood Flow and Metabolism*, 30(7), 1263–1264. doi: 10.1038/jcbfm.2010.51.

385. Sena, E.S., van der Worp, H.B., Bath, P.M.W., Howells, D.W., & Macleod, M.R. (2010). Publication Bias in Reports of Animal Stroke Studies Leads to Major Overstatement of Efficacy. *PLOS Biol*, 8(3), e1000344. doi: 10.1371/journal.pbio.1000344.

386. Riegler, J., Tiburcy, M., Ebert, A., Tzatzalos, E., Raaz, U., Abilez, O.J., Shen, Q., Kooreman, N.G., Neofytou, E., Chen, V.C., Wang, M., Meyer, T., Tsao, P.S., Connolly, A.J., Couture, L.A., Gold, J.D., Zimmermann, W.H.H., & Wu, J.C. (2015). Human Engineered Heart Muscles Engraft and Survive Long Term in a Rodent Myocardial Infarction Model. *Circulation research*, 117(8), 720–730. doi: 10.1161/CIRCRESAHA.115.306985.

387. Pfeffer, M.A., Pfeffer, J.M., Fishbein, M.C., Fletcher, P.J., Spadaro, J., Kloner, R.A., & Braunwald, E. (1979). Myocardial infarct size and ventricular function in rats. *Circulation research*, 44(4), 503–512. doi: 10.1161/01.RES.44.4.503.

388. Zornoff, L.A.M., Paiva, S.A.R., Minicucci, M.F., & Spadaro, J. (2009). Experimental myocardium infarction in rats: analysis of the model. *Arquivos brasileiros de cardiologia*, 93(4), 434–440. doi: 10.1590/S0066-782X2009001000018.

389. Ciulla, M.M., Paliotti, R., Ferrero, S., Braidotti, P., Esposito, A., Gianelli, U., Busca, G., Cioffi, U., Bulfamante, G., & Magrini, F. (2004). Left ventricular remodeling after experimental myocardial cryoinjury in rats. *The Journal of surgical research*, 116(1), 91–97.

390. Stuckey, D.J., Carr, C.A., Tyler, D.J., & Clarke, K. (2008). Cine-MRI versus two-dimensional echocardiography to measure in vivo left ventricular function in rat heart. *NMR in biomedicine*, 21(7), 765–772. doi: 10.1002/nbm.1268.

391. de Jong, R., Houtgraaf, J.H., Samiei, S., Boersma, E., & Duckers, H.J. (2014). Intracoronary stem cell infusion after acute myocardial infarction: a meta-analysis and update on clinical trials. *Circulation. Cardiovascular interventions*, 7(2), 156–167. doi: 10.1161/CIRCINTERVENTIONS.113.001009.

392. Pons, J., Huang, Y., Takagawa, J., Arakawa-Hoyt, J., Ye, J., Grossman, W., Kan, Y.W., & Su, H. (2009). Combining angiogenic gene and stem cell therapies for myocardial infarction. *The journal of gene medicine*, 11(9), 743–753. doi: 10.1002/jgm.1362.

393. Li, L., Chen, X., Wang, W.E., & Zeng, C. (2016). How to Improve the Survival of Transplanted Mesenchymal Stem Cell in Ischemic Heart? *Stem cells international*, 2016, 9682757. doi: 10.1155/2016/9682757.

394. Cheng, K., Blusztajn, A., Shen, D., Li, T.S., Sun, B., Galang, G., Zarembinski, T.I., Prestwich, G.D., Marbán, E., Smith, R.R., & Marbán, L. (2012). Functional performance of human cardiosphere-derived cells delivered in an in situ polymerizable hyaluronan-gelatin hydrogel. *Biomaterials*, 33(21), 5317–5324. doi: 10.1016/j.biomaterials.2012.04.006.

395. Chen, L., Qin, F., Ge, M., Shu, Q., & Xu, J. (2014). Application of Adipose-Derived Stem Cells in Heart Disease. *Jour-*

nal of Cardiovascular Translational Research, 7(7), 651–663. doi: 10.1007/s12265-014-9585-1.

396. Holladay, C., Power, K., Sefton, M., O'Brien, T., Gallagher, W.M., & Pandit, A. (2011). Functionalized scaffold-mediated interleukin 10 gene delivery significantly improves survival rates of stem cells in vivo. *Molecular Therapy*, 19(5), 969–978. doi: 10.1038/mt.2010.311.

397. Holladay, C.A., Duffy, A.M., Chen, X., Sefton, M.V., O'Brien, T.D., & Pandit, A.S. (2012). Recovery of cardiac function mediated by MSC and interleukin-10 plasmid functionalised scaffold. *Biomaterials*, 33(5), 1303–1314. doi: 10.1016/j.biomaterials.2011.10.019.

398. Gaballa, M.A., Sunkomat, J.N.E., Thai, H., Morkin, E., Ewy, G., & Goldman, S. (2006). Grafting an acellular 3-dimensional collagen scaffold onto a non-transmural infarcted myocardium induces neo-angiogenesis and reduces cardiac remodeling. *The Journal of Heart and Lung Transplantation*, 25(8), 946–954. doi: 10.1016/j.healun.2006.04.008.

399. Baldwin, J., Antille, M., Bonda, U., De-Juan-Pardo, E.M., Khosrotehrani, K., Ivanovski, S., Petcu, E.B., & Hutmacher, D.W. (2014). In vitro pre-vascularisation of tissue-engineered constructs A co-culture perspective. *Vascular Cell*, 6, 13. doi: 10.1186/2045-824X-6-13.

400. Tien, J. (2014). Microfluidic approaches for engineering vasculature. *Current opinion in chemical engineering*, 3, 36–41. doi: 10.1016/j.coche.2013.10.006.

401. Golden, A.P. & Tien, J. (2007). Fabrication of microfluidic hydrogels using molded gelatin as a sacrificial element. *Lab on a Chip*, 7(6), 720–725. doi: 10.1039/b618409j.

402. Miller, J.S., Stevens, K.R., Yang, M.T., Baker, B.M., Nguyen, D.H.T., Cohen, D.M., Toro, E., Chen, A.A., Galie, P.A., Yu, X., Chaturvedi, R., Bhatia, S.N., & Chen, C.S. (2012). Rapid casting of patterned vascular networks for perfusable engineered three-dimensional tissues. *Nature materials*, 11(9), 768–774. doi: 10.1038/nmat3357.

403. Morgan, J.P., Delnero, P.F., Zheng, Y., Verbridge, S.S., Chen, J., Craven, M., Choi, N.W., Diaz-Santana, A., Kermani, P., Hempstead, B., López, J.A., Corso, T.N., Fischbach, C., & Stroock, A.D. (2013). Formation of microvascular networks in vitro. *Nature Protocols*, 8(9), 1820–1836. doi: 10.1038/nprot.2013.110.

404. Kolesky, D.B., Truby, R.L., Gladman, A.S., Busbee, T.A., Homan, K.A., & Lewis, J.A. (2014). 3D Bioprinting of Vascularized, Heterogeneous Cell-Laden Tissue Constructs. *Advanced Materials*, 26(19), 3124–3130. doi: 10.1002/adma.201305506.

405. Thomson, K.S., Korte, F.S., Giachelli, C.M., Ratner, B.D., Regnier, M., & Scatena, M. (2013). Prevascularized Microtemplated Fibrin Scaffolds for Cardiac Tissue Engineering Applications. *Tissue Engineering Part A*, 19(7-8), 967–977. doi: 10.1089/ten.tea.2012.0286.

APPENDIX A

ADDITIONAL MATERIALS AND METHODS

Table A.1: Primers for quantitative PCR for the analysis of gene expression in human iPS and iPS-CMs.

Category	Gene	Sequence - Direction		E (%)
Housekeeping	POLR2A	AGTCCGGATGAACTGAAGCG	FW	97
		CACGTGAAACACAGGCTTGG	RV	
Housekeeping	TBP	TGACCCAGCATCACTGTTTCTT	FW	98
		CAAGCCCTGAGCGTAAGGTG	RV	
Housekeeping	HPRT1	CCTGGCGTCGTGATTAGTGA	FW	101
		GGGCTACAATGTGATGGCCT	RV	
Housekeeping	B2M	AGCAGCATCATGGAGGTTTGA	FW	108
		AGCCCTCCTAGAGCTACCTG	RV	
Pluripotency	NANOG	ACCTCAGCTACAAACAGGTGA	FW	102
		AAAGGCTGGGGTAGGTAGGT	RV	
Ectoderm	NCAM1	GCAGCGAAGAAAAGACTCTGG	FW	98
		TGGTTCCCCTCCCAAGTGTA	RV	

Table A.1 (continued):

Category	Gene	Sequence - Direction		E (%)
Mesoderm	RUNX1	AACCTCGAAGACATCGGCAG	FW	96
		GGCTGAGGGTTAAAGGCAGT	RV	
Heart	NKX-2.5	GAGCCGAAAAGAAAGCCTGAAAT	FW	90
		CCACCGACACGTCTCACTCA	RV	
Heart	TNNT2	GACAGAGCGGAAAAGTGGGA	FW	95
		CTCCTTGGCCTTCTCCCTC	RV	
Heart	MYL7	GGAGTTCAAAGAAGCCTTCAGC	FW	97
		GTCCCATTGAGCTTCTCCCC	RV	
Heart	MYH6	TCCTGCGGCCCAGATTCTTC	FW	106
		TCTTCCTTGTCATCGGGCAC	RV	
Heart	MYH7	AAGGTCAAGGCCTACAAGCG	FW	100
		CCAGGGCTGAGCAGATCAA	RV	
Heart	CX43	TACCAAACAGCAGCGGAGTT	FW	98
		TGGGCACCACTCTTTTGCTT	RV	
Heart	SERCA2A	CGAACCCTTGCCACTCATCT	FW	102
		CCAGTATTGCAGGTTCCAGGT	RV	
Heart	CACNA1D	GGATCACCCAAGCTGAGGAC	FW	99
		GGCTTGACAGAGACTTCCACA	RV	
Heart	KCNJ2	CTGGGTCTTGGGAATTCTGGTT	FW	103
		AGAACATGTCCTGTTGCTGGC	RV	
Heart	CALR	CGCTTTTATGCTCTGTCGGC	FW	95
		CCACAGATGTCGGGACCAAA	RV	
Heart	CASQ2	ACTTTCCTCTGCTCGTTGCC	FW	99
		GCTCCTCAGCAGTTGGAAGA	RV	

Table A.1 (continued):

Category	Gene	Sequence - Direction		E (%)
Heart	RYR2	CTAATGTCTGGGTGGGCTGG	FW	101
		TGCTGCGTTTGATGCTTTCA	RV	
Heart	ITPR3	CAAGTTTGCCCGTCTCTGGA	FW	104
		AGGCTGACCACCTCAAAAGT	RV	
Heart	JPH2	CGCTTACCAGAGCCAGAAGTT	FW	98
		CATTCCTCTTGGCACCACCA	RV	
Heart	PLN	CAGCTGCCAAGGCTACCTAA	FW	98
		TTTGACGTGCTTGTTGAGGC	RV	
Metabolism	GLUT1	TGGCATCAACGCTGTCTTCT	FW	102
		CTAGCGCGATGGTCATGAGT	RV	
Metabolism	GLUT4	GTTCTTTCATCTTCGCCGCC	FW	99
		CAATCACCTTCTGAGGGGCA	RV	
Metabolism	CS	CCAGTGCTTCCTCCACGAAT	FW	94
		GGAAACGGATGCCCTCATCA	RV	
Metabolism	IRS1	ACTGGACATCACAGCAGAATGA	FW	99
		ACTGAAATGGATGCATCGTACC	RV	
Metabolism	IRS2	GCCACCATCGTGAAAGAGTG	FW	104
		CCATCCGGGAACAAGGGAAA	RV	
Metabolism	PDK4	TGGTCCAAGATGCCTTTGAGT	FW	104
		GTTGCCCGCATTGCATTCTT	RV	
Metabolism	PPARA	GGACAAGGCCTCAGGCTATC	FW	97
		AACGAATCGCGTTGTGTGAC	RV	
Metabolism	PGC1A	TCTCAGTAAGGGGCTGGTTG	FW	112
		ACCAGAGCAGCACACTCGAT	RV	

Table A.1 (continued):

Category	Gene	Sequence - Direction		E (%)
ECM	COL1A1	GGACACAGAGGTTTCAGTGGT	FW	108
		GCACCATCATTTCCACGAGC	RV	
ECM	COL3A1	GCTGGCATCAAAGGACATCG	FW	101
		GGGAGCCCTCAGATCCTCTT	RV	

Table A.2: Primary antibodies used for immunohistochemistry and immunocytochemistry

Target	Manufacturer	Host	Dilution
CD68	AbD Serotec,	Mouse	1/50
vWF	Millipore, AB7356	Rabbit	1/200
Cardiac Troponin-T	Abcam, ab10214	Mouse	1/200

Table A.3: Secondary antibodies used for immunohistochemistry and immunocytochemistry

Label	Manufacturer	Species reactivity	Dilution
Alexa-488	Life Technologies Ltd	donkey anti-goat	1/200
Alexa-488	Life Technologies Ltd	donkey anti-rabbit	1/200
Alexa-488	Life Technologies Ltd	goat anti-rat	1/200
Alexa-568	Life Technologies Ltd	donkey anti-rabbit	1/200
Alexa-568	Life Technologies Ltd	goat anti-rabbit	1/200
Alexa-647	Life Technologies Ltd	donkey anti-mouse	1/200

APPENDIX B

BIOREACTOR: DETAILED DESIGN DESCRIPTION

Table B.1: Instructions list. List of single character instructions to set the destination channel for further processing on the master MCU

Command	Instruction
I	transmit identifier sequence
D	data (analog) channel
L	T&H channel
S	slave channel
V	full validation of all settings
F	debug mode

Table B.2: Instructions list. List of single character instructions for analog data gathering and transmission

Command	Instruction
O	timer based sampling, set rate to 500 Hz
P	timer based sampling, set rate to 1 kHz
Q	timer based sampling, set rate to 2 kHz
A	measure channel 1 (pressure, timer based)
a	measure channel 1 (pressure)
B	measure channel 2 (pressure, timer based)
b	measure channel 2 (pressure)
C	measure channel 3 (electrical activity, timer based)
c	measure channel 3 (electrical activity)
E	measure all channels (timer based)
R	measure reference channel
0	set gain, G=1 ×100
4	set gain, G=2 ×100
5	set gain, G=4 ×100
6	set gain, G=8 ×100
7	set gain, G=16 ×100
8	set gain, G=32 ×100
9	set gain, G=64 ×100
q	set gain, G=128 ×100
z	set gain, G=256 ×100

Table B.3: Instructions list. List of single character instructions for T&H

Command	Instruction
M	order temperature and humidity measurements
m	restart climate slave timer module
t	transmit room temperature
T	transmit bioreactor temperature
h	transmit room humidity
H	transmit bioreactor humidity

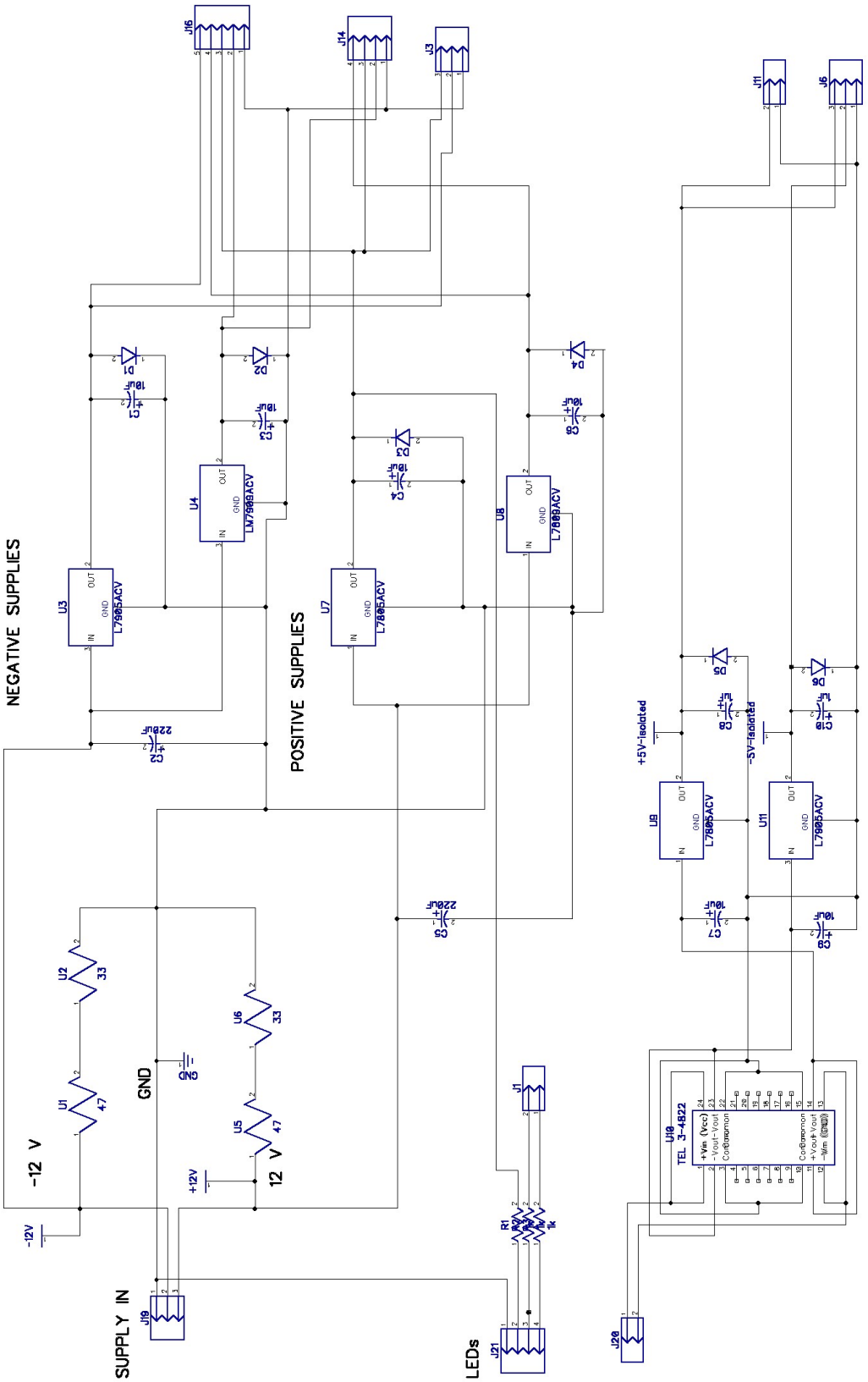


Figure B.1: Power board: Schematics.

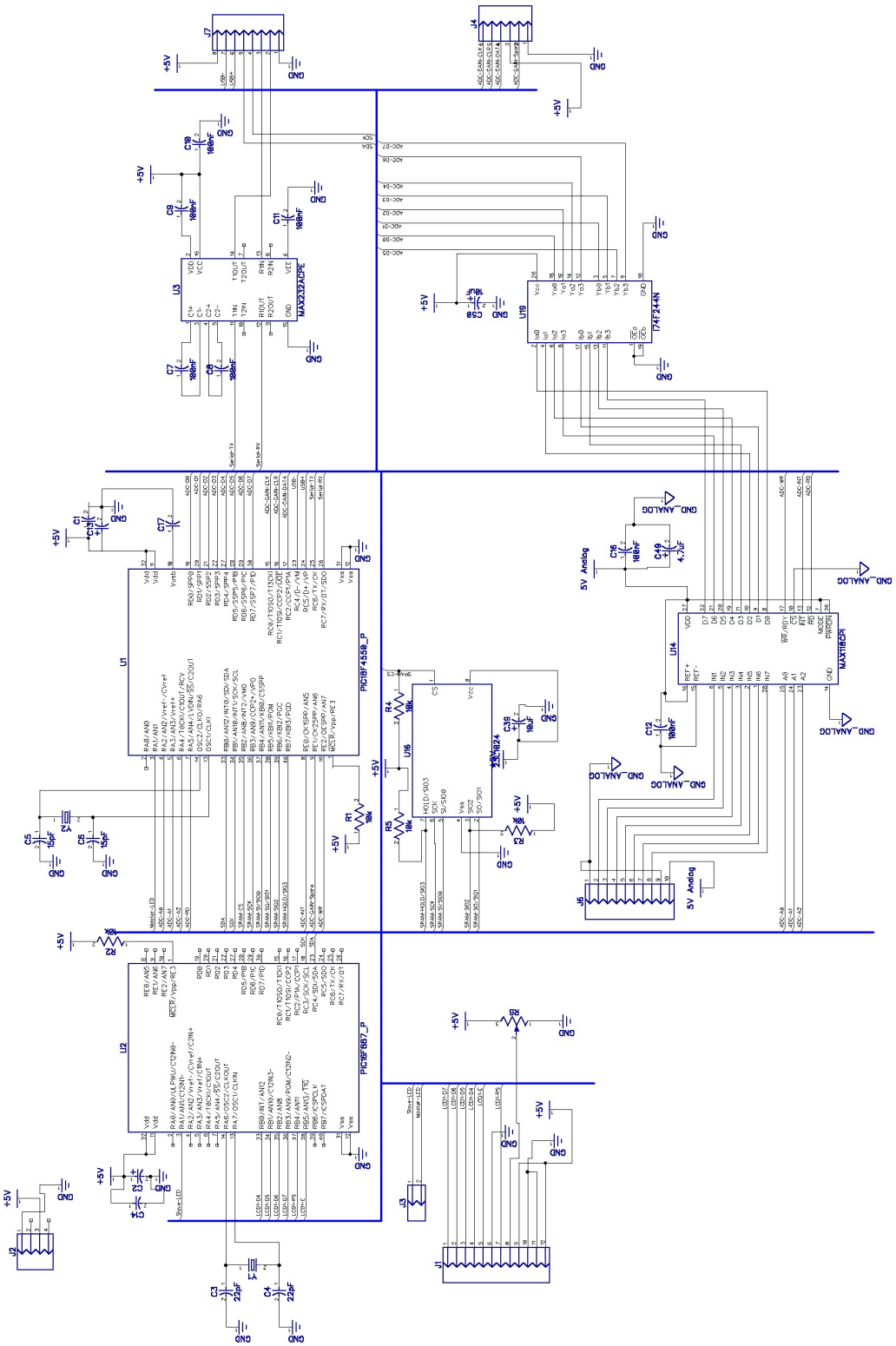


Figure B.2: MCU board PCB: Schematics.

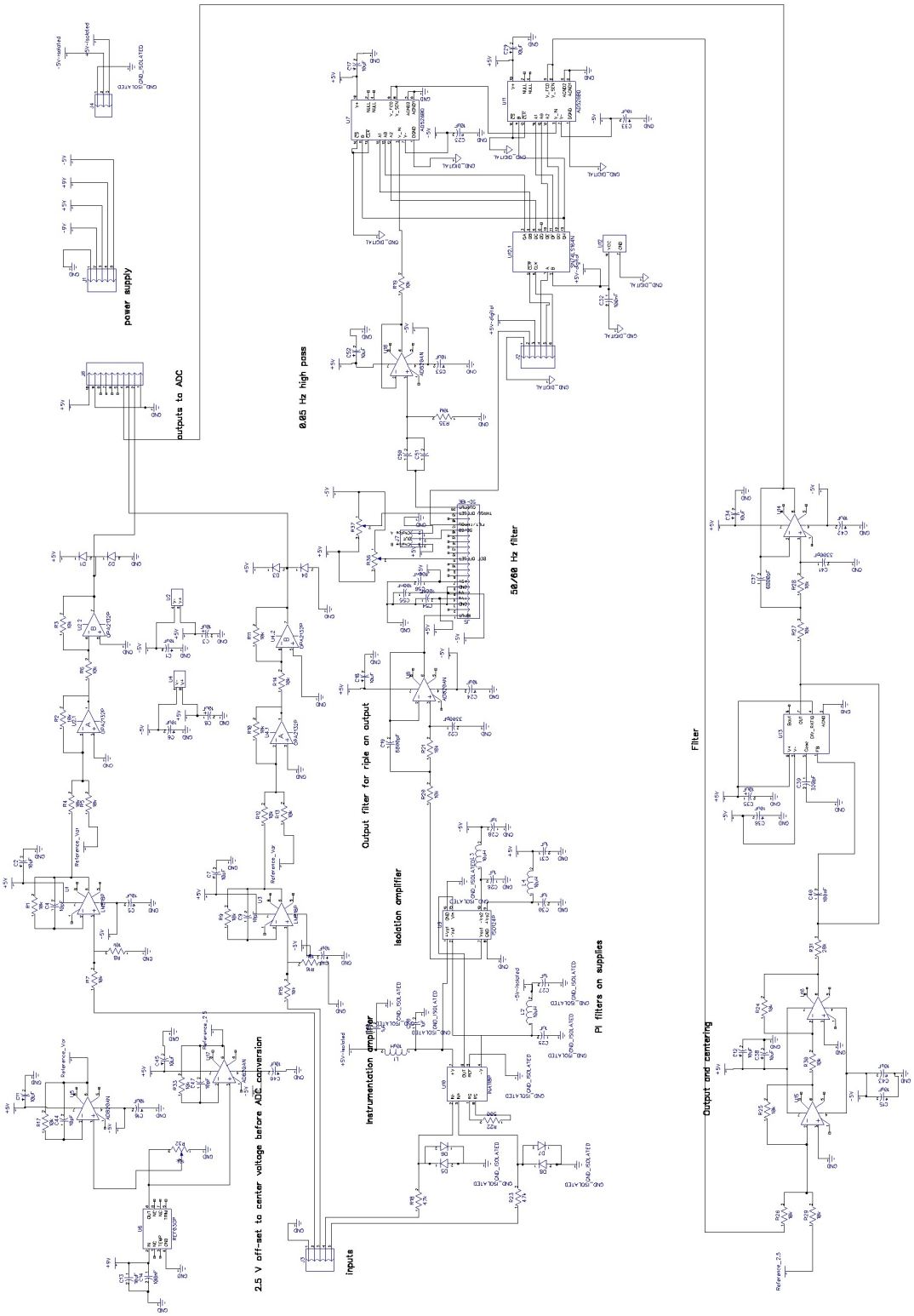


Figure B.3: Amplifier board PCB: Schematics.

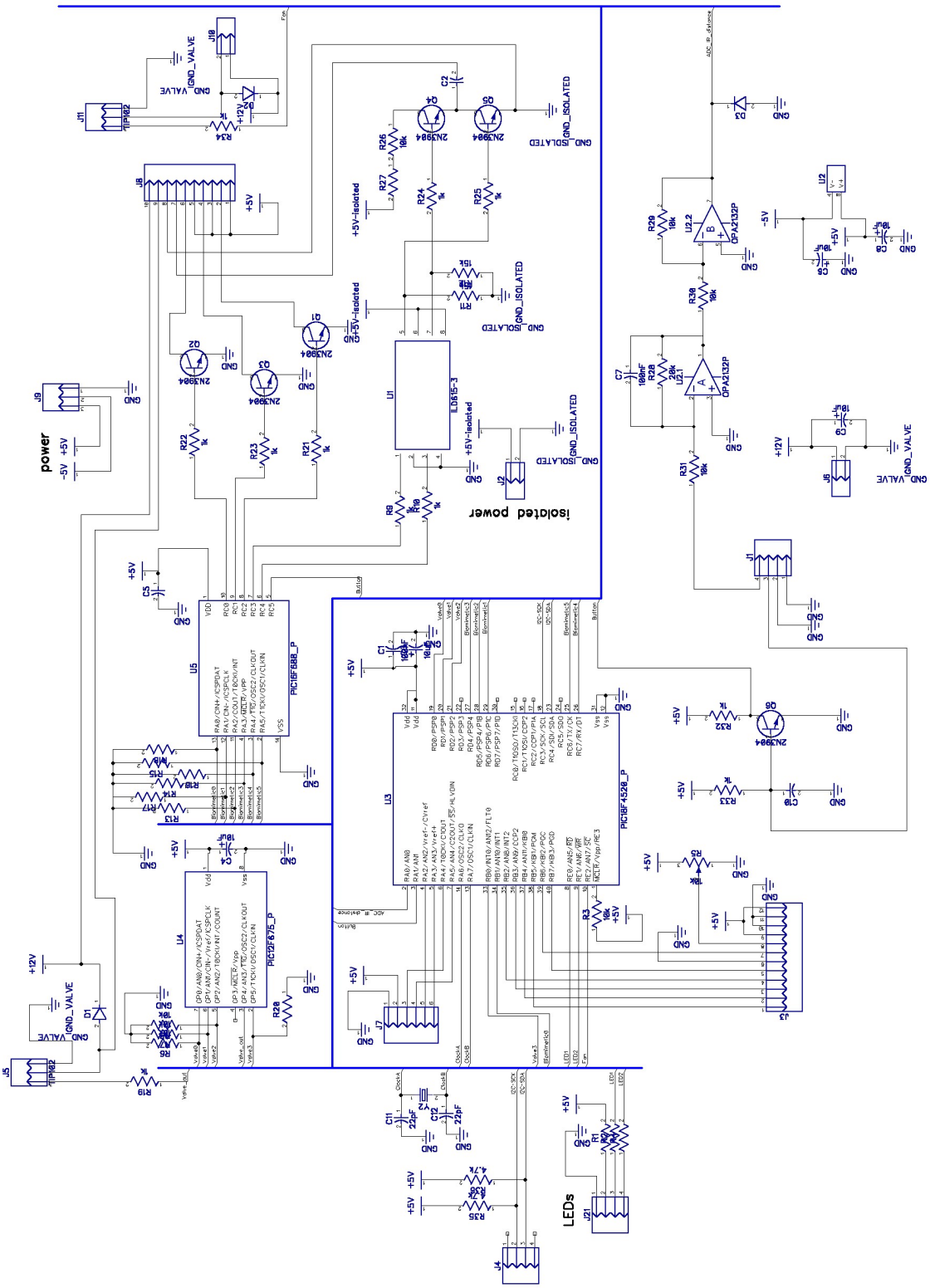


Figure B.4: Stimulation board PCB: Schematics.

Table B.4: Stimulation instructions list. List of single character instructions for stimulation configuration

Command	Instruction
r	oxygenation: off
u	oxygenation: 1-3
v	oxygenation: 1-5
w	oxygenation: 1-7
x	oxygenation: 1-9
y	oxygenation: 1-11
h	mechanical transducer: to home
a	mechanical transducer: FW 10
b	mechanical transducer: FW 100
c	mechanical transducer: FW 1000
d	mechanical transducer: RV 10
e	mechanical transducer: RV 100
f	mechanical transducer: RV 1000
T	mechanical transducer: start
s	mechanical transducer: stop
g	mechanical transducer: set deflated position (min)
G	mechanical transducer: set inflated position (max)
t	mechanical transducer: demo
i	electrical stimulation: on (synchronised)
j	electrical stimulation: off
5	stimulation: stimulate at 0.5 Hz
1	stimulation: stimulate at 1 Hz
2	stimulation: triangular mechanical pulse
3	stimulation: trapezoidal mechanical pulse

Table B.5: Parallel communication instructions to configure oxygenation Parallel communication instructions send by the 18F4520 slave to the 12f675 valve controller chip to configure oxygenation.

Command	Instruction
0b0100	stop
0b0110	set, config 4
0b0111	execute, config 6
0b1100	config 8
0b1101	close and cancel communication, config 10
0b1110	open communication, config 12
0b0101	confirm
0b1111	full validation

Table B.6: Parallel communication instructions to configure electrical and mechanical stimulation Parallel communication instructions send by the 18F4520 slave to the 16f688 stimulation controller chip to configure electrical and mechanical stimulation.

Command	Instruction
0b000100	goto deflated position, stop
0b111111	goto deflated position, start
0b010100	FW 10
0b100100	FW 100
0b110100	FW 1000
0b011100	RV 10
0b101100	RV 100
0b111100	RV 1000
0b000110	save current position as deflated
0b000101	save current position as inflated
0b000111	home position
0b111110	do trial/demo
0b010111	stimulate at 0.5 Hz
0b100111	stimulate at 1 Hz
0b110111	triangular mechanical pulse
0b001111	trapezoidal mechanical pulse
0b101101	confirm
0b100101	open communication
0b011101	set
0b110101	execute
0b111101	cancel command
0b010101	full validation